



Papanatsiou, Maria (2014) Stomatal clustering and hydrogen sulfide: unraveling novel aspects of stomatal behavior. PhD thesis.

<http://theses.gla.ac.uk/6514/>

Copyright and moral rights for this work are retained by the author

A copy can be downloaded for personal non-commercial research or study, without prior permission or charge

This work cannot be reproduced or quoted extensively from without first obtaining permission in writing from the author

The content must not be changed in any way or sold commercially in any format or medium without the formal permission of the author

When referring to this work, full bibliographic details including the author, title, awarding institution and date of the thesis must be given

Enlighten:Theses
<http://theses.gla.ac.uk/>
theses@gla.ac.uk

**Stomatal Clustering and Hydrogen
Sulfide: Unraveling novel aspects of
stomatal behavior**

Thesis submitted for the degree of Doctor of
Philosophy

Maria Papanatsiou

Institute of Molecular, Cellular and Systems Biology
College of Medical, Veterinary and Life Sciences
University of Glasgow

October 2014

Abstract

Stomata are pores found on the epidermis of most aerial parts of plants and are formed by a specialized pair of cells, the guard cells. Stomata enable the uptake of CO₂ in expense of water vapour release and therefore optimize the trade-off between transpirational water loss and carbon gain. Regulation of gas exchange is achieved by controlling the stomatal pore aperture involving the osmotic solute accumulation. Fluxes of K⁺ are mediated by the plasma membrane inward and outward rectifying K⁺ channels (K_{IN} and K_{OUT}), while the anion channels enable Cl⁻ fluxes. Stomata in most plants follow the “one cell spacing rule” implying that the separation of stomata by at least one epidermal cell. However, there are several genera exhibiting stomata clusters, such as the genus *Begonia*.

In this study I have used two *Begonia* species as well as *Arabidopsis* stomatal patterning mutants to explore the impact of stomatal clustering in plant physiology. In the *tmm1* mutants the stomatal movements suppressed gas exchange responses when plants were exposed to light and darkness. Kinetic analysis of the K⁺ channels uncovered changes in the gating characteristics that affected the activity of K_{OUT} channels as well as the voltage-dependence of K_{IN} channel opening. Tail current analysis of K⁺ channels demonstrated that the effect was to reduce accumulation of K⁺ ions in the cytosol of guard cells from *tmm1* plants. Raising light intensity and lowering evaporative demand enhanced WUE and growth of plants exhibiting single stomata, albeit the *tmm1* mutant plants failed to respond likewise. Astonishingly, the *tmm1* mutants were more resilient to prolonged drought stress via minimizing the transpirational water loss. Phenotypic analysis also revealed that the impaired stomatal behaviour of the *tmm1* plants attenuated root growth under sucrose abundant conditions.

I have also made use of the novel gasotransmitter hydrogen sulfide (H_2S) to examine its effect on stomata. H_2S -induced stomatal closure in both *Arabidopsis* and tobacco plants was dependent on the exclusive inhibition of K_{IN} channels. The data implied a partial sensitivity of H_2S effect to the intracellular Ca^{2+} levels, and modelling also suggest a role for pH in the H_2S -mediate response. The *tmm1* mutants did not respond to H_2S in a wild type fashion, indicating that stomatal movements are altered irrespectively to the nature of stimuli.

Collectively, my data suggest that stomatal spacing and their associations with neighbouring epidermal cells is important for the K^+ relations of guard cells and their capacity to drive stomatal movements. The role of spacing was crucial for gaseous exchange as well as plant growth under favourable conditions. The data also provided novel insights into the network governing stomatal behaviour and positioned H_2S to an independent branch of the ABA pathway. Finally, the data suggested an adaptive role for stomatal clustering under water-limited habitats and a potential use of H_2S as a tool to minimize transpirational water loss.

Table of Contents

Abstract	i
Table of Contents	iii
List of Figures	v
List of Tables	xi
List of Equations	xii
Acknowledgements	xiii
Author's declaration	xiv
Abbreviations	xv
1 INTRODUCTION	1
1.1 Stomatal development and patterning	3
1.1.1 Genes regulating stomatal initiation and production	5
1.1.2 Genes regulating spacing pattern	5
1.2 Stomata and the environment	11
1.2.1 Light	13
1.2.2 Carbon dioxide	15
1.2.3 Water status	16
1.1.4 Temperature	17
1.3 Stomata and other signalling compounds	18
1.3.1 Abscisic acid	18
1.3.2 Nitric oxide	20
1.3.3 Hydrogen sulfide	21
1.4 Stomatal movements depend on plasma membrane ion transport	23
1.4.1 K ⁺ channels	24
Inward-rectifying K ⁺ channels	25
Outward-rectifying K ⁺ channels	26
Anion channels	27
Tonoplast K ⁺ and anion channels	28
1.5 <i>Begonia</i>	29
1.6 Thesis objectives	35
2 MATERIAL & METHODS	36
2.1 Materials	36
2.1.1 Plant material	36

2.1.2	Chemicals, reagents and buffers	36
2.2	Plant Growth	39
2.2.1	<i>Begonia</i> growth conditions	39
2.2.2	<i>Arabidopsis</i> growth conditions	40
2.2.3	Tobacco growth conditions	40
2.3	Experimental design for phenotypic analysis	41
2.3.1	Light-Humidity experiment	41
2.3.2	Drought stress experiment	42
2.3.3	Root phenotypic analysis	42
2.3.4	Osmotic content analysis	43
2.4	Gas exchange measurements	44
2.4.1	Basic concepts of gas exchange	44
2.4.2	General gas exchange experimental design	45
2.4.3	Light Curves	46
2.4.4	Time-Course gas exchange measurement	46
2.4.5	Steady-state gas exchange measurement	46
2.4.6	Gas exchange measurement analysis	47
2.5	Stomatal biology	47
2.5.1	Preparation of epidermal peels	47
2.5.2	Stomatal patterning	48
2.5.3	Stomatal closure	50
2.6	Electrophysiology	50
2.6.1	Basic concepts of electrophysiology	50
2.6.2	Electrophysiological experimental design	52
2.6.3	Ion current separation	54
2.6.4	Analysis of ion currents	56
2.7	Molecular Biology	56
2.7.1	RNA extraction	56
2.7.2	Polymerase chain reaction	58
2.7.3	Quantitative PCR	59
2.8	Data analysis	61
2.8.1	Image analysis	61
2.8.2	Statistical analysis	61
3	STOMATAL CLUSTERING INFLUENCES STOMATAL MOVEMENTS	62
3.1	Introduction	62
3.2	Results	65
3.2.1	Epidermal patterning depends on stomatal geometry	65
3.2.2	Light-induced gas exchange responses	74
3.2.3	Stomatal clustering influences light-induced gas exchange response	89
3.2.4	Stomatal clustering results in altered ion transport	94
3.3	Discussion	104

3.3.1	Clustering type differs between experimental and natural populations _____	105
3.3.2	Spacing between stomata is essential for plant physiology _____	106
3.3.3	Alterations to guard cell ion transport is associated with the impaired movements of stomata in clusters ____	108
3.3.4	Outlook _____	111
4	STOMATAL CLUSTERING INFLUENCES CONDITIONAL GROWTH PHENOTYPES _____	112
4.1	Introduction _____	112
4.2	Results _____	114
4.2.1	Stomatal clustering affects plant growth _____	114
4.2.2	Stomatal clustering promotes resilience to severe drought stress _____	120
4.2.3	Stomatal patterning mutants affected in root architecture _____	127
4.3	Discussion _____	132
4.3.1	Does stomatal clustering hinder plants growth under growth-favourable conditions? _____	132
4.3.2	Evidence on drought resilience due to stomatal clustering? _____	134
4.3.3	Does stomatal patterning restrain root system architecture? _____	137
4.3.4	Outlook _____	140
5	H₂S REGULATES STOMATAL MOVEMENTS VIA A NOVEL PATHWAY _____	141
5.1	Introduction _____	141
5.2	Results _____	145
5.2.1	Stomatal clustering prevents H ₂ S-induced stomatal closure _____	145
5.2.2	H ₂ S-induced stomatal closure is linked to inhibition of inward-rectifying K ⁺ channels _____	148
5.2.3	H ₂ S acts via ABA-independent pathway _____	153
5.2.4	H ₂ S effect is partially dependent on intracellular Ca ²⁺ rises _____	156
5.2.5	H ₂ S does not influence the activity of anion channels _____	158
5.2.6	Changes in intracellular Ca ²⁺ and pH mediate H ₂ S response _____	160
5.3	Discussion _____	170
5.3.1	Evidence on stomatal closure? _____	170

5.3.2	H ₂ S-induced stomatal closure via modulation of ion channels? _____	172
5.3.3	H ₂ S a new branch of the guard cell signalling? _____	174
5.3.4	Outlook _____	177
6	GENERAL DISCUSSION _____	178
6.1	Summary _____	178
6.2	Stomatal clustering in <i>Arabidopsis</i> and <i>Begonia</i> _____	180
6.3	Stomatal clustering influences plant growth _____	182
6.4	Stomatal clustering entails changes in stomatal movements via altered ion transport _____	184
6.5	H ₂ S a novel effector of stomatal behaviour _____	188
	REFERENCES _____	191
	APPENDIX I _____	I
	APPENDIX II _____	V

List of Figures

Chapter 1

Figure 1. Developmental pathway of stomata _____	4
Figure 2. Type of stomatal clusters _____	4
Figure 3. Model showing the specific interactions between EPF signalling peptides and LRR/LRRKs that promote stomatal development and spacing _____	8
Figure 4. Schematic representation of genes involved in stomatal production and spacing. _____	10
Figure 5. Schematic representation of major environmental factors and their influence on guard cells and leaf tissue. _____	12
Figure 6. Schematic representation of the major ion channels and pumps residing at the plasma membrane. _____	24
Figure 7. Diversity of leaf shape across <i>Begonia</i> species. _____	29
Figure 8. Characteristic leaf shape of sections Gireoudia and Pritzelia _____	30
Figure 9. Characteristics of <i>B. coccinea</i> from Gireoudia section and <i>B. plebeja</i> from Pritzelia section. _____	31
Figure 10. Distribution of <i>B. coccinea</i> and <i>B. plebeja</i> species. ____	32

Chapter 2

Figure 1. LI6400 XT basic principle of operation _____	45
Figure 2. FDA staining of living cells _____	50
Figure 3. Schematic representation of two-electrode voltage circuit _____	52
Figure 4. Images of the equipment used to perform electrophysiological studies _____	53
Figure 5. Double-barrelled microelectrodes pulled for <i>N. tabacum</i> (top) and <i>A. thaliana</i> (bottom) guard cells _____	54

Chapter 3

Figure 1. <i>TMM1</i> transcript level in <i>Arabidopsis</i> lines _____	66
Figure 2. Representative micrographs of epidermal peels from the abaxial side of <i>Arabidopsis</i> and <i>Begonia</i> leaves _____	68

Figure 3. Quantification of stomatal patterning of epidermal peels from <i>Arabidopsis</i> and <i>Begonia</i> plants _____	70
Figure 4. Stomatal clustering inhibits stomatal opening in <i>Arabidopsis tmm1</i> mutant _____	72
Figure 5. Relationship between maximum stomatal conductance to water vapour and stomatal pattern of <i>Arabidopsis</i> and <i>Begonia</i> plants _____	73
Figure 6. Effect of photosynthetic active radiation on CO ₂ assimilation _____	75
Figure 7. Time-series of gas exchange responses from <i>Arabidopsis</i> plants _____	77
Figure 8. Time-series of gas exchange responses from <i>Begonia</i> plants _____	88
Figure 9. Half-times of gas exchange responses triggered by light or darkness _____	85
Figure 10. Steady-state rates of gas exchange responses triggered by light or darkness _____	87
Figure 11. Water use efficiency of <i>Arabidopsis</i> and <i>Begonia</i> plants under three light regimes _____	88
Figure 12. Stomatal patterning affects the gas exchange responses _____	91
Figure 13. Stomatal clustering suppresses stomatal conductance _____	93
Figure 14. Stomatal clustering inhibits closure of in <i>Arabidopsis tmm1</i> mutant _____	95
Figure 15. Stomatal clustering inhibits closure of in <i>Arabidopsis tmm1</i> mutant independently of the availability of ions in the apoplast _____	95
Figure 16. Stomatal clustering alters currents carried by outward- and inward-rectifying K ⁺ channels _____	99
Figure 17. Stomatal clustering suppresses I _{KOUT} _____	100
Figure 18. Transcript level of major plasma membrane transport genes in <i>Arabidopsis</i> lines _____	101
Figure 19. Tail current analysis for K _{OUT} channels from single and clustered stomata _____	103

Chapter 4

Figure 1. Phenotype of <i>A. thaliana</i> stomatal patterning mutants under four distinct light and humidity regimes _____	117
---	-----

Figure 2. Quantification of the biomass of <i>A. thaliana</i> stomatal patterning mutants under four distinct light and humidity regimes	118
Figure 3. Quantification of sensitivity of <i>A. thaliana</i> stomatal patterning mutants to short-term drought stress	122
Figure 4. Effects of long-term drought stress on <i>A. thaliana</i> stomatal patterning mutants	124
Figure 5. Quantification of sensitivity of <i>A. thaliana</i> stomatal patterning mutants to long-term drought stress	125
Figure 6. Osmotic content of <i>A. thaliana</i> stomatal patterning mutants	126
Figure 7. Effects of sucrose starvation on <i>A. thaliana</i> stomatal patterning mutants	130
Figure 8. Quantification of sensitivity of <i>A. thaliana</i> stomata mutants to sucrose starvation	131

Chapter 5

Figure 1. Simplified schematic diagram of the ABA signalling pathway	142
Figure 2. Hydrogen sulfide is involved in ABA-dependent stomatal closure in <i>Vicia faba</i>	144
Figure 3. H ₂ S triggers stomatal closure in a dose-dependent manner	146
Figure 4. Stomatal clustering inhibits H ₂ S-induced stomatal closure	147
Figure 5. H ₂ S selectively inactivates currents from inward-rectifying K ⁺ channels in <i>N. tabacum</i>	149
Figure 6. Activation half times of currents from inward-rectifying K ⁺ channels	150
Figure 7. Sensitivity of conductance of inward-rectifying K ⁺ channels to H ₂ S	151
Figure 8. H ₂ S affects currents from inward-rectifying K ⁺ channels in a dose-dependent manner	153
Figure 9. H ₂ S effect on stomata is independent of the ABA pathway	155
Figure 10. H ₂ S inactivates currents from inward-rectifying K ⁺ channels in Ca ²⁺ - independent manner	157

Figure 11. H ₂ S does not stimulate anion channels _____	159
Figure 12. Quantitative modelling reproducing H ₂ S effect on stomatal opening and closure _____	162
Figure 13. Quantitative modelling reproducing H ₂ S effect on K ⁺ ions in guard cells _____	164
Figure 14. Quantitative modelling reproducing H ₂ S effect on Cl ⁻ ions in guard cells _____	165
Figure 15. Quantitative modelling predicting changes in pH due to H ₂ S-induced changes in ion channels _____	168
Figure 16. Quantitative modelling predicting changes in intracellular Ca ²⁺ due to H ₂ S-induced changes in ion channels _____	169

Chapter 6

Figure 1. Stomatal clustering impacts plant physiology and growth via changes in ion transport and ionic exchange _____	187
Figure 2. H ₂ S induces stomatal closure via altering ion transport at the guard cell plasma membrane _____	189

APPENDIX I

Figure 1. Quantitative modelling predicting changes in the fluxes through the K ⁺ and Cl ⁻ channels at the plasma membrane _____	I
Figure 2. Quantitative modelling predicting changes in Ca ²⁺ fluxes at the plasma membrane and tonoplast _____	II
Figure 3. Quantitative modelling predicting changes in Ca ²⁺ fluxes at the plasma membrane and tonoplast _____	III
Figure 4. Quantitative modelling predicting changes in the membrane potential at the plasma membrane and tonoplast _____	IV

List of Tables

Chapter 2

Table 1. List of solutions and media used _____	37
Table 2. List of primers for qPCR _____	38
Table 3. <i>Begonia</i> growth medium _____	39
Table 4. Microelectrode-filling and bathing solutions _____	55
Table 5. Standard PCR master mix _____	58
Table 6. Cycling conditions of standard PCR _____	59
Table 7. qPCR reaction mix _____	60
Table 8. Cycling conditions for qPCR _____	60

Chapter 3

Table 1. Gas exchange data from <i>Arabidopsis</i> and <i>Begonia</i> plants under three different light regimes were fitted to non-linear regression models to extrapolate the kinetics for CO ₂ assimilation response, transpiration under light and transpiration under darkness _____	82
Table 2. Maximum water use efficiency from <i>Arabidopsis</i> and <i>Begonia</i> plants under three different light regimes _____	88
Table 3. Gating parameters of I _{KOUT} and I _{KIN} _____	100

Chapter 4

Table 1. Water use efficiency (μmol CO ₂ per mmol H ₂ O) of <i>Arabidopsis</i> under four light and humidity regimes _____	119
--	-----

Chapter 5

Table 1. Gating characteristics of conductance of inward-rectifying K ⁺ channels _____	152
---	-----

List of Equations

Equation 1. Nernst equation _____	11
Equation 2. Percentage of water content _____	41
Equation 3. Exponential rise _____	47
Equation 4. Exponential decay _____	47
Equation 5. Sigmoidal function _____	47
Equation 6. Anatomical stomatal conductance to water vapour ____	49
Equation 7. Boltzmann function _____	56
Equation 8. Modified Boltzmann function to measure G_{KIN} _____	150

Acknowledgments

I would like to thank my two supervisors Prof. Mike Blatt and Prof. Anna Amtmann, whose guidance and advice added considerably to this project.

Especially, I am deeply grateful to Prof. Mike Blatt for having always an open door for me and willing to discuss any of my questions. But mostly, I am grateful for your encouragement to produce this piece of work and overcoming any difficulties. You really pushed me to be a better scientist!

Also, I thank all the past and present members of Stevenson lab -, Giorgio Perella, Rucha Karnik, YiZhou Wang, Naomi Donald, George Boswell, Fabian Kellermeier, Emily Larson, Carla Minguet, Cecile Lefoulon, Ben Zhang, Mary-Ann Madsen and Sakharam Waghmare for the relaxing times during working and for our fruitful discussions. Special thanks to:

Dr. Carlos Garcia-Mata for letting me work on the hydrogen sulfide story.

Amparo Ruiz-Prado, whose help to harvest and growth the plants, was tremendous.

My “stoma” buddy, Dr. Cornelia Eisenach, for all of our discussions about general science and particular experimental matters, be it in the lab or the pub.

My dear Annegret, Dr. Annegret Honsbein, for being there every time for me to listen my crazy thoughts. Also, I thank you for being critical reading my thesis.

I would like to thank my family and all my friends for their support and belief on me.

Of course, McIntyre Begonia trust for funding my PhD.

Finally, I thank you Aris for always be next to me throughout the good and difficult times, and for keeping remind me that is

the journey that makes it interesting, not the arrival...!

Author's Declaration

I declare that, except where explicit reference is made to the contribution of others, that this dissertation is the result of my own work and has not been submitted for any other degree at the University of Glasgow or any other institution.

Maria Papanatsiou

Abbreviations

A	Photosynthetic assimilation
ABA	Abscisic acid
ABI1 / 2	ABA insensitive 1 / 2
AHA	Arabidopsis H ⁺ -ATPase
AKT1	Arabidopsis K ⁺ transporter 1
ALMT	Al ³⁺ -activated malate transporter
a _{max}	Maximum stomatal aperture
AP2C3	ARABDOPSIS PROTEIN PHOSPHATASE 2C
BCA	β-carbonic anhydrases
cADPR	Cyclic adenosine 5'-diphosphoribose
CBS	Cystathionine β synthetase
CSE	Cystathionine γ lyase
CO	Carbon monoxide
COP1	<i>CONSTITUTIVE PHOTOMORPHOGENESIS 1</i>
CRY1 / 2	Cryptochrome 1 / 2
DES	L-Cys-desulhydrase
E	Transpiration
EPF	EPIDERMAL PATTERNING FACTOR
EPFL	EPIDERMAL PATTERNING FACTOR -LIKE
ER	ERECTA
ERL1 / 2	ERECTA-LIKE 1 / 2
FDA	Fluorescein diacetate
FLP	FOUR LIPS
G _s	Stomatal conductance
G _{wmax}	Anatomical conductance to water
G _{KIN}	Conductance of inward-rectifying K ⁺ channels
GORK	Guard cell K ⁺ outward rectifier
GTL1	GT2-like 1
H ₂ S	Hydrogen sulfide

HIC	<i>HIGH CARBON DIOXIDE</i>
HT	Hypotaurine
IRGA	Infrared gas analysis
KAT1 /2	K ⁺ transporter of Arabidopsis thaliana 1 / 2
KC1	K ⁺ rectifying channel 1
KCS	3-ketoacyl CoA synthase
K_{IN}	K ⁺ - inward
K_{OUT}	K ⁺ - outward
LOV	Light, voltage, oxygen
LR	Lateral root
LRD2	lateral root development 2
LRR	Leucine-rich repeat
LRR-RLKs	Leucine-rich repeat- like kinases
MAPK	Mitogen-activated protein kinases
MRP5	Multidrug-resistance protein 5
NO	Nitric oxide
NR	Nitrate reductase
OST1	Open stomata 1
PAR	Photosynthetic active radiation
P_e	Turgor of epidermal cells
P_g	Turgor of guard cells
Phyt	Phytochrome
PHOTO1 /2	Phototropin 1 /2
PP2A / C	Phosphatase protein 2 A / C
PYR1	Pyrabactin resistance 1
RALF	Rapid alkanisation factor
ROS	Reactive oxygen species
SCRM / 2	SCREAM/2
SDD1	STOMATAL DENSITY AND DISTRIBUTION 1
SKOR	Stellar K ⁺ outward rectifier

SLAC1	Slow anion channel 1
SLAH3	SLAC1 homologue 3
SNAP	S-nitroso-N-acetyl- penicillamine
SNP	Sodium nitroprusside
SnRK	Snf1- related protein kinase
SPCH	SPEECHLESS
SUR	Sulphonylurea 1
TEVC	two-electrode voltage clamp
TMM	TWO MANY MOUTH
TPK1	Two- pore K ⁺ channel 1
TUB9	TUBULIN 9
UVR8	UV RESISTANCE LOCUS 8
VCL	Vacuolar chloride channel
VPD	Vapour pressure deficit
V_m	Membrane voltage
YDA	YODA
WUE	Water use efficiency
Ψ_{leaf}	Leaf water potential

1 Introduction

Stomata are pores found on the epidermis of most aerial parts of plants and are formed by a specialized pair of cells, the guard cells. Stomata facilitate the uptake of CO₂ at the expense of water vapour release via transpiration (Hetherington & Woodward 2003). Transpiration allows leaf cooling and nutrient translocation from roots to shoots via the xylem (Cramer et al. 2009). Hence, stomata optimize the trade-off between transpirational water loss and carbon gain and therefore the water use efficiency (WUE), which is generally described as the amount of dry matter produced per unit of water transpired through stomata. In line with mathematical models, it is suggested that in recent years increases in the continental run-off as well as changes in the freshwater resources are partly the result of transpiration, and it has been argued that stomatal transpiration will be one of the major factors affecting water availability in the next 20-30 years (UNESCO World Water Assessment Program 2003). This together with the increasing demand of water for agricultural purposes puts pressure on scientists and breeders for adapting crops with higher WUE that will result in higher yields with less water usage.

Regulation of gas exchange is achieved by controlling the stomatal pore size, which dynamically responds to environmental changes including light quality and intensity, ambient CO₂ concentration and humidity (Aphalo & Jarvis 1991; Hetherington & Woodward 2003; Shimazaki et al. 2007) (see section 1.2). The stomatal aperture is regulated by osmotically-driven movements of the stomatal guard cells. Stomatal movements are the result of changes in guard cell volume and turgor that in turn depend on solute fluxes into and out of the guard cells. Fluxes of osmotically active molecules, like K⁺ and Cl⁻, are facilitated by transport proteins residing at the plasma membrane. For instance, the activation of the voltage-dependent inward-rectifying K⁺ channels predominantly accounts for stomatal opening, while stomatal closing depends on the activity of the outward-rectifying K⁺ channels and anion channels (Schroeder et al. 1984; Blatt 1991; Roelfsema et al. 2012) (see section 1.4). Osmotic solute accumulation drives the influx of water causing a rise in the turgor pressure, which results in

the swelling of guard cells and eventually the opening of the pore, whereas the opposite is observed during the closing process (Blatt 2000; Roelfsema & Hedrich 2005). Additionally, opening of stomata requires the overcoming of the hydraulic limitation exerted by epidermal cells before they reach a fully open state (Meidner 1990). Plants rely on endogenous molecules that affect stomatal movements by directly or indirectly regulating ion channels. ABA has been in the focus of research and is described as the hub of many stimuli inducing stomatal closure. Recently an additional small signalling gas molecule, hydrogen sulfide (H₂S), has been reported to trigger stomatal closing response via an ABA-dependent pathway (García-Mata & Lamattina 2010) (see section 1.3).

Apart from the environmental factors and their mediators, stomatal patterning also influences the plant physiology. The majority of plant species follow the “one-cell spacing rule” that implies the separation of stomata by at least one epidermal cell (Peterson et al. 2010; Pillitteri & Dong 2013) (see section 1.2). However, there are several genera that diverge from this rule such as the *Begonia* genus (Nebauer, 1967). Stomatal clustering in *Begonia* has been considered to be an adaptation to niches requiring higher evaporative demand (Hoover 1986; Tang et al. 2002) (see sections 1.1 & 1.5). Even so, no quantitative data are available confirming an advantage of “clustered” species to grow on dry environments. Several reports have established a relationship between high stomatal density and photosynthesis, while plants with less numerous stomata displayed lower transpirational water loss (Yoo et al. 2010; Doheny-Adams et al. 2012; Tanaka et al. 2013). Both these aspects resulted in higher WUE and place stomatal patterning as a key factor for manipulation of gas exchange according to the environmental conditions (Lawson & Blatt 2014). Given the special arrangement of stomata in stomatal clusters, it was of my interest to examine the mechanisms driving their stomatal movements as well as whether the lack of neighbouring cells between stomata influenced the growth and physiology of the plant but also the guard cell physiology. In fact, this study challenges a long-standing notion of the importance of adjacent neighbouring cells to facilitate ion fluxes across the plasma membrane of guard cells.

1.1 *Stomatal development and patterning*

Plants have developed a sophisticated program for proper stomatal development, which ensures the survival and fitness of plants in adverse environmental conditions. This developmental program includes a range of transcription factors, peptide ligands, cell-surface receptors, mitogen-activated protein kinases (MAPK), proteinases and other molecular players that make up a complex regulatory network dependent on both internal and environmental signals (Casson & Gray 2008; Pillitteri & Dong 2013). A stoma is produced from an undifferentiated epidermal cell, the protodermal cell, which undergoes a series of cell-state transitions to eventually form two guard cells and the stoma. Figure 1 illustrates the successive stages contributing to stomatal development. The protodermal cell firstly differentiates into meristemoid mother cell, a process that still remains obscure. The meristemoid mother cell divides asymmetrically to produce two cells, the sister cell and the meristemoid. The former can undergo up to three amplifying divisions that will increase the number of epidermal cells and also provide ground for more stomata formation. The meristemoid cell differentiates into guard mother cell that symmetrically divides into two guard cells, which ultimately produce the stoma (Geisler et al. 2000; Peterson et al. 2010). This pathway makes up the above mentioned “one cell spacing rule” that ensures each stoma is separated from each other by at least one epidermal cell (Pillitteri & Dong 2013).

Nevertheless, as stated above there are few species that show stomata in clusters, such as species from the genus *Begonia* (see section 1.5). Cluster formation is a deviation from the “one cell spacing rule” and is of interest for its physiological consequences, but the steps leading to it are not confirmed. It has been suggested that the only difference, in comparison with the single stomata, occurs at the first division step (Peterson et al. 2010). In particular, the MMC instead of undergoing an asymmetric division, it divides symmetrically to produce two meristemoid mother cells, which subsequently will follow the same series of steps as in single stomata development to yield a stomatal cluster. Stomatal clusters can be classified as non-contiguous and contiguous clusters (Figure 2). The latter describes stomata being in contact with each other while

in the non-contiguous clusters the stomata are separated by small cells, called subsidiary cells (Gan et al. 2010).

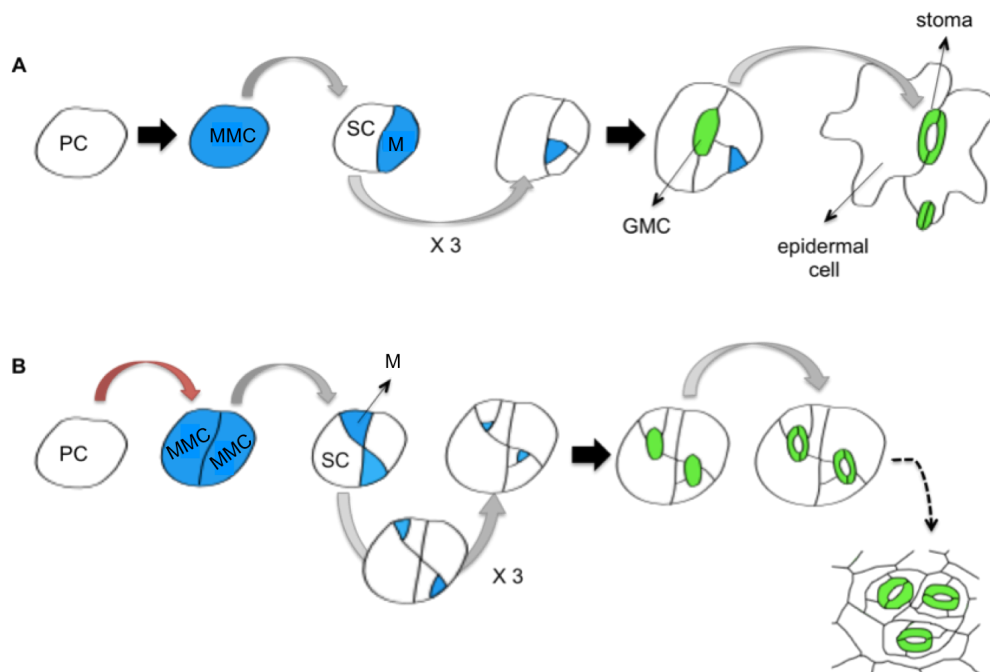


Figure 1. Developmental pathway of stomata.

Developmental pathway of single stomata (A) and stomatal clusters (B). A Protodermal cell undergoes a series of cell-state transitions (black arrows) and cell divisions (grey arrows) to yield a stoma. The protodermal cell differentiates into a meristemoid mother cell (MMC) that symmetrically divides to produce a sister and meristemoid (M) cell. The sister cell can amplify up to three times whereas the meristemoid cell differentiates into a guard mother cell. The latter divides symmetrically to produce two guard cells and thereby form the stoma. In the case of stomatal clusters, the protodermal cell undergoes a symmetric division (red arrow) and then follows same pathway as single stomata. Adapted and redrawn from Peterson et al. (2010).

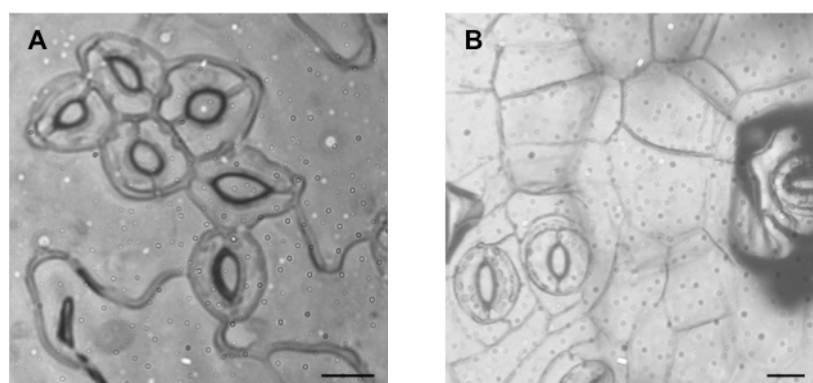


Figure 2. Type of stomatal clusters.

Non-contiguous clusters (A) found in *Begonia* species, where stomata are separated by subsidiary cells (asterisk). Contiguous clusters (B) found in *Arabidopsis tmm* mutant. Scale bar = 10 μm

1.1.1 Genes regulating stomatal initiation and production

There are five basic helix-loop-helix genes, encoding for transcription factors, that regulate stomatal-lineage initiation; these are the gene products of *SPEECHLESS (SPCH)*, *MUTE*, *FAMA*, *SCREAM (SCRM)* and *SCREAM 2 (SCRM2)* (Ohashi-Ito & Bergmann 2006; MacAlister et al. 2007; Pillitteri et al. 2007; Lampard et al. 2008; Kanaoka et al. 2008). *SPCH* is expressed in MMCs and promotes entry to stomatal lineage. Loss-of-function mutations in *SPCH* result in a no stomata epidermis (MacAlister et al. 2007). *MUTE* is required to terminate the stomatal-lineage entry divisions and is only present in meristemoid cells. Mutants in the *MUTE* gene do not show any stomata in the epidermis but the number of meristemoid cells is increased (Pillitteri et al. 2007). *FAMA* inhibits guard mother cell differentiation in order to promote guard cell formation. Mutations in the *FAMA* gene result in more guard mother cell divisions, producing elongated guard mother cell-like cells that lie in parallel with each other. Finally, *SCRM* and *SCRM2* act throughout the stomatal lineage and coordinate the *SPCH*, *MUTE* and *FAMA* activities via heterodimerisation. The single *scrm* mutant and double *scrm/scrm2* mutant showed similar phenotypes to *fama* and *spch*, respectively. However, the *scrm-D*, a gain-of-function mutation, was found to result in an epidermis solely made of stomata (Kanaoka et al. 2008). *SCRM*, also known as *ICE1*, is considered to assist on the integration of environmental signals to stomatal development because it is associated with cold tolerance phenotype (Kanaoka et al. 2008). The MYB transcription factors, *FOUR LIPS (FLP)* and *MYB88*, additionally regulate stomatal-lineage by acting in parallel with *FAMA* to promote GC transition (Yang & Sack 1995).

1.1.2 Genes regulating spacing pattern

Stomata are commonly found to follow the “one cell spacing rule”. Several genes encoding for leucine-rich repeat receptor (LRR) proteins, cysteine-rich secreted peptides and MAPK components act to ensure this spacing pattern. Four genes belonging to the *EPIDERMAL PATTERNING FACTOR (EPF)* and *EPIDERMAL PATTERNING FACTOR-LIKE (EPFL)* family have been shown to regulate stomatal spacing. *EPF1*, *EPF2*, *EPFL9/STOMAGEN* and *EPFL6/CHAL* encode for cysteine-

rich secreted peptides having six to eight cysteines at the carboxyl-terminal (Torii 2012). *EPF1* is expressed in guard mother cells and guard cells and is thought to provide positional information for spacing divisions in sister cells, since *epf1* mutants showed stomatal clusters (Hara et al. 2007). On the other hand, *EPF2* is secreted in the early-stage stomatal precursor cells where it prevents entry to stomatal-lineage. Its absence produces leaf epidermis with many small arrested epidermal cells and increased stomatal number (Hunt & Gray 2009). The double mutant *epf1/epf2* showed an additive phenotype with high stomatal density, modest stomatal cluster formation and arrested epidermal cells (Doheny-Adams et al. 2012). The functions of *EPF1* and *EPF2* are not interchangeable and both act in leaf epidermis. In contrast, *EPFL9/STOMAGEN* and *EPFL6/CHAL* are involved in stomatal development by mediating signalling between epidermis and internal tissue. *EPFL9/STOMAGEN* is expressed in mesophyll cells and is implicated in coordination of stomatal production with photosynthetic demand. RNAi knockdown lines of *EPFL9/STOMAGEN* resulted in a reduced number of stomata whereas its ectopic expression produced numerous stomata and stomatal clusters (Kondo et al. 2010). *EPFL6/CHAL* is expressed in internal tissues of stems and it is suggested to be a negative regulator of stomatal production acting through association with *ERECTA* proteins (Abrash & Bergmann 2010).

The LRR-like kinases (LRR-RLKs) include the *ERECTA (ER)*, *ERECTA-LIKE1* and *ERECTA-LIKE2 (ERL1* and *ERL2)* that have 20 continuous LRRs and a cytoplasmic-threonine kinase domain. The LRR-RLKs are redundant and therefore null mutations to each of them result in subtle phenotypes, whereas the triple mutation *er/erl1/erl2* produced an excessive stomatal clustering phenotype (Torii et al. 1996; Shpak et al. 2005). They have distinct expression patterns and therefore act at different developmental stages. *ER* inhibits stomatal-lineage entry while *ERL1* regulates the orientation of meristemoid cells in a manner to exclude guard cell differentiation in adjacent cells. The role of *ERL2* is still unclear (Shpak et al. 2005).

LRR-RLKs function in combination with another LRR protein, the *TOO MANY MOUTHS (TMM)* gene product. *TMM* possess 10 continuous LRRs with no kinase domain and it is expressed throughout the stomatal-lineage up to guard mother

cell stage (Nadeau & Sack 2002). Mutants in the *TMM* gene showed stomatal clusters and ectopic meristemoid cells in leaf epidermis, while no stomata were found in hypocotyls and stems (Yang & Sack 1995; Geisler et al. 1998; Geisler et al. 2000). This contrasting phenotype is context-specific and probably depends on the association of *TMM* with other receptors and available ligands. Although the role of *TMM* is still ambiguous, it appears to be actively involved in signal transduction, either through interaction with LRRs or alternatively through titration of signals/receptors which therefore prevent associations between EPFs and LRRs (Abrash & Bergmann 2010; Lee et al. 2012a). What is clear is that the formation of stomata involves a tissue-specific mix-and-match process where different combinations of ligands and receptors ensure the proper spacing of stomata and therefore their proper function. Genetic and biochemical studies have shown that LRRs act as primary receptors for binding EPFs. Specifically, EPF1 binds to ERL1 and EPF2 binds to ER. The *TMM* protein is a modulator of both pairs and likely functions through heterodimerisation with LRRs (Lee et al. 2012b). Figure 3 shows the *in vivo* associations between LRR/LRRs and EPFs resulting in wild type and *tmm1* mutant stomatal phenotype.

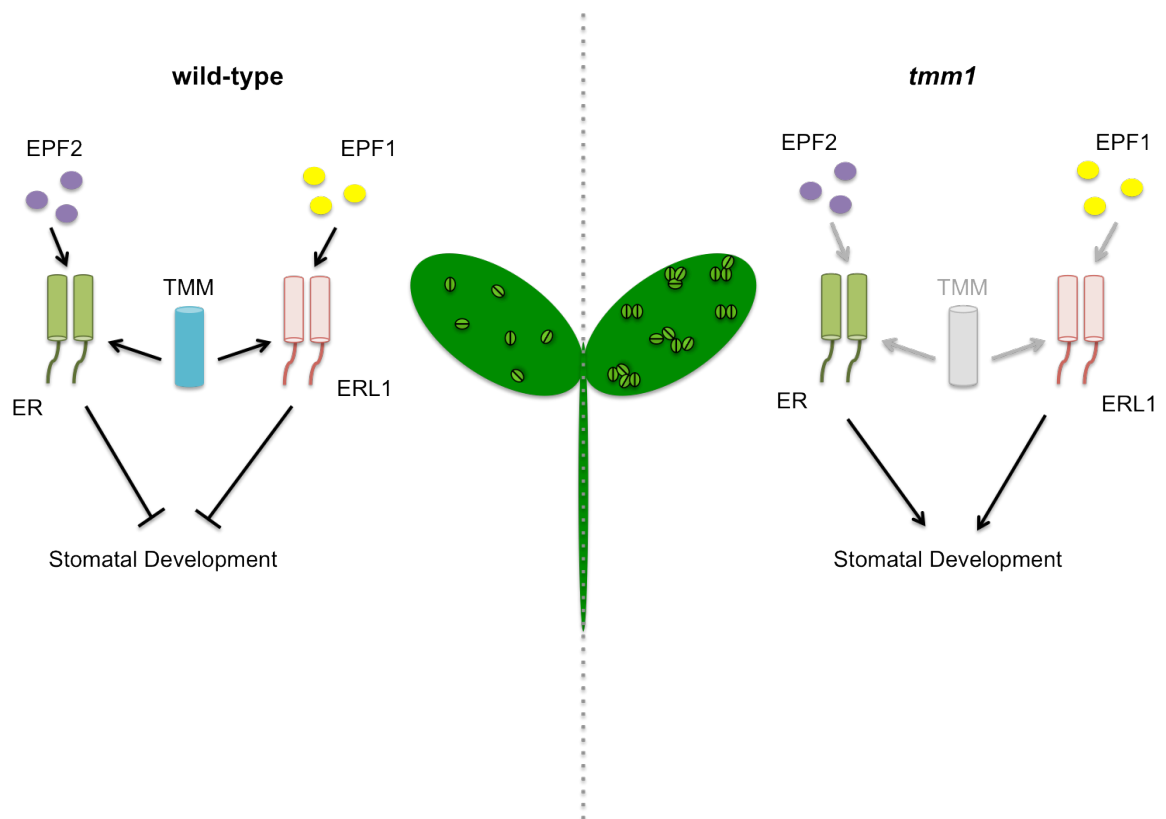


Figure 3. Model showing the specific interactions between EPF signalling peptides and LRR/LRRKs that promote stomatal development and spacing.

EPF2 binds to ER whereas EPF1 binds to ERL1. Presence of TMM enables these bindings and inhibits stomatal development by titrating the signals and/or receptors to ensure proper patterning, as it occurs in the wild type context (left side). Mutation in *TMM* gene affects inhibition of stomatal development resulting in stomatal cluster formation (right side). Adapted and redrawn from Abrash et al. (2011)

Signal transduction from these associations occurs via a MAPK pathway, including the MAPKKK YODA (*YDA*), MKK4/5, MKK7/9 and MPK3/6 proteins. The MAPK proteins are involved in many plant processes but in the stomatal context they promote pavement cell differentiation and inhibition of stomatal-lineage entry (Pillitteri & Dong 2013). Overexpression of *YDA* and *MKK4/5* resulted in an epidermis made solely by pavement cells, while clustering phenotypes were observed in the null mutants (Bergmann et al. 2004). Stomatal clusters were also observed in plants overexpressing *MKK7/9*, and together with transcriptomic evidence it is suggested that the *MKK7/9* gene is involved in guard mother cell differentiation (Lampard et al. 2009). The described phenotypes of MAPKs resemble that of the *spch* mutant implying that the genes act upstream of *SPCH*. *SPCH* contains a MAPK domain that is shown to be a phosphorylation target for MPK3/6, which in turn leads to the suppression of *SPCH* activity (Lampard et al.

2008). Regulation of MAPK activity depends on the ARABDOPSIS PROTEIN PHOSPHATASE 2C 3 (AP2C3). *AP2C3* is specifically expressed in the late stomatal lineage and its null mutation produced a leaf epidermis with numerous stomata. Co-localization studies showed that AP2C3 is localized to the nucleus, where MPK3/6 is also found, implying its direct effect on MPK3/6 (Umbrasaite et al. 2010).

A summary of the major genes and their roles discussed above is illustrated in Figure 4. *SPCH*, *MUTE* and *FAMA* are master gene regulators of stomatal development and are expressed in meristemoid cells, guard mother cells and guard cells, respectively. All of them are associated with *SCREAM/SCREAM2* via heterodimerisation to promote stomatal differentiation. Additionally, the transcription factors, *FLP* and *MYB88*, act in the guard cells to also regulate stomatal formation. Although the mechanism through which *MUTE* and *FAMA* act remains unclear, more information is available on *SPCH*. Activation of *SPCH* and thus stomatal-lineage entry involves a set of MPKKK proteins (Bergmann et al. 2004). In particular, *MPK3/6* phosphorylates *SPCH* and inhibits its activity, whereas *AP2C3* suppresses *MPK3/6* activity and therefore regulates initiation of the stomatal developmental pathway. *MPK3/6* activity depends on three additional MPKKK proteins, the *MKK4/5*, *MKK7/9* and *YDA* (Wang et al. 2007). The latter potentially transduces an upstream signal from EPF-LRR/LRRK associations that govern stomatal spacing divisions. EPFs are expressed in specific cell stages to inhibit adjacent cells from acquiring stomatal fate. *EPF1* is expressed in guard mother cells and guard cells and interacts with *ERL1*, while *EPF2* is expressed in meristemoid cells and associates with *ER*. *TMM* is a modulator of these interactions and inhibits stomatal development ensuring proper stomatal patterning. Recently it was shown that *SPCH* binds and activates upstream genes including *EPF2*, *TMM* and *ER* creating a positive feedback loop to ensure proper spacing (Lau et al. 2014). Finally, it is proposed that another EPF protein, *EPFL9/STOMAGEN*, is involved in signal transduction between mesophyll and epidermis to promote stomatal formation (Sugano et al. 2010), albeit via a mechanism that is still unclear.

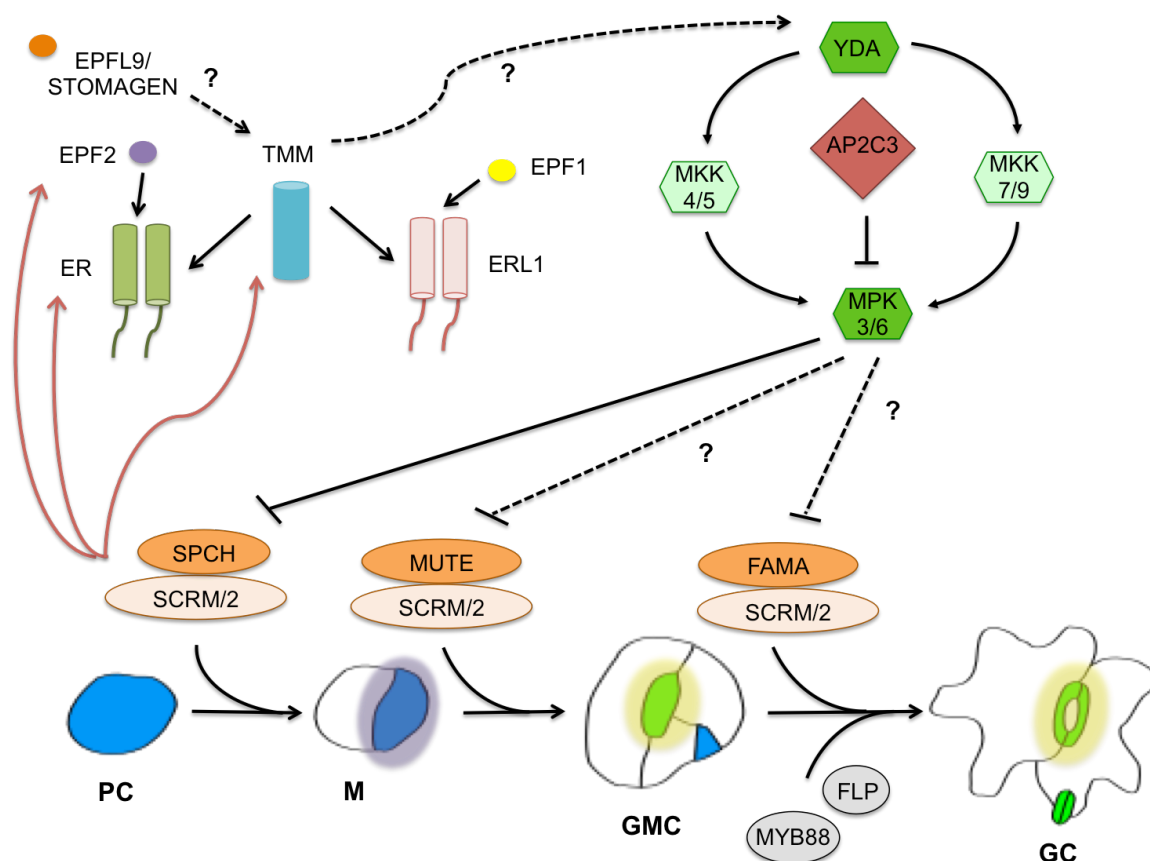


Figure 4. Schematic representation of genes involved in stomatal production and spacing.

SPCH, MUTE and FAMA are expressed in meristemoid cells, guard mother cells and guard cells, respectively. Their association with SCRM/2 via heterodimerisation promotes stomatal differentiation. Transcription factors, FLP and MYB88, act specifically in guard cells to also regulate stomatal formation. Activation of SPCH involves a set of MPKKK proteins. MPK3/6 inhibits SPCH via phosphorylation, whereas AP2C3 suppresses MPK3/6 activity ensuring entry to stomatal lineage. MPK3/6 activity depends on MKK4/5, MKK7/9 and YDA, with the latter potentially transducing a signal from EPF-LRR/LRRK associations. EPFs are expressed in specific cell stages inhibiting adjacent cells from acquiring stomatal fate. EPF1 (yellow) is expressed in guard mother cells and guard cells and interacts with ERL1, while EPF2 (purple) is expressed in meristemoid cells and associates with ER. TMM is a modulator of these interactions and inhibits stomatal development ensuring proper stomatal patterning. The EPFL9/STOMAGEN is involved in signal transduction between mesophyll and epidermis to promote stomatal formation via a still unclear mechanism. Finally, the positive feedback loop of *SPCH* activating the upstream genes *EPF2*, *TMM* and *ER* is shown (red arrows). Adapted and redrawn from Pillitteri & Dong (2013).

1.2 Stomata and the environment

Given their sessile nature, plants have to adapt to the environmental conditions in order to promote their growth and reproduction. Similarly stomata are highly influenced by their surroundings, both in their development and subsequent physiological functioning. Indeed, changes in both stomatal pattern and aperture depend on environmental factors, plant hormones and other signalling compounds. Such changes can be described as rapid or long-standing based on the nature of the environmental stimulus and the coupled response. For instance, stomata can rapidly respond to changing light and humidity throughout the day to balance the trade-off between CO₂ and water loss (Roelfsema & Hedrich 2005). However, long-term differences in environmental conditions, like CO₂ enrichment or growth in shade, result in alterations to stomatal patterning through the process of leaf growth and expansion (Woodward et al. 2002; Coupe et al. 2006; Casson & Gray 2008). Environmental factors affect stomatal behavior directly by altering guard cell water relations and metabolism, but also act via an indirect manner, when water relations of other tissues and mesophyll photosynthesis are altered and influence guard cells. Stomatal behaviour ascribes a complex network of interrelated environmental signalling components rather than a stand-alone stimulus-specific process (Hetherington & Woodward 2003). Stomata show high plasticity and so loss of one signalling component is usually compensated through the remaining components of the network. Figure 5 displays a schematic representation of the major environmental signals influencing stomata and their mode of action. In natural environments stomata must respond to the combined effects of environmental signals, however, for the purpose of better-understanding I here describe the major environmental factors and their signalling components separately.

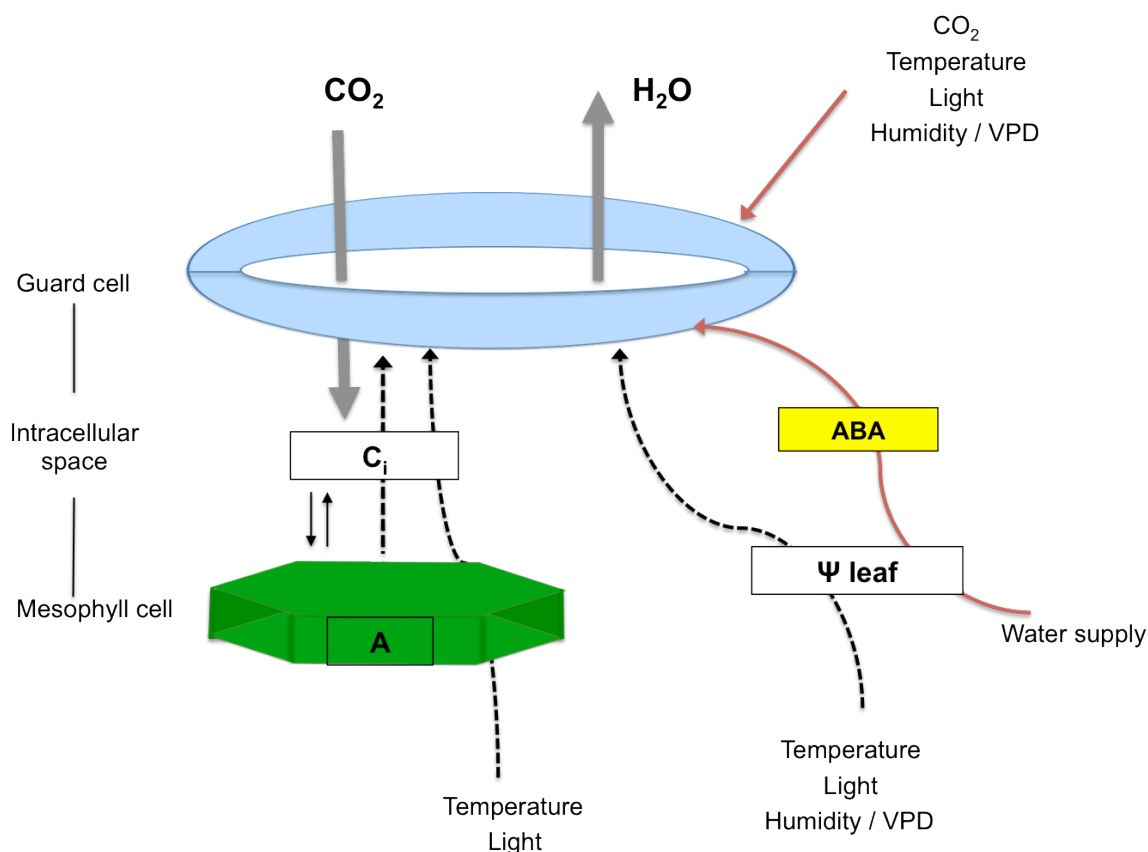


Figure 5. Schematic representation of major environmental factors and their influence on guard cells and leaf tissue.

Cartoon depicts a simplified situation of how stomatal behaviour and gas exchange are influenced by CO_2 , light, temperature, humidity and water supply. From top to bottom are shown the guard cells, intracellular space and mesophyll tissue. Black dashed lines show the indirect effects on stomatal behaviour, while solid red lines show the direct ones. CO_2 influx (grey downward arrow) alters internal CO_2 (C_i), which enables mesophyll photosynthetic assimilation (A). A negative feedback loop between A and C_i results in stomatal movements (left side, black dashed arrow). Temperature and light also indirectly affect stomatal behaviour through the same route. Additionally, temperature, light, humidity and vapour pressure deficit indirectly influence stomatal movements by changing leaf water potential (Ψ_{leaf} ; right side, black dashed arrow). A drop in Ψ_{leaf} brought by water deprivation potentiates stomatal movements via abscisic acid (ABA; yellow box), which directly acts on the guard cell process inducing stomatal closure. CO_2 , temperature, light and humidity can also directly affect the guard cell process via metabolic and ion transport processes occurring in guard cells. Adapted and redrawn from (Willmer 1988).

1.2.1 Light

Plants respond to a broad range of radiation including visible, ultraviolet (UV) and infrared wavelengths of light. In general, stomata from C3 and C4 plants open in response to light and close in response to darkness, with opening being a slower process than closing. Stomata also respond to the quantity of light. Studies of gaseous exchange of various species have shown that increasing light radiation provokes higher photosynthetic CO₂ fixation and stomatal conductance (Wilmer & Fricker, 1996).

At equal fluence rates, light of different wavelengths results in substantially different stomatal responses. Blue light induces stomatal opening by directly affecting the guard cells, since both guard cell protoplasts and stomata in epidermal strips respond to it. Blue light causes proton extrusion to the apoplast via electrogenic pumping by H⁺-ATPases (Shimazaki et al. 2007). This activation in turn hyperpolarizes the plasma membrane and leads to the activation of voltage-gated inward-rectifying K⁺-channels (K_{IN}) and therefore to K⁺ and other solute uptake that are required for stomatal opening (Hedrich & Schroeder 1989; Blatt 1991). Activation of H⁺-ATPase depends on the binding of 14-3-3 proteins (Shimazaki et al. 2007). These proteins also bind phototropins prior to binding the H⁺-ATPase at the plasma membrane, but their exact role in blue light induced stomatal opening remains unclear (Sullivan et al. 2009). There are two identified phototropins, phot1 and phot2, which contains two light, oxygen, voltage (LOV) domains at the N-terminus and a Ser/Thr kinase domain at the C-terminus. The presence of the Ser residues enables autophosphorylation upon blue light excitation and the subsequent binding of 14-3-3 proteins (Christie 2007). LOV domains are the binding sites for flavin mononucleotides responsible for absorption at blue light wavelengths. phot1 and phot2 act redundantly because single mutations respond normally to blue light while the double mutant *phot1 phot2* did not show blue light-induced stomatal opening. These phototropins also mediate phototropism, chloroplast and leaf movements to optimize photosynthesis by enhancing light capture (Briggs & Christie 2002; Christie 2007).

Red light influences stomatal response in both direct and indirect ways via the guard and mesophyll cells, respectively. Although guard cells contain

chloroplasts with limited electron transport and photophosphorylation activity, the ATP and NADH generated by this light can drive K^+ uptake and partly sugar accumulation resulting in stomatal opening, as in the case of blue light (Wilmer & Fricker, 1996; Shimazaki et al. 2007). For instance, achlorophyllous guard cells from the orchid *Paphiopedilum harrisianum* did not show red light response in isolated epidermal peels (Zeiger et al. 1983). In contrast, mesophyll cells are highly abundant in chlorophyll-containing chloroplasts, which absorb both in blue and red light, albeit the absorption efficiency is smaller in blue light. In this case, red light acts as energy source promoting photosynthetic carbon assimilation and therefore a reduction in intracellular CO_2 , which in turn is sensed by stomata and triggers their opening (Shimazaki et al. 2007).

Both blue and red light exhibit synergistic effects on stomatal responses. Weak blue light pulses resulted in stomatal opening only under a red light background (Assmann 1988). When *Arabidopsis* plants were placed under high red light intensity, photosynthesis rose sharply to reach a steady state after 20 minutes, whereas stomatal conductance showed a gradual increase. Superimposing blue light of weak intensity to these plants resulted in a new steady-state stomatal conductance in 10 minutes, implying that stomatal opening in blue light can be up to 20 times faster than in red light (Shimazaki et al. 2007). Also, stomatal conductance under the influence of white light (blue + red) is higher than the sum of the conductance at separated lights, suggesting an interaction between the different light qualities (Wilmer & Fricker, 1996).

There is also evidence for the influence of light in stomatal development, with increasing density of quantum flux resulting in greater stomatal index (Casson & Gray 2008; Pillitteri & Torii 2012). Several light signalling-related mutants have been found to be defective in stomatal patterning. For example, the double mutant of *CRYPTOCHROME 1* and *2* (*cry1 cry2*) as well as the single *PHYTOCHROME* (*phy*) mutants, *phyA* and *phyB*, exhibited lower stomatal density in blue and far-red light, respectively. By contrast, mutation in the *CONSTITUTIVE PHOTOMORPHOGENESIS 1* (*COP1*) gene, which acts downstream in the *CRY* signalling pathway, resulted in stomatal clustering in both light and dark conditions, an opposite phenotype of the *cry1 cry2* double mutant (Pillitteri & Torii 2012). Coupe et al. (2006) showed that light intensity alters stomatal

patterning via long-distance signalling by using cuvette systems. Simultaneous shading of mature leaves and illumination of developing leaves resulted in lower stomatal index, reduced photosynthetic capacity and sugar levels as well as altered genetic expression in the developing leaves (Coupe et al. 2006).

1.2.2 Carbon dioxide

CO₂ levels have a significant impact on both stomatal development and function. Stomatal aperture shows an inverse relationship with increasing CO₂ concentration. Nevertheless, great changes in atmospheric CO₂ levels are not found in natural habitats, except in the dense canopies during night (Wilmer & Fricker, 1996). The mechanism underlying coordination of CO₂ perception and stomatal development is not well understood, but several genes have been found to potentially link these two processes. Mutations in β-carbonic anhydrase (BCA) genes *CA1* and *CA4* resulted in the impairment of both stomatal function and patterning (Hu et al. 2010; Engineer et al. 2014). The BCAs are expressed in both mesophyll and guard cells and catalyse the conversion of CO₂ into H⁺ and HCO₃⁻. Although blue light- and ABA- induced stomatal movement was observed in the *ca1/ca4* double mutant, stomata did not respond to elevated CO₂ and showed higher stomatal conductance and density under ambient CO₂. Additionally, guard cell-targeted expression of BCA compensated for the stomatal phenotype inferring a potential role of BCAs in CO₂ signalling and stomatal development (Hu et al. 2010).

Geological and laboratory evidence from various species indicates that stomata density is reduced with increasing concentration of CO₂ (Woodward & Kelly 1995; Doheny-Adams et al. 2012). Integration of altered CO₂ levels in stomatal development depends on long-distance signalling, similar to what is observed under light. Mature leaves grown inside cuvettes with an elevated CO₂ concentration caused a reduction of the stomatal index in developing leaves grown under ambient CO₂ conditions, while in reciprocal experiment the stomatal index of developing leaves was enhanced (Lake et al. 2001). Gray et al. (2000) reported the involvement of *HIGH CARBON DIOXIDE (HIC)* gene in the regulation of stomatal pattern with respect to CO₂ conditions. The authors

proposed that *HIC* acts in a dominant-negative or gene-dosage manner, because both *hic/hic* and *hic/+* plants showed an increase in stomatal index under high CO₂. *HIC* encodes for a putative 3-ketoacyl CoA synthase (KCS), which has a role in wax biosynthesis (Gray et al. 2000). Additional mutants defective in the production of wax polymers showed altered stomatal indices, implying an important role of cuticular wax profile in permeability to water and gas as well as other signalling compounds (Casson & Gray 2008; Pillitteri & Torii 2012).

1.2.3 Water status

Water status depends on water uptake from the soil and water loss from guard cells via transpiration. Leaf water potential (Ψ_{leaf}) is largely influenced by these two processes, and thereby any factor like humidity, temperature and wind that affects them will alter Ψ_{leaf} . It is proposed that use of the term leaf-to-air water vapour pressure deficit (VPD) is more appropriate to describe effects of humidity and temperature on stomatal behaviour (Aphalo & Jarvis 1991). Processes enabling stomatal movements in response to changes in VPD are defined as hydropassive or hydroactive (Franks 2013; McAdam & Brodribb 2014).

Water deficit triggers passive stomatal closing due to reduction in Ψ_{leaf} . When species-specific Ψ_{leaf} levels are reached, stomatal aperture gradually starts closing, followed by a more rapid closure as Ψ_{leaf} further decreases (Wilmer & Fricker, 1996). McAdam & Brodribb have argued that lycophytes and ferns depend solely on passive mechanisms and especially in the decline of guard cell turgor as the Ψ_{leaf} is suppressed, since guard cells are not in immediate contact with epidermal cells (McAdam & Brodribb 2014). These authors also argued that in species in which hydraulic coupling between epidermal and guard cells occurs, stomata must overcome the “mechanical advantage” exerted by epidermal cells to reduce their pore diameter. The term “mechanical advantage” describes the property of epidermal cells to initially impede stomatal movements according to the given stimuli, since changes in epidermal cell turgor antagonize those of guard cells (Meidner 1990; Wilmer & Fricker, 1996; Mott et al. 1999; Franks & Farquhar 2007). In angiosperms, this restriction must be overcome by the means of active control of stomatal closing that implies the osmotic adjustment of

guard cells via the activation of ion transport system. In particular, during stomatal closing this active mechanism is mostly mediated by augmented levels of ABA (Franks 2013), a drought stress-related hormone that influences major ion channels residing at the plasma membrane and the tonoplast (see section 1.3.1). In recent studies, McAdam & Brodribb (2014) also reported that ABA-induced stomatal closure in the coniferous *Metasequoia glyptostroboides* occurred only after 6 hours of water deprivation, suggesting that stomatal function regarding water supply is also dependent on phylogeny.

Regarding the stomatal development, there are few reports of altered stomatal patterning brought by water availability and/or presence of ABA (Quarrie & Jones 1977; Davies 1978; Franks & Farquhar 2001). Additionally, atmospheric humidity has been shown to alter stomatal patterning in *Arabidopsis* and particularly produce stomatal clusters, though it is not known if this is a direct effect (Pillitteri & Torii 2012).

1.2.4 Temperature

Although temperature is an important parameter influencing plant physiology and fitness, little is known about its effect on stomatal behaviour and development. The consensus holds that a rise in temperature results in higher metabolic activity of the guard cells and upon reaching an optimum stomatal opening is triggered (Wilmer and Fricker, 1996). Yet different species reach maximum stomatal opening at different temperatures. For example, stomatal opening of *Vicia faba* was reached a maximum at 35 °C, whereas stomata from leaves of *Polypodium vulgare* open at 28 °C (Wilmer and Fricker, 1996). An indication of how temperature can indirectly control stomatal movements is illustrated by the “midday stomatal closure” (Tenhunen et al. 1984; Hirasawa & Hsiao 1999). The term depicts the phenomenon where stomatal aperture and conductance decrease during the middle of the day when evaporative demand is high. It is suggested that this is an adaptive strategy of plants to retain water loss especially in dry and hot conditions, as observed from studies with several Mediterranean perennial species (Lösch et al. 1978; Tenhunen et al. 1984). Few reports suggest that midday stomatal closure is a CO₂ response rather than a

water-related effect. In particular increasing temperature enhances respiration and photorespiration that eventually overpass photosynthesis and thereby promote internal CO₂ build-up, which in turn causes stomata closing (Wilmer & Fricker, 1996). The temperature effect on stomatal behaviour remains highly obscure, while there is no information on its effects on stomatal development.

1.3 Stomata and other signalling compounds

It is well-established that stomatal behaviour is highly influenced by hormones and other endogenous signals. In addition, the potential use of compounds to manipulate the stomatal behaviour and therefore increase water use efficiency (WUE) has led to the hunt for new signalling compounds affecting stomatal movements. In this section, I briefly discuss the effects of ABA and nitric oxide (NO) on stomata as well as the limited information available on a novel signalling molecule, the gaseous compound hydrogen sulfide (H₂S).

1.3.1 Abscisic acid

Among the various phytohormones, ABA is the most well-investigated regarding stomatal behaviour and is reported to affect diverse processes in plants, such as seed germination, shoot growth, gene transcription and pathogen tolerance (Cutler et al. 2010). Here I only focus on the hydroactive control of ABA over stomatal behaviour. ABA triggers stomatal closing when applied via the transpiration stream, exogenously to leaves or even to epidermal peels, and it is considered to be the signal mediating plant responses to water stress (Blatt & Thiel 1993; Wilmer & Fricker, 1996; Roelfsema & Hedrich 2005; Lee & Luan 2012). ABA is found in most tissues of higher plants, but its synthesis is often restricted to specific tissues and little, if any, is synthesized in guard cells. Normally, upon water deprivation ABA is synthesized in roots and it is reallocated via xylem to shoots (Wilkinson & Davies 2002). Because ABA is a weak acid, its modulation and distribution among different plant tissues as well as cell compartments is highly influenced by the pH of the environment (Wilmer & Fricker, 1996).

Generally, it is thought that ABA travels through both apoplast and symplast, but only the former results in ABA accumulation in guard cells (Wilkinson & Davies 2002). Although the mechanism through which ABA is recognized by the guard cells is still obscure, studies have shown that proteins with such putative ABA-binding domains include members of the PYR/PYL/RCAR family (Park et al. 2009; Nishimura et al. 2010). Pyrabactin resistance 1 (PYR1) bound pyrabactin, an ABA agonist, but *pyr1* mutants did not show any ABA-related phenotype suggesting that additional interaction partners might be involved (Park et al. 2009; Cutler et al. 2010). In fact, interaction and structural studies showed that PYR/PYL/RCAR proteins bind ABA in a conserve helix that is flanked by two β -loops; these loops create a gate securing the binding site (Melcher et al. 2009). ABA binding to PYR/PYL/RCAR protein results in structural conformation and gate closing, which in turn creates an interaction surface for the type 2 C protein phosphatase (PP2C) (Melcher et al. 2009; Cutler et al. 2010). In *Arabidopsis*, the *ABA-INSENSITIVE 1* and 2 (*ABI-1* and *ABI-2*) genes have been shown to encode for PP2C proteins involved in ABA signalling (Leung et al. 1997; Gosti et al. 1999). Mutations in these genes reversed the ABA-inhibited seed germination, root growth and stomatal function. The ABA signalling cascade involves the binding of ABA to PYR/PYL/RCAR receptors as well as the stabilization of this interaction by the additional binding of ABI1 to the complex. This prevents ABI1 from inhibiting downstream targets. Such targets include proteins from the Snf1- related protein kinase (SnRK2) family, for instance, the *Arabidopsis* OST1 protein (Vlad et al. 2009). OST1 promotes changes in several intermediates including H_2O_2 and cytosolic calcium, that induce stomatal closure via regulation of ion channels (Mustilli et al. 2002; Siegel et al. 2009; Vlad et al. 2009; Kim et al. 2010;).

ABA-mediated elevations in cytosolic-free calcium ($[Ca^{2+}]_i$) resulted in enhanced stomatal closure as shown in experiments with increased extracellular Ca^{2+} concentration and in studies using Ca^{2+} -reporter dyes (Schroeder & Hagiwara 1989; Blatt 1990; Hedrich et al. 1990; Blatt & Armstrong 1993; Blatt & Thiel 1993; Roelfsema & Hedrich 2005). This ABA-induced rise of $[Ca^{2+}]_i$ relies on the activation of plasma membrane Ca^{2+} channels as well as Ca^{2+} channels residing in intracellular compartments (Grabov & Blatt 1998; MacRobbie 1998; Grabov & Blatt 1999). Plasma membrane ion channels are also modulated by ABA, in both

Ca^{2+} -independent and Ca^{2+} -dependent manner. In particular, ABA induces anion efflux by activating anion channels that lead to a depolarization of plasma membrane (Roelfsema & Hedrich 2005). The latter is further amplified by the suppression of H^+ -ATPase by ABA and the combined depolarization effect will result in activation of K^+ -outward (K_{OUT}) channels. ABA causes elevation of pH by 0.2 units and that further modulates K^+ -outward (K_{OUT}) channels by potentiating the K^+ efflux (Blatt 1990; Blatt & Armstrong 1993). The consequent steps described here are simplified as ABA acts via additional mediators like reactive oxygen species.

1.3.2 Nitric oxide

Like ABA, NO has been shown to trigger stomatal closing as well as reduction in transpiration rate and photosynthesis (Willmer & Fricker, 1996). NO is a small water- and lipid-soluble gaseous free radical involved in many plant processes such as programmed cell death, protection against biotic agents and drought. The beneficial action of NO depends on the levels found in cell tissues or compartments. For example, high levels of NO inhibit growth of tomato seedlings, whereas low levels of NO promote growth of lettuce and pea plants (Neill et al. 2003). NO synthesis in plants is tissue-specific and involves nitric-synthases (NOS), nitric reductases (NR) and non-enzymatic processes via a redox- or pH-dependent manner (Neill et al. 2002; García-Mata & Lamattina 2003; Guo et al. 2003; Neill et al. 2003). In the context of stomata, NO causes reduction of stomatal apertures via an ABA-dependent manner (Neill et al. 2002). Garcia-Mata et al. (2003) showed that NO-induced stomatal closure in *V. faba* was dependent on the Ca^{2+} release from internal stores that caused the activation of K_{IN} and anion. The rise in cytosolic Ca^{2+} ($[\text{Ca}^{2+}]_{\text{cyt}}$) involves the action of cyclic adenosine 5' -diphosphoribose (cADPR) that activates the ryanodine-sensitive Ca^{2+} channels found at the plasma membrane. Using blocking agents for these Ca^{2+} channels, the authors showed no inhibition of K_{OUT} channels and concluded that NO only effects K_{IN} and Cl^- channels. Thus, NO action only constitutes a part of the ABA-signalling pathway that causes stomatal closure through the modulation of the endomembrane Ca^{2+} channels.

1.3.3 Hydrogen sulfide

In recent years, evidence for an additional gaseous second messenger affecting stomata has emerged. H₂S is a bioactive molecule and is highly permeable to membranes. Given its functional similarities to carbon monoxide (CO) and NO, H₂S has been regarded as the third gasotransmitter (Wang 2002). H₂S is generated from L-cysteine via the action of two enzymes, cystathionine γ lyase (CSE) and cystathionine β synthetase (CBS). Both enzymes also catalyse the condensation reaction of homocysteine to cysteine in order to generate H₂S. Mammalian CSE and CBS are expressed in many tissues, including the liver, brain and kidney, and inhibition of these enzymes results in altered H₂S production in different tissues (Wang 2002; Kimura 2011). Expression and activity of CSE is augmented by treatment with the NO donors, S-nitroso-N-acetylpenicillamine (SNAP) or sodium nitroprusside (SNP) (Kimura 2011). H₂S synthesis also occurs via non-enzymatic processes and so it can be dependent on redox reactions and the acidity of pH of the environment (Peers et al. 2012). H₂S is a well-known player in multiple mammalian processes like cardioprotection, neuromodulation and apoptosis. Although the list of possible molecular targets is growing, a major group consists of ion channels. In mammals, H₂S has been shown to modulate ATP-sensitive K⁺, Ca²⁺-activated K⁺, K⁺ and Cl⁻ channels (Peers et al. 2012). A suggested mode of action for modulation of these ion channels is via sulphydration, which entails the addition of an extra sulfur in the cysteine thiol groups of proteins (Mustafa et al. 2009).

In plants, cysteine is a precursor for a number of essential biomolecules containing sulfur moieties, including the antioxidant glutathione. However, the thiol groups of these molecules are easily oxidized to produce molecules with sulfur of higher oxidative state that in turn inhibit several enzymes. Hence, the pool of cysteine has to be balanced and this process involves the desulphydration of L- and D-cysteines to produce H₂S, pyruvate and ammonia in a 1:1:1 ratio. The enzyme responsible for this reaction are the L-Cys-desulphydrase (DES) (Alvarez et al. 2010). Additionally, H₂S is synthesized by D-Cys-desulphydrases that catalyze D-Cysteine degradation (Riemenschneider et al. 2005), and by desulphydrases that degrade cysteine in order to provide sulfur for the assembly of

iron-sulfur clusters required in several proteins of mitochondria, chloroplasts and cytosol (Li & Lancaster 2013). H₂S production in plants was considered to be a defence response against pathogens, because higher activity of DES was observed with fungal infection (Bloem et al. 2004; Bloem et al. 2007). More recent studies implicate H₂S in tolerance mechanisms against drought, osmotic and heavy metal stress, through the regulation of reactive oxygen species (ROS) scavenging systems as well as lipoxygenases (Zhang et al. 2010a; Zhang et al. 2010b; Zhang et al. 2010c).

H₂S has been shown to affect stomata, though the available data provide conflicting evidence. Treatment of epidermal peels of *Capsicum annuum* leaves with NaHS or GYY 4137, two H₂S donors, resulted in stomatal opening in the light and reduction of stomatal closure in darkness (Lisjak et al. 2010; Lisjak et al. 2011). García-Mata & Lamattina (2010) reported stomatal closure when epidermal peels of *V. faba* and *Impatiens walleriana* leaves were treated with NaHS. H₂S-induced stomatal closing was partially dependent on ABA, because epidermal peels pre-treated with hypotaurine (HT), a H₂S scavenger, exhibited a reduction in ABA-mediated closure in comparison to the treatment with ABA alone (García-Mata & Lamattina 2010). In addition, the authors carried out experiments using glibenclamide, which inhibits the multidrug-resistance protein AtMRP5. AtMR5, a homologue of the mammalian sulphonylurea 1 (SUR1), belongs to the ATP-binding cassette (ABC) transporter family and is known to control a number of ion channels (Gaedeke et al. 2001). For example, in mammals, K_{ATP} channels are formed by four pore-forming K_{IN} subunits and four SUR receptors (Peers et al. 2012). Pharmacological data indicated that NaHS-induced stomatal closure was blocked by glibenclamide, suggesting that H₂S might act via regulation of SURs or other ion channels residing at the plasma membrane of guard cells (García-Mata & Lamattina 2010).

1.4 Stomatal movements depend on plasma membrane ion transport

Stomatal movements depend on the turgor of guard cells that, in turn, depends on the fluxes of osmotically active solutes in and out of the guard cells. Transport of such molecules is fundamental to stomatal behaviour and requires the function of ion pumps, H⁺-coupled transporters and ion channels. The primary solutes comprise K⁺, Cl⁻ and the organic solutes malate and sucrose.

Ion fluxes across the membrane and through ion channel proteins require an electrochemical driving force, which is influenced by the membrane potential (V_m; also referred to as membrane voltage). V_m is the difference of the electrical potential between the inside and the outside of the plasma membrane; and it depends on the combined activity of ion pumps and channels to maintain different charges between the two sides of the membrane. V_m is highly dependent on the equilibrium potential of a given ion (E_x) that is defined by the Nernst equation (Eq. 1):

$$E_x = \frac{RT}{zF} \ln \frac{[X]_{out}}{[X]_{in}} \quad \text{Eq. 1,}$$

where [X]_{out} and [X]_{in} are the concentration of ion X outside and inside of the cell, respectively. R is the gas constant (8.314 J K⁻¹ mol⁻¹), T is the absolute temperature in Kelvin, z is the charge of the ion X and F is the Faraday constant (9.648 x 10⁴ C mol⁻¹).

It is known that V_m has a direct effect on a group of ion channels, termed voltage-gated channels, and regulates ion permeation through them, a process known as “gating”. Gating simply refers to the opening (activation) and closing (inactivation) of the channel pore. The voltage range over which ion channels are gated is an intrinsic feature of each channel (Hille, 2001). Figure 6 illustrates the major ion channels residing at the plasma membrane. In the following sections, I review only the plasma membrane K⁺ and anion channels and their importance on stomatal movements. Note, however, that stomatal function

depends equally on the activities of ion channels and pumps at endomembranes, the tonoplast. Therefore, the major tonoplast transporters are also briefly introduced.

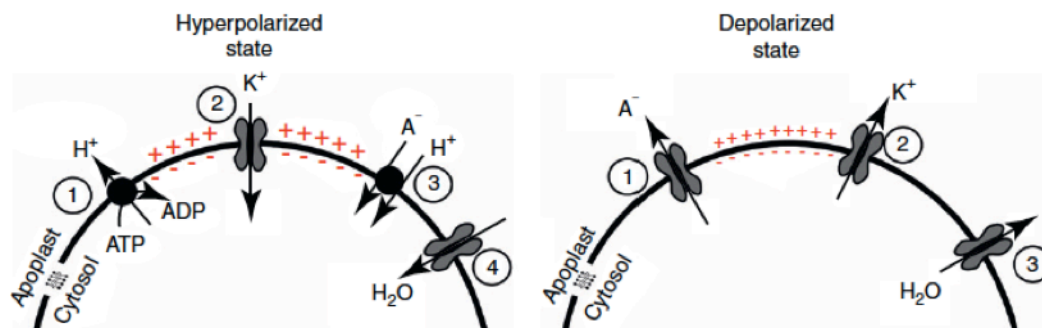


Figure 6. Schematic representation of the major ion channels and pumps residing at the plasma membrane.

Changes in membrane potential drive ion and accompanied water fluxes into and out of the cell. The left side represents the hyperpolarized state that results in opening of stomata. Hyperpolarization is driven by H⁺-ATPase that create an electrochemical gradient through the extrusion of protons. This in turn drives K⁺ and anion uptake through voltage-dependent K⁺ channels and H⁺/anion co-transport proteins. Due to the increased osmotic pressure inside the cell, water follows the same route resulting in opening of stomata. The right side shows the depolarized state that is mainly characterized by the activation of anion channels. Anion efflux further depolarizes the membrane potential that in turn activates the outward-rectifying K⁺ channels. Eventually anion and K⁺ efflux drives water out of the cell and thus facilitates stomatal closing. Adapted and redrawn from (Roelfsema et al. 2012)

1.4.1 K⁺ channels

Potassium is the most abundant cation in plants and is involved in many physiological processes. K⁺ channels have been identified in all plant tissues and every cell type studied so far, including guard cells. As mentioned above, K⁺ has a crucial role in driving stomatal movements. The predominant K⁺ channels found at the plasma membrane of guard cells are of the Shaker type that entails the sensitivity of the K⁺ channels to the membrane potential. These together with the Shaker K⁺ channels of *Drosophila melanogaster* they constitute the K_v⁺ superfamily of K⁺ channels (Pilot et al. 2003). The K_v⁺ channels are formed by four subunits, with each subunit consisting of six transmembrane spanning domains and a loop (P-loop) between the 5th and 6th domain. A consensus amino acid sequence (TXGYG) is located in the P-loop and the four P-loops of the tetramer form the selectivity pore (Dreyer & Blatt 2009) . K⁺ passage across the

plasma membrane mainly relies on the function of two types of K^+ channels distinguished by their voltage dependence: hyperpolarization- and depolarization- activated K^+ channels. The voltage gating of K^+ channels implies that the channel senses the electrical potential across the membrane in order to open or close. Gating in these channels is known to depend on movement of the charged residues found in the 4th transmembrane of each subunit that are displaced by the V_m . This displacement, in turn, causes the structural rearrangement of the channel and therefore its activation or inactivation (Dreyer et al. 2004).

Inward-rectifying K^+ channels

Hyperpolarization-activated channels in guard cells generally open at voltages more negative than -100 mV and function as inward-rectifiers (K_{IN}). As described above, the electric driving force for K_{IN} activation is established by the H^+ -ATPase found at the plasma membrane that pumps H^+ out of the cell and thus creates a negatively-charged environment on the inside (Dreyer et al. 2004). K_{IN} channels show a higher selectivity to K^+ than Na^+ . K_{IN} channels are characterised by their sensitivity to external acidification, external Ca^{2+} concentration, as well as the phosphorylation status of the protein. Extracellular Ca^{2+} , in the millimolar range, modulates K_{IN} channels by triggering the entry of Ca^{2+} . For instance, increasing free cytosolic $[Ca^{2+}]_{cyt}$ from 0.1 to 1.5 μM resulted in reduction of the currents passing through K_{IN} channels (I_{KIN}) and a negative shift to voltage. (Blatt 1991).

The first gene identified to encode a K_{IN} channel was the *Arabidopsis K⁺ transporter 1 (AKT1)* that is highly expressed in roots. Mutation in the *AKT1* gene resulted in the complete abolishment of K_{IN} currents in the roots (Hirsch et al. 1998). Root growth of *akt1* mutants was also reduced when subjected on K^+ deficient media supplemented with ammonium, which inhibits the non-AKT1 K^+ uptake mechanisms (Hirsch et al. 1998; Spalding et al. 1999). Several other inward-rectifiers have been discovered including the K^+ transporter of *Arabidopsis thaliana* 1 (KAT1) and 2 (KAT2) and the regulatory subunit K^+ rectifying channel 1 (KC1). KAT1 activates at approximately -100 mV and

represents the major channel responsible for K^+ uptake in guard cells. Expression of a dominant-negative KAT1 mutant protein resulted in a reduction of stomatal aperture upon light treatment due to impaired K^+ influx into the cell (Kwak et al. 2001). In contrast, KC1 is considered electrically-silent because it does not lead to any K^+ current when expressed heterologously. Yet, loss-of-function mutations in *KC1* gene resulted in a decrease in plant biomass suggesting that its activity is required for normal growth (Honsbein et al. 2009; Jeanguenin et al. 2011). KC1 is a modulator of AKT1 channel gating by shifting its voltage dependence when forming heteromeric complexes (Duby et al. 2008; Honsbein et al. 2009).

Outward-rectifying K^+ channels

K_{OUT} channels constitute the major route for K^+ efflux from the cell, which triggers stomatal closure. K_{OUT} channels are activated upon depolarisation and at more positive voltages than the equilibrium potential for E_K (Blatt 1991; Dreyer et al. 2004; Johansson et al. 2006). In intact guard cells, half-times for K_{OUT} channel activation were increased with higher external K^+ concentration and K_{OUT} channel gating was shifted to more positive voltages, ensuring that it constantly functions as an outward rectifier regardless of K^+ concentration (Blatt 1991). Additionally, K_{OUT} channels exhibit a dependency on intracellular pH (pH_i). Experiments where the cytosol of guard cells was loaded with weak acid butyrate showed a suppression of K_{OUT} channel activity (Blatt & Armstrong 1993).

The first identified outward rectifying K^+ channel was the stelar K^+ outward rectifier (*SKOR*) from *Arabidopsis*. *SKOR* is expressed in root stelar tissues and its knockout mutation resulted in lower K^+ content both in xylem sap and shoots. These data suggested that the *SKOR* channel facilitates the K^+ loading from the roots into the xylem sap, allowing its translocation to the shoots (Gaymard et al. 1998). In guard cells, the only K_{OUT} channel contributing to K^+ efflux and therefore stomatal closure is the guard cell K^+ outward rectifier (*GORK*; Ache et al. 2000). Dominant-negative or null mutations in the *GORK* gene resulted in a reduction or complete abolishment of outward K^+ conductance. Stomatal apertures of *gork* mutants were significantly larger in both dark and light

conditions and physiological experiments showed increased transpirational rates in comparison to wild type plants (Hosy et al. 2003).

Anion channels

As discussed in the previous section, activation of K_{OUT} channels depends on the depolarisation of the plasma membrane - i.e. to voltages positive of E_K . To initiate membrane depolarization in plants, anion channels must open to allow efflux of Cl^- and malate. It is the concerted release of anions and K^+ from the cells that drives the loss of turgor causing stomatal closing. In guard cells, two types of anion channels have been described based on the activation kinetics, the rapid-activating (R-type) and slow-activating (S-type) channels (Roelfsema et al. 2012).

R-type channels do not open at a fixed V_m because they are sensitive to both internal and external anion concentrations and display higher permeability for monovalent anions than divalent anions. However, it is shown that most of them are also largely selective for malate. Meyer et al. (2010) reported that mutation in *aluminum-activated malate transporter 12* (*ALMT12*) resulted in partially impaired R-type anion currents and suppressed dark-induced stomatal closure. Also, expression of *ALMT12* in *Xenopus* oocytes produced R-type anion currents (Meyer et al. 2010). Taking together these findings, the authors suggested that the R-type channels are related to ALMTs with additional unknown factors also contribute to the R-type anion currents.

The *SLOW ANION CHANNEL 1* (*SLAC1*) was the first gene identified to encode for a S-type anion channel residing at plasma membrane (Negi et al. 2008; Vahisalu et al. 2008). Knocking-out this gene resulted in weakened stomatal closure upon treatment with various stomatal closure-inducing stimuli, and in the reduction of S-type anion currents (Vahisalu et al. 2008; Wang et al. 2012). Another member of the S-type channels found at the guard cell plasma membrane is the *SLAC1* homologue 3 (*SLAH3*). In contrast to *SLAC1*, *SLAH3* is more permeable to NO_3^- than Cl^- and requires the presence of NO_3^- in the extracellular space to be activated (Roelfsema et al. 2012). Thus, *SLAC1* and *SLAH3* show a complementary but distinct role in stomatal closure by allowing passage of Cl^-

and NO_3^- , respectively. The S-type channels are also sensitive to organic acids found in the cytosol linking the ion transport with malate metabolism (Wang & Blatt 2011). The authors showed that modulation of anion channels by oxaloacetate, which is an immediate malate metabolite, is coupled with the diurnal changes in the accumulation of malate and therefore the opening and closing of stomata.

Tonoplast K^+ and anion channels

The guard cell vacuole makes up the most of the total volume of the guard cell, which changes during the diurnal cycle due to the fluxes of osmolytes. The majority of the osmolytes is shuttled across the tonoplast into the vacuole during the start of the day, while the reversed is observed during dark period (Blatt 2000; Chen et al. 2012). As in the case of plasma membrane transport, ion channels residing at the tonoplast facilitate fluxes of K^+ and Cl^- from and in the vacuole. In *Arabidopsis*, the two-pore K^+ (TPK) 1 channel largely mediates K^+ flux across tonoplast and in both directions. Mutations in the *TPK1* gene resulted in defective vacuolar K^+ release and slower stomatal closure (Gobert et al. 2007). Moreover, Cl^- fluxes across the tonoplast are partly dependent on the activation of vacuolar chloride (VCL) channel that results from the negative potential of the cytosolic side of the vacuole (Pei et al. 1996). Additional anion transporters of the tonoplast, such as those of *Arabidopsis* Al^{3+} -activated malate family, have been shown to contribute on the ion homeostasis and therefore on the stomatal movements. In particular, the *Arabidopsis altm6* and *almt9* mutants were defective in malate transport across the vacuole that in turn impaired control of stomatal movements (Kovermann et al. 2007; Meyer et al. 2011; De Angeli et al. 2013).

1.5 *Begonia*

Begonia is one of the largest genera of angiosperms consisting of approximately 1600 species and of many more ornamental cultivars (Doorenbos et al. 1998). The *Begonia* genus appears to be monophyletic and together with the monotypic *Hillebrandia sandwicensis* makes up the family *Begoniaceae*. Several synapomorphies distinguish *Begoniaceae* family from other families such as asymmetric leaf shape, succulent petioles and a ring collar of cells between the seed lid and testa cells (Bouman & de Lange, 1983; Doorenbos et al. 1998; Tebbitt, 2005). Most of the *Begonia* species are monoecious perennials, though a few dioecious or annuals species also exist. Begonias show big variation on the whole plant level and their plant habit. Figure 7 presents the range of leaf morphologies found across the genus *Begonia*.



Figure 7. Diversity of leaf shape across *Begonia* species.

In terms of their habit, they can be prostrate, trailing, shrubby or upright, and they can also be bamboo-like, tuberous, rhizomatous or herbaceous. *Begonia* genus exhibits an almost pantropical distribution, except for its complete absence from the Australian tropical forests (Goodall-Copestake et al. 2010). The genus is subdivided into 66 sections, with each section being restricted to a

single continent. For example, section *Gireoudia*, consisting of 66 species, is found exclusively in Central America, while section *Pritzelia* is one of the largest sections with 125 species restricted to eastern Brazil (Doorenbos et al. 1998, Tebbitt, 2005). Morphological and habit variation is lower on members of a section than between different sections. Figure 8 illustrates the leaf shape from members of two sections that will be discussed in this thesis. Most of the species in section *Gireoudia* have palmate leaves while section *Pritzelia* shows higher variation in leaf shape such as ear-like, ovate and palmate.

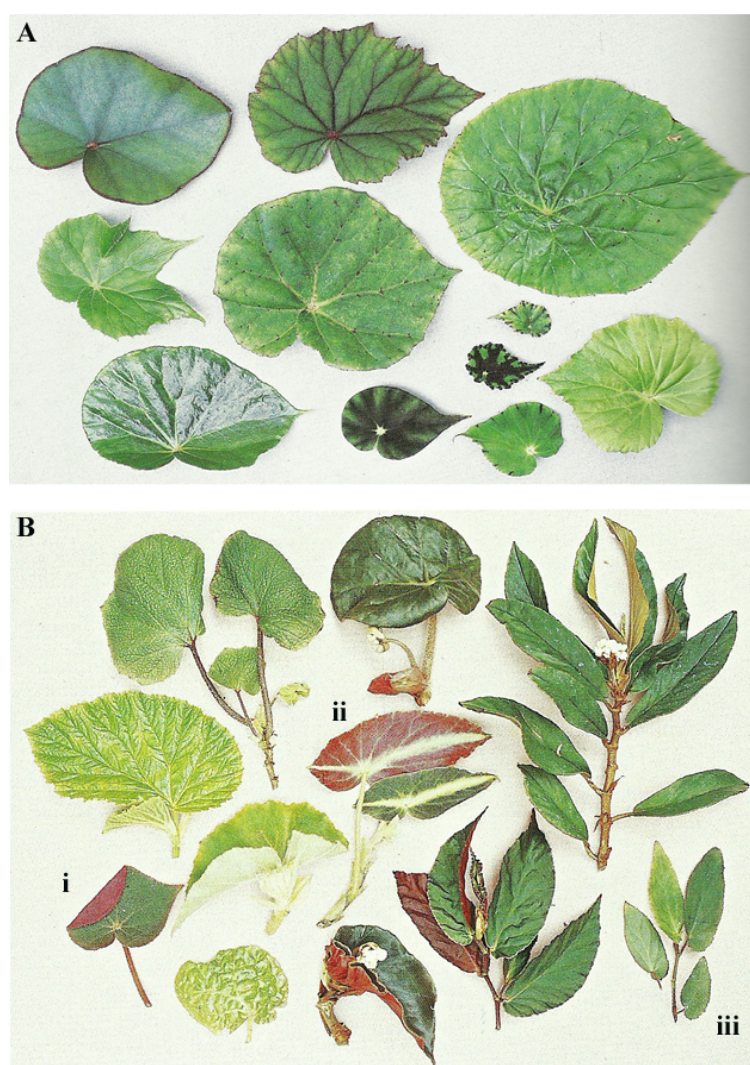


Figure 8. Characteristic leaf shape of sections *Gireoudia* and *Pritzelia*.

Palmate leaves mainly characterize section *Gireoudia* (A), while leaf shape in section *Pritzelia* (B) can be described as palmate (i), ear-like shape (ii) or ovate (iii).

The natural population of plants investigated in this research project consists of two Begonias, *Begonia coccinea* and *Begonia plebeja*, from sections Pritzelia and Gireoudia, respectively. Figure 9 shows the shoot attributes and the plant habit of the two *Begonia* species. *B. coccinea* is a monoecious perennial with a bamboo-like morphology and an upright habit. Its leaves are hairless, have an ear-like shape and its flowers have a dazzling red colour, hence the species name (coccinea= Greek for red). *B. plebeja* is also a monoecious perennial, however, it has a prostrate rhizomatous habit. Its flowers are of white colour and the leaves have the typical palmate shape of section Gireoudia. Particularly, *B. plebeja* posses a characteristic red spot found on the point where petiole joints leaf blade (arrow in Fig 3E)



Figure 9. Characteristics of *B. coccinea* from Gireoudia section and *B. plebeja* from Pritzelia section.

B. coccinea (A-C) and *B. plebeja* (D-F). Flower colour (A,D) and leaf shape (B,E). Arrow on (E) indicates red spot characteristic of *B. plebeja*. Plant habit shown in (C,D). *B. coccinea* has bamboo-like upright habit while *B. plebeja* is prostrate rhizomatous.

Despite the variation in habitat across the sections, each *Begonia* species is located to a very restricted geographical niche (Tebbutt, 2005). For instance, *B. plebeja* is adapted to seasonally deciduous forests of Central America while *B. coccinea* is native to the rainforests of southeast Brazil as shown in Figure 10 (Burt-Utley, 1985). In line with this distribution, the climatic conditions for the two species differ. Mean annual temperature is 19 °C and 23.5 °C where *B. coccinea* and *B. plebeja* grow, respectively. *B. plebeja* encounters more precipitation as the mean annual precipitation is 1945 mm per year while *B. coccinea* faces 1591 mm/year (<http://www.diva-gis.org/>).

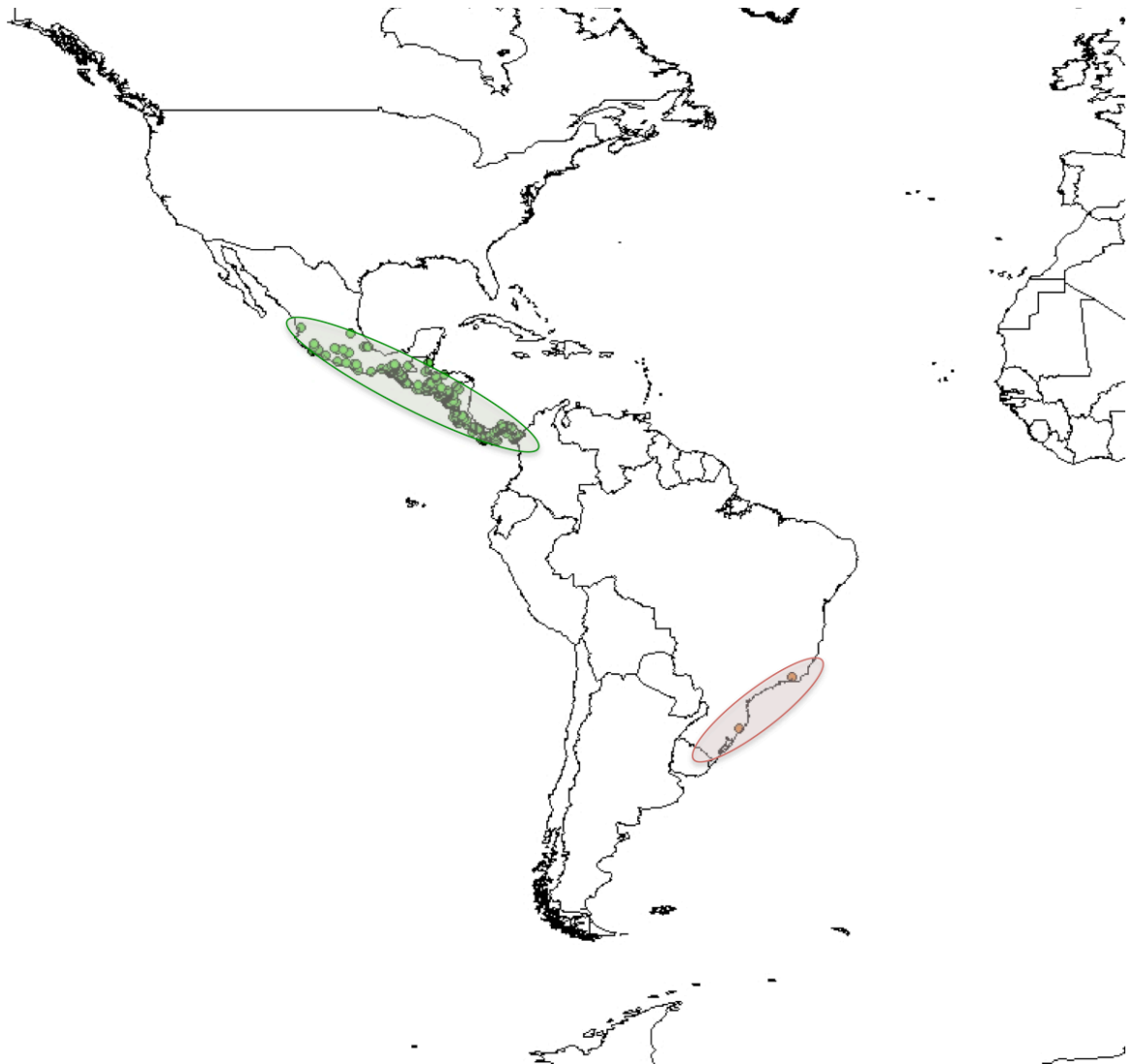


Figure 10. Distribution of *B. coccinea* and *B. plebeja* species.

B. plebeja is found throughout Mexico (green circles) whereas *B. coccinea* is more restricted to eastern coastal Brazil (pink circles).

The endemic distribution of *Begonia* species can be explained in part by the very poor ability of seed dispersal. Most begonias rely on either wind or water run-off as ways to disperse their seeds (Tebbitt, 2005). A number of population genetic studies have confirmed such low rates of gene flow between *Begonia* populations (Hughes et al., 2003; Hughes & Hollingsworth 2008). Additionally, variation in the *Begonia* genus is also apparent on a genomic level. For example, diploid chromosome number can range from $2n=16$ for *B. rex* to $2n=156$ for *B. acutifolia* (Doorenbos et al., 1998). In particular, *B. plebeja* has $2n=28$ and *B. coccinea* has twice this amount with $2n=56$. As expected, molecular-based studies have shown that *Begonia* genotypes from the same section have the same diploid chromosome number while different sections differ in this feature (Dewitte et al. 2009).

Significant differences among the species are also detected on a cellular level. *Begonia* is one of the few genera naturally exhibiting stomatal clusters. However, stomatal clusters do not appear in all *Begonia* species. Nebauer (1967) studied several Begonias and listed the numbers of stomata per cluster, if any, were present. For example, *B. coccinea* has single stomata, whereas *B. plebeja* shows stomata in non-contiguous clusters with an average of two stomata per cluster. Even though a few studies have reported the presence of stomatal clustering in *Begonia* (Nebauer, 1967; Hoover et al., 1986; Tang et al., 2002) and propose its influence on plant adaptation, no quantitative data relevant to the physiology of the leaf and accordingly of the plant are available. However, there is a small piece of evidence inferring that stomatal clustering in *Begonia* is species-specific and dependent on the ecology of the plant, and this might be in relation to the endemic distribution of *Begonia* species. Hoover (1986) described a correlation of stomatal density and stomatal clustering with elevation. *B. heracleifolia* showed higher stomatal density as elevation, i.e. altitude and moisture increased, whereas the opposite was observed in *B. nelumbiifolia*. Stomatal clustering exhibited a parabolic relationship, with cluster number and size decreasing at the extremes of elevation. Also, *Begonia heracleifolia* and *Begonia nelumbiifolia* populations were found to have more stomatal clusters when grown on rocks near waterfalls in comparison with populations grown on well-watered soils (Hoover 1986). Several *Begonias* species show a multilayered epidermis. It is reported that a positive relationship between stomatal clusters and the

number of sub-epidermal layers exists, though this observation was not quantified (Boghdan & Barkley 1972). Both stomatal clustering and a multilayered epidermis is considered as an adaptive trait to grow on water-limited environments such as rocks and low nutrient-containing soils (Boghdan & Barkley 1972; Tang et al. 2002).

1.6 Thesis objectives

The significance of stomata ranges from their impact on water cycles and atmospheric CO₂ composition down to their effect on plant fitness. Stomatal behaviour and its influence by environmental and endogenous signals has been in the focus of plant research for decades. Yet many questions remain to be answered. The main aim of this project was to address the question whether stomatal clustering infers any physicommechanical restrictions onto stomatal behaviour. Furthermore, I was interested in the impact of stomatal clustering onto the cell at the cellular level - i.e. ion transport - and at the macroscopic level - i.e. plant growth and physiology. As mentioned above, *Begonia* species show a natural variation in stomata, with few species exhibiting stomatal clusters. However, several experimental procedures could not be performed in *Begonias* and also the species differ on the genetic background. Therefore, I decided to include on my research the plant model *A. thaliana* to allow the in-depth investigation of the stomata in clusters. For this purpose, I used two *Arabidopsis* mutants showing altered stomatal patterning; the *tmm* mutant has stomata in clusters, while the *epf1/epf2* double mutant shows high stomatal density. I also included two *Begonia* species into my research, *B. coccinea* showing single stomata on the epidermis and *B. plebeja* with stomatal clusters. Hence, the comparison was undertaken on multiple levels - i.e. between *Begonias*, between *Arabidopsis* and between *Begonias* with *Arabidopsis*.

Firstly, I will present quantitative data for two *Begonia* species with regard to their stomatal characteristics. The effect of stomatal clustering in stomatal movements was addressed through studies of stomatal apertures using opening and closing stimuli in both natural (*Begonia*) and experimental (*Arabidopsis*) populations.

To explore if and how stomatal clustering affects the physiology and therefore water use efficiency of the plant, I performed gas exchange measurements in *Arabidopsis* whole plants and in *Begonia* leaves using light and dark treatments to drive opening and closing of stomata, respectively.

In addition, I aimed to address if the stomatal clustering is an adaptive strategy for plants inhabiting challenging environments, like the Begonias. For this purpose, I examined the growth and gas exchange responses of *Arabidopsis* plants exposed to a range of stresses including light, humidity and water. Also, the root system architecture of the *Arabidopsis* stomatal patterning mutants was examined in order to explain the conditional phenotypes observed.

Given the unique spatial arrangement of stomata in clusters, I employed an electrophysiological approach to study ion transport in the *tmm* mutant in order to examine if the major ion channels residing in plasma membrane of the guard cells were impaired. Using a similar approach, the K^+ content of guard cells of single stomata and stomata within clusters was also measured to identify whether stomatal clustering results in differences on the solute accumulation into the guard cells.

If single stomata and stomata in clusters perceive differently gaseous signals was examined, using the novel gasotransmitter hydrogen sulfide. Considering the little information on this novel molecule, I carried out electrophysiological studies to establish the mechanism by which hydrogen sulfide exerts its effect on stomata. Finally, the possibility of hydrogen sulfide being a part of the well-known ABA-signalling pathway was also investigated.

2 Material & Methods

2.1 Materials

2.1.1 Plant material

Two *Begonia* species were used in this project, *B. coccinea* and *B. plebeja*, and were obtained from Glasgow Botanic Gardens. Four *Arabidopsis thaliana* lines were used; Col0, *tmm1*, the *tmm1* complementation (hereafter referred as PTMM1) and *epf1/epf2*. All *Arabidopsis* lines were on Columbia (Col0) background. The *tmm* transgenic lines were obtained from Prof F. Sack (University of British Columbia), while *epf1/epf2* double mutant was provided by Prof J. Gray (University of Sheffield).

2.1.2 Chemicals, Reagents and Buffers

Except where otherwise stated, all chemicals used were from Sigma (Poole, UK) and Fischer-Scientific (Southampton, UK). Enzymes for molecular biology were from Invitrogen (Paisley, UK), Promega (Southampton, UK), Stratagene (UK) and Qiagen (Crawley, UK). Kits for RNA extraction, gel extraction and cDNA synthesis were from Qiagen. Custom primers were designed using Primer3 (<http://primer3.ut.ee/>) or NetPrimer (<http://www.premierbiosoft.com/>) platforms and were purchased from Invitrogen. List of solutions, media and primers used are indicated in Tables 1 and 2.

Table 1. List of solutions and media used.

Name	Description
General Use Solutions	
Sterilizing solution	2.5% sodium hypochlorite + 0.01% Tween 20
Molecular Biology Buffers	
TRIZOL	0.8 M guanidinium thiocyanate, 0.4 M ammonium thiocyanate, 0.1 M sodium acetate (pH 5), 5% glycerol, 38% phenol (pH 4, saturated in double-distilled H ₂ O)
Buffers for stomata	
Standard Buffer	5 mM MES-CaOH, pH 6.1 + 10 mM KCl
Opening Buffer	5 mM MES-NaOH, pH 6.1 + 60 mM KCl
Closing Buffer	5 mM MES-NaOH, pH 6.1 + 0.1 mM KCl + 6 mM CaCl ₂
FDA staining	Standard buffer + 20 μM fluorescein diacetate
Electrophysiology bathing solutions	
K ⁺ channel-related buffers	5 mM MES-CaOH, pH 6.1 + 10 mM KCl
Anion channel-related buffers	5 mM MES-CaOH, pH 6.1 + 10 mM KCl + 15 mM TEA-Cl + 15 mM CsCl
Growth Media	
Control medium	0.5 MS + 0.5 % Sucrose, pH 5.6
- SUC medium	0.5 MS + 0 % Sucrose, pH 5.6

Table 2. List of primers for qPCR.

Gene	AGI	Primers		Amplicon
AHA1	At2g18960	FOR	CACAACCAAGAAAGATTACGG	159
		REV	CTTCTCTTGGCTTGCTCTG	
AKT2	At4g22200	FOR	GTACTTGCGTTCTTGGTTCC	88
		REV	CTGCGTGGTACTCCAACAG	
GORK	At5g37500	FOR	GCTCAGTCGTCTATCTACCCG	125
		REV	CGTGCTTTCTACTACGCTCTTC	
KAT1	At5g46240	FOR	TCTCAAATACTGCGGATAAGC	125
		REV	TCTATTGCTATTGACTGTTGCC	
KAT2	At4g18290	FOR	GCTGATAATCCTTCCTGCTTC	116
		REV	CATCTTCATCATCTATTTCTGCG	
TMM1	At1g80080	FOR	AGTCTTCGGGTCCTTCACCT	206
		REV	TCACTGTCCCGGTTAACACA	
TUB9	At4g20890	FOR	AGTGTCCCTGAGCTAAC	225
		REV	AGTGGGAGCTATATCGC	

2.2 Plant Growth

2.2.1 *Begonia* growth conditions

Begonia plants were grown on airy soil mix consisting of medium coir compost (Sinclair) and bark supplemented with lime and fertilizer (Osmocote) in a composition as shown in Table 3. Plants were placed in long-day conditions (light/darkness 16/8 hours; light intensity 50-70 $\mu\text{mol m}^{-2} \text{sec}^{-1}$; temperature approximately 22 °C/18 °C day/night; RH of 60%/70% day/night). Propagation of plants was done by stem cuttings, which were sown on soil mix consisting 50:50 coconut fibre and bark. *B. coccinea* stem cuttings were firstly placed in water to produce roots and then sown on the propagation medium.

Table 3. *Begonia* growth medium

Ingredients	Composition per litre
COIR	1 litre
Bark	½ litre
Garden Lime	3 g
Dolomite	4.5 g
Osmocote (Scotts)	6 g

2.2.2 *Arabidopsis* growth conditions

A. thaliana seeds were sown onto moist Levington F2+S compost (Coulthers, Glasgow, UK) supplemented with systemic insecticide, Intercept 70WG (Scots, Ipswich, UK) inside a standard circular plant pot (4 cm in diameter). Pots were placed under a propagator in darkness at 4 °C for 2 days to allow stratification. Pots were subsequently transferred in controlled growth chamber (Sanyo Fitotron) in long-day conditions (light/darkness 16/8 hours; temperature approximately 22 °C/18 °C day/night; RH of 60%/70% day/night) under 70-90 $\mu\text{mol m}^{-2} \text{sec}^{-1}$ of light. After one week, plants were transplanted in individual pots (60 mm in diameter). For avoidance of any potential harm due to biotic agents, soil was covered with polyester mesh (mesh width 0.5 cm; Remnant Kings, Glasgow UK) that prevented contact of leaves with soil. All plants were placed under customised propagator with NITEX open mesh (mesh width 20 μm ; Sefar, Heiden, Switzerland) at all four sides, to keep relative RH same as the growth room conditions. For all physiological experiments, the same set-up was used, unless otherwise stated.

For seed collection, Aracon (LHELE SEEDS, Texas, USA) tubing was placed on top of the rosettes and watering stopped once the first siliques became discoloured. Plants were allowed to first completely dry out at greenhouse (temperature 18-24 °C; 100-200 $\mu\text{mol m}^{-2} \text{sec}^{-1}$ light) before collecting the seeds in 2 ml Eppendorf tubes and stored at room temperature.

2.2.3 Tobacco growth conditions

Sowing of *Nicotiana tabacum* seeds was carried out in the same way as for the *Arabidopsis* plants. Plants were placed in long-day conditions (light/darkness 16/8 hours; temperature approximately 26 °C/22 °C day/night; RH of 60%/70% day/night) under $\sim 100 \mu\text{mol m}^{-2} \text{sec}^{-1}$ light.

2.3 Experimental design for phenotypic analysis

2.3.1 Light-Humidity experiment

Plants were grown in long-day conditions (light/darkness 16/8 hours; temperature approximately 22 °C/18 °C day/night; RH of 60%/70% day/night) and were randomly distributed. Four different combinations of light and humidity regimes were used:

	Light Intensity ($\mu\text{mol m}^{-2} \text{s}^{-1}$)	Relative Humidity (%)
Control Conditions	70	60
High Humidity	70	90
High Light	200	60
High Light + High Humidity	200	90

High Humidity was achieved by covering the plants with a normal propagator (with no mesh at sides). Three-week old plants were photographed using a Nikon D1X camera. Steady-state gas exchange responses of each individual plant were quantified as described below (see section 2.4.5), with light and RH for gas exchange measurements being adjusted according to the levels used to grow the plants. Whole rosettes were harvested and scanned for area quantification as well as weighted for fresh weight (FW) measurement. Pooled rosettes of each genotype were wrapped in aluminum foil, placed at 70 °C for at least 72 hours to dry and subsequently weighted to determine the dry weight (DW). Water content (%) was calculated using the following formula

$$WC (\%) = 100 \left[\frac{(FW - DW)}{DW} \right] \quad \text{Eq. 2}$$

2.3.2 Drought stress experiment

Drought stress was carried out in three-week old plants grown in short-day conditions (light/darkness 9/15; light intensity 70-90 $\mu\text{mol m}^{-2} \text{sec}^{-1}$; temperature approximately 22 °C/18 °C day/night; relative humidity of 60%/70% day/night) under 70-90 $\mu\text{mol m}^{-2} \text{sec}^{-1}$ light.

For short-term drought stress, water was withheld for 21 days and rosettes were harvested at day 0, 5, 8, 16 and 21. On day 16 and 21 plants were re-watered and rosettes were harvested on 21st day. Harvested material was quantified for area and fresh weight. Individual rosettes were pooled and placed in aluminum foil at 70 °C for 72 hours to measure the dry weight and thereby water content. Soil water content was also measured by weighing the FW and DW of the soil, as done for the plant material.

For long-term drought stress, 4 plants were grown on standard pots (4 cm in diameter) for 4 weeks. Subsequently, water was withheld for 30 days, followed by weighing FW of pooled rosettes per genotype. DW and WC were also determined after drying the pooled plant material at 70 °C for 72 hours.

2.3.3 Root phenotypic analysis

A. thaliana seeds were surfaced sterilized. About 400 seeds were placed in 1.5 ml Eppendorf tube with 1 ml 100% ethanol for 1 minute and mixed by inverting tube several times. The ethanol was discarded and 1 ml of sterilizing solution was added into the tube and mixed by inverting several times. After incubation for 5 minutes, the sterilizing solution was replaced by 1 ml of double distilled water (ddH₂O). Washing was repeated 5 times to ensure complete removal of bleach solution and the seeds kept in water. Tubes were wrapped in aluminum foil and placed in darkness at 4 °C for 2 days to ensure stratification.

Muraskige and Skoog (MS; Sigma M5519) medium was used to prepare both Control and -SUC media at half strength, with pH adjusted to 5.6 using 0.5 M NaOH. Control media were supplemented with sucrose to a concentration of 0.5% while sucrose was 0 in SUC- medium. To solidify the media, 1% Agar (Type A,

Sigma) was added before autoclaving at 121 °C for 20 minutes. Once the autoclaved medium had cooled to about 60 °C, it was suspended into square plates (120 x 120 mm, Greiner) using titration pipettes.

Seeds were sown individually onto the solidified media using a sterile cut P200 pipette tip attached to a Gilson pipette. Generally, 6 seeds sown per plate containing 50 ml medium and spaced evenly into horizontal line approximately 15 mm from the top of the plate. The plates were sealed with 3M Micropore Tape (MidMeds Ltd, Nazeing, UK) and placed in short-day conditions under 150 $\mu\text{mol m}^{-2} \text{sec}^{-1}$ of light. At the 8th day after germination, plates were scanned to determine the root system architecture using the *EZ-Rhizo* software (Armengaud et al. 2009).

2.3.4 Osmotic content analysis

For osmotic content analysis, 2 leaves from three-week old plants grown in short-day conditions were harvested into 2 ml screw-cap tube, snap frozen in liquid N₂ and ground using TissueLyser (Retsch Qiagen, Crawley, UK). The ground tissue was homogenized with 100 μl ddH₂O and debris was subsequently pelleted by centrifugation for 2.5 minutes at 13,000 g. Supernatant was transferred into a new 0.5 ml Eppendorf tube. 10 μl of supernatant was placed on filter pads to allow osmotic content quantification using VAPROTM 5520 vapour pressure osmometer (WESCOR, EliTechGroup, Berkhamsted, UK). Calibration every 5th sample was performed using 100, 290 and 1000 mOS standards (EliTechGroup).

2.4 Gas exchange measurements

2.4.1 Basic concepts of gas exchange

LI-6400XT open system (LI-COR Bioscience GmbH, Bad Homburg, Germany) was used to measure CO₂ and H₂O differentials of air fluxes coming in and out of plant tissue, based on infrared gas analysis (IRGA) principle. Measurements were carried out either on whole rosette area for *Arabidopsis* using the Whole Arabidopsis Chamber (LI-COR 6400-17) or on leaves from *Begonia* species using the leaf chamber (LI-COR, 6400-08).

The operating principle of LI-6400 involves air stream pumped through reference and sample cuvette at same flow rate (mol air s⁻¹) and the mole fractions of CO₂ and H₂O are determined. The incoming air stream can also be conditioned and therefore control for humidity, CO₂ concentration and temperature. The mole fractions differentials for CO₂ and H₂O from reference and sample cuvettes are determined and used to calculate photosynthetic assimilation rate (A) and transpiration rate (E), respectively. When leaf temperature was measured, additional estimation of stomatal conductance was feasible. In particular, infrared light is passed through air stream with CO₂ and H₂O absorbing at specific and distinct wavelengths. Comparison of air mole fractions differentials between sample and reference was done by firstly transforming the absorbance-specific wavelengths into voltage signals. It is important that the IRGA analysers must be regularly checked to ensure that read the same air mole fractions. This was achieved by matching; a process where sample air is passed through reference cuvette and the former is adjusted according to the reference air. Figure 1 shows a layout of LI-6400XT's basic operating principle.

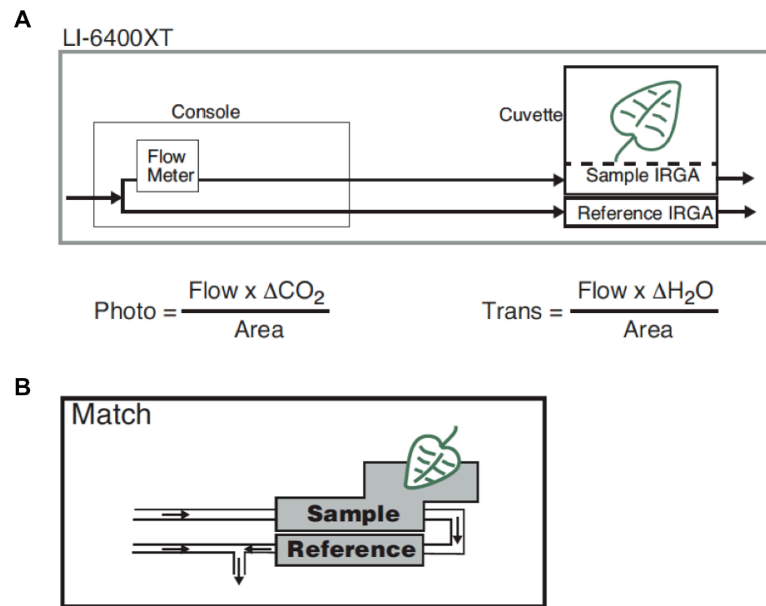


Figure 1. LI6400 XT basic principle of operation.

Air is simultaneously pumped through the console into the sample and reference cuvettes, which each contains an IRGA analyser. Air is pumped at constant flow rate set by flow meter residing in the console. (A) The differentials of mole air fractions are used to determine photosynthetic assimilation ($\mu\text{mol m}^{-2} \text{s}^{-1}$) and transpiration ($\text{mmol m}^{-2} \text{s}^{-1}$) rate by also taking into account the flow rate and area of plant tissue measured. (B) Matching between sample and reference air occurs by adjusting the former to the latter (Adapted by LI-COR, ftp://ftp.licor.com/perm/env/LI-6400/Manual/Using_the_LI-6400XT-v6.2.pdf)

2.4.2 General gas exchange experimental design

Instrument was warmed-up and checked for different parameters according to manufacturer's instructions. CO_2 concentration was set at 390 ppm using either CO_2 injector with pure liquid CO_2 cylinder (LI-COR, 6400-01) or external CO_2 tank. Once CO_2 concentration reached 390 ppm and remained stable, the reference and sample air were matched. Dark-adapted plant material was placed into the sample chamber, and temperature and humidity were set at 22°C and 55-60%, respectively. Gas exchange under darkness was measured for about 1 hour by matching every 20 min to ensure that photosynthesis, transpiration and conductance have reached a stable baseline before running any program. A RGB light source (LI-COR, 6400-18) was used to irradiate plant material at set photosynthetic active radiation (PAR; $\mu\text{mol m}^{-2} \text{s}^{-1}$). For *Arabidopsis* plants, individual pots, containing three-week plants grown in long-day conditions, were

wrapped with cling film before mounting to the whole Arabidopsis chamber to prevent gas diffusion from soil. Gas exchange in *Begonia* was carried out in the 3rd leaf from the tip of the stem. At least three different plants were studied at three different days and all experiments were carried out from 10-14 pm, to avoid deviations due to diurnal changes.

2.4.3 Light Curves

Dark-adapted plants were irradiated with a gradually decreasing PAR of 1000, 800, 600, 400, 200, 50 and 0 $\mu\text{mol m}^{-2} \text{s}^{-1}$. Light regime was changed every 10 minutes and before each change sample and reference air were matched. Data were logged every 1 minute and mean value of photosynthetic assimilation rate was calculated at each light intensity.

2.4.4 Time-course gas exchange measurement

Dark-adapted plant material was illuminated with either 70, 200, or 400 $\mu\text{mol m}^{-2} \text{s}^{-1}$ photosynthetic active radiation. Once gas exchange reached steady-state, plants were subjected to darkness until another stable baseline was reached. Throughout the program, data were logged every 1 minute, with matching automatically occurring every 20 minutes.

2.4.5 Steady-state gas exchange measurement

For Light-Humidity phenotypic analysis, steady-state gas exchange measurements were carried out holding temperature constant to 22 °C and [CO₂] to 390 ppm, while RH was set to either 60 or 90% according to the experimental conditions. Whole Arabidopsis chamber was covered with propafilm (LI-COR, 250-01885) and therefore ambient light was used as light source. Each plant was investigated for 2 minutes and data logged every 10 seconds resulting in 11 points that were averaged for assimilation and transpiration rate.

2.4.6 Gas exchange measurement analysis

All gas exchange data were normalized to rosette area for *Arabidopsis* plants and to leaf area (6 cm²) for *Begonia*. For light curve and the time-course gas exchange analysis, individual set of data were fitted to three-parameter exponential rise to maximum (Eq. 3), three-parameter exponential decay (Eq. 4) or four-parameter sigmoidal function (Eq. 5) depending on the parameter measured.

$$f(x) = Y_0 + a^{1-e^{-bx}} \quad \text{Eq.3,}$$

$$f(x) = Y_0 + a e^{-bx} \quad \text{Eq.4,}$$

$$f(x) = Y_0 + \frac{a}{1-e^{-(x-x_0)/b}} \quad \text{Eq.5.}$$

From the above equations, maximum rates and half times were estimated and averaged for each genotype.

2.5 Stomatal biology

2.5.1 Preparation of epidermal peels

For *Arabidopsis*-related experiments, epidermal peels were obtained from abaxial leaf side of three- to four-week old plants. Leaves were excised close to hypocotyl. For both *Begonia* and tobacco plants, epidermal peels were obtained from abaxial side and from areas close to the tip of the leaf, as leaves appeared softer and more flexible to touch. Leaf or leaf sections (especially for *Begonia* due to the big leaf size) were placed over index finger and hold with thumb and middle finger with abaxial side facing upwards. Using fine and sharp forceps, an initial cut onto the leaf was made followed by a gentle lift of epidermis, avoiding stretching of the peel. Once sufficient area of epidermis was peeled,

the epidermis was placed back onto the mesophyll and a new sterile razor blade used to make a cut at the end of the peel. Leaf together with the peel was softly pressed onto an adhesive-covered cover slip (Pressure-sensitive Adhesive, Factor II Inc., Lakeside AZ, USA) and the leaf tissue was removed. Epidermal peels were immediately submerged to opening buffer and treated with light of $\sim 100 \mu\text{mol m}^{-2} \text{sec}^{-1}$ for 2 hours.

Epidermal peels of at least three leaves from different plants were studied under Axiovert200 microscope (ZEISS, Jena, Germany) with $100 \mu\text{mol m}^{-2} \text{sec}^{-1}$ PAR and a LD Acroplan 40x/0.6 objective (ZEISS, Germany). Imaging was done using AxioCam HRc digital camera (ZEISS, Germany) and AxioVision LE software (ZEISS Vision GmbH, version 3.0.6 SP4), where >20 random 512x512 image fields for each leaf sample were acquired.

2.5.2 Stomatal patterning

Three independent experiments were carried out investigating stomatal patterning, which includes the following parameters:

Parameter	Description
Stomatal Density	Number of stomata per mm^2
Stomatal Size	Measured in μm^2
Stomatal Index	Number of stomata/number of epidermal cells
Stomatal Cluster	Number of stomata per cluster
Max stomatal aperture (a_{max})	Measured in μm^2

Maximum stomatal aperture was estimated as

$$a_{max} = \frac{\pi * W_a * L_a}{4}$$

where W_a is aperture width and L_a is aperture length.

Stomatal size was obtained from

$$SS = \frac{\pi * W_s * L_s}{4} - a_{max}$$

where W_s is stoma width and L_s is stoma length.

Maximum anatomical stomatal conductance to water vapour (G_{Wmax}) was calculated as before (Franks et al. 2009). The formula used is based on stomatal geometry characteristics

$$G_{Wmax} = \frac{d * SD * a_{max}}{v(l + \frac{\pi}{2} \sqrt{\frac{a_{max}}{\pi}})} \quad Eq\ 6$$

where d is the diffusivity of water vapour in air ($m^2\ s^{-1}$), v is the molar volume of air at 1 atm and 22 °C ($m^3\ mol^{-1}$), SD is stomatal density (m^{-2}) and l is the pore depth (m), estimated as the half of fully inflated guard cell width. Anatomical stomatal conductance to CO_2 can also be determined from Eq.6 since it equals to the 1/6 of G_{Wmax} (Hetherington & Woodward 2003).

After imaging, epidermal peels were incubated for 5 minutes in standard buffer supplemented with 20 μM fluorescein diacetate (FDA) to check for cell vitality. Only stomata that showed fluorescence under confocal microscopy were analysed. Also, this procedure confirmed that the epidermal cells were destroyed while the stomata were still alive. Therefore, I was ensured that the altered stomatal movements on plants with stomatal clusters were not dependent on the physical constraints of the adjacent non-stomatal cells.

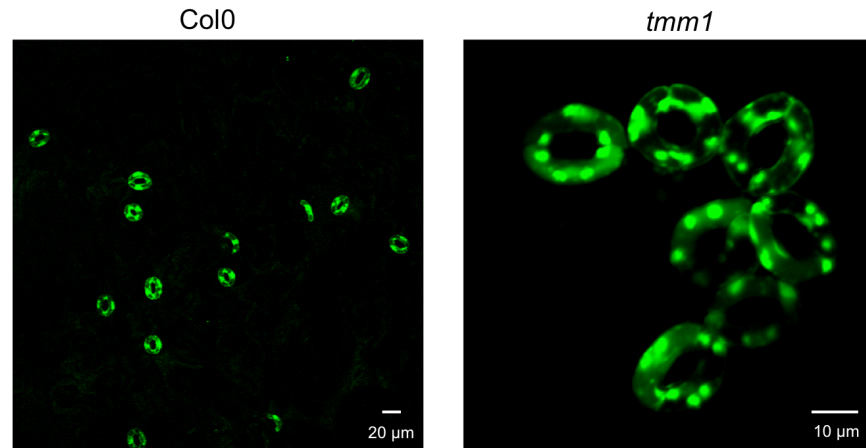


Figure 2. FDA staining of living cells.

Representative photos of cells stained with 20 μM FDA from *Arabidopsis* wild type and *tmm1* mutant plants. Only living cells were stained, confirming that the preparation of epidermal peels did destroy the cells adjacent of stomata.

2.5.3 Stomatal closure

Stomatal closure was investigated in epidermal peels pre-treated with opening buffer and light and subsequently placed in closing buffer for 1 hour. Images were taken before and after treatment and apertures were measured from the same stoma. Closure was also investigated under the presence of the plant hormone ABA and the H_2S donor, GYY 4137. In this case standard buffer was supplemented with 20 μM ABA or 10 μM GYY 4137. In addition, concentration response of stomatal aperture to GYY 4137 ranging from 0.1 to 10 μM was carried out in tobacco epidermal peels.

2.6 Electrophysiology

2.6.1 Basic concepts of electrophysiology

Electrophysiological studies allow the analysis of ion transport across membranes and the understanding of the mechanisms controlling ion currents and stomatal movements. Here I made use of two-electrode voltage clamp (TEVC) technique that entails the control of membrane potential and measurement of ion current across the membrane. The kinetic characteristics and gating of the ion current

depend on the membrane voltage and measuring steady-state currents across a defined voltage range enables characterization of major ion channels at the plasma membrane. Figure 2 illustrates a schematic representation of the TEVC circuit. The technique comprises the use of two electrodes, the “voltage electrode”, which measures voltage relative to the ground and the “current electrode”, which supplies current into the cell. The membrane voltage (V_m) is recorded via the “voltage electrode” and read-out by a feedback amplifier that feeds the signal into a “voltage clamp” amplifier. The latter amplifier also receives a voltage command (V_c) and the difference between V_c and V_m is used to generate a current proportional to this difference. The current eventually is fed back into the cell via the “current electrode” to minimize the $V_m - V_c$ signal to zero. Hence, the current produced by the TEVC circuit is equal and opposite of the ionic current at a given voltage. To prevent disturbances due to junction potentials - i.e. half-cells - a reference electrode connected to the ground was inserted into the bathing solution as well.

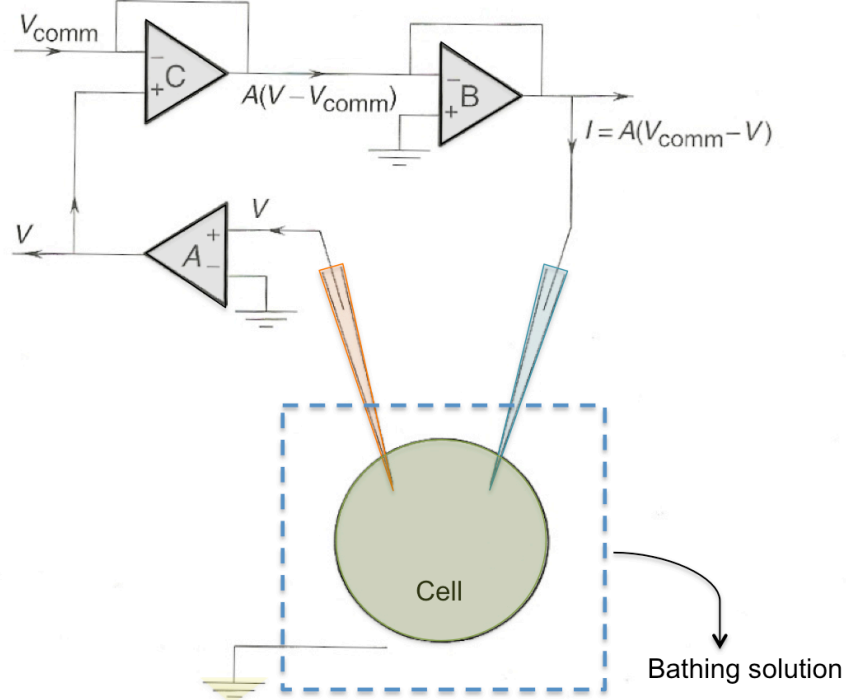


Figure 3. Schematic representation of two-electrode voltage circuit.

Membrane voltage (V_m) is measured through a voltage electrode (orange) and is fed into a feedback amplifier (A). The signal is transmitted into a voltage clamp (C). A voltage command (V_{comm}) is also fed into C. The difference ($V - V_{comm}$) is supplied back to the cell as current (I) through a differential amplifier (B) and through a “current electrode (blue). The bathing solution is ground to compensate for junction potential created by half-cells through a reference half-cell (yellow). Adapted and redrawn by (Blatt, 2004).

2.6.2 Electrophysiological experimental design

Currents were recorded under TEVC using Henry’s EP software (Y-Science, <http://www.psrg.org.uk>). Epidermal peels were pressed on adhesive-covered chamber and bathed with opening buffer. A cover slip was placed on top of the chamber and placed under light for 2 hours to ensure maximum stomatal opening, as it allows better current measurements (Chen et al. 2012). Subsequently, the chamber was secured in a holder stage and the reference electrode was inserted in the chamber. Flow of solutions occurred by delivery needles and a suction needle placed at the side of the chamber and in contact with the bathing solution.

Microelectrodes are used as salt bridge connecting cytosol and true electrode, which is formed by a silver wire coated with silver chloride (AgCl) precipitate. The junctions of metal and electrolyte, known as half-cells, were bathed in 1 M KCl solution to avoid any cell-derived variations in salt composition or concentration. To prepare half-cells, a 2 ml disposable pipette was cut (approx. 6 cm in length) and into that a silicone rubber was inserted. The silver wire was of 0.5 mm in diameter and 4 cm in length and soldered onto the end of a 2 mm socket. The silver was sanded to remove the silver oxide layer and inserted through the silicone rubber into the half-cell. The half-cells were filled with 10% sodium hypochlorite for 12 hours to deposit an AgCl layer on them. Following that, sodium hypochlorite was removed and replaced with 1 M KCl. Half-cells were stored in 1 M KCl and connected together ensuring electrical equivalence between them. A reference half-cell was constructed on the same way and in order to make electrical connection with the microelectrodes a special salt-bridge was constructed. The latter included the filling of a about 0.5 mm in diameter polyethylene tubing with 2% agar dissolved in 1 M KCl. Figure 3 presents the whole assembly of chamber, holder stage and a reference half-cell as well as the two distinct types of half-cells used.

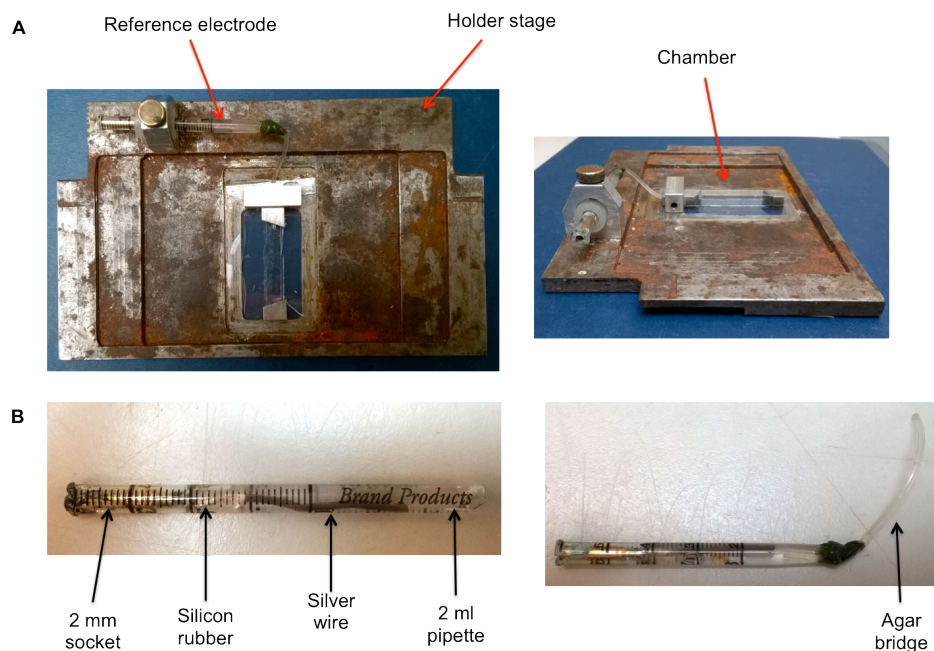


Figure 4. Images of the equipment used to perform electrophysiological studies.

(A) Top view (left) and side view (right) of whole assembly of holder stage, reference electrode and chamber. (B) The two types of half-cells used, the typical half-cell (left) and reference half-cell (right).

Microelectrodes were mounted on the amplifiers and moved using a Huxley-type micromanipulator. Microelectrodes were formed by two borosilicate glass capillaries mounted on a PD5 horizontal puller (Narashige Instruments, Oxford, UK), heated and twisted for 360°. Microelectrodes were pulled apart to give tip resistances of 300-500 M Ω for *Arabidopsis* impalements and >100 M Ω for tobacco impalements. Therefore, distinct settings for preparing the microelectrodes were used. In particular, coil heat was adjusted in order to result in a pull time of approximately 30 seconds for *Arabidopsis* and about 40 seconds for tobacco. Figure 4 shows the microelectrode tips of the two different double-barrelled microelectrodes used in this study.

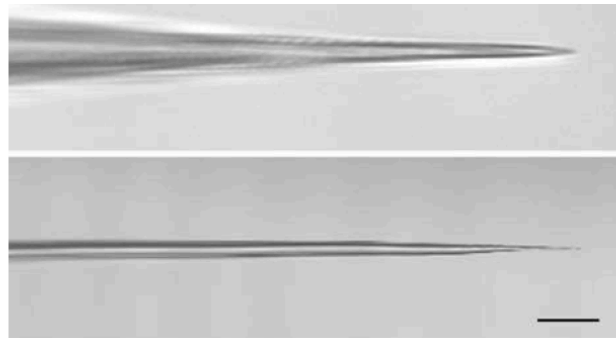


Figure 5. Double-barrelled microelectrodes pulled for *N. tabacum* (top) and *A. thaliana* (bottom) guard cells.

The tip of *Arabidopsis* microelectrode was tapered with a smaller angle than that of tobacco's microelectrode. The extreme tip is beyond the resolution of the light microscope used in this study. Scale bar = 10 μm (Adapted from (Chen et al. 2012)).

2.6.3 Ion current separation

TEVC firstly requires the separation of ionic currents in order to identify and measure for the specific characteristics of a given channel. One way to achieve that is to use different toxins or blocking agents that eliminate a given channel. Hence, for K⁺ channel measurements, microelectrodes were filled with 200 mM K⁺-Acetate (KAc), pH 7.5, to minimize interference due to anion current (I_{Cl}) (Wang & Blatt 2011). KAc was prepared by titrating acetic acid solution with 1 M KOH. 200 mM caesium chloride (CsCl) was used to eliminate K⁺ currents (I_K) in anion measurements. In both cases, microelectrodes supplemented with a small

amount of Ca^{2+} sponge to avoid interference due to Ca^{2+} . Comparison of K^+ channel currents in *Arabidopsis* guard cells was conducted using bathing solution of standard buffer (5 mM MES-Ca, pH 6.1 +10 mM KCl). For anion channels, bathing solution consisted of standard buffer supplemented with 15 mM tetraethylammounium chloride (TEA-Cl) and 15 mM CsCl.

For investigating the effect of H_2S on K^+ and anion channels, the same as the above bathing solutions were used, but they were additionally supplemented with 0.1, 1 or 10 μM GYY 4137, a H_2S donor. Additionally, treatments with hypotaurine (HT), which is a H_2S scavenger, were performed. To investigate if H_2S effect was Ca^{2+} -dependent, ethylene glycol tetraacetic acid (EGTA), which has high affinity for Ca^{2+} and chelates Ca^{2+} into the cytosol, was used. Finally ABA-dependence was investigated by using bathing solution supplemented with 20 μM ABA \pm 10 μM HT. Table 4 presents all the solutions used in electrophysiological studies. Finally, surface area of the impaled guard cells was calculated assuming spheroid geometry using Henry's EP software.

Table 4. Microelectrode-filling and bathing solutions.

	Microelectrode filling solutions	Bathing solution composition
K^+ channels	200 mM KAc	SB +10 mM KCl + 0.1, 1 or 10 μM GYY
		SB + 10 mM KCl + 10 μM GYY + 10 μM HT
		SB + 10 mM KCl + 20 μM ABA + 10 μM HT
		SB + 10 mM KCl + 20 μM ABA
	200 mM KAc + 50 mM EGTA	SB +10 mM KCl + 10 μM GYY
Anion channels	200 mM CsCl	SB + 15 mM TEA-Cl +15 mM CsCl
		SB + 15 mM TEA-Cl +15 mM CsCl +10 μM GYY

2.6.4 Analysis of ion currents

TEVC allows identification of voltage-dependent currents, however, additional transporters, like H⁺ ATPases, are active at all voltages. Separation of such currents is necessary and requires the subtraction of the steady-state currents, which are identified by their slower gating from the instantaneous currents, which make the sum of all the channels activated at the first few milliseconds. This manipulation enables the construction of a current-voltage (I-V) curve for the channel. From this curve, one can extrapolate the kinetic characteristics of the channel. For instance, K⁺ channel characteristics are obtained by fitting a Boltzmann function (Eq.7) on the I-V curve.

$$I = \frac{G_{max}(V-E_K)}{1+e^{\frac{\delta zF(V-V_{1/2})}{RT}}} \quad \text{Eq.7}$$

where G_{max} is the maximum conductance, V is the command voltage, E_K it the equilibrium voltage for K⁺, $V_{1/2}$ is the voltage at which half maximum activation of channels occurs, z is the ion charge, F the Faraday constant, δ is the gating charge, R is the gas constant and T is the absolute temperature. In effect, analysis using Boltzmann function results in determination of δ , which describes the change in activity with voltage and $V_{1/2}$ that reports the midpoint where this change occurs. Finally, from such fittings the parameters half-time ($t_{1/2}$) can be obtained through Henry's software. $t_{1/2}$ describes the time required the current to relax to a new steady-state.

2.7 Molecular Biology

2.7.1 RNA extraction

For the extraction of RNA, 2 leaves from three-week plants grown in long-day conditions were harvested into 2 ml screw-cap tube and snap frozen in liquid N₂. The tubes were placed in a pre-cooled rack and plant material was ground using

the TissueLyser (Qiagen) for 1-1.5 minutes depending on the amount of plant material, with a frequency of ~28 Hz.

To prepare RNase free water, 1 ml of DEPC (Diethyl pyrocarbonate, Fluka) was added to 1 L of double distilled water and stirred for approximately two hours. This water was subsequently autoclaved and used in all methods involving RNA.

RNA was extracted from *A. thaliana* by using either the RNase® Mini kit (Qiagen) according to the manufacturer's instructions or TRIZOL-based method. For the latter method, 1.4 ml of TRIZOL solution was added to 100 mg of ground frozen plant material. The samples were mixed by vortexing for 1 minute and incubated at room temperature for 5 minutes. The plant debris was pelleted by centrifugation at 8000g for 2 minutes. The supernatant was transferred into a new 2 ml Eppendorf tube with additionally 300 µl of chloroform : isoamylalcohol (24:1) solution. The samples were mixed by vortexing for 1 minute, incubated at room temperature for 2 minutes and subsequently centrifuged at 13000g and 4 °C for 10 minutes to separate organic and inorganic phases. Up to 750 µl of aqueous inorganic phase was carefully transferred into a fresh 1.5 ml tube followed by adding isopropanol in a volume ratio of 1:1. The samples were mixed by inverting the tubes for several times and left at room temperature for 5 minutes to allow the precipitation of RNA. The samples were further centrifuged at 13000 g and 4 °C for 10 minutes and supernatant was discarded. The resulted pellet was washed with 1 ml of 70% ethanol and centrifuged at 13000g and 4 °C for 5 minutes. The supernatant was removed and the pellet allowed to dry at air and resuspended in 50 µl of DEPC-treated water. The samples were placed at 42 °C to ensure dissolving of dried RNA.

RNA quantity and purity was measured by spectrophotometry using Eppendorf Biophotometer Plus 6132 (Eppendorf, Germany). RNA was diluted 1:10 in DEPC-treated water and absorbance was measured from 220 to 320 nm into an Eppendorf UVette® (Eppendorf, Hamburg, Germany). RNA concentration ($\text{ng } \mu\text{l}^{-1}$) was calculated following the formula: $(A_{260-230}) \times 40 \times \text{Dilution factor}$. The purity of RNA was estimated from the A_{260}/A_{280} ratio and RNA was stored at -80°C.

Approximately 500 ng of RNA were used to synthesize cDNA using the QuantiTech RT kit (Qiagen) according to manufacturer’s instructions. The produced cDNA was stored at -20 °C and used for both PCR and qPCR.

2.7.2 Polymerase Chain Reaction

PCR was performed using the Gen Amp PCR System 9700 (Applied Biosystems, UK). Standard PCR was carried out using GoTaq Flexi DNA polymerase (Promega, Madison, USA). Table 4 and 5 display the composition of the standard PCR mix prepared to a final volume of 20 ml and cycling conditions, respectively. Template was cDNA diluted in 1:10 while genomic DNA was also used as positive control. Primers used are shown in Table 2 (see section 2.2.2).

Table 5. Standard PCR master mix

Component	Volume (µL)
10x Green Buffer	5
MgCl ₂ (25mM)	1.5
dNTP Mix (10mM of dATP, dCTP, dGTP and dTTP)	0.5
DMSO	0.5
Forward Primer (10mM)	0.5
Reverse primer (10mM)	0.5
GoTaq (5µg/µL)	0.13
Double distilled water	16.12
Template	0.75

Table 6. Cycling conditions of standard PCR.

Cycles	Step	Temperature	Time (min)
1	Denaturation	95 °C	2
30	Denaturation	95 °C	0.5
	Primer Annealing	58 °C	0.5
	Extension	72 °C	2
1	Final extension	72 °C	3

2.7.3 Quantitative PCR (qPCR)

qPCR was performed in 96-well plates using StepOne PlusTM real-time PCR system (Applied Biosystems) and the Brilliant SYBR Green qPCR kit (Stratagene). Table 4 and 5 display the composition of the qPCR reaction mix prepared to a final volume of 15 ml and cycling conditions, respectively. The template was cDNA, DNA standards or nucleotide-free water. DNA standards were prepared from gel-extracted PRC products by performing standard PCR using the same primers as for qPCR. Purified PCR products were adjusted to 1 pg μl^{-1} and following serial dilutions, six standards ranging from 0.1 to 10^{-7} pg μl^{-1} were made.

At the end of the annealing step of every PCR cycle, SYBR green fluorescence was measured and the Ct (the number of cycles required to reach threshold fluorescence) was calculated. Plotting the Ct value of each standard dilution against the log initial template quantity created a standard curve, which were used for normalization of Ct values for each gene. To control and correct any errors occurring in each qPCR, the expression of the gene of interest was tested relative to the stably expressed gene, *TUBULIN 9 (TUB9)* (Gutierrez et al. 2008). qPCR reactions were made in technical duplicates and cDNA from 3

independently grown plant material was used. Primers for genes tested are shown in Table 2 (see section 2.2.2).

Table 7. qPCR reaction mix.

Component	Volume per reaction (µL)
SYBR green qPCR Master mix	10
Forward Primer (10mM)	0.4
Reverse primer (10mM)	0.4
Double distilled water	4.2
Template	5

Table 8. Cycling conditions for qPCR.

	Cycles	Temperature	Time (min)
Denaturation stage	1	95 °C	3
Extension stage	40	95 °C	0.10
		60 °C	0.20
Denaturation Stage	1	95 °C	1
		55 °C	0.30
		95 °C	0.35

2.8 Data analysis

2.8.1 Image analysis

For all experiments in which image acquisition was employed, image analysis was performed using ImageJ, v. 1.43u (<http://rsb.info.nih.gov/ij>; Rasband and Bright, 1995) and especially exercising the Measure Area and Measure Particles plugins. Scales were set using a reticule-containing image acquired at each objective used throughout this study. Scanned or photographed rosette areas of gas exchange experiments were also normalized to a defined scale.

2.8.2 Statistical analysis

Data analysis and curve fitting was carried out using SigmaPlot 12 (Systat Software Inc.). Results are the means \pm SE of three independent biological replicates, unless otherwise stated. Statistical significances were tested using either t-test or ANOVA at $p < 0.001$ or < 0.05 , as specified for each experiment. Graphs were created using SigmaPlot 12 and Photoshop 6.0.

3 Stomatal clustering influences stomatal movements

3.1 Introduction

Stomata play a crucial role on physiology of plants, because they permit gaseous exchange between the environment and the inside of the leaf that in turn influences the growth of the plant. For example, plants with no stomata display limited growth (MacAlister et al. 2007). Several studies have been focused on specific stomatal parameters, such as stomatal size and density, and their effect on plant physiology. Based on mathematical models, higher stomatal density has been shown to correlate with higher stomatal conductance (Drake et al. 2013). Various groups have provided experimental evidence supporting this prediction. For instance, studies with the *STOMAGEN* overexpressing, having more numerous stomata, suggested a positive correlation between photosynthetic capacity and stomatal density (Tanaka et al. 2013). Accordingly, mutation in the *GTL1* gene, which encodes for a transcription factor regulating the *STOMATAL DENSITY AND DISTRIBUTION1* (*SDD1*) gene, resulted in a low density stomatal phenotype that in turn was translated into a reduction in the transpiration rate (Yoo et al. 2010). However, the discussion about how stomatal density influences gas exchange responses remains controversial. Schluter et al. (2003) carried out physiological experiments with mutants of the subtilisin-type serine proteinase *SDD1*, which shows high stomatal density, and found no differences in CO₂ assimilation under constant light conditions. Albeit, the *sdd1* mutants did show greater carbon assimilation and metabolism comparing to wild type plants under fluctuating light conditions (Schluter et al. 2003). The authors suggested that in such conditions, where stomatal conductance is the limiting factor for CO₂ diffusion, increasing stomatal density would overcome the photosynthetic limitation. Indeed, the diffusional theory implies that high stomatal density in association with the small stomatal size results in faster and greater stomatal responses (Willmer & Fricker, 1996). Thus, a greater volume to surface area ratio of stomata should be favoured to optimize gaseous exchange. This latter notion is reinforced by the fact that a negative correlation between the stomatal density

and size has been reported from various groups based on both geological and laboratory (Hetherington & Woodward 2003; Franks & Beerling 2009; Doheny-Adams et al. 2012).

Nevertheless, stomatal conductance and thus plant physiology is also dependent on the stomatal aperture and therefore on the mechanistic properties of cells to accumulate osmotically active solutes to drive stomatal movements (Blatt 2000; Lawson & Blatt 2014). The sensitivity of stomatal movements on the ionic exchange with neighbouring cells has been indeed postulated for decades (Raschke & Fellows 1971; Outlaw 1983; Wilmer & Fricker, 1996). Also, Franks & Farquhar (2007) suggested the importance of the neighbouring cells of stomata for stomatal movements and conductance by studying four species with different arrangements of the stomatal complex. Most of the plant species follow the “one cell spacing rule” that entails the separation of stomata by each other by at least one epidermal cell (Geisler et al. 2000; Peterson et al. 2010). Yet, in nature, there are genera deviating from this rule, like the *Begonia* genus, that shows stomatal clusters on leaf epidermis. To date, only one study with *Arabidopsis* transgenic lines has reported on the impact of stomatal clustering in plant physiology (Dow et al. 2014). The authors showed a deviation from the maximum potential for stomatal conductance and CO₂ assimilation rate as the degree of clustering increased. Despite the fact that they did not conclude on the exact mechanism underlying the improper stomatal function in clusters, they exclude the possibility of that being dependent on the stomatal density of the lines with stomatal clusters.

Hence, I was interested in addressing 5 major questions regarding the impact of stomatal clustering on plant and guard cell physiology: 1) Does stomatal clustering leads to changes in stomatal index and density? 2) And if so, does the plants with stomatal clusters follow the same positive correlation between stomatal density and stomatal conductance as the plants with single stomata do? 3) Does stomatal clustering impacts the gaseous exchange when light intensity is varied? 4) Does the pore of stomata occurring in clusters equally functions as it does in the single stomata? 5) And finally, does stomatal clustering impacts the guard cell physiology through altering ion transport and solute accumulation?

To address the above questions, I used two separate populations of plants exhibiting either single stomata or stomata in clusters. The experimental population consisted of four *Arabidopsis* lines, wild type (Col0), *tmm1* mutant showing stomatal clusters, complementation line of *tmm1* (PTMM1), and *ep1/epf2* double mutant showing high stomatal density. Two *Begonia* species made up the natural population of plants, with *B. coccinea* showing single stomata phenotype and *B. plebeja* showing stomatal clusters. Firstly, I carried out quantitative analysis of stomatal characteristics on epidermal peels of the abaxial side of leaves to distinguish between stomatal clustering in the two distinct plant populations. I used mathematical models to estimate the stomatal conductance based on the stomatal anatomy. I examined if the reported relationships between stomatal conductance and size or density as well as between stomatal density and size were held true for the lines used in this study. Moreover, performing IRGA measurements I studied the gas exchange responses between clustered and single stomata plants using light of different intensities to drive stomatal opening and closing. Also, stomatal aperture measurements were carried out in epidermal peels treated with opening and closing stimuli to investigate for the functionality of stomatal pore in the “clustered” species. To dissect the mechanism driving stomatal movements in the “clustered” plants, I employed voltage clamp technique in order to determine the kinetics of K^+ channels in single and “clustered” stomata. Finally, the K^+ content of the two types of stomata was measured by performing tail current analysis to investigate for the importance of surrounding epidermal context in stomatal behaviour.

3.2 Results

3.2.1 Epidermal patterning depends on stomatal geometry

The *Arabidopsis* lines were first examined for the transcript level of *TMM1* gene by RT-PCR and compared with that of the housekeeping gene, *TUBULIN 9* (*TUB9*, Figure 1A). The *TMM1* transcript in *tmm1* mutant was highly reduced compared to wild type and PTMM1 plants, whereas it appeared higher in the *epf1/epf2* double mutant compared to wild type plants. The *tmm1* line was originally generated by ethyl methanesulfonate (EMS) mutagenesis (Yang & Sack 1995), which results in 33 missense residues before premature termination that removes 2 ½ LRRs and the transmembrane domain. However, the transcript still retains some activity. PTMM1 indicate the *tmm1* plants complemented with *TMM1* gene driven under 35S CaMV promoter and tagged with GFP at the C-terminus. To further check the *TMM1* transcript levels, quantitative PCR was carried out, using RNA extracted from three-week old *Arabidopsis* wild type, *tmm1*, PTMM1 and *epf1/epf2* leaves as template. The transcript level of the *TMM1* gene from the transgenic lines was normalized to the transcript level of the endogenous gene and to that of the wild type plants. Figure 1B shows the relative difference in the amount of *TMM1* transcript from the *tmm1*, PTMM1 and *epf1/epf2* mutants. The data showed 2.7-fold down-regulation of the *TMM1* in *tmm1*, whereas the opposite was observed in the *epf1/epf2* plants. In contrast, the *TMM1* transcript of the PTMM1 plants was not significantly different from that of wild type plants, confirming the expected wild type levels of the *TMM1* gene in this complementation line.

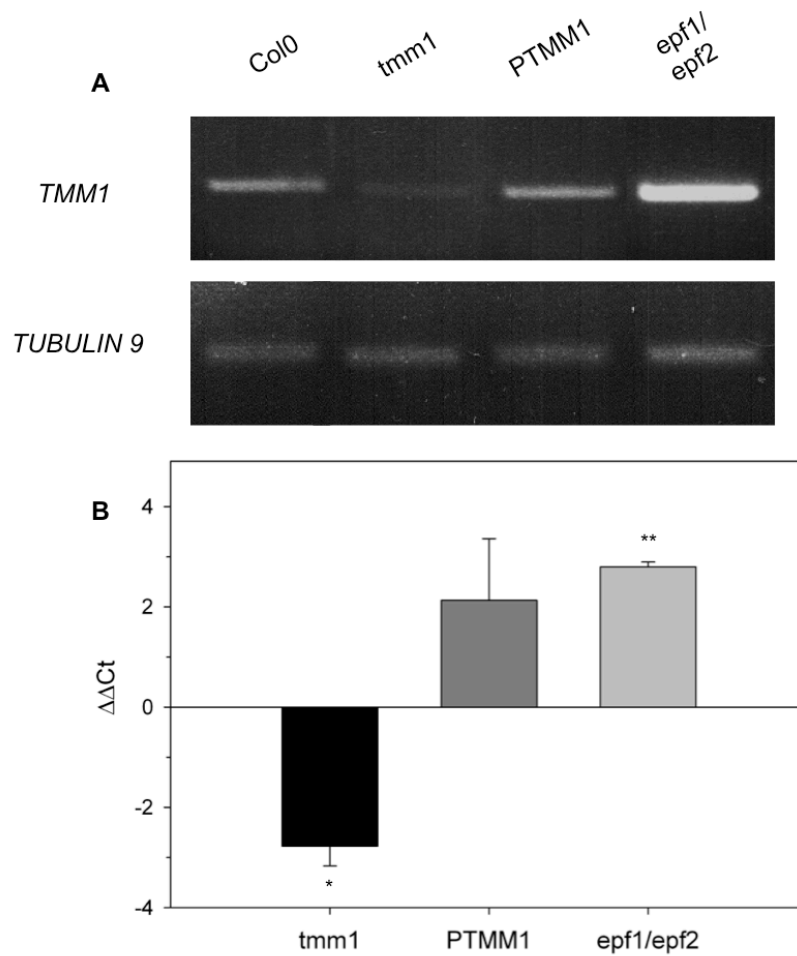


Figure 1. *TMM1* transcript level in *Arabidopsis* lines.

RNA was extracted from leaves of 3-week old *Arabidopsis* Col0, *tmm1*, PTMM1 and *epf1/epf2* plants to quantify transcript levels using the *TUBULIN 9* gene as endogenous control. Graphs represent (A) RT-PCR and (B) quantitative PCR. Data report on the difference between the endogenous control and the target gene, *TMM1*, and between wild type and rest of *Arabidopsis* lines. Data are means \pm SE of n=3 technical replicates. Asterisks indicate statistical differences (after ANOVA ($p < 0.05$), as determined by Student-Newman-Keuls test).

The effect of the reduced *TMM1* transcript in *tmm1* mutants was highly significant when epidermal peels from abaxial side of *Arabidopsis* leaves were examined under light microscopy. Figure 2 presents the stomatal phenotypes of the *Arabidopsis* and *Begonia* plant populations used throughout this project. The wild type (Col0), complementation line (PTMM1), and *B. coccinea* displayed stomata that were separated by at least one epidermal cell, henceforward referred to as “single stomata” plants. Stomata of the *epf1/epf2* plants appeared single, but few arrested meristemoid cells were also apparent on the leaf epidermis, as described before (Doheny-Adams et al. 2012). However, the authors have also reported the presence of pairs of stomata in the *epf1/epf2* mutants. Here, I did not observed any stomatal clusters on the *epf1/epf2* mutants that might be due to the different conditions used to grow the plants. By contrast, the *tmm1* mutant did not follow the “one cell spacing rule” and exhibited stomatal clusters on leaf epidermis. Additionally, *B. plebeja* showed stomatal clusters on abaxial side of the leaf but the stomata were separated with a special type of non-epidermal cells, known as subsidiary cells. Henceforward *tmm1* and *B. plebeja* are referred to as “clustered” plants. The stomatal clustering differed between the *Arabidopsis* and the *Begonia* species, with the *tmm1* exhibiting contiguous clusters while *B. plebeja* showing non-contiguous clusters.

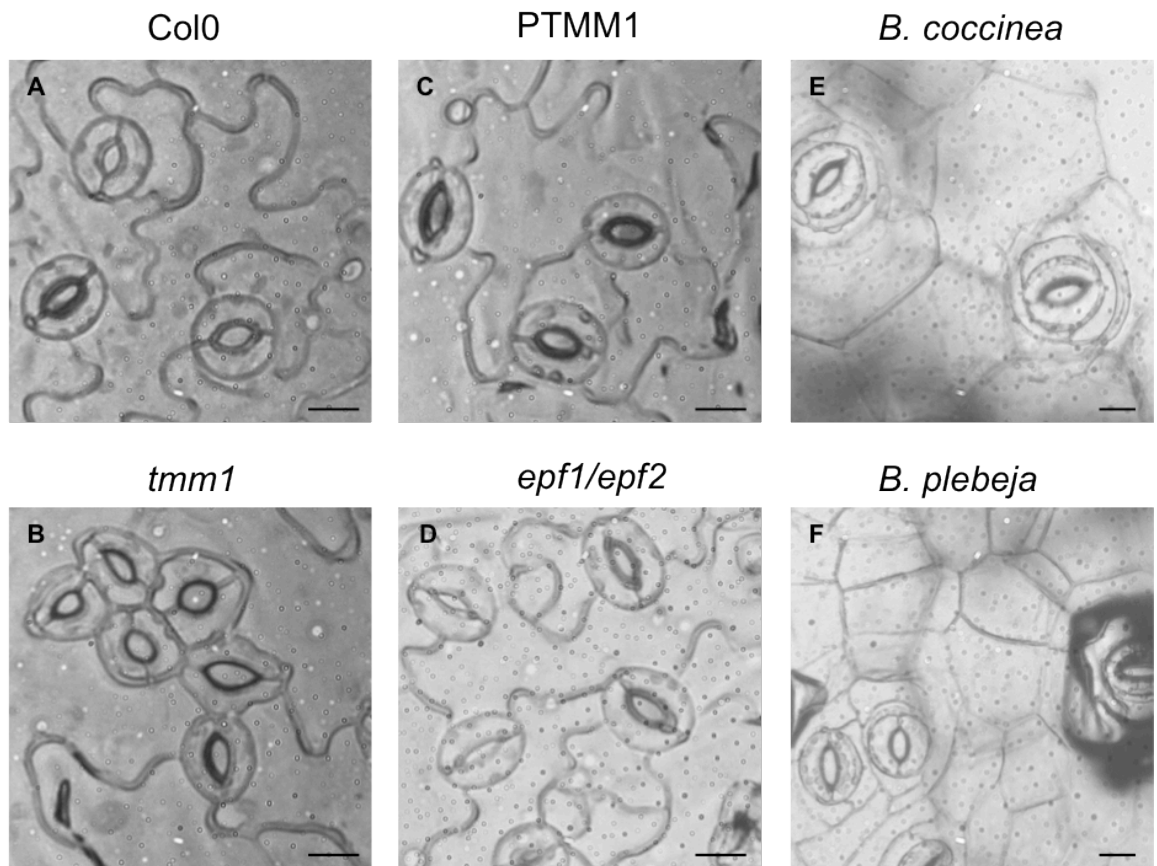


Figure 2. Representative micrographs of epidermal peels from the abaxial side of *Arabidopsis* and *Begonia* leaves.

Arabidopsis Col0 (A), *tmm1* (B), PTMM1 (C), *epf1/epf2* (D), *B. coccinea* (E) and *B. plebeja* (F). Images at upper panel represent “single stomata” phenotype. At bottom panel, plants with distinct stomatal patterning are presented. The *epf1/epf2* mutant showed single stomata, but it also exhibited arrested meristemoid cells on the leaf epidermis. The *tmm1* mutant exhibited contiguous stomatal clusters, while *B. plebeja* showed non-contiguous stomatal clusters.

Bars = 10 μ m

Quantification of the stomatal patterning phenotypes from the *Arabidopsis* and *Begonia* species is presented in Figure 3. The mean stomatal density ranged between 290 to 740 stomata per mm² for *Arabidopsis* lines and 70 to 200 stomata per mm² for *Begonia* species. The *tmm1* and *epf1/epf2* mutants showed significantly higher SD compared to wild type and PTMM1 plants. Similarly, *B. plebeja* had more stomata than *B. coccinea*. Stomatal size did not significantly vary among the *Arabidopsis* lines, except in the case of the *epf1/epf2* double mutant that showed much smaller stomata in comparison to wild type. The stomatal size of the “clustered” *B. plebeja* was significantly reduced when compared to *B. coccinea*. Also, all six genotypes followed the previously reported strong inverse correlation between stomatal density and size, with a decrease in stomatal size resulting in more numerous stomata (Fig. 3A).

The difference in stomatal numbers and size is also depicted by the stomatal index, which is the ratio of the number of stomata over the number of non-stomata cells and basically is a measure of the leaf area covered by stomata. The difference among the *Arabidopsis* lines is more pronounced than that of the *Begonia* species (Figure 3B). The *tmm1* mutant showed an approximately 4-fold higher stomatal index than the “single stomata” lines. The difference in stomatal index of the *epf1/epf2* double mutant comparing to wild type was also significant, but it was smaller comparing to that of the *tmm1* plants. Conversely, the *Begonias* did not follow the above trend and stomatal index appeared very similar between *B. coccinea* and *B. plebeja*, yielding values of 0.13 ± 0.003 and 0.14 ± 0.01 (Figure 3B). The differences in stomatal size as well as the different type of stomatal cluster in *B. plebeja* underscore this latter observation. In particular, stomata from *B. plebeja* were smaller in size, with the average stomatal size being about $545 \mu\text{m}^2$ compared to $722 \mu\text{m}^2$ from *B. coccinea* (Figure 3A). Notably, the stomata in *B. plebeja* are surrounded by subsidiary cells, which lead to the reduction of the leaf area being covered by stomata. Regarding the “clustered” phenotype, the *tmm1* mutant had more stomata within the cluster than *B. plebeja* plants, with a mean cluster size of 2.8 and 1.64 stomata per cluster, respectively (Figure 3C).

Stomatal clustering influences stomatal movements

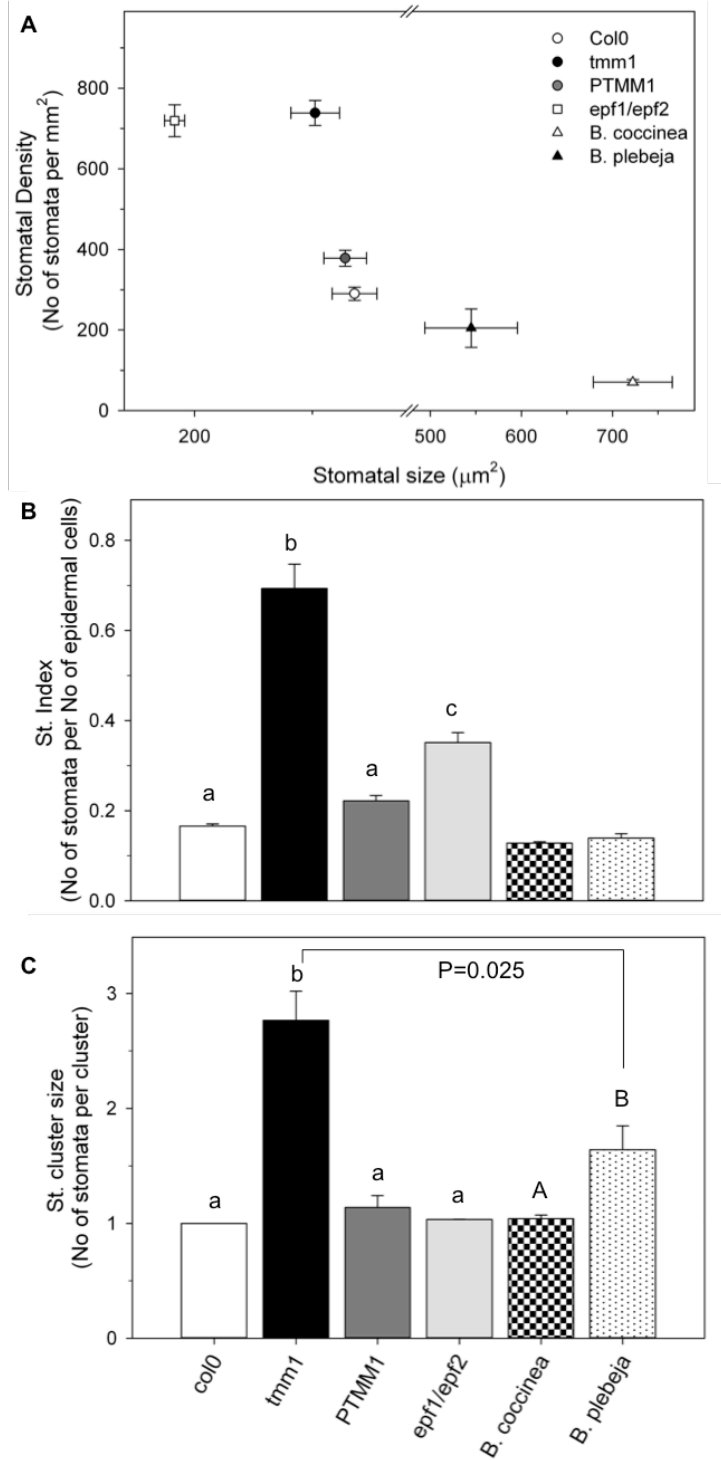


Figure 3. Quantification of stomatal patterning of epidermal peels from *Arabidopsis* and *Begonia* plants.

Stomatal patterning was estimated from wild type (white circle and bars), *tmm1* (black circle and bars), complementation line PTMM1 (dark grey circle and bars), *epf1/epf2* (white square and grey bars), *B. coccinea* (white triangle and square-shaded bars) and *B. plebeja* (black triangle and dotted bars). Graphs display the relationship between stomatal density and stomatal size (A), stomatal index (B) and stomatal cluster size (C). Data are means \pm SE of $n > 60$ stomata from three independent experiments. Lettering indicates statistical differences after ANOVA ($p < 0.05$), as determined by Student-Newman-Keuls test performed between *Arabidopsis* lines and between *Begonia* species. P value in graph (C) indicates significant differences between *tmm1* and *B. plebeja* plants

The mathematical model described by Franks et al. (2009) allows the estimation of maximum diffusive stomatal conductance to water vapour (G_{Wmax}) based on the anatomy stomata and stomatal aperture. Figure 4 displays maximum aperture of stomata from *Arabidopsis* and *Begonia* epidermal peels treated with opening buffer (+60 mM KCl-MES, pH 6.1) and placed under light of high intensity ($\sim 200 \mu\text{mol m}^{-2} \text{s}^{-1}$) for 2 hours. Stomatal aperture was measured by calculating the geometry of individual guard cells as well as the guard cell complex itself, as shown before (Doheny-Adams et al. 2012). Both the “clustered” *Arabidopsis* and *Begonia* plants showed impairment in stomatal opening. The *tmm1* mutant reached 24% of the *Arabidopsis* wild type stomatal aperture while stomata of *B. plebeja* opened 22% less compared to *B. coccinea*. However, the differences among the *Begonia* species were not statistically significant. The PTMM1 and *epf1/epf2* plants resulted in stomatal apertures of 24.57 ± 1.71 and 18.09 ± 1.15 μm compared to the 22.58 ± 1.54 μm of wild type, albeit the differences were not significant (Figure 4).

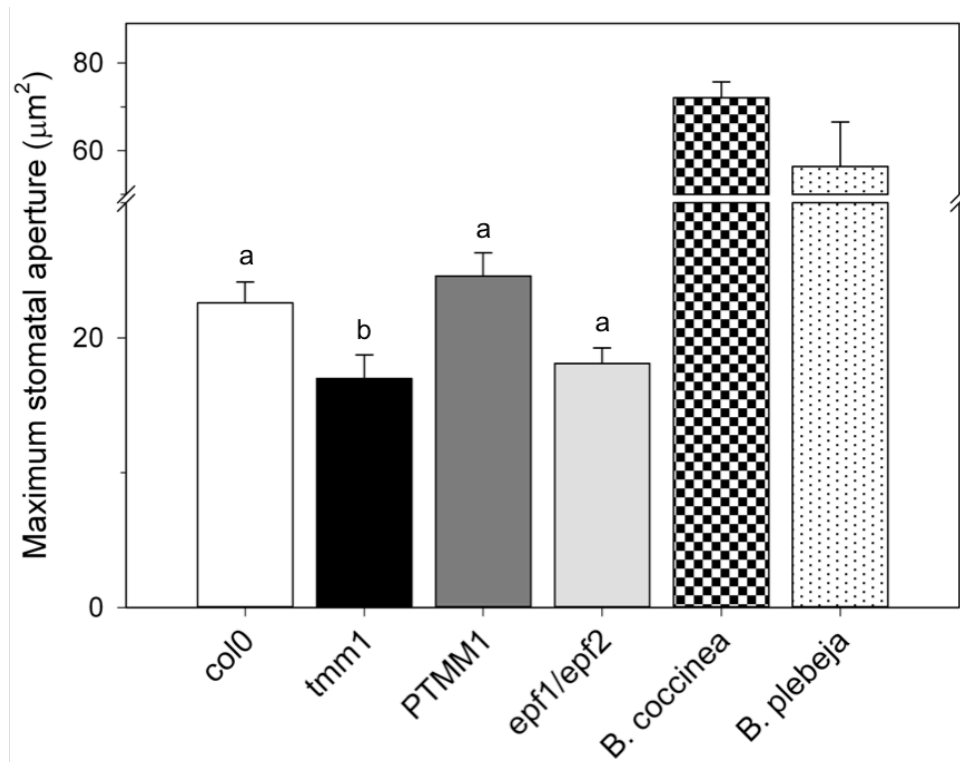


Figure 4. Stomatal clustering inhibits stomatal opening in *Arabidopsis tmm1* mutant.

Maximum stomatal aperture was measured from wild type, *tmm1*, complementation line PTMM1, *epf1/epf2*, *B. coccinea* and *B. plebeja* epidermal peels placed in opening buffer (+60 mM KCl-MES, pH 6.1). Data are means \pm SE of $n > 60$ stomata from three independent experiments. Lettering indicates statistical differences after ANOVA ($p < 0.05$), as determined by Student-Newman-Keuls test performed between *Arabidopsis* lines and between *Begonia* species.

G_{Wmax} was positively correlated with the stomatal density (Fig. 5A; $R^2=0.98$) and negatively correlated with the stomatal size (Fig 5B; $R^2=0.97$), an observation also consistent with previous reports (Franks et al. 2009; Franks & Beerling 2009). In particular, the G_{Wmax} of *tmm1* was twice of the wild type plants. The *epf1/epf2* and PTMM1 plants showed 55% and 26% higher G_{Wmax} than the wild type plants, respectively. Similarly, *B. plebeja* exhibited a 1.5-fold increase to G_{Wmax} when compared to *B. coccinea*.

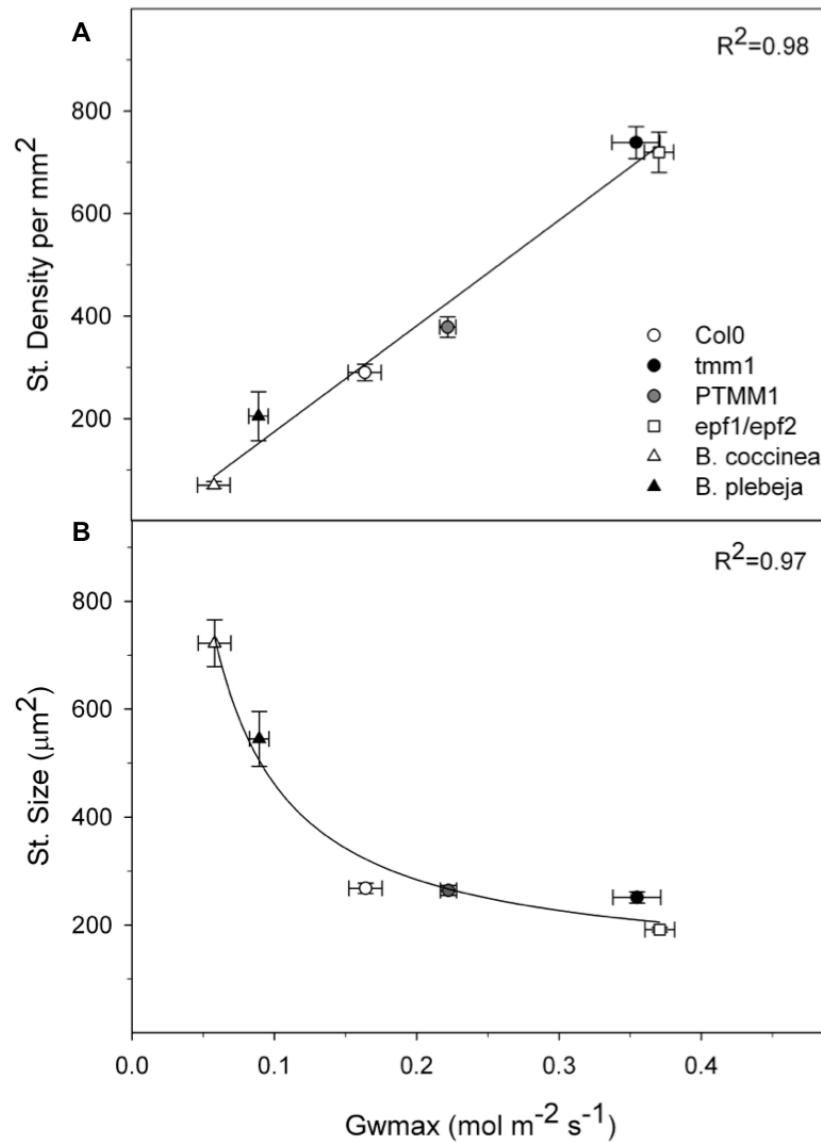


Figure 5. Relationship between maximum stomatal conductance to water vapour and stomatal pattern of *Arabidopsis* and *Begonia* plants.

Stomatal conductance was calculated based on anatomical characteristics of wild type (white circles), *tmm1* (black circles), complementation line PTMM1 (dark grey circles), *epf1/epf2* (white squares), *B. coccinea* (white triangles) and *B. plebeja* (black triangles). Maximum stomatal conductance was positively correlated with stomatal density (A; $R^2=0.98$) and negatively correlated with stomatal size (B; $R^2=0.97$). Data are means \pm SE of $n>60$ stomata from three independent experiments.

3.2.2 Light-induced gas exchange responses

The above data showed that the *Arabidopsis tmm1* and *epf1/epf2*, as well as the *B. plebeja* plants followed the relationships between stomatal conductance and stomatal density or stomatal size of the “single stomata” plants. Yet, the “clustered” stomata were defective in stomatal opening, since they did not reach the stomatal apertures of the “single stomata” lines. Hence, I was interested to address whether the stomatal clustering had an effect on the actual stomatal conductance and the gas exchange responses. For doing so, I perform IRGA measurements using light as the stimuli to drive stomatal movements. Light induces the opening of stomata allowing CO₂ entrance in the expense of water vapour release, with the two processes being measured as the CO₂ assimilation rate (A) and the transpiration rate (E). In selecting the level of the photosynthetic active radiation (PAR) to be used, I performed light curves that showed the response of A over different quantum flux densities, ranging from 0 to 800 $\mu\text{mol m}^{-2} \text{s}^{-1}$ (Figure 6). The aim was to identify the conditions that were not light-limited for photosynthesis. The *Begonia* species showed a steep response of A relative to the increased PAR reaching a steady state at approximately 100 $\mu\text{mol m}^{-2} \text{s}^{-1}$ (Figure 6A), whereas the *Arabidopsis* plants had a more gradual response, with A being saturated at PAR of approximately 370 $\mu\text{mol m}^{-2} \text{s}^{-1}$ (Figure 6B).

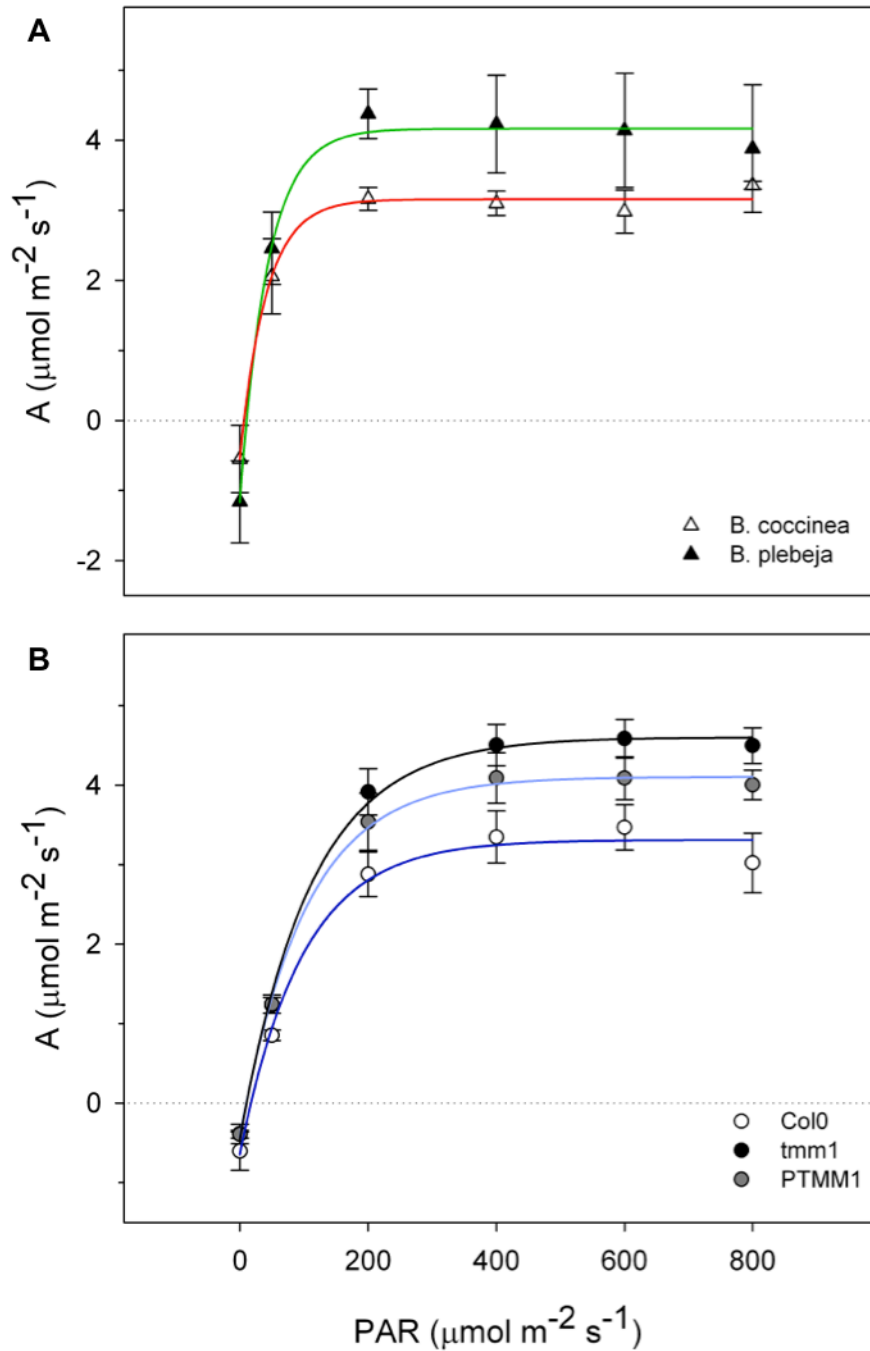


Figure 6. Effect of photosynthetic active radiation on CO₂ assimilation.

Light curves from *Begonia* (A) and *Arabidopsis* (B) plants grown under standard conditions display the assimilation of CO₂ over a range of PAR (from 0 to 800 $\mu\text{mol m}^{-2} \text{s}^{-1}$). Data were fitted to exponential rise curve and fittings are shown for *B. coccinea* (red line), *B. plebeja* (green line) and *Arabidopsis* wild type (blue line), *tmm1* (black line) and PTMM1 (light blue line). Data are means \pm SE of n=3 independent experiments.

Hence, I decided on using the three following PARs as light stimuli, $70 \mu\text{mol m}^{-2} \text{s}^{-1}$ of PAR (low light), $200 \mu\text{mol m}^{-2} \text{s}^{-1}$ of PAR (high light) and $400 \mu\text{mol m}^{-2} \text{s}^{-1}$ of PAR (saturating light). Light-induced changes of gas exchange responses were recorded by keeping constant $[\text{CO}_2]$ at 390 ppm, relative humidity at 55 - 60% and temperature at 22°C . IRGA was performed to dark-adapted *Begonia* leaves or whole three-week old *Arabidopsis* plants. Once plants have reached a steady-state of A and E under the light treatment, they were exposed back to darkness to measure transpiration during stomatal closure. Figure 7 and 8 illustrate the characteristic gas exchange responses as a function of time of all the genotypes when exposed to saturating light of $400 \mu\text{mol m}^{-2} \text{s}^{-1}$. Figure 7A and 8A presents the CO_2 assimilation of *Arabidopsis* plants and *Begonia* leaves, respectively. During the light treatment also the transpiration (E_{light}) rate was measured (Figure 7B and 8B). The transpiration rates under darkness (E_{dark}) of both *Arabidopsis* plants and *Begonia* leaves are shown in Figures 7C and 8C. Across all the genotypes, a typical biphasic response of CO_2 assimilation was observed with an initial steep increase of A followed by a slower rise to a steady-state. However, the changes between the two steady-states of E - i.e. dark to light and the reverse - appeared more gradual.

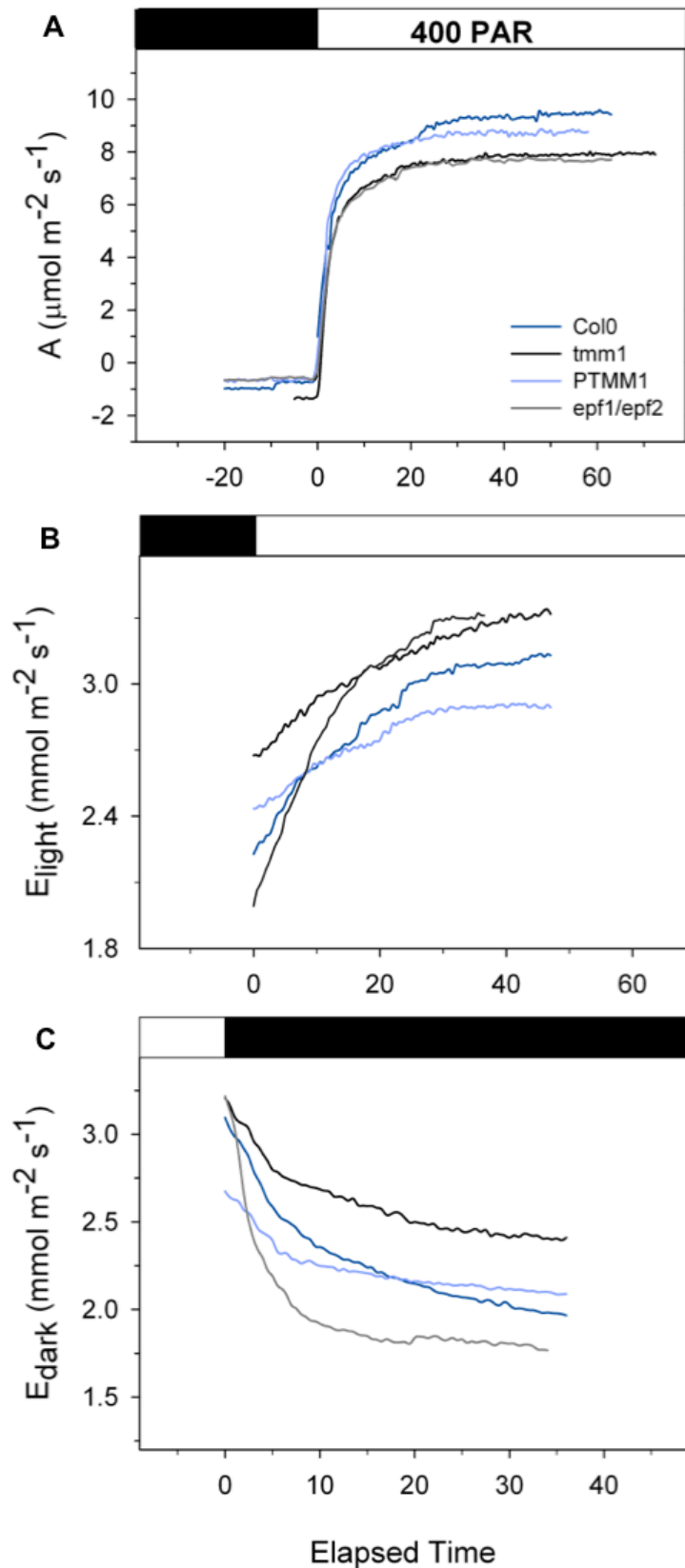


Figure 7. Time-series of gas exchange responses from *Arabidopsis* plants.

Dark-adapted *Arabidopsis* wild type (dark blue), *tmm1* (black), PTMM1 (light blue) and *epf1/epf2* (grey) plants were treated with light of $400 \mu\text{mol m}^{-2} \text{s}^{-1}$ to measure CO_2 assimilation (A) and transpiration rate (B). Plants were subsequently exposed to darkness and transpiration rate was measured (C). Data are means of $n=3$ plant per species.

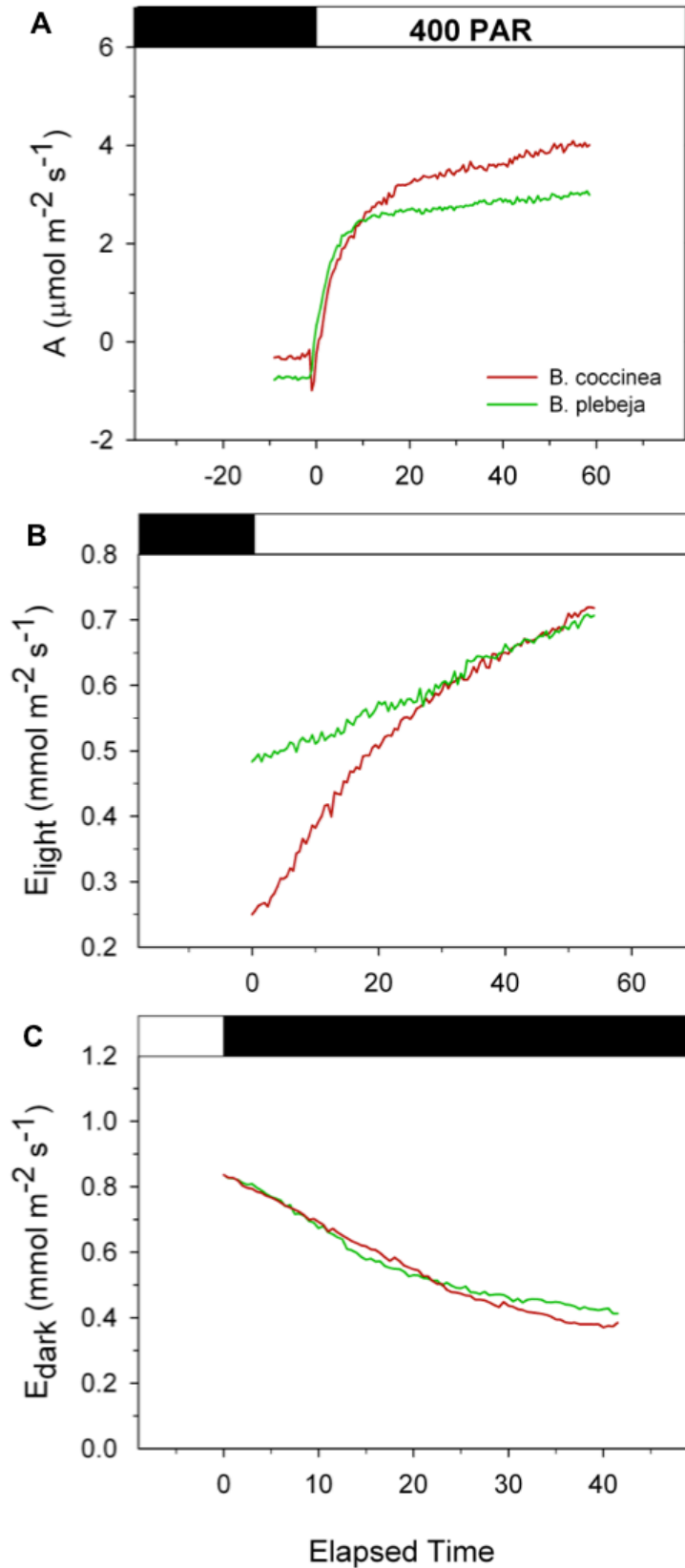


Figure 8. Time-series of gas exchange responses from *Begonias* plants.

Dark-adapted *B. coccinea* (red) and *B. plebeja* (green) leaves were treated with light of $400 \mu\text{mol m}^{-2} \text{s}^{-1}$ to measure CO₂ assimilation (A) and transpiration rate (B). Leaves were subsequently exposed to darkness and transpiration rate was measured (C). Data are means of $n=3$ plant per species.

The kinetics of the light-induced gas exchange responses were analysed by fitting a sigmoidal function to the A data and exponential rise function to the E_{light} data. For analysis of E_{dark} response, an exponential decay function was used. The averaged half-times and maximum rates of the gas exchange responses are presented in Table 1, Figure 9 and 10. In general, exposing the plants to higher intensities of light slowed down the relaxation in changes to gas exchange, as it is depicted from the half-time data. This observation was more obvious in the A and E_{dark} responses. The $t_{1/2}$ of A was about 10-fold higher at $400 \mu\text{mol m}^{-2} \text{s}^{-1}$ than at $70 \mu\text{mol m}^{-2} \text{s}^{-1}$. Similarly, the $t_{1/2}$ of E_{dark} was approximately 60% increased at $400 \mu\text{mol m}^{-2} \text{s}^{-1}$ (Figure 9). In particular, the rate of A was extremely fast and it was saturated within a few minutes from the onset of light treatment across all genotypes and light regimes (Figure 9A). By contrast, plants reached a new steady-state of E_{light} rate after 5 minutes of illumination, with the $t_{1/2}$ of *Begonias* being double of that of *Arabidopsis* plants (Figure 9B). E_{dark} response was faster than the E_{light} response, confirming the concept of stomatal closure being a faster process than stomatal opening. Stomatal clustering did not affect the speed of gas exchange response since no substantial differences in the $t_{1/2}$ observed between the “single stomata” and “clustered” plants, (Figure 9). One exception to this was the slower E_{light} response of *tmm1* comparing to wild type at $200 \mu\text{mol m}^{-2} \text{s}^{-1}$ of PAR. Additionally, the *epf1/epf2* mutant showed slightly faster gas exchange response - especially at saturating light - comparing to wild-type plant, but still this difference was not significant.

Nonetheless, stomatal clustering had a big impact on the stomatal gas exchange responses by shifting the maximum rates of A (Figure 10A), E_{light} (Figure 10B) and E_{dark} (Figure 10C). Increasing the quantum flux density resulted to higher rates of A and E_{light} . Similarly, adaptation to increasing PARs elevated the E_{dark} in all *Arabidopsis* genotypes, whereas *B. plebeja* and *B. coccinea* exhibited the highest gas exchange rates at $200 \mu\text{mol m}^{-2} \text{s}^{-1}$ of PAR. The *Begonia* species did not differ between each other in A under any light treatment, however significant differences were observed among the *Arabidopsis* lines (Figure 10A). In particular, at $70 \mu\text{mol m}^{-2} \text{s}^{-1}$ the mean maximum photosynthetic rate (A_{max}) of *epf1/epf2* double mutant was $2.43 \pm 0.08 \mu\text{mol m}^{-2} \text{s}^{-1}$ comparing to the $1.99 \pm 0.11 \mu\text{mol m}^{-2} \text{s}^{-1}$ of wild type plants. The A_{max} of *tmm1* mutants was 1.79 ± 0.05

and did not substantially differ from that of the wild type and PTMM1 plants. Increasing the light at $200 \mu\text{mol m}^{-2} \text{s}^{-1}$, the *epf1/epf2* double mutant showed similar A_{max} to wild type, as also the *tmm1* plants did. However, at saturating light, the *tmm1* plants failed to reach the “single stomata” steady-state of A , whereas no difference was observed on the A_{max} of *epf1/epf2* double mutants comparing to the wild type plants. At this condition, the *tmm1* plants exhibited a 20% decrease in A_{max} , corresponding to a value of $7.8 \pm 0.23 \mu\text{mol m}^{-2} \text{s}^{-1}$ comparing to the $9.26 \pm 0.53 \mu\text{mol m}^{-2} \text{s}^{-1}$ of wild type plants. This latter finding inferred to a failure of stomatal opening when conditions favour maximum photosynthetic rates (Figure 10A).

Light treatment also resulted in an enhancement of the transpiration rate, with higher the PAR the higher the E_{light} being. As the G_{Wmax} data suggested, transpiration rate of mutants with high stomatal density should be higher compared to wild type plants. Indeed, the *epf1/epf2* double mutants exhibited greater E_{light} rate compared to wild type at all PARs, but this observation was only statistically significant at $70 \mu\text{mol m}^{-2} \text{s}^{-1}$ of PAR (Figure 10B). In contrast, the E_{light} rate of *tmm1* mutants was not substantially different from the wild type, despite their greater stomatal number, indicating an impaired stomatal function to reach their maximum stomatal conductance. At the two light extremes (70 and $400 \mu\text{mol m}^{-2} \text{s}^{-1}$), *Begonias* did not differ in the E_{light} rate, though when the light intensity was set at $200 \mu\text{mol m}^{-2} \text{s}^{-1}$ the “clustered” *B. plebeja* reached a 1.5-fold suppressed steady state of E_{light} compared to *B. coccinea* (Figure 10B). The latter observation further highlights the compromised opening of stomata due to clustering, and it hints to a potential role of stomatal clustering in minimizing the transpirational water loss.

By exposing the plants back to darkness, I was able to measure the transpiration rate and associate it with the short-term adaptation to the given light regime (Figure 10C). The wild type and PTMM1 plants showed very similar E_{dark} rates at the three light regimes. The highest E_{dark} rate was detected when *Arabidopsis* plants were adapted to high light intensity, with this phenomenon being more apparent for the stomatal patterning mutants. In particular, exposure of the *tmm1* and *epf1/epf2* plants to darkness, after being adapted to $70 \mu\text{mol m}^{-2} \text{s}^{-1}$, resulted to 65% and 98% increase in E_{dark} rate in comparison with the wild type.

Additionally, the *tmm1* mutant plants did show 1.2-fold increase in E_{dark} rate at $400 \mu\text{mol m}^{-2} \text{s}^{-1}$ of PAR, corresponding to $2.33 \pm 0.07 \text{ mmol m}^{-2} \text{s}^{-1}$ compared to $1.88 \pm 0.06 \text{ mmol m}^{-2} \text{s}^{-1}$ of wild type plants. When the leaves were adapted at low and high light, the mean steady-state of E_{dark} rate ranged between 0.18 ± 0.02 and $0.30 \pm 0.05 \text{ mmol m}^{-2} \text{s}^{-1}$ for both *Begonia* species. At $200 \mu\text{mol m}^{-2} \text{s}^{-1}$, the E_{dark} rate was higher for *B. coccinea* comparing to the other two light regimes, while it remained the same for *B. plebeja*. However, the stomatal clustering in *Begonia* did not influence the E_{dark} responses under any light regime, since no significant differences between the two species occurred. The distinct effects of stomatal clustering in the E_{dark} responses in *Arabidopsis tmm1* mutant and *B. plebeja* further emphasize on the significance of proper stomatal spacing to facilitate gas exchange responses, and they distinguish the two types of stomatal clustering.

Table 1. Gas exchange data from *Arabidopsis* and *Begonia* plants under three different light regimes were fitted to non-linear regression models to extrapolate the kinetics for CO₂ assimilation response, transpiration under light and under darkness.

CO ₂ assimilation	70 μmol m ⁻² s ⁻¹ of PAR		200 μmol m ⁻² s ⁻¹ of PAR		400 μmol m ⁻² s ⁻¹ of PAR	
	t _{1/2} (mins)	A _{max} (μmol m ⁻² s ⁻¹)	t _{1/2} (mins)	A _{max} (μmol m ⁻² s ⁻¹)	t _{1/2} (mins)	A _{max} (μmol m ⁻² s ⁻¹)
Col0	0.2 ±0.01	1.99 ±0.11	0.78 ±0.11	4.43 ±0.4	2.03 ±0.67	9.26 ±0.53
<i>tmm1</i>	0.23 ±0.00	1.79 ±0.05	0.52 ±0.08	4.77 ±0.07	1.48 ±0.3	7.80 ±0.23
PTMM1	0.42 ±0.1	1.94 ±0.23	0.54 ±0.02	5.68 ±0.35	1.21 ±0.08	8.87 ±0.28
<i>epf1/epf2</i>	0.29 ±0.03	2.43 ±0.08	0.51 ±0.04	4.57 ±0.41	1.41 ±0.19	8.94 ±0.29
<i>B. coccinea</i>	0.45 ±0.05	2.27 ±0.13	1.26 ±0.15	3.39 ±0.10	2.7 ±0.61	2.79 ±0.31
<i>B. plebeja</i>	0.63 ±0.09	2.51 ±0.25	1.6 ±0.14	3.11 ±0.36	2.6 ±0.71	4.07 ±0.47

Stomatal clustering influences stomatal movements

Transpiration under light	70 $\mu\text{mol m}^{-2} \text{s}^{-1}$ of PAR		200 $\mu\text{mol m}^{-2} \text{s}^{-1}$ of PAR		400 $\mu\text{mol m}^{-2} \text{s}^{-1}$ of PAR	
	$t_{1/2}$ (min)	E_{max} ($\text{mmol m}^{-2} \text{s}^{-1}$)	$t_{1/2}$ (min)	E_{max} ($\text{mmol m}^{-2} \text{s}^{-1}$)	$t_{1/2}$ (min)	E_{max} ($\text{mmol m}^{-2} \text{s}^{-1}$) 1)
Col0	5.98 \pm 0.46	1.68 \pm 0.15	7.16 \pm 0.66	2.01 \pm 0.15	12.62 \pm 2.46	3.23 \pm 0.17
<i>tmm1</i>	5.81 \pm 0.37	1.49 \pm 0.05	15.9 \pm 2.77	2.03 \pm 0.11	14.01 \pm 2.65	3.37 \pm 0.03
PTMM1	4.74 \pm 0.58	1.26 \pm 0.22	9.76 \pm 0.92	2.56 \pm 0.34	11.15 \pm 1.18	2.94 \pm 0.06
<i>epf1/epf2</i>	7.9 \pm 1.02	2.39 \pm 0.14	9.73 \pm 2.18	2.45 \pm 0.18	9.35 \pm 1.70	3.42 \pm 0.54
<i>B. coccinea</i>	18.54 \pm 3.35	0.58 \pm 0.06	44.4 \pm 9.77	1.17 \pm 0.12	19.14 \pm 3.24	0.91 \pm 0.07
<i>B. plebeja</i>	15.37 \pm 2.58	0.46 \pm 0.04	23.4 \pm 10.2	0.74 \pm 0.01	18.70 \pm 2.42	1.28 \pm 0.25

Stomatal clustering influences stomatal movements

Transpiration under darkness	70 $\mu\text{mol m}^{-2} \text{s}^{-1}$ of PAR		200 $\mu\text{mol m}^{-2} \text{s}^{-1}$ of PAR		400 $\mu\text{mol m}^{-2} \text{s}^{-1}$ of PAR	
	$t_{1/2}$ (min)	E_{min} ($\text{mmol m}^{-2} \text{s}^{-1}$)	$t_{1/2}$ (min)	E_{min} ($\text{mmol m}^{-2} \text{s}^{-1}$)	$t_{1/2}$ (min)	E_{min} ($\text{mmol m}^{-2} \text{s}^{-1}$)
Col0	4.42 \pm 0.89	0.73 \pm 0.06	3.3 \pm 1.07	1.3 \pm 0.05	12.62 \pm 2.46	1.88 \pm 0.06
<i>tmm1</i>	5.47 \pm 1.16	1.20 \pm 0.02	12.7 \pm 4.41	1.22 \pm 0.07	14.01 \pm 2.65	2.33 \pm 0.07
PTMM1	3.44 \pm 0.92	0.83 \pm 0.19	5.71 \pm 0.89	1.53 \pm 0.14	11.15 \pm 1.18	1.99 \pm 0.1
<i>epf1/epf2</i>	3.03 \pm 0.06	1.44 \pm 0.11	5.26 \pm 1.37	1.68 \pm 0.24	9.35 \pm 1.7	1.78 \pm 0.34
<i>B. coccinea</i>	6.46 \pm 1.6	0.25 \pm 0.02	10.3 \pm 1.34	0.50 \pm 0.08	19.14 \pm 3.24	0.30 \pm 0.05
<i>B. plebeja</i>	5.51 \pm 0.72	0.18 \pm 0.02	5.97 \pm 1.04	0.31 \pm 0.02	18.7 \pm 2.42	0.24 \pm 0.08

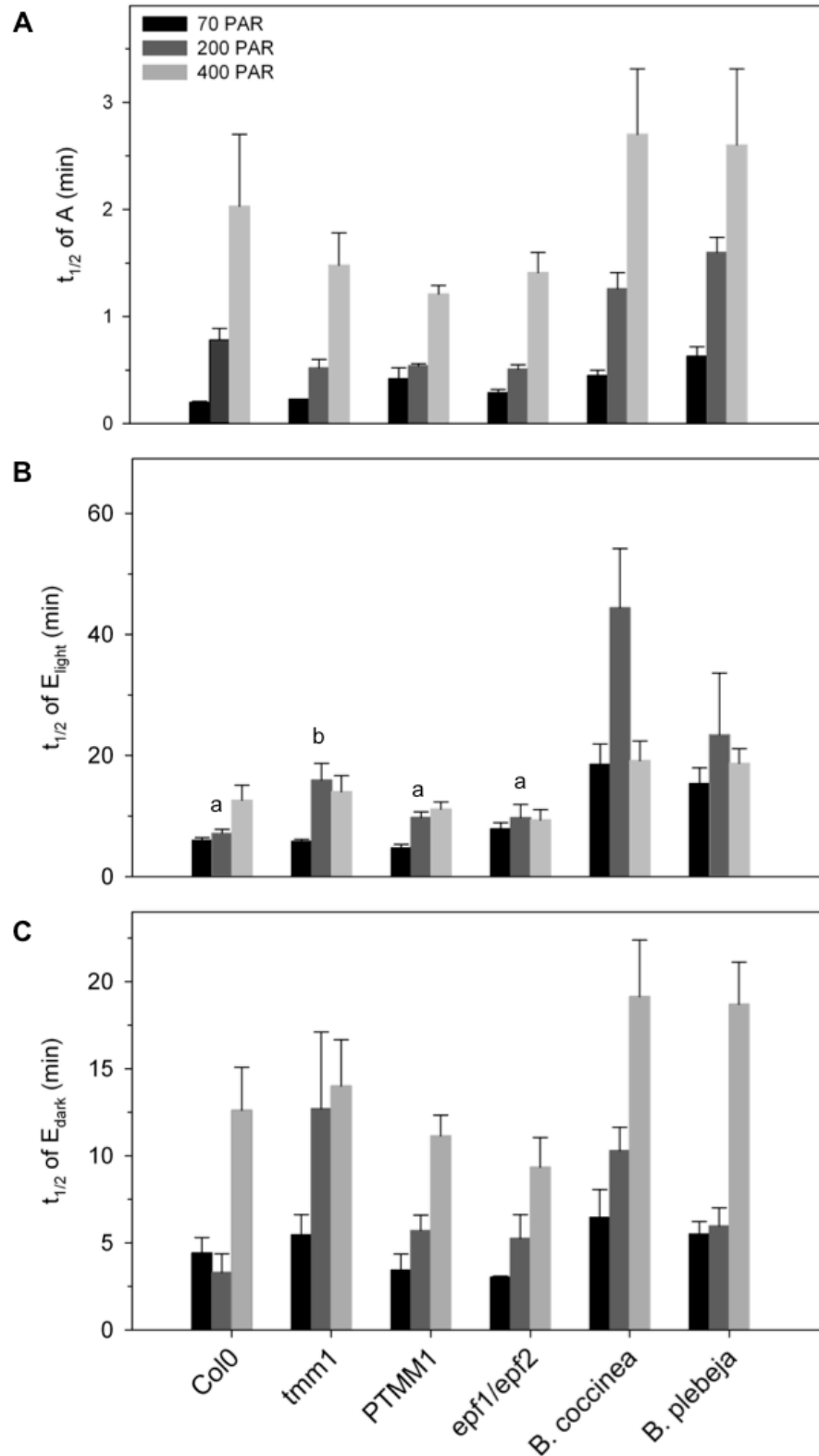


Figure 9. Half-times of gas exchange responses triggered by light or darkness.

Dark-adapted plants were treated with PAR of 70 (black), 200 (dark grey) and 400 (grey) $\mu\text{mol m}^{-2} \text{s}^{-1}$ and then exposed to darkness. Graphs present half-times ($t_{1/2}$) for CO_2 assimilation (A), transpiration under light (B) and transpiration under darkness (C). Data are means \pm SE of $n=3$ plant per species. Lettering indicates significant differences after ANOVA ($p < 0.05$), as determined by Student-Newman-Keuls test performed between *Arabidopsis* lines and between *Begonia* species at each light condition.

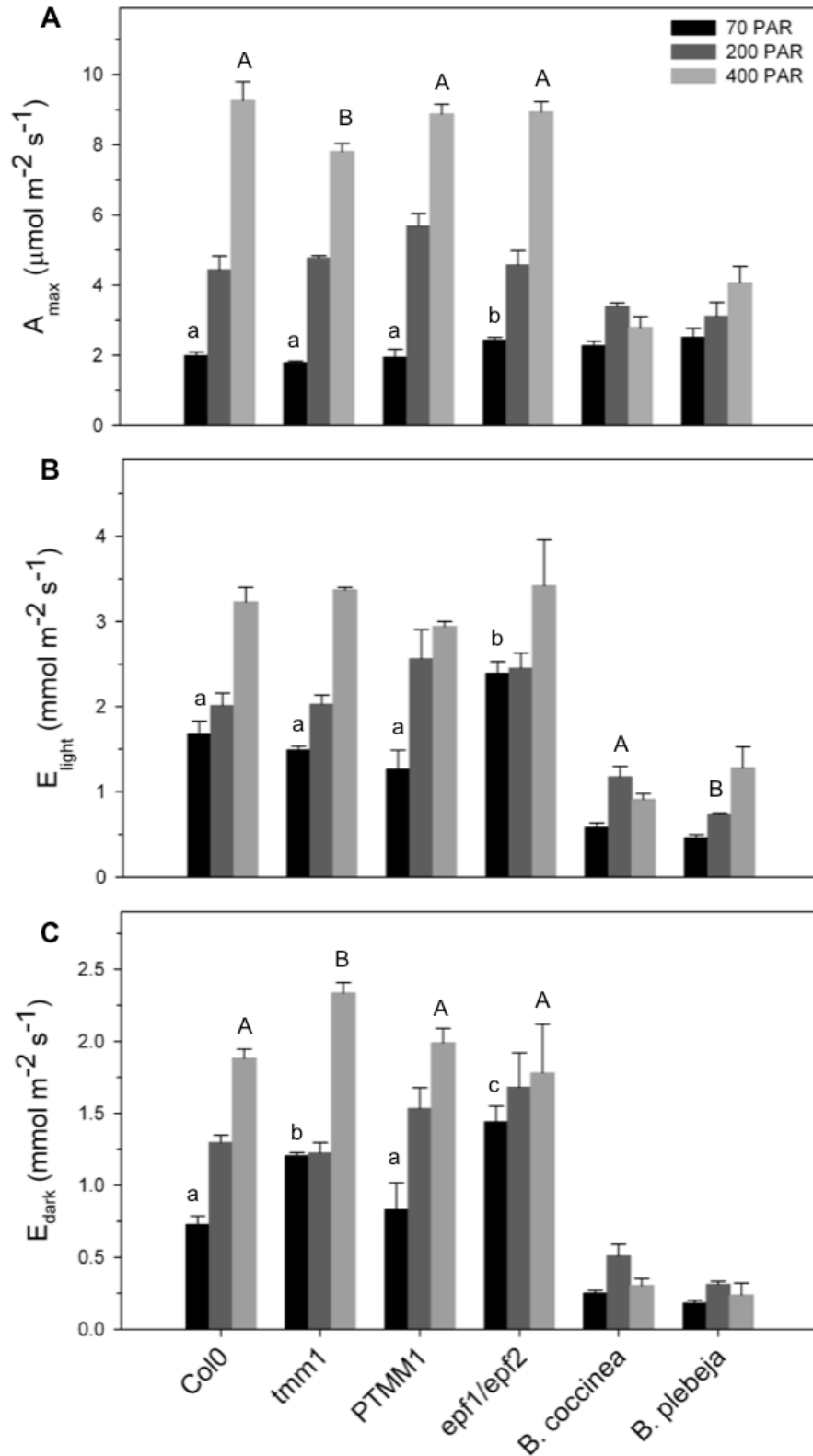


Figure 10. Steady-state rates of gas exchange responses triggered by light or darkness.

Dark-adapted plants were treated with PAR of 70 (black), 200 (dark grey) and 400 (grey) $\mu\text{mol m}^{-2} \text{s}^{-1}$ and then expose to darkness. Graphs present maximum rates of CO₂ assimilation (A), transpiration under light (B) and transpiration under darkness (C). Data are means \pm SE of n=3 plant per species. Lettering and asterisks indicate statistical differences after ANOVA ($p < 0.05$), as determined by Student-Newman-Keuls test performed between *Arabidopsis* and between *Begonias* at each light condition.

To further investigate the potential advantage for water conservation of the “clustered” plants, I estimated the water use efficiency (WUE) as the ratio of A to E (Table 2). WUE describes the amount of dry matter produced per unit of water transpired through stomata of the plant, and therefore plants optimize WUE through balancing the trade off between CO₂ influx and H₂O efflux. Figure 11 presents the calculated WUE of all genotypes at the three distinct light regimes. Raising light intensity results in higher WUE as more CO₂ is assimilated per water unit transpired. Indeed, this trend was observed across the *Arabidopsis* plants with single stomata, including the *epf1/epf2* double mutant. At 400 $\mu\text{mol m}^{-2} \text{s}^{-1}$ of PAR, the WUE of wild type, PTMM1 and *epf1/epf2* plants was 2.89 ± 0.28 , 3.07 ± 0.23 and 2.74 ± 0.09 $\mu\text{mol CO}_2 \text{ mol}^{-1} \text{ H}_2\text{O}$, respectively. In contrast, the *tmm1* mutant did not show an elevation in WUE at saturating light, which was approximately 20% reduced in comparison with the wild type plants. The picture in *Begonias* is completely reversed. The plants showed a reduction in WUE as the light intensity got higher. The maximum potential for WUE was evident at low light, where *B. coccinea* and *B. plebeja* resulted in 4.02 ± 0.4 and 5.53 ± 0.73 $\mu\text{mol CO}_2 \text{ mol}^{-1} \text{ H}_2\text{O}$, respectively. This finding might be due to the ecological adaptation of *Begonias* in lower light intensities given that they are usually found at the lower part of the canopy. Also, stomatal clustering in *Begonias* allowed the enhancement of WUE, as at 70 and 200 $\mu\text{mol m}^{-2} \text{s}^{-1}$ of PAR the *B. plebeja* plants exhibited 1.4-fold increase in WUE comparing to *B. coccinea* plants. The WUE data suggested an advantage of *B. plebeja* to optimize the water usage, especially at low light. This was not apparent for the *tmm1* mutant, also highlighting on the difference between contiguous and non-contiguous clustering.

Table 2. Maximum water use efficiency from *Arabidopsis* and *Begonia* plants under three different light regimes.

WUE (μmol of CO_2 per mmol H_2O)	70 $\mu\text{mol m}^{-2} \text{s}^{-1}$ of PAR	200 $\mu\text{mol m}^{-2} \text{s}^{-1}$ of PAR	400 $\mu\text{mol m}^{-2} \text{s}^{-1}$ of PAR
Col0	1.20 \pm 0.12	2.20 \pm 0.05	2.89 \pm 0.28
<i>tmm1</i>	1.21 \pm 0.07	2.37 \pm 0.16	2.32 \pm 0.06
PTMM1	1.72 \pm 0.54	2.28 \pm 0.25	3.07 \pm 0.23
<i>epf1/epf2</i>	1.02 \pm 0.04	1.90 \pm 0.26	2.74 \pm 0.09
<i>B. coccinea</i>	4.02 \pm 0.4	2.94 \pm 0.24	3.07 \pm 0.39
<i>B. plebeja</i>	5.53 \pm 0.73	4.21 \pm 0.51	3.53 \pm 0.10

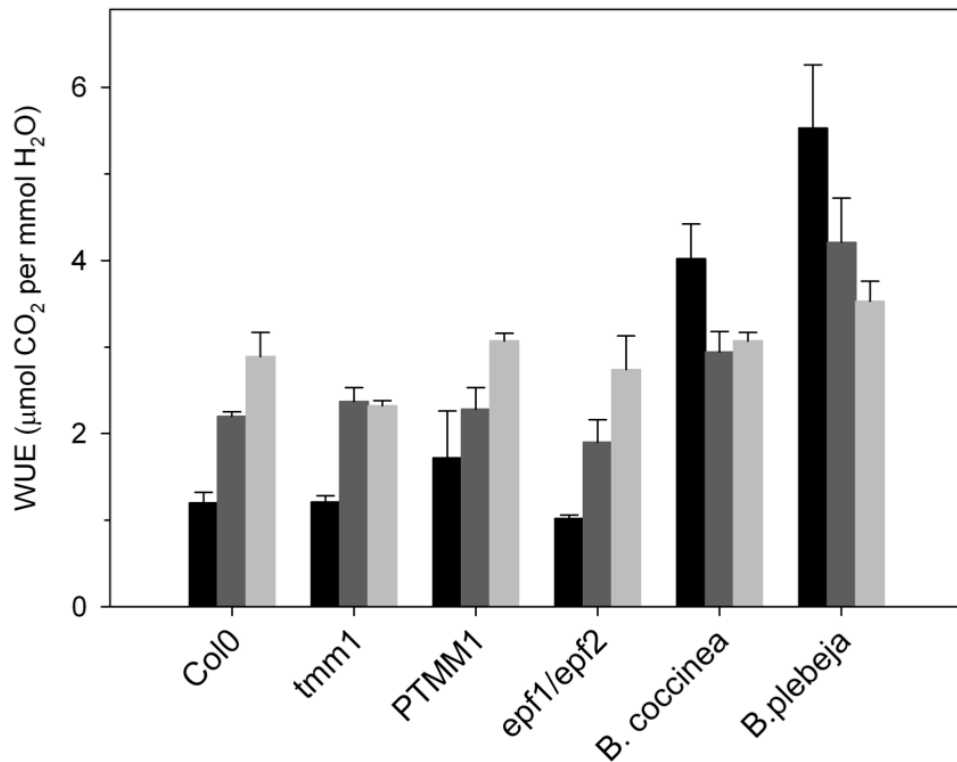


Figure 11. Water use efficiency of *Arabidopsis* and *Begonia* plants under three light regimes.

Water use efficiency estimated as the ratio of maximum A rate over transpiration at light rate at PAR of 70 (black), 200 (dark grey) and 400 (grey) $\mu\text{mol m}^{-2} \text{s}^{-1}$. Data are means \pm SE of n=3 plant per species. No statistical differences were detected after ANOVA ($P < 0.05$).

3.2.3 Stomatal clustering influences light-induced gas exchange responses

The gas exchange data as well as their deviation from the estimated G_{Wmax} data pointed to an altered stomatal behaviour in the “clustered” genotypes, and especially suggesting the impairment of stomatal movements in the plants exhibiting contiguous stomatal clusters. To further clarify that, I normalized the data to the evaporative unit area assuming that each stoma constitutes one evaporative unit (Figure 11A) or that each cluster makes one evaporative unit (Figure 11B and C). I performed this analysis only on the gas exchange data at saturating light ($400 \mu\text{mol m}^{-2} \text{s}^{-1}$), where differences were more prominent.

The genotypes with higher stomatal density (valleys in area plots; Figure 11A) displayed a significant reduction in gas exchange at the evaporative unit level comparing to the plants with normal stomatal patterning (peaks of area plots; Figure 11A). This observation could be expected as the size of stoma in the *epf1/epf2* plants and *B. plebeja* is much smaller than that of the *Arabidopsis* wild type and *B. coccinea*, respectively (Figure 3A). In contrast, because the *tmm1* mutant did not exhibit smaller stomata than the wild type plants, the reduced gas exchange responses under light can be accounted to the suppressed stomatal opening. Similarly, high stomatal density was associated with a reduction in E_{dark} response per stoma, with the *epf1/epf2* mutant and *B. plebeja* showing 65% and 72% reduction comparing to their respective “single stomata” genotypes. The *tmm1* showed only 40% suppression in E_{dark} per stoma when compared to the wild type plants, implying that the stomatal movements in these plants were attenuated.

Considering the stomatal cluster as being an individual evaporative unit, gas exchange responses per stomatal unit were indeed significantly reduced in *tmm1* mutants compared to the “single stomata” *Arabidopsis* lines (Figure 11 B and C). In particular, the maximum CO_2 assimilation rate of *tmm1* plants was 61% declined in comparison with the wild type plants. The *epf1/epf2* resulted in similar CO_2 assimilation rate to the wild type, while the PTMM1 plants showed a slight increase. The transpiration rate of *tmm1* plants, at $400 \mu\text{mol m}^{-2} \text{s}^{-1}$ but also when switched back to darkness, was half of the wild type whereas no discernible differences among the “single stomata” lines were detected. The gas

exchange responses of *B. plebeja* at the stomatal cluster level did not differ from those of *B. coccinea*. Altogether the data suggested that stomata in non-contiguous clusters are indeed functional, while the lack of spacing between stomata in contiguous clusters prevents stomatal movements in a “single stomata” fashion.

Stomatal clustering influences stomatal movements

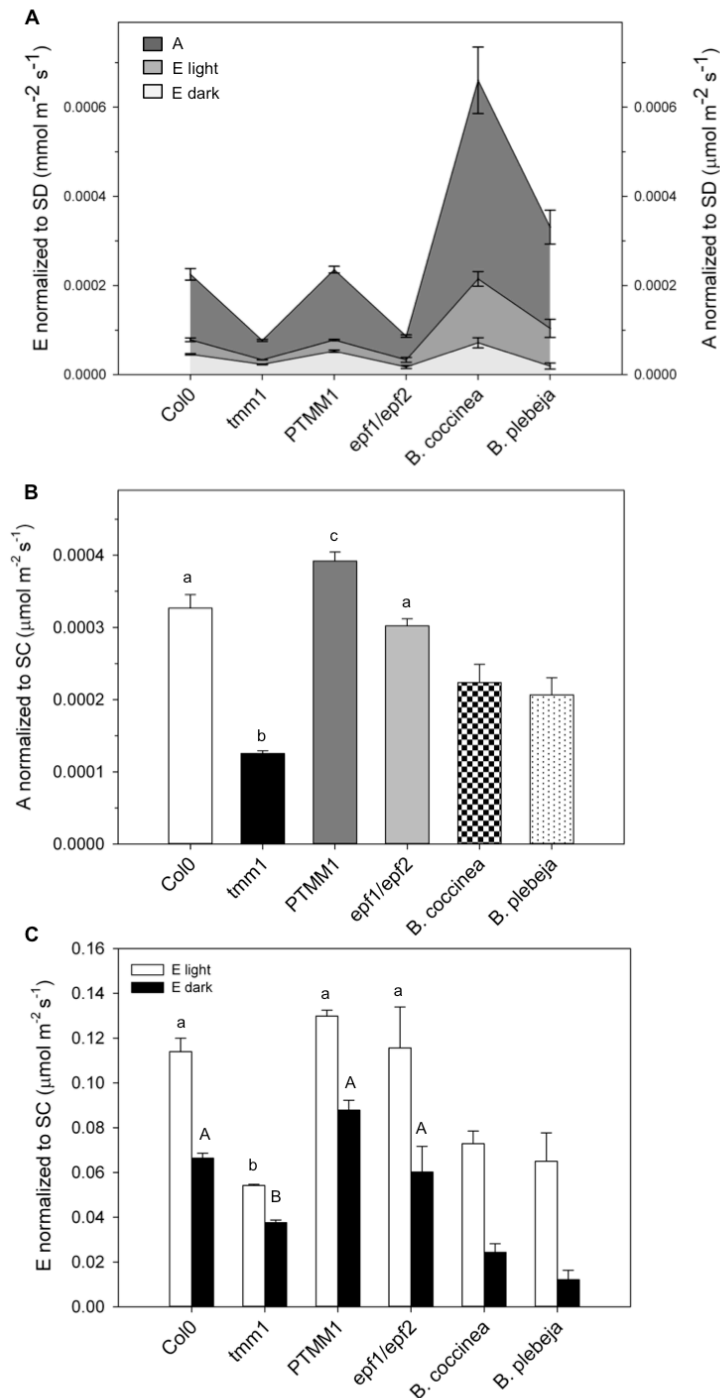


Figure 12. Stomatal patterning affects the gas exchange responses.

Maximum rates of gas exchange from *Arabidopsis* and *Begonia* plants measured at $400 \mu\text{mol m}^{-2} \text{s}^{-1}$ of PAR were normalized to either stomatal density or cluster. (A) Graph represents the normalization of CO₂ assimilation (dark grey), transpiration under light (grey) and under darkness (light grey) to stomatal density. Graphs represent normalization of maximum rate of CO₂ assimilation to stomatal cluster (B), whereas normalized maximum rate of transpiration under light (white bars) and darkness (black bars) to stomatal cluster is shown in (C). Data are means \pm SE of n=3 plant per species. Lettering indicates statistical differences after ANOVA ($p < 0.05$), as determined by Student-Newman-Keuls test performed between *Arabidopsis* lines and between *Begonia* species.

In order to further investigate the reduced gas exchange responses and impaired stomatal movements of the “clustered” plants, measurement of stomatal conductance (G_s) at the leaf level was carried out, as it is a more direct measure of the stomatal behaviour. Figure 13 presents the stomatal conductance at $400 \mu\text{mol m}^{-2} \text{s}^{-1}$. Surprisingly, wild type, *tmm1* and PTMM1 plants showed similar steady-states of G_s , corresponding to values of 0.30, 0.35 and $0.27 \text{ mmol m}^{-2} \text{s}^{-1}$, respectively. The *epf1/epf2* double mutant exhibited approximately 22% higher G_s than the wild type and *tmm1* plants. *B. plebeja* also reached the same steady-state of G_s as *B. coccinea*, yielding G_s of 0.081 ± 0.003 and $0.074 \pm 0.007 \text{ mol m}^{-2} \text{s}^{-1}$, respectively. These findings implied that stomatal clustering actually prevented plants to reach the maximum $G_{W_{\max}}$, while the *epf1/epf2* mutant with high stomatal density followed the relationship presented in Figure 5A. Furthermore, I compared the anatomical and diffusive stomatal conductance considering the “single stomata” and “clustered” plants as two separate groups (Figure 13B). Both groups showed a positive relationship between the two parameters when regression models were fitted to the data. Regression analysis was performed for each of the groups and was compared against a 1:1 reference regression, which entails a perfect match between $G_{W_{\max}}$ and G_s . Only, the slope of the regression model for “clustered” plants was significantly different ($p < 0.001$) than the 1:1 reference regression model, reinforcing the previous data and particularly the negative effect of stomatal clustering on stomatal movements.

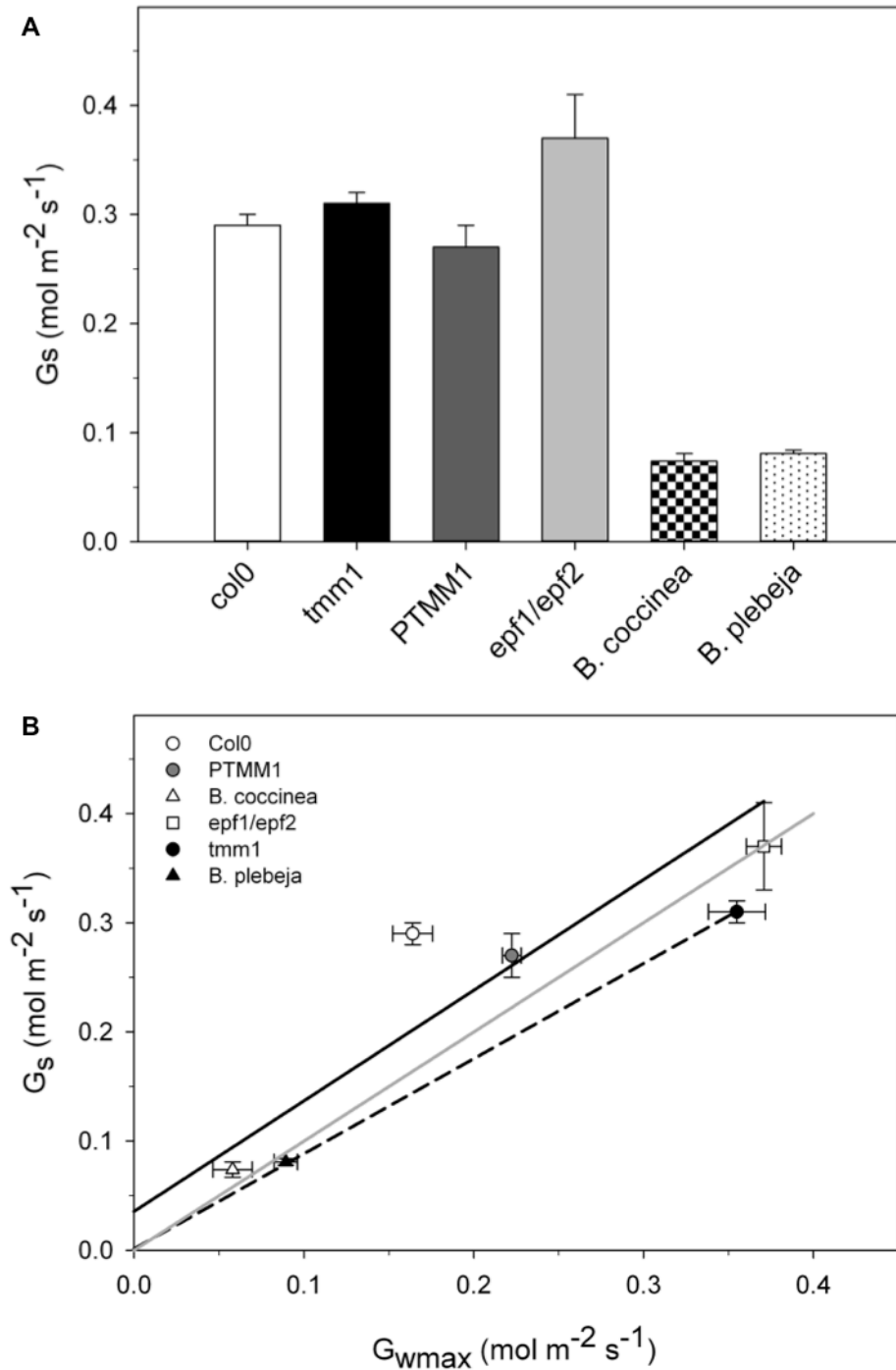


Figure 13. Stomatal clustering suppresses stomatal conductance.

(A) Diffusive stomatal conductance from whole *Arabidopsis* or *Begonia* mature leaves at 400 $\mu\text{mol m}^{-2} \text{s}^{-1}$ of PAR. (B) Correlation between the anatomical ($G_{w\text{max}}$) and diffusive (G_s) stomatal conductance from whole *Arabidopsis* plants or *Begonia* leaves. 1:1 reference regression model is shown in grey solid line. Slope of regression model for single stomata-bearing plants (solid black line) does not differ from that of the 1:1 reference ($p < 0.34$), while the slope of regression model for «clustered» plants (black dashed line) is significant different than 1:1 regression ($p < 0.001$). Data are means \pm SE of $n=3$ independent experiments.

3.2.4 Stomatal clustering results in altered ion transport

Up to this point, I have presented the impaired gas exchange responses due to stomatal clustering as well as the failure of the “clustered” plants to reach the maximum stomatal aperture of “single stomata” plants. I was also interested to examine the functionality of the pore in “single stomata” and “clustered” plants during stomatal closure. For this purpose, epidermal peels, which were pretreated with opening buffer and light for 2 hours, were placed in buffer containing 6 mM CaCl_2 (closing buffer; Figure 14A). It is known that external Ca^{2+} coupled with membrane depolarization result in the activation of the outward- K^+ channels that lead to the K^+ efflux and so stomatal closure (Grabov & Blatt 1998; Blatt 2000). Stomatal aperture was measured before and after the treatment and the relative stomatal closure was estimated on cell-by-cell basis. The stomata of *tmm1* mutant appeared defective in closing, as the mutant showed less than 50% stomatal closure in comparison with the approximately 60% closure of the single stomata-bearing *Arabidopsis* lines. In contrast, the *Begonia* species did not show such pronounced difference in stomatal closing. Additionally, I carried out a time-course of stomatal closure under the influence of ABA. For this experiment, the same procedure as above was followed, except of that the cells were treated with 20 μM ABA and imaged every 10 minutes and up to 90 minutes after exposure to the treatment (Figure 14B). The “single stomata” from the wild type and the *epf1/epf2* lines exhibited smaller stomatal pores than the *tmm1* and *PTMM1* lines. The hindered closure of *PTMM1* plants under the ABA treatment might be the result of overexpression on *TMM1* under 35S promoter or even the presence of GFP tag at the C-terminus. However, the closing process of *tmm1* was significantly inhibited than the rest of the lines, resulted in 26% relative maximum closure when compared to the 56%, 43% and 59% of wild type, *PTMM1* and *epf1/epf2* stomata, respectively. To address whether the defective stomatal closure was dependent on the ion concentration found on the apoplast, considering the high SI of *tmm1* mutants, I performed a time-course of stomatal closure under a constant flow of standard buffer solution containing 20 μM ABA. Figure 15 presents stomatal closure of wild type and *tmm1* plants under constant or no flow of buffer solution. The *tmm1* plants also failed to close as the wild type plants under continuous flowing solution,

suggesting that the observed differences were not dependent on the availability of ions since the apoplast volume was constantly exchanged with flowing solution. Fitting exponential decay curves to compare the kinetics of the closing process did not reveal any significant differences on the half-times between the wild type and *tmm1* plants.

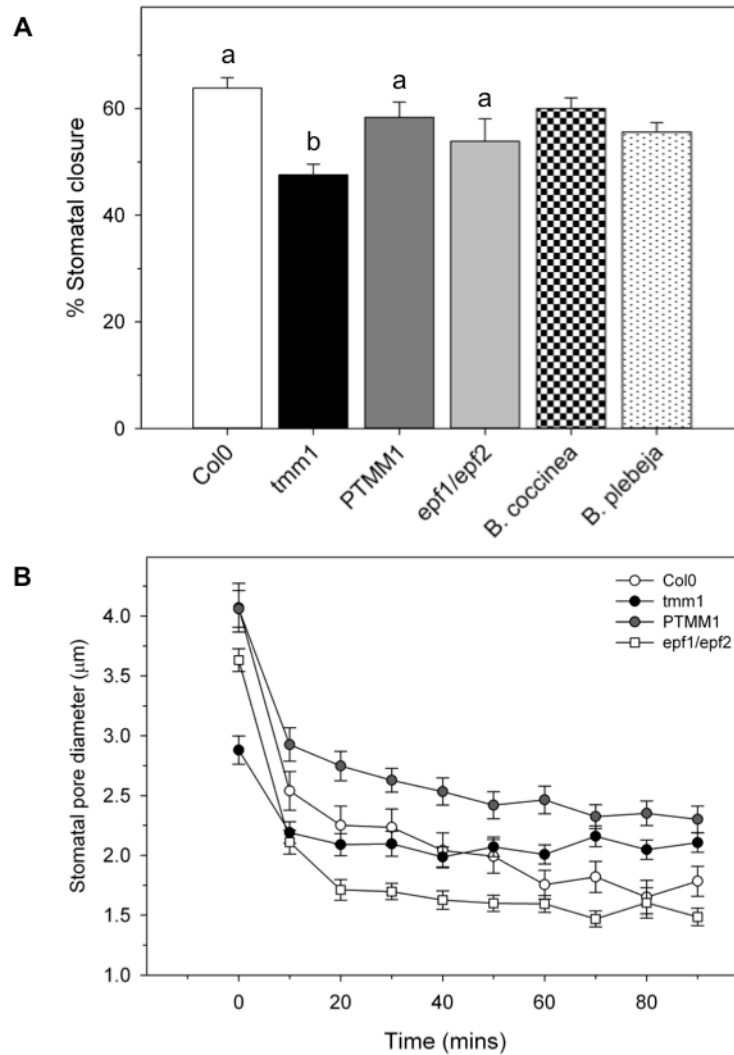


Figure 14. Stomatal clustering inhibits closure in *Arabidopsis tmm1* mutant.

Epidermal peels from wild type, *tmm1*, complementation line PTMM1, *epf1/epf2*, *B. coccinea* and *B. plebeja* plants were placed in opening buffer and under light to ensure maximum stomatal opening. They were subsequently treated with buffer containing 6 mM CaCl₂ (**A**) or 20 μM ABA (**B**) to induce stomatal closure. Relative stomatal closing was measured on cell-by-cell basis. Data are means ±SE of n>80 stomata from three independent experiments. Lettering indicates statistical differences after ANOVA (p<0.001), as determined by Student-Newman-Keuls test performed between *Arabidopsis* lines.

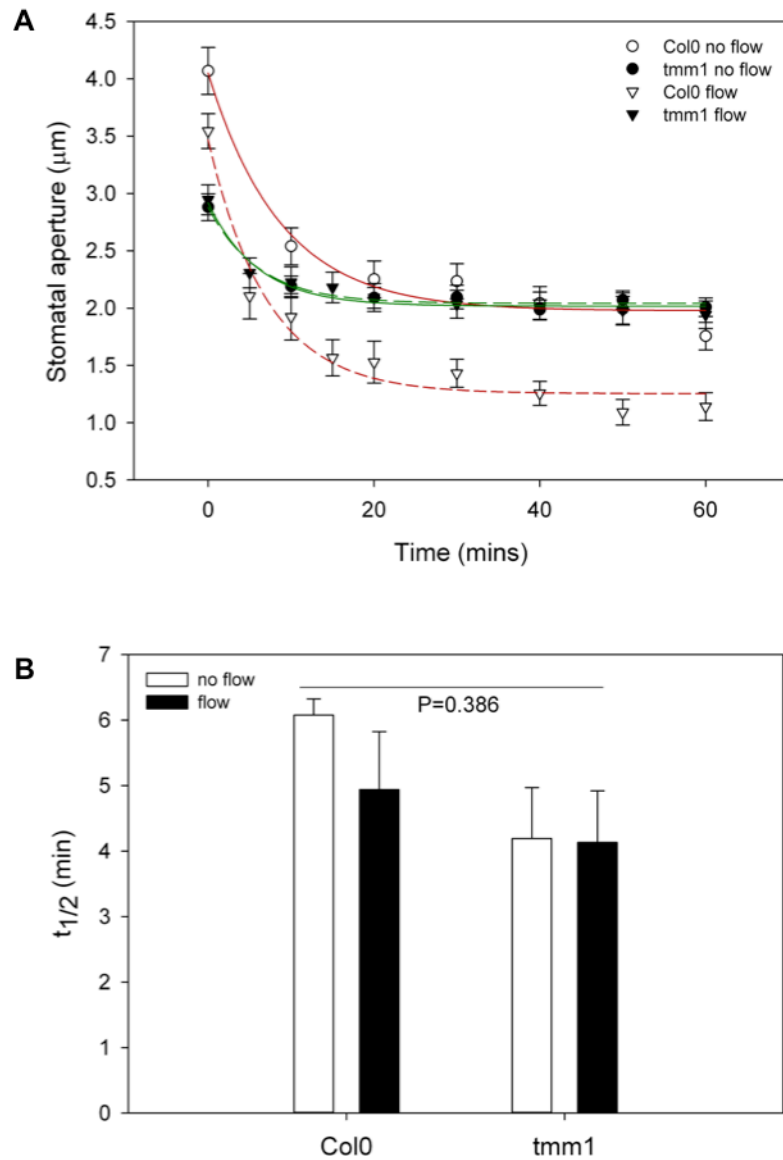


Figure 15. Stomatal clustering inhibits closure in *Arabidopsis tmm1* mutant independently of the availability of ions in the apoplast.

Epidermal peels from wild type and *tmm1* plants were placed in opening buffer and under light to ensure maximum stomatal opening. They were subsequently treated with standard buffer containing 20 μM ABA to induce stomatal closure (**A**). Relative stomatal closure was measured on cell-by-cell basis. Data are means ±SE of n>30 stomata from three independent experiments. Fitting exponential decay curves, the half-times of the stomatal closure response was determined. No statistical differences were detected after ANOVA (P<0.05).

The question of whether the impaired stomatal movements in *tmm1* plants was caused by altered guard cell physiology led me to perform electrophysiological studies in the *Arabidopsis* Col0 and *tmm1* lines, and compare the ion transport of single and clustered stomata. Stomatal movements are driven by the fluxes of ion from the epidermal cells into the guard cells thanks to a repertoire of various transporters residing at the plasma membrane (see section 1.4). Because K^+ is the most abundant solute driving stomatal movements, I focused on the K^+ transport and particularly investigated the outward- and inward-rectifying K^+ channels (K_{OUT} and K_{IN} , respectively) by using two-electrode voltage clamp technique (Chen, Eisenach, et al. 2012). Epidermal peels of wild type and *tmm1* plants were bathed in buffer containing 10 mM K^+ (10 mM KCl-MES; pH 6.1). Current recordings were carried out by clamping at voltages ranging from -220 to +40 mV, following a holding voltage at -100 mV. Figure 16 presents current traces and average steady-state currents as a function of voltage (I-V curve) from guard cells of *Arabidopsis* wild type and the “clustered” *tmm1* mutant. Changes in the voltage resulted in the activation of the K^+ channels allowing higher fluxes of K^+ ions through them. For instance, at -100 mV the outward-rectifying K^+ channel is inactive but upon elevation in the voltage the channel opens and relaxes to a new steady-state. Currents from the outward-rectifying K^+ channel are here designated as I_{KOUT} and those from the inward-rectifying K^+ channels as I_{KIN} . Specifically, voltages positive of -40 mV yielded I_{KOUT} that were higher in amplitude as the voltages were increased. The mean amplitude of I_{KOUT} at +27 mV of the *tmm1* mutant was reduced by 53%, yielding mean current amplitude of $103 \pm 20 \mu A cm^{-2}$ compared to the $220 \pm 40 \mu A cm^{-2}$ of the wild type (Figure 17A). Voltages negative of -100 mV were marked by I_{KIN} , with decreasing voltages resulting in higher amplitudes of I_{KIN} . The mean amplitude of I_{KIN} at -220 mV was $-92 \pm 27 \mu A cm^{-2}$ for wild type and $-77 \pm 12 \mu A cm^{-2}$ for *tmm1* plants, but this difference was not statistically significant (Figure 17A).

The I-V curves were jointly fitted to a Boltzmann function (Eq. 7) to determine the half-maximal activation voltage ($V_{1/2}$), which describes voltage range for the gating of the channel, the gating charge (δ), which relates to the charge moved across the membrane electric field during gating, and the G_{max} (Table 3). The G_{max} describes the conductance of K_{IN} and K_{OUT} at saturating voltages and reflects

on the number of channels and the individual capacity of each channel. I-V curves for the K_{OUT} channels were jointly fitted, with the δ and $V_{1/2}$ being held in common resulting to values of 1.52 ± 0.12 and -7 ± 1 mV, respectively. The G_{max} for the K_{OUT} channels of *tmm1* lines was significantly reduced by 62% compared to the wild type plants. Holding only the δ constant for the joint fittings of the K_{IN} channels yielded a value of -2.9 ± 0.5 . Similar with the K_{OUT} channels, the G_{max} for K_{IN} channels of the wild type was significantly higher than the *tmm1* plants, yielding values of 0.6 ± 0.02 and $0.5 \pm 0.01 \mu S cm^{-2}$, respectively. The $V_{1/2}$ of K_{IN} channels for *tmm1* plants was displaced by approximately 30 mV towards more positive values, reaching membrane potential of -148 ± 3 mV compared to -178 ± 1 mV of wild type. The data suggested that stomatal clustering resulted in a decrease of the maximum I_{KOUT} and I_{KIN} , but it also affected the open probability of the K_{IN} channels, as indicated by the voltage displacement to more positive voltages. The stomatal clustering also affected the activation half times of K^+ channels (Figure 17B). The mean half times of I_{KIN} at -220 mV were 435 ± 138 ms for wild type and 269 ± 88 ms for *tmm1*, whereas the half-time of I_{KOUT} activation at $+33$ mV was similar between wild type and *tmm1*, showing values of 293 ± 74 and 325 ± 109 ms, respectively.

To check if the altered K^+ channel activities in the *tmm1* mutants were the result of changes in the gene transcription, I checked by quantitative PCR the levels of transcript from five genes encoding for the outward-rectifying K^+ channel *GORK*, the inward-rectifying K^+ channels *KAT1* and *KAT2* and the plasma membrane H^+ -ATPase, *AHA1* (Figure 18). I used cDNA isolated from the leaves of three-week old *Arabidopsis* wild type, *tmm1* and *PTMM1* plants that were harvested at the beginning of the day. The transcript level was normalized to the housekeeping gene *TUB9*. Expression of *GORK* and *KAT1* appeared slightly higher than that of plants with single stomata, though the differences were not significant. One could assume that the higher number of guard cells in *tmm1* should result in higher transcript levels of the K^+ channels in these mutants. However, the genes tested here are also expressed in other cell types apart from guard cells (Gambale & Uozumi 2006). Also, the fact that I used whole leaves to quantify the transcript levels might result in the dilution of the transcript levels

in *tmm1* mutant plants. Thus, I concluded that the altered ion transport was not dependent on the regulation of genes at the transcript level.

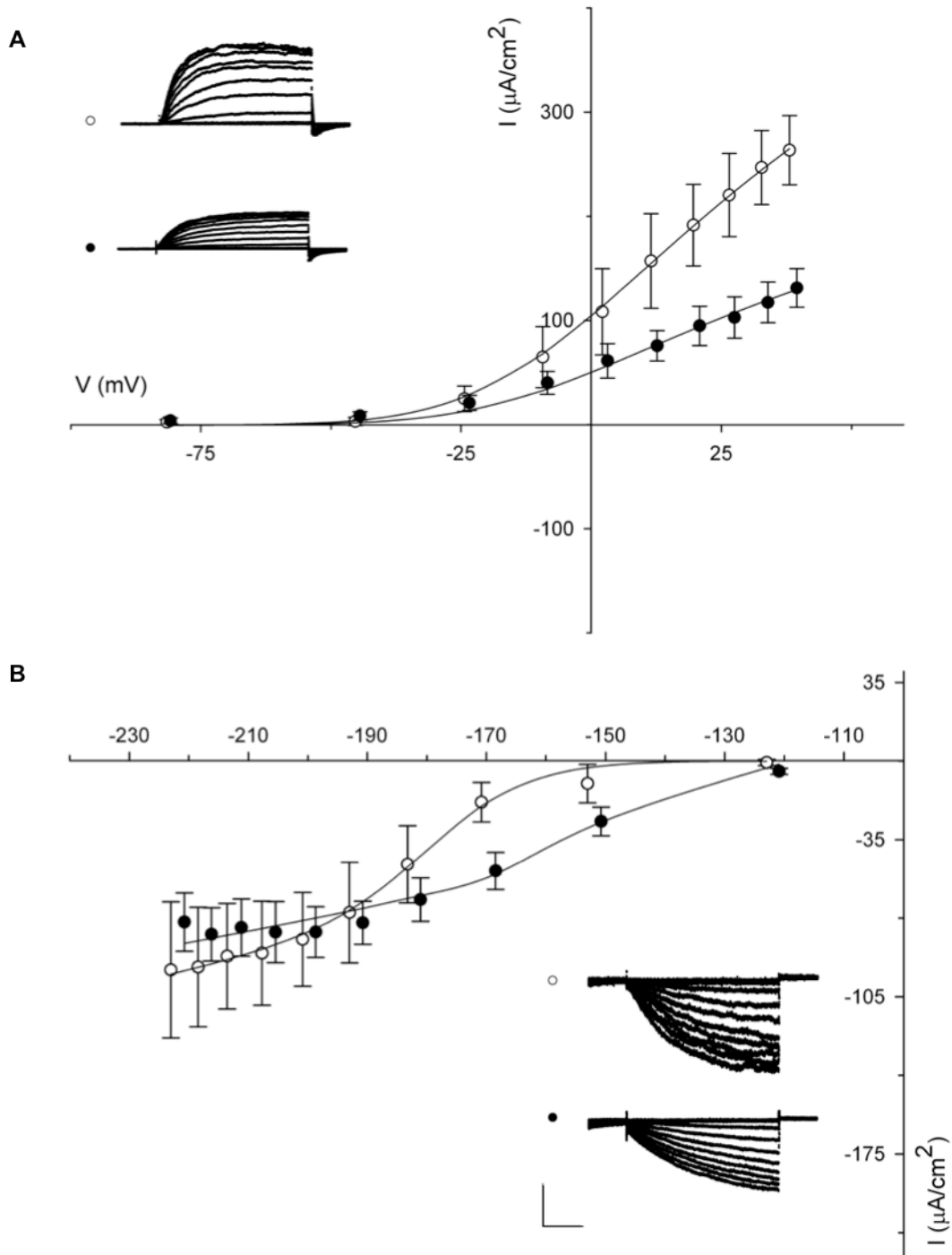


Figure 16. Stomatal clustering alters currents carried by outward- and inward-rectifying K⁺ channels.

Steady state currents recorded for I_{KOUT} (A) and I_{KIN} (B) under voltage clamp. Voltage clamp protocol consists of steps (20 mV) of 4 seconds between -220 and +40 mV, following a holding voltage at -100 mV. Data are means \pm SE from guard cells of wild type (white circle, n=5) and *tmm1* (black circle, n=4). Insets present current traces recorded under voltage clamp. Scale bar: horizontal, 2 ; vertical, 200 $\mu\text{A}/\text{cm}^2$. Curves were jointly fitted to Boltzmann function, with only the gating charge δ being held constant.

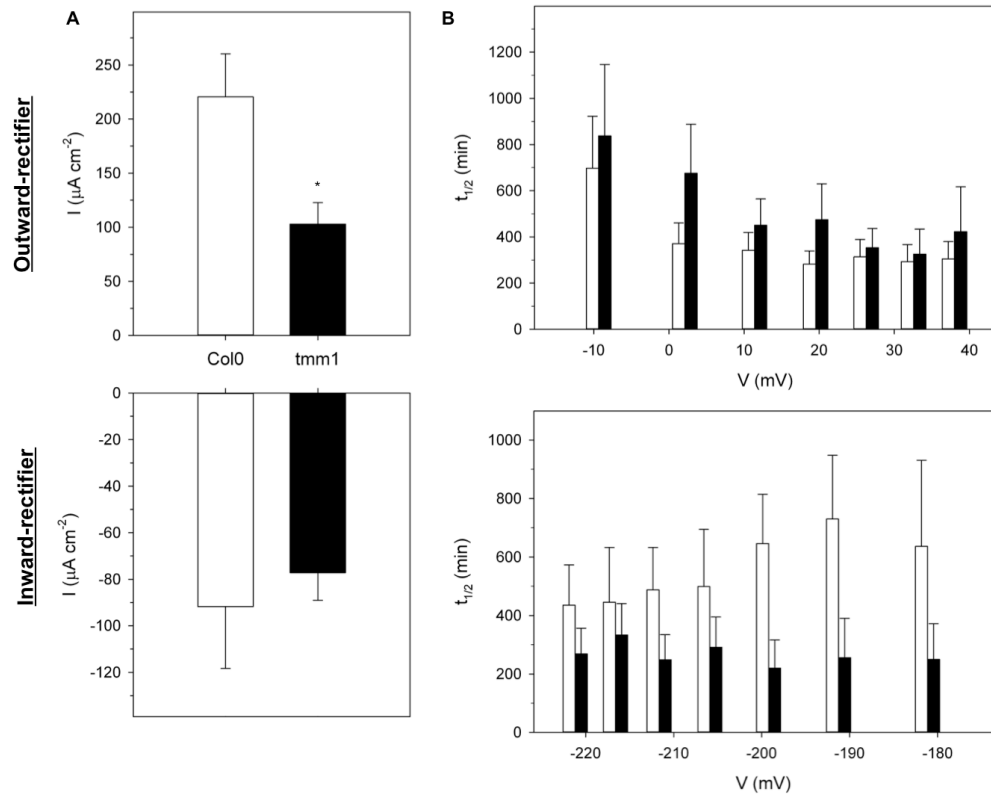


Figure 17. Stomatal clustering suppresses I_{KOUT} .

(A) Steady state currents as described in Figure 12 for I_{KOUT} at +40 mV (upper panel) and for I_{KIN} at -220 mV (bottom panel). (B) Current relaxation half times ($t_{1/2}$) as a function of voltage for I_{KOUT} (upper panel) and for I_{KIN} (bottom panel). Data are means \pm SE from guard cells of wild type (white; $n=5$) and *tmm1* (black; $n=4$) plants. Asterisk indicates statistical differences as determined by t-test ($P<0.001$).

Table 3. Gating parameters of I_{KOUT} and I_{KIN} .¹

	I_{KOUT}			I_{KIN}		
	g_{max} ($\mu S\ cm^{-2}$) ($p<0.001$)	δ	$V_{1/2}$ (mV)	g_{max} ($\mu S\ cm^{-2}$) ($p=0.016$)	δ	$V_{1/2}$ (mV) ($p=0.001$)
Col0	2.90 ± 0.06	1.52	-7 ± 1	0.58 ± 0.02	-2.9	-178 ± 2
<i>tmm1</i>	1.31 ± 0.03	± 0.12		0.50 ± 0.01	± 0.5	-147 ± 3

1. Statistical differences determined by t-test. P values are shown in blue under each parameter tested between Col0 and *tmm1* plants.

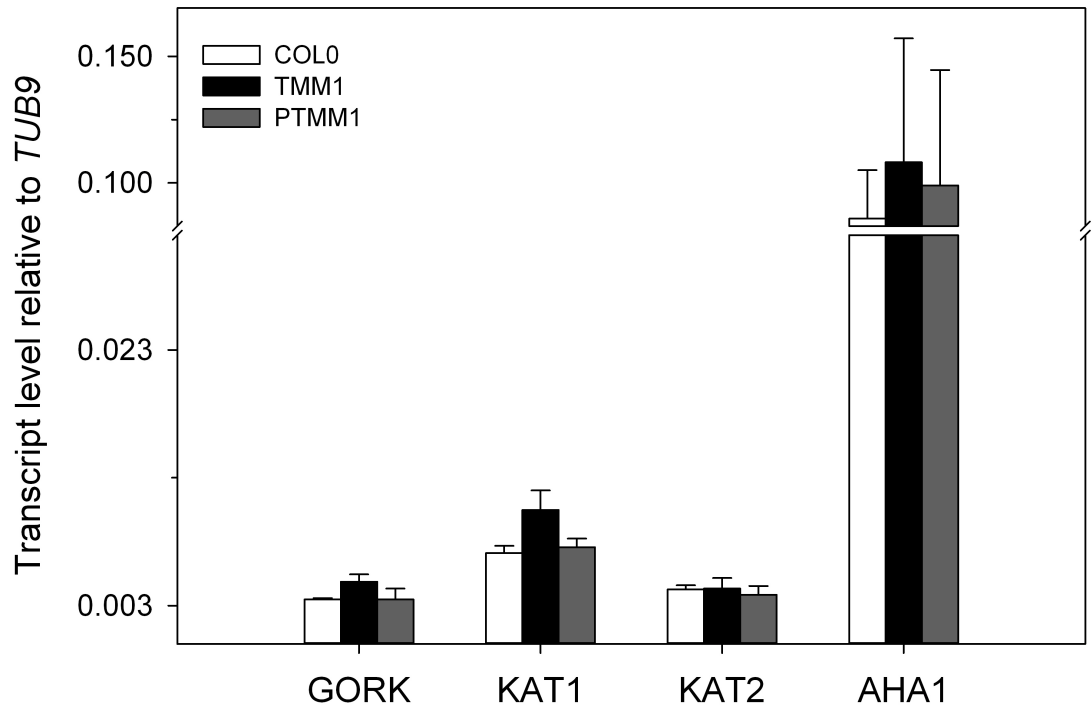


Figure 18. Transcript level of major plasma membrane transport genes in *Arabidopsis* lines.

RNA extracted from leaves of 3-week old *Arabidopsis* wild type (white), *tmm1* (black) and PTMM1 (dark grey) plants to perform quantitative PCR using *TUB9* gene as endogenous control. Data are means \pm SE of n=3 biological replicates. No statistical significant differences were detected after ANOVA (P<0.05).

Using the two-electrode voltage clamp protocol, I was able to measure the K^+ content of the guard cells from single and clustered stomata. For this purpose, epidermal peels from wild type and *tmm1* plants were placed in standard buffer supplementing with 10 mM KCl. Current recordings were carried out by clamping at voltages ranging from -220 to +40 mV, following a holding voltage at +50 mV. The currents were activated by holding the voltage at +50 mV for 5 seconds. Decrease of voltages in steps of 20 mV resulted in the relaxation of I_{KOUT} to a deactivated state. Figure 16A presents current traces and average tail currents for the K_{OUT} channels as a function of voltage from guard cells of *Arabidopsis* wild type and the “clustered” *tmm1* mutant. The point, which no current relaxation was seen, makes up the reversal of membrane potential. As shown in Figure 16B, the reversal of membrane potential was displaced towards more positive values by about 50 mV for *tmm1* mutant. Thus, based on the Nernst equation (Eq. 1), the K^+ content of the *tmm1* guard cells was estimated at 54 mM in comparison with the 199 mM of wild type. The values indicate a very substantial reduction in the K^+ content of the *tmm1* guard cells and imply that they were not able to accumulate K^+ to the same degree as wild type. Although these values appeared to be slightly offset, possibly resulting from the big capacitance of the electrode, the conditions used for this study were the same for either wild type or *tmm1* stomata and therefore a constructive conclusion can be derived from this study. Despite the observation that stomatal clustering hindered the accumulation of K^+ ions, the response was not sensitive to supply of ions from epidermal cells. All the electrophysiological studies were carried out under constant flowing solution, which in effect provided unlimited supply of ions to the guard cells.

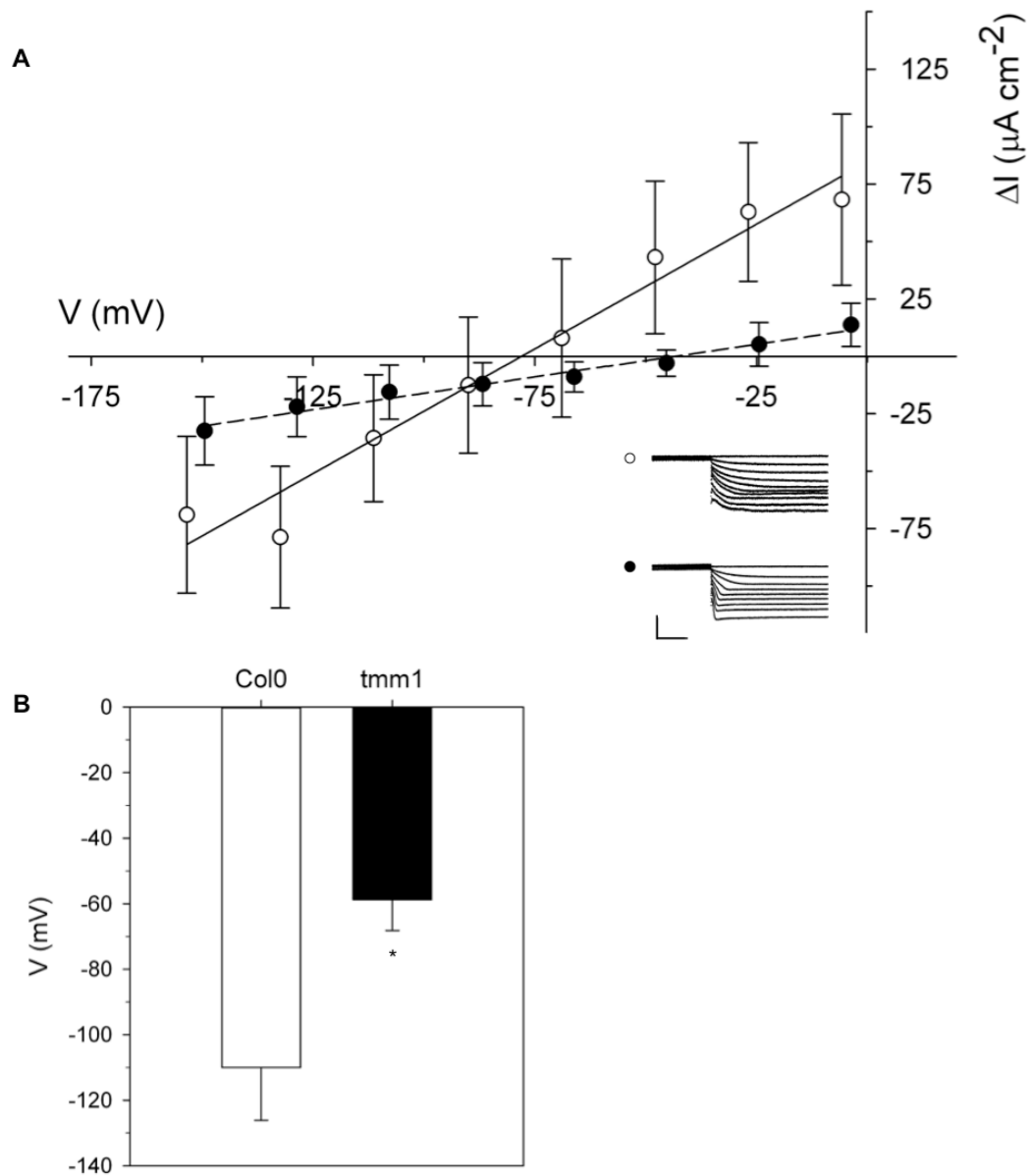


Figure 19. Tail current analysis for K_{OUT} channels from single and clustered stomata.

(A) Data are from wild type (white) and *tmm1* (black) guard cells were recorded by two-electrode voltage clamp with the presence of 10 mM KCl in the buffer. Voltage clamp protocol consists of 20 mV voltage steps of 6 seconds, following a holding voltage at +50 mV. Insets present current traces recorded under voltage clamp. Scale bar: horizontal line 2 seconds and vertical line 200 $\mu\text{A cm}^{-2}$. Inset present current traces recorded under voltage clamp. Scale bar: horizontal line 0.2 seconds and vertical line 100 $\mu\text{A cm}^{-2}$.

(B) Reversal potential of K_{OUT} channel as depicted from the above tail current analysis. Decrease in voltage steps led to a negative reversal potential around -110 ± 16 mV for wild type plants, whereas stomatal clustering of *tmm1* mutant shifted the reversal potential to more positive value of $-58 \text{ mV} \pm 9 \text{ mV}$. Lettering indicates statistical differences as determined by t-test ($P < 0.05$).

Discussion

Manipulation of stomatal density has been proposed as a potential strategy to improve WUE of plants grown in harsh environments, especially in such habitats where water is scarce (Lawson & Blatt 2014). Although there are reports suggesting the enhancement of stomatal conductance and photosynthetic capacity in species with altered number of stomata (Schluter et al. 2003; Franks et al. 2009; Yoo et al. 2010; Fanourakis et al. 2011; Tanaka et al. 2013; Drake et al. 2013), little information is available concerning the stomatal spacing and its influence on stomatal biology. The majority of the plants show single stomata on the leaf epidermis where the stoma is separated by the neighbouring stomata by at least one epidermal cell. *Begonia* is one of the few genera consisting of species that are naturally showing stomatal clusters. Stomatal clustering in *Begonia* species is considered an adaptation to water-stressed habitats, though not quantitative data exist to support this (Boghdan & Barkley 1972; Hoover 1986; Tang et al. 2002). Apart from the study of Nebauer (1967) on the stomatal patterning of various *Begonia* species, no complete and detailed record exists till today regarding the stomatal clustering or its physiological implications. My main objective in this chapter was to address the effect of stomatal clustering in stomatal movements by examining the physiology at the stoma and whole plant level, using two different populations of plants. *Arabidopsis* mutants made up the experimental population that exhibited defects in stomatal patterning, while two *Begonia* species constituted the natural population that included species with naturally-having stomatal clusters. Five main outcomes emerged: 1) *B. plebeja* exhibited non-contiguous clusters that differ from the type of cluster observed in the *Arabidopsis tmm1* mutant. 2) The data suggested a clear effect on gas exchange responses from solely the *Arabidopsis tmm1* mutant. Thus, the type of clustering plays a crucial role, with only the contiguous clustering adversely affecting plant physiology. 3) The contiguous stomatal clustering in *Arabidopsis* also impeded the stomatal movements under both opening and closing stimuli. 4) The impaired stomatal behaviour in *Arabidopsis* was mediated by defects in ion transport across the guard cell plasma membrane. And 5) the ion - notably K^+ - accumulation into the guard cells of the “clustered” *Arabidopsis* plants was suppressed.

3.3.1 Clustering type differs between experimental and natural plant populations.

There are several distinctions at the leaf level between *Arabidopsis* and *Begonias*, such as the latter have multiple layers of epidermis and stomata only on the abaxial side of the leaf (Boghdan & Barkley 1972; Tebbit, 2005). Another striking difference presented here is the structure of stomatal clusters from *Arabidopsis* and *Begonia* plants. Stomata of *B. plebeja* were not in contact with each other due to the presence of small subsidiary cells and therefore stomatal clustering in *B. plebeja* is described as non-contiguous. By contrast, stomatal clusters in *Arabidopsis tmm1* mutants were contiguous, with stomata in the cluster being in contact with each other (Figure 2). Gan et al. (2010) reported on this distinct type of stomatal clustering in the species *Sedum dfredii*. Apart from the stomatal clusters, *Arabidopsis tmm1* and *B. plebeja* also exhibited more numerous stomata in comparison to the “single stomata” *Arabidopsis* wild type and *B. coccinea*, respectively. Higher stomatal density was also observed in the *epf1/epf2* double mutant that is consistent with a previous study (Doheny-Adams et al. 2012; Hunt & Gray 2009). Several reports have described an inverse relationship between stomatal density and size (Hetherington & Woodward 2003; Franks et al. 2009; Franks & Beerling 2009b; Doheny-Adams et al. 2012), a phenomenon also evident here for the stomata in clusters as well as the high stomatal density mutant, *epf1/epf2* (Figure 3A). Indeed, stomata of *B. plebeja* and *epf1/epf2* double mutant were more numerous and smaller than *B. coccinea* and *Arabidopsis* wild type, respectively. This was also reflected on the stomatal index, which did not differ from that of the “single stomata” genotypes. However, the *tmm1* plants, when compared to the “single stomata” lines, showed a higher stomatal index that resulted from the combination of more numerous stomata of a similar stomatal size to the wild type (Figure 3B).

Taken together the stomatal patterning data, one can suggest that the non-contiguous stomatal clustering phenotype of *B. plebeja* rather mirrors the phenotype of the *epf1/epf2* plants than the “clustered” phenotype of *tmm1* plants. This suggestion is based on the observation that *B. plebeja* has small and numerous stomata that are not in direct contact with each other. The

development of high number of stomata together with small stomatal size has been postulated as a key strategy to adapt faster a higher stomatal conductance, without increasing the evaporative area of the leaf (Drake et al. 2013). The smaller stomata entail the greater ratio of membrane surface area to volume and thus they should respond faster in the environmental changes. The improvement of gas exchange responses due to such developmental strategies have been previously presented through studies with *Arabidopsis* mutants (Schluter et al. 2003; Tanaka et al. 2013) as well as with other species (Franks & Farquhar 2007; Drake et al. 2013; Lawson & Blatt 2014). However, what is the force maintaining stomatal clustering in certain species such as *B. plebeja*? The answer can be explained from the diffusional theory. Stomatal pores allow the diffusion of water vapour from the interior leaf spaces to the atmosphere, creating a water gradient between the two sides. Under standard conditions (i.e. low VPD), single stomata behave independently and therefore gas diffusion increases proportionally to the pore diameter (Ting & Loomis 1963; Ting & Loomis 1965). Nonetheless, when stomata are found in close proximity, like in stomatal clusters, the diffusion stream lines are merged resulting in saturation of the outside surface of the leaf that in turn leads to the reduction of water gradient and eventually to lower transpirational water loss (Ting & Loomis 1965; Wilmer & Fricker, 1996; Gan et al. 2010). Thus, one can distinguish between the two types of clusters and their implications in plant physiology. The smaller size of stomata in *B. plebeja* minimizes the evaporative area, and the presence of small cells between stomata in non-contiguous stomatal clusters might provide an ecological advantage to plants inhabiting niches where water conservation is required or even when plants have to respond fast to environmental changes.

3.3.2 Spacing between stomata is essential for gaseous exchange

When light is abundant and evaporative demand low, stomatal conductance is the main factor influencing CO₂ assimilation and transpiration (Farquhar & Sharkey 1982; Lawson 2009; Hummel et al. 2010). Based on mathematical model that takes into account the geometry of guard cells and guard cell complex, a positive correlation of stomatal conductance with stomatal density has been

described (Doheny-Adams et al. 2012; Dow et al. 2014). The same prediction also held true for the genotypes tested here, as the *tmm1*, *epf1/epf2* and *B. plebeja* plants showed higher G_{Wmax} , which was positively correlated with the stomatal density (Figure 5).

Nevertheless, the gas exchange data suggested that the stomatal behaviour of *tmm1* plants is altered. The plants failed to reach similar levels of gas exchange as the “single stomata” *Arabidopsis* lines, when conditions became favourable (Figure 9). This observation was more obvious from the transpiration data under dark exposure where the *tmm1* plants showed more than twice the E_{dark} rate than the genotypes with single stomata. Additionally, at saturating light the *tmm1* showed a suppressed CO_2 assimilation rate compared to the wild type plants. In contrast, *B. plebeja* did not show such substantial differences in gas exchange responses when compared to *B. coccinea*, highlighting the importance of the type of clustering on plant physiology. The latter finding underpins the similarity of *B. plebeja* with *epf1/epf2* and dictates the coupling of stomatal aperture with CO_2 assimilation and transpiration in order to achieve greater WUE under favourable conditions.

The stomatal impairment in *tmm1* plants was more apparent when I considered the stomatal cluster as sole functional unit (Figure 11). The *tmm1* gas exchange responses were indeed suppressed in comparison with those of “single stomata” plants, whereas *B. plebeja* did not differ from *B. coccinea*. A similar observation was described for several “clustered” *Arabidopsis* mutants that showed reduced CO_2 assimilation when exposed to high CO_2 concentrations (Dow et al. 2014). The authors ascribed this effect to the misplacement of stomata relative to the interior tissues. In the “single stomata” arrangement, each stoma is located over the substomatal cavity, the interior air space, that enables gas diffusion from the atmosphere to the mesophyll cells (Wilmer & Fricker, 1996; Zeiger, 2006). However, here I also presented differences into the transpiration rate from plants subjected to light and darkness. Therefore, one cannot exclude the possibility that the altered gas exchange responses were due to impaired stomatal movements in contiguous stomatal clusters. Indeed, when the diffusive stomatal conductance was measured, the “clustered” *tmm1* and *B. plebeja* plants did not show higher G_s than their respective single stomata genotypes

despite their higher stomatal density (Figure 13A). Additionally, regression analysis of G_{Wmax} and G_s data highlighted the effect of stomatal clustering in the maximum potential of gas diffusion, since the clustered regression model significantly deviated from the 1:1 regression (Figure 13B). Dow et al. (2014) also reported on the significance of proper spacing between stomata for plant physiology, as the diffusive stomatal conductance of lines with high stomatal clustering was significantly different from their theoretical stomatal conductance. However, it has to be mentioned that the equation used to estimate G_{Wmax} does not reflect on the spatial environment of guard cells and therefore one assumes that the individual stomata in stomatal cluster function independently and regardless of the neighbouring cells. Yet is this the case?

3.3.3 Alterations to guard cell ion transport is associated with the impaired movements of stomata in clusters

Stomatal opening and closing depends on changes in the turgor of guard cells, which in turn requires the movement of osmotically active compounds and water across the plasma membrane of guard cells (Blatt 2000). The stomatal aperture measurements performed here indicated that stomatal movements were only affected in the “clustered” *Arabidopsis* line, underscoring the importance of the geometry of the cluster. *tmm1* plants showed a reduction in stomatal aperture of approximately 25% in comparison to wild type during both stomatal opening and closing, whereas stomatal movements of *B. plebeja* did not differ from that of *B. coccinea* (Figure 4 and 13). One can assume that the reason for this discrepancy lies on the fact that the presence of non-stomata cells in *B. plebeja* stomatal clusters provide the lateral space that is required for the swelling and shrinkage of guard cells. Apart from the ion fluxes in and out of the guard cells, stomatal movements also depend on the mechanistic properties of the guard cells. For instance, in earlier plants, the enlargement of guard cells during opening process involves their vertical displacement without depending on interaction with adjacent cells. Yet, opening in the grass *Triticum aestivum* requires the lateral displacement of guard cells and therefore the shrinkage of adjacent subsidiary cells (Franks & Farquhar 2007). The authors argued that

widening of stomatal aperture requires the increase of guard cell turgor pressure, the decrease of epidermal turgor pressure as well as the decline in epidermal osmotic pressure. The latter depends on the transfer of solutes between the subsidiary or epidermal cells and guard cells (Raschke & Fellows 1971; Outlaw 1983; Wilmer & Fricker, 1996). In particular, studies with *Zea mays* have shown that K^+ and in a lesser extent Cl^- ions were accumulated into guard cells once the epidermal peels were illuminated, while the opposite was observed in the subsidiary cells, suggesting that these cells might serve as storage of major osmolytes. The reversal of this response was detected upon exposure of epidermal peels to darkness (Raschke & Fellows 1971). Similarly, stomatal opening of several species such as *Vicia* and *Nicotiana* was positively correlated with K^+ accumulation into the guard cells (Wilmer & Fricker, 1996).

Taking the above facts together, there are three possible ways to explain the impaired stomatal function in *tmm1* mutants:

- 1) The number, activity and exact localization of ion channels and transporters at the plasma membrane of the clustered stomata might be completely different than the single stomata. Remarkably, the electrophysiological analysis implied that K^+ transport is highly compromised in the *tmm1* plants. The activity of K_{OUT} channels was about 55% reduced compared to wild type, whereas the gating characteristics of the K_{OUT} channels were not affected by clustering (Figure 16 and 17). K_{OUT} channels are sensitive to the external K^+ concentration (Blatt 1992; Johansson et al. 2006; Dreyer & Blatt 2009; Eisenach et al. 2014) and this together with the fact that apoplast volume in *tmm1* plants is reduced due to higher stomatal index, one should expect a shift on the gating characteristics of K_{OUT} channels in these plants. Yet, this was not observed since in the experimental procedures followed the external K^+ concentration was not limited (constant flowing buffer solution). However, I did observe a positive displacement of $V_{1/2}$ for the K_{IN} channels implied that the changes in the open probability of the K_{IN} channels occurred. The K_{IN} channels are not sensitive to the external K^+ concentration implying that additional regulatory mechanisms such as intracellular Ca^{2+} and pH should have a role in the defective stomatal behaviour of *tmm1* plants. Moreover, the similar transcript levels of the major plasma membrane transporters excluded the possibility that the lower activity of

K^+ channels is dependent on the down-regulation of the genes encoding for these channels (Figure 18).

Whether the altered conductance and gating properties of K^+ channels in the *tmm1* mutants are the result of changes at the protein level remains elusive. Stomatal movements have been associated with trafficking of proteins to and from the plasma membrane to drive the changes in cell volume (Zonia & Munnik 2007). ABA treatment has been shown to induce the internalization of KAT1 channels, suggesting that the trafficking of channels was an adaptive change of solute flux into the guard cells (Sutter et al. 2007). Also, Eisenach et al. (2014) showed the GORK channels were not homogeneously distributed across the plasma membrane, but they were rather apparent as punctate, of which dispersal was associated with the external K^+ . The authors proposed that this unique phenomenon is a mechanism of channel regulation by sensing the surrounding environment. Hence, it will be interesting to assess the localization of K^+ channels in *tmm1* mutants and identify whether the activity of these channels was influenced by the close proximity of multiple stomata in stomatal clusters.

2) Given that stomata in contiguous clusters share the same reservoir of ions, this might cause scarcity of osmotically solutes and therefore obstruct stomatal opening. As mentioned above, stomatal movements depend on lateral movements of guard cells driven by opposite changes in osmotic and turgor pressure of epidermal and guard cells (Franks & Farquhar 2007). If we accept that the adjacent cells provide the osmolytes (Raschke & Fellows 1971; MacRobbie & Lettau 1980; Outlaw 1983; Franks & Farquhar 2007), then one can assume that in plants exhibiting contiguous stomata clusters, the reservoir of osmolytes is not sufficient to drive stomatal movements. Here, I presented data highlighting the lower accumulation of K^+ in the guard cells of *tmm1* mutants when compared to the wild type plants (Figure 18). However, the data do not elucidate the mechanism underlying this response, since the ion supply in the electrophysiological studies was not limited. Of course one cannot exclude the possibility that on a leaf or even whole plant level, like in the case of gas exchange measurements, the reduced amount of epidermal cells in the *tmm1* does influence the ion supply into guard cells and thus the stomatal movements.

Finally, 3) stomata *per se* might apply backpressure to each other when found in contiguous clusters and therefore they hinder the proper opening - closing processes. Although no evidence is presented here for this argument, one can hypothesize that under the presence of an opening stimulus swelling of stomata would result in the mutual extrusion of adjacent guard cells that in turn would impede the opening process. Despite that no data exist from stomata in clusters, the dependence of stomatal movements and conductance on neighbouring cells has been considered the reason for the patchy stomatal behaviour observed in *Xanthium strimarium* (Mott & Buckley 1998; Mott & Buckley 2000; West et al. 2005).

3.3.4 Outlook

In conclusion, quantitative analysis of stomata *per se* and stomatal complex geometry led to the identification of two distinctive types of cluster, the contiguous clusters of *Arabidopsis tmm1* mutant and the non-contiguous clusters of *B. plebeja*. A correlation between stomatal density and stomatal size with the theoretical stomatal conductance was shown among the lines used here, which is in accordance with previous studies. Hence, the more numerous and smaller stomata the higher stomatal conductance is. The impact of stomatal clustering in the plant physiology was presented, with plants exhibiting contiguous clusters failing to reach similar steady-states of CO₂ assimilation and transpiration rates as the “single stomata” or the stomata in non-contiguous cluster formation. Also, I proposed that the suppressed gas exchange responses due to stomatal clustering were associated with impaired stomatal movements, as the *tmm1* plants did not respond to opening or closing stimuli as the “single stomata” plants did. The altered stomatal behaviour of *tmm1* mutants was identified to be the result of changes in ion transport of guard cells. Surprisingly, the activity of K⁺ channels was significantly affected due to the unique spatial arrangement of stomata in *tmm1* plants. Finally, the significance of spacing between stomata was discussed, since guard cells of *tmm1* mutants failed to accumulate the same amount of K⁺ as the wild type plants.

4 Stomatal clustering influences conditional growth phenotypes

4.1 *Introduction*

Research on the *TMM1* gene has been mainly concentrated on its role in stomatal development (Yang & Sack 1995; Geisler et al. 1998; Geisler et al. 2000; Bhave et al. 2009), on its protein product and the interaction with other proteins involved in this developmental pathway (Shpak et al. 2005; Abrash & Bergmann 2010; Lee et al. 2012), and recently on the impact of *tmm1* mutation to gas exchange responses and stomatal conductance (Dow et al. 2014). Similar studies have been carried out for the *EPF1* and *EPF2* genes and their products (Hara et al. 2007; Hunt & Gray 2009; Lee et al. 2012). Moreover, Doheny-Adams et al. (2012) reported the better growth of the *EPF* transgenic lines with reduced number of stomata in water-scarce environments as well as the involvement of the gene in adjusting stomatal patterning according to atmospheric CO₂ concentrations.

The requirement for proper spacing of stomata to enable gas exchange responses was extensively discussed in the previous chapter. Hence, one can ask what is the impact of stomatal clustering in water use efficiency and plant growth. Stomata have a fundamental role in controlling WUE by facilitating the diffusion of CO₂ and water vapour with their immediate environment (Hetherington & Woodward 2003; Lawson & Blatt 2014). However, there is a debate on which specific stomatal parameter mostly influences WUE; is this parameter the number of stomata or the stomatal aperture? Different groups have argued in favour of one or the other parameter as the most important for WUE depending on the genotypes and experimental conditions used (Lawson 2009; Yoo et al. 2010; Doheny-Adams et al. 2012; McAusland et al. 2013; Dow et al. 2014).

Improving WUE is considered to be the key strategy for higher crop yields combined with improved sustainability, especially in water-restricted habitats

(Mueller et al. 2012). Paradoxically, several reports have concluded on the enhancement of WUE under water deficit, when light, humidity and [CO₂] were kept constant. Under such conditions, the stomatal conductance is reduced promoting the slower expansion of the leaf (Tardieu et al. 2000; Medrano 2002; Flexas 2002), which in turn leads to the reduction in evaporative area associated with the unaltered photosynthetic capacity and carbon metabolism that influence the production of biomass (Hummel et al. 2010; Tardieu et al. 2014). Indeed, the non-linear relationship between stomatal conductance and CO₂ assimilation has been observed in various species (Franks & Farquhar 1999; Drake et al. 2013). Moreover, the water deficit also results in large changes in additional processes affecting the plant physiology and morphology, such as induction of root growth (Hummel et al. 2010), activation of anti-oxidant machinery (Kubo et al. 1999; Zhang et al. 2010) and redistribution of osmolytes (Hare et al. 1998). Hence, regulation of WUE does not constitute a “black-and-white” case, but the process rather depends on the converge action of several factors that shape the final response.

Here, I investigated the influence of the altered stomatal patterning on plant biomass and physiology in response to environmental stimuli that drove two opposite responses: 1) opening of stomata to promote photosynthesis and biomass production under low evaporative demand and 2) stomatal closure to prevent transpirational water loss under water-scarce conditions. To address the first point, I exposed three-week old *Arabidopsis* plants to different degrees of evaporative demand by adjusting the light and humidity conditions. To address the second point, three-week old *Arabidopsis* plants were subjected to progressive mild or severe drought stress. Assessment of the growth phenotypes relied on measurements of the rosette area, fresh and dry weight of shoots. Where possible, I also carried out IRGA measurements to estimate the CO₂ assimilation and transpiration rate and thus calculate the WUE. In addition, for the first time, the root system architecture of stomatal patterning mutants was investigated using a quantitative analysis of 5 root-related parameters in the absence or presence of external carbon supply.

4.2 Results

4.2.1 Stomatal clustering affects plant growth

Stomata should balance gaseous flux between photosynthesis and transpiration to optimize carbon assimilation and water loss by adapting their apertures to variable environmental conditions. High humidity eliminates the restriction posed due to foliar transpiration allowing stomata to fully open. Hence, high humidity in combination with exposure to high light intensity which promotes light-limited photosynthetic reactions, will result in a rise in water use efficiency and consequently in an increase of biomass. Here, I investigated the biomass of three week-old wild type and *tmm1* transgenic lines under four distinct light and humidity conditions: control conditions (70 $\mu\text{mol m}^{-2} \text{s}^{-1}$ of PAR + 60% RH), high humidity (70 $\mu\text{mol m}^{-2} \text{s}^{-1}$ of PAR + >90% RH), high light (200 $\mu\text{mol m}^{-2} \text{s}^{-1}$ of PAR + 60% RH) and high light and humidity (200 $\mu\text{mol m}^{-2} \text{s}^{-1}$ of PAR + >90% RH). Fresh shoot weight and rosette area measurements were utilized as a proxy of biomass (Figure 2A and B). I also determined the WUE of the three *Arabidopsis* lines in the four different conditions based on measures of assimilation of CO_2 and transpiration rate (Figure 2C and D).

Figure 1 displays the phenotype of the wild type, *tmm1* and PTMM1 plants grown under the four light and humidity regimes. At first glance, it is obvious that as the parameters were increased the “single stomata” plants exhibited higher biomass with the largest plants occurring under 200 $\mu\text{mol m}^{-2} \text{s}^{-1}$ of PAR + >90% RH. The *tmm1* plants only appeared larger than the control conditions when both light and RH were saturated. This is the first report on growth phenotype regarding the *tmm1* mutants. Indeed, under control conditions (70 $\mu\text{mol m}^{-2} \text{s}^{-1}$ of PAR + 60% RH), no discernible differences in the biomass were detected. In particular, the average fresh shoot weight of *tmm1* was 0.16 ± 0.01 g compared to 0.18 ± 0.01 g of wild type and 0.17 ± 0.01 g of PTMM1. Estimation of rosette area via imaging indicated that the average rosette size was not statistically different among the lines, ranging from 8.9 to 10.5 cm^2 . When the relative humidity was saturated, the average fresh shoot weight of “single stomata” plants was 40% greater than that in control conditions, while the average rosette area remained unchanged corresponding to $10.35 \pm 0.58 \text{ cm}^2$ for wild type and

8.67 ±0.98 cm² for PTMM1. However, the *tmm1* mutant did not show such an increase in both parameters, resulting in fresh shoot weight of 0.16 ±0.01 g and rosette area of 6.35 ±0.93 cm². Raising the light to 200 μmol m⁻² s⁻¹ of PAR slightly augmented the rosette area of “single stomata” plants, while it resulted in further 45% increase in the average fresh shoot weight compared to control conditions. In contrast, the *tmm1* plants did not show any change in the fresh shoot weight compared to control conditions, and therefore it appeared 46% smaller when compared with wild type plants grown at high light conditions. The average rosette area of *tmm1* mutants also remained unchanged comparing to control conditions, and it was 1.4-fold decreased compared with the wild type under 200 μmol m⁻² s⁻¹ of PAR. By saturating both light and humidity, the biomass of all three lines was elevated. However, the fresh weight and rosette area of the *tmm1* mutants was significantly suppressed in comparison to the “single stomata” lines, yielding values of 0.38 ±0.04 g and 11.29 ±1.16 cm² compared to 0.66 ±0.009 g and 16.82 ±0.43 cm² of wild type plants.

The gas exchange responses of the three *Arabidopsis* lines reflected the changes observed in the above morphological parameters. Under control conditions the wild type, *tmm1* and PTMM1 plants exhibited statistically undifferentiated rates of CO₂ assimilation (A), resulting in 2.72 ± 0.10, 2.44 ±0.08 and 3.03 ±0.20 μmol m⁻² s⁻¹, respectively. The transpiration rate (E) did not differ between wild type and *tmm1* plants, whereas it was approximately 35% increased for PTMM1 plants. When relative humidity was raised at >90%, the gas exchange responses of all three *Arabidopsis* lines remained close to the rates quantified at control conditions, ranging between 2.25 to 2.75 μmol m⁻² s⁻¹ for A and 1.47 to 1.79 mmol m⁻² s⁻¹ for E. Interestingly, under 200 μmol m⁻² s⁻¹ of PAR, the A rate of *tmm1* mutants did not show any elevation, whereas both wild type and PTMM1 plants reach A of approximately 5.3 μmol m⁻² s⁻¹. The E rate was increased with the elevation of light intensity, but it did not differ among the lines resulting in a rate of approximately 3 mmol H₂O m⁻² s⁻¹ in water loss per plant. Saturating both light and humidity did not affect the A, resulting in similar values for each genotype to those at 200 μmol m⁻² s⁻¹ of PAR. Interestingly, the E rate of *tmm1* mutants appeared 45% higher than the “single stomata” plants, corresponding to a E rate of 3.8 ±0.4 mmol m⁻² s⁻¹.

Table 1 presents the measures of WUE from wild type, *tmm1* and PTMM1 plants grown under the four light and humidity regimes, as determined by the ratio of A and E rates. At low light intensity, WUE did not substantially differ among the lines. When light intensity was raised to $200 \mu\text{mol m}^{-2} \text{s}^{-1}$ of PAR, the WUE of wild type and PTMM1 plants remained unchanged in comparison to the control conditions. However, the *tmm1* plants reached a WUE of $1.15 \pm 0.28 \mu\text{mol CO}_2$ per mmol H_2O , which was suppressed by 33% compared to wild type plants at the same conditions and by 23% compared to *tmm1* at control conditions. Once the gas exchange constraints were eliminated (i.e. under $200 \mu\text{mol m}^{-2} \text{s}^{-1}$ PAR + >90% RH), the WUE of wild type and PTMM1 plants was elevated to 2.77 ± 0.23 and $2.41 \pm 0.39 \mu\text{mol CO}_2$ per mmol H_2O , respectively. In contrast the *tmm1* plants did not show an enhanced WUE under these conditions, resulting in 2.3-fold decrease compared with wild type plants ($p=0.011$). The results imply that the stomatal behaviour in *tmm1* mutants is dynamically suppressed and therefore the plants cannot adjust for an equivalent optimum in their gas exchange when these constraints are eased for growth.

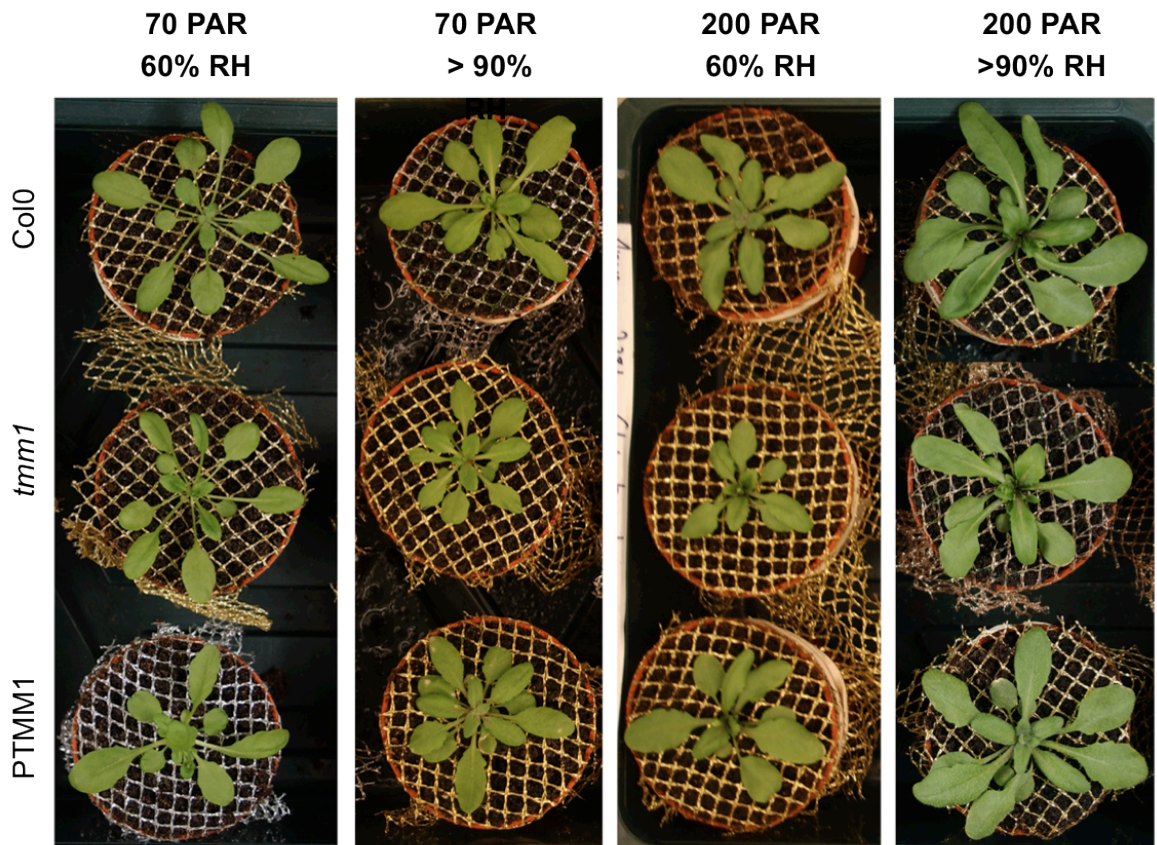


Figure 1. Phenotype of *A. thaliana* stomatal patterning mutants under four distinct light and humidity regimes.

Representative pictures of three week-old *Arabidopsis* wild type (upper row), *tmm1* (middle row) and PTMM1 (bottom row) plants grown under normal conditions ($70 \mu\text{mol m}^{-2} \text{s}^{-1}$ of PAR + 60% RH), high humidity ($70 \mu\text{mol m}^{-2} \text{s}^{-1}$ of PAR + >90% RH), high light ($200 \mu\text{mol m}^{-2} \text{s}^{-1}$ of PAR + 60% RH) and high light and humidity ($200 \mu\text{mol m}^{-2} \text{s}^{-1}$ of PAR + >90% RH).

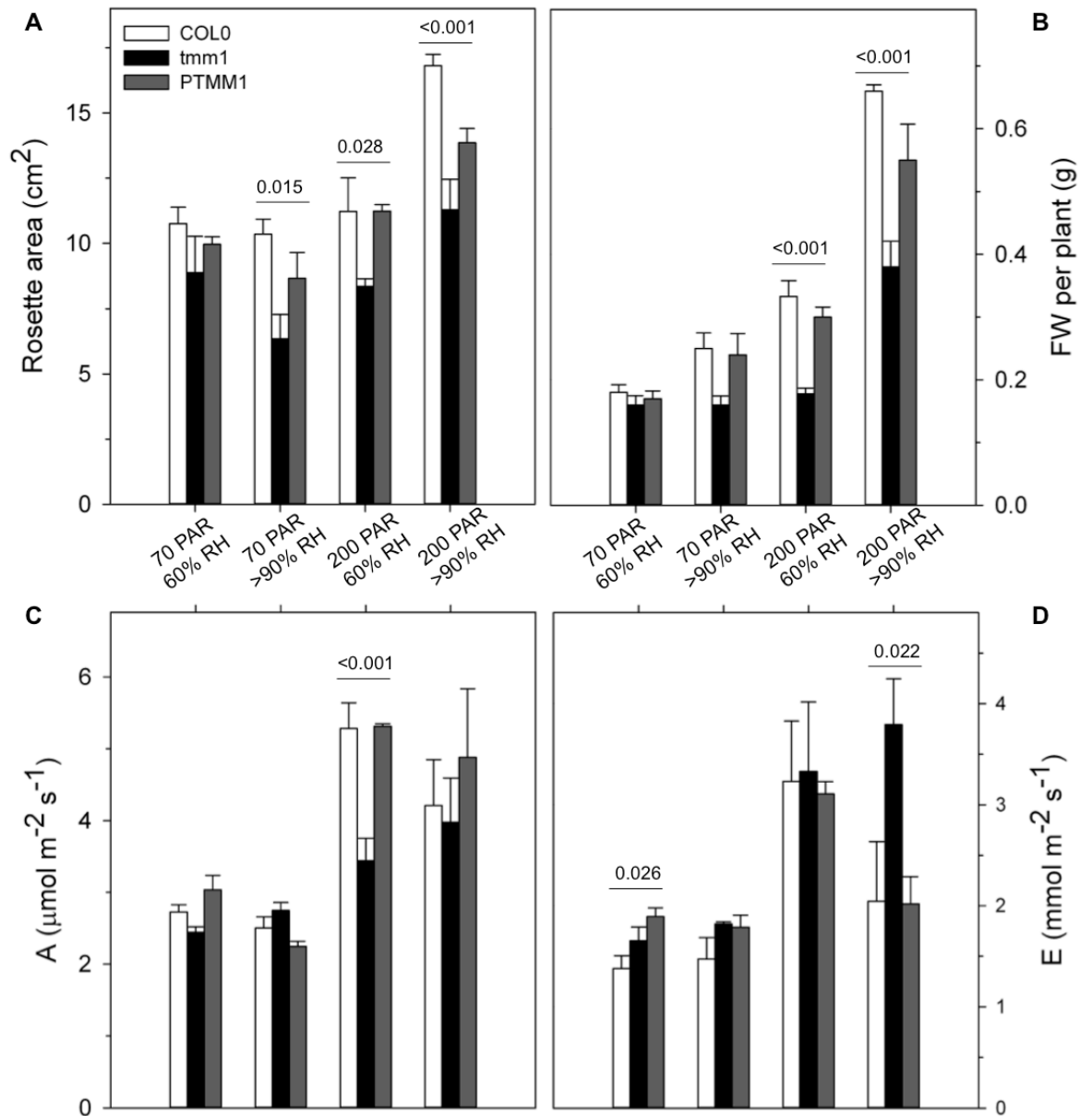


Figure 2. Quantification of the biomass of *A. thaliana* stomatal patterning mutants under four distinct light and humidity regimes.

Three week-old *Arabidopsis* wild type (white), *tmm1* (black) and PTMM1 (dark gray) plants were grown in normal conditions (70 $\mu\text{mol m}^{-2} \text{s}^{-1}$ of PAR + 60% RH), high humidity (70 $\mu\text{mol m}^{-2} \text{s}^{-1}$ of PAR + >90% RH), high light (200 $\mu\text{mol m}^{-2} \text{s}^{-1}$ of PAR + 60% RH) and high light and humidity (200 $\mu\text{mol m}^{-2} \text{s}^{-1}$ of PAR + >90% RH). Graphs represent (A) rosette area, (B) fresh weight, (C) CO₂ assimilation and (D) transpiration. Data are means \pm SE of n=6 independent experiments. Statistical differences after ANOVA ($P < 0.05$) are indicated by numbers above bars, as determined by Student-Newman-Keuls test.

Table 1. Water use efficiency ($\mu\text{mol CO}_2$ per $\text{mmol H}_2\text{O}$) of *Arabidopsis* under four light and humidity regimes ¹.

	70 PAR + 60% RH (P=0.061)	70 PAR + >90% RH (P=0.238)	200 PAR + 60% RH (P=0.170)	200 PAR + >90% RH (P=0.011)
Col0	2.11 \pm 0.23	1.79 \pm 0.34	1.74 \pm 0.29	2.77 \pm 0.23
<i>tmm1</i>	1.50 \pm 0.18	1.51 \pm 0.07	1.15 \pm 0.28	1.21 \pm 0.35
PTMM1	1.49 \pm 0.04	1.37 \pm 0.11	1.71 \pm 0.07	2.41 \pm 0.39

1. Water use efficiency was determined as the ratio of A and E rates of wild type, *tmm1* and PTMM1 plants grown in normal conditions (70 $\mu\text{mol m}^{-2} \text{s}^{-1}$ of PAR + 60% RH), high humidity (70 $\mu\text{mol m}^{-2} \text{s}^{-1}$ of PAR + >90% RH), high light (200 $\mu\text{mol m}^{-2} \text{s}^{-1}$ of PAR + 60% RH) and high light and humidity (200 $\mu\text{mol m}^{-2} \text{s}^{-1}$ of PAR + >90% RH) . Data are means \pm SE of n=6 independent experiments. Statistical differences after ANOVA were determined by Student-Newman-Keuls test. Comparison was carried out between *Arabidopsis* lines from the same condition and P values are indicated in blue.

4.2.2 Stomatal clustering promotes resilience to severe drought stress

Bearing in mind the seasonally dry habitat where *B. plebeja* is found, the association of stomatal clustering with water conservation (Gan et al. 2010) as well as the presented defective stomatal closure in *tmm1* plants, I was interested in investigating the effect of stomatal clustering on growth under mild drought stress. For this reason, I exposed three week-old *Arabidopsis* wild type, *tmm1*, PTMM1 and *epf1/epf2* plants to drought stress by withholding watering for 16 days. To follow the growth rate, I harvested the shoots at 5, 8, 12 and 16 days after the stop of watering. I also re-watered the plants on days 16 and 20, to eventually harvesting the shoots on day 21 in order to assess the recovery in growth. Growth was determined by measuring the rosette area of the plants (Figure 3A) and weighing the fresh shoot material (Figure 3B). Additionally, I determined the dry weight in order to calculate the water content of the plants (Figure 3C). To ensure that plants were exposed to the same drought stress, the water content of the soil per plant at each time point was also estimated (Figure 3D).

At the onset of the drought stress, the biomass of all three *Arabidopsis* lines was similar to the wild type plants; the average fresh shoot weight per plant was 0.16 ± 0.03 g and the average rosette area was 11.29 ± 1.24 cm². On withholding watering, the *tmm1* and *epf1/epf2* mutants exhibited a slower growth rate compared to wild type plants, as it is depicted from the fresh weight measurements (Figure 3A). However, no substantial differences in fresh shoot weight among the lines were detected. On day 16, the average rosette area of the four *Arabidopsis* lines did not differ among the lines (Figure 3B). Similarly, the average fresh shoot weight of *tmm1* and *epf1/epf2* plants was 32% and 36% less than the wild type, but still the differences were not statistically significant. This led me to measure the percentage of water content (WC) of the plants to address whether the small differences in the fresh shoot weight were the outcome of the higher water loss in the stomatal patterning mutants. Interestingly, no substantial differences were detected among the lines on day 5, 8 and 12, with mean WC ranging from 88% to 93%. On day 16, the mean % WC of the *epf1/epf2* mutant was reduced to 91.22 ± 0.03 compared to 93.56 ± 0.28 of

wild type, suggesting the higher water loss in these mutants (Figure 3C). The *tmm1* mutants did not display such a significant difference in comparison to wild type and PTMM1 plants, implying that stomatal movements on these mutants are indeed impaired, despite the higher number of stomata. All together the data suggested that the plant growth was not inhibited due to the short-term water deprivation and posed the question of whether the plants did sense the drought stress.

Measuring the percentage of soil water content, I was able to observe the progression of drought stress as well as to ensure that re-watering was sufficient to alleviate the stress (Figure 3D). This set of data suggested the drought stress effect was only apparent on day 16, when relative soil WC was 20-23% lower than the rest of time points (Figure 3D). This observation is in accordance with the rosette area measurements that reached a plateau at this time point, pointing to the expected drought-induced inhibition of leaf expansion. Additionally, the data did not indicate any difference in the amount of watering between the four lines tested. The same held true for the soil % WC on day 21 that was about 60% for all four lines, indicating that the plants faced the same amount of re-watering. On day 21, the average fresh shoot weight of the wild type and PTMM1 plants was 40% elevated compared to that on day 16. The *epf1/epf2* double mutants also show 60% increase in fresh shoot weight, resulting in values of 0.93 ± 0.09 g that were similar to 0.97 ± 0.1 g of wild type plants. Although the *tmm1* mutant did follow the same pattern as the above lines, they still showed a 1.3-fold lower fresh shoot weight compared to wild type plants, corresponding to values of 0.72 ± 0.06 g (Figure 3A). A similar outcome was found for the rosette area measurements, with the wild type 32% larger mean rosette areas after re-watering compared to that on the last day of drought stress (Figure 3B). The rosette area of *tmm1* plants was also increased by 36% compared to that at day 16. The mean WC of the “single stomata” plants was slightly reduced compared to day 16 and it was approximately 91% across all three lines. This observation suggested that the plants with normal stomatal patterning responded to re-watering by enhancing their gas exchange responses, which eventually resulted in higher transpirational water loss. However, the mean % WC of the *tmm1* mutants was slightly but not significantly reduced after

re-watering. This outcome is in agreement with the smaller recovery observed in growth of the *tmm1* mutants and it argues in favour of the impaired stomatal behaviour associated with clustering.

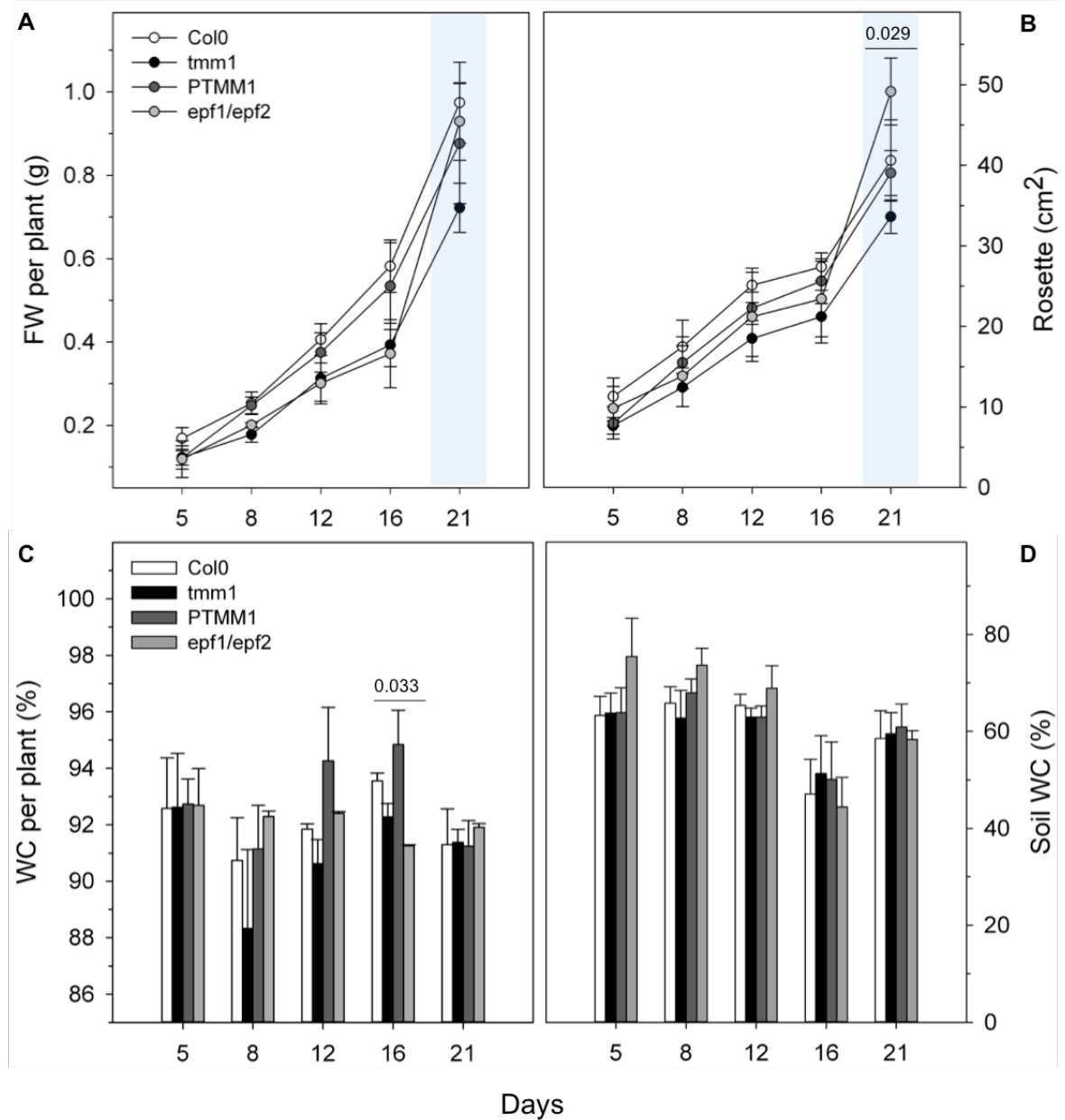


Figure 3. Quantification of sensitivity of *A. thaliana* stomatal patterning mutants to short-term drought stress.

Three week-old *Arabidopsis* wild type, *tmm1*, PTMM1 and *epf1/epf2* plants were grown under normal conditions before subjecting to drought stress. Plants were harvested at 5, 8, 12 and 16 days after watering was withheld. Plants were rewatered on day 16 and 20, and harvested on day 21 (blue shaded section). Graphs represent (A) fresh weight, (B) rosette area. (C) water content per plant and (D) water content of soil. Data are means \pm SE of $n=5$ independent experiments. Statistical differences after ANOVA ($P<0.05$) are indicated by numbers above bars, as determined by Student-Newman-Keuls test.

To further examine whether the impairment in stomatal movement of the *tmm1* mutants provides an advantage when the water balance and status of the plant is crucial for its survival, I exposed the plants to long-term drought stress. For this purpose, I subjected three week-old *Arabidopsis* wild type, *tmm1*, PTMM1 and *epf2/epf2* plants to four weeks of water deprivation. Figure 4 displays the phenotype of all four lines on day 30 after the stop of watering. The photos clearly show that *tmm1* plants coped better with severe drought stress. To quantify this phenotype, I estimated the fresh weight and the percentage of WC of the shoots (Figure 5). The mean fresh shoot weight of *tmm1* plants was 25% increased compared to wild type, corresponding to a value of 0.70 ± 0.05 g (Figure 5A). Although the mean fresh shoot weight of PTMM1 and *epf1/epf2* was 10-15% higher than that of wild type plants, this difference was not statistically significant. Additionally, the mean % WC of the *tmm1* plants was 90 ± 2 compared to 86 ± 1 for the wild type plants, whereas the “single stomata” lines PTMM1 and *epf1/epf2* showed lower % WC values of 88 ± 2 and 87 ± 2 , respectively (Figure 5B). The data suggested that the *tmm1* mutant showed an enhanced tolerance in water-limited conditions. Hence, one can hypothesize that stomatal clustering might benefit plant performance via the reduced transpirational water loss when water is scarce for long periods.

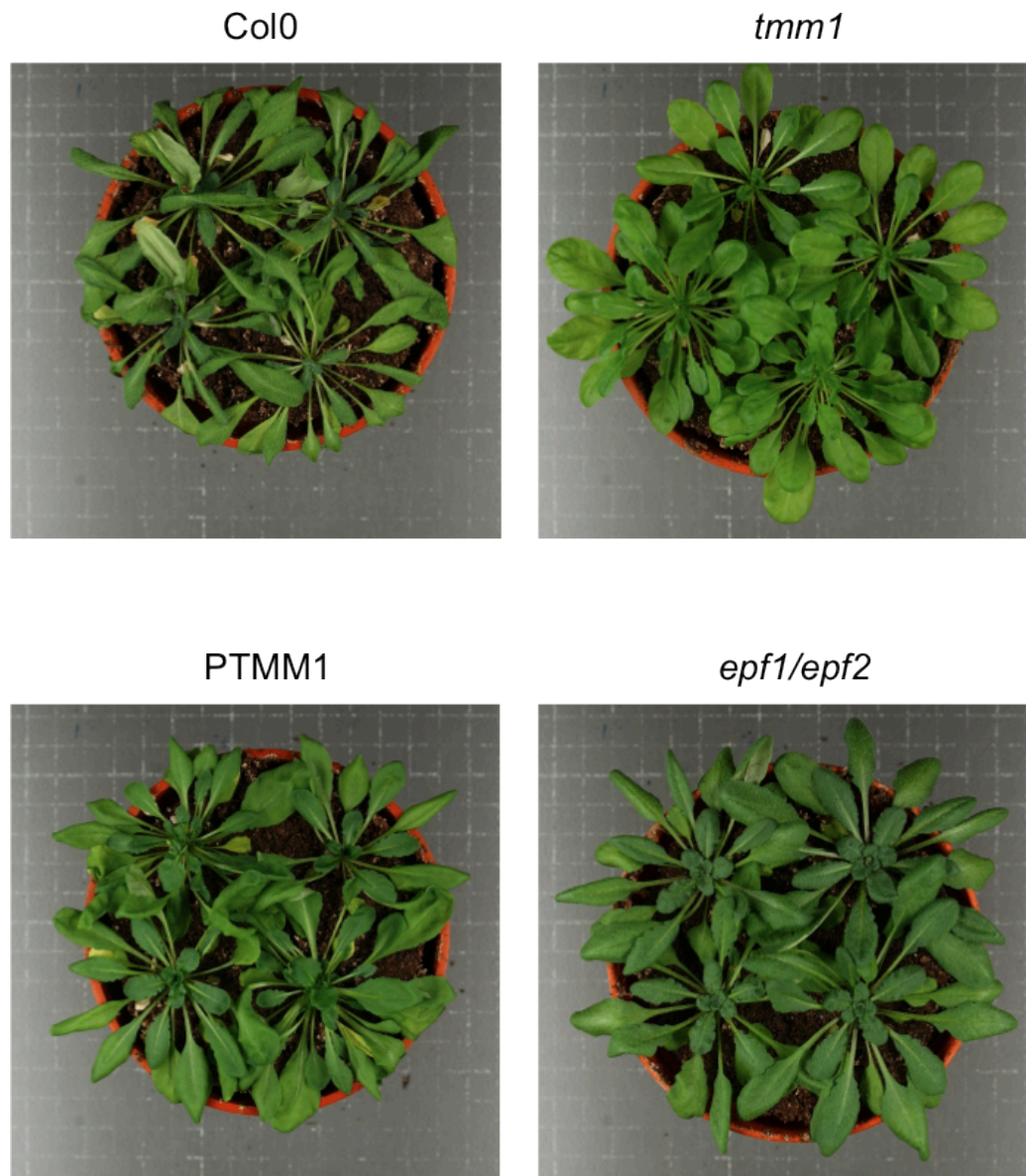


Figure 4. Effects of long-term drought stress on *A. thaliana* stomatal patterning mutants. Representative pictures of three week-old wild type, *tmm1*, PTMM1 and *epf1/epf2* plants exposed to drought stress by withholding watering for 4 weeks.

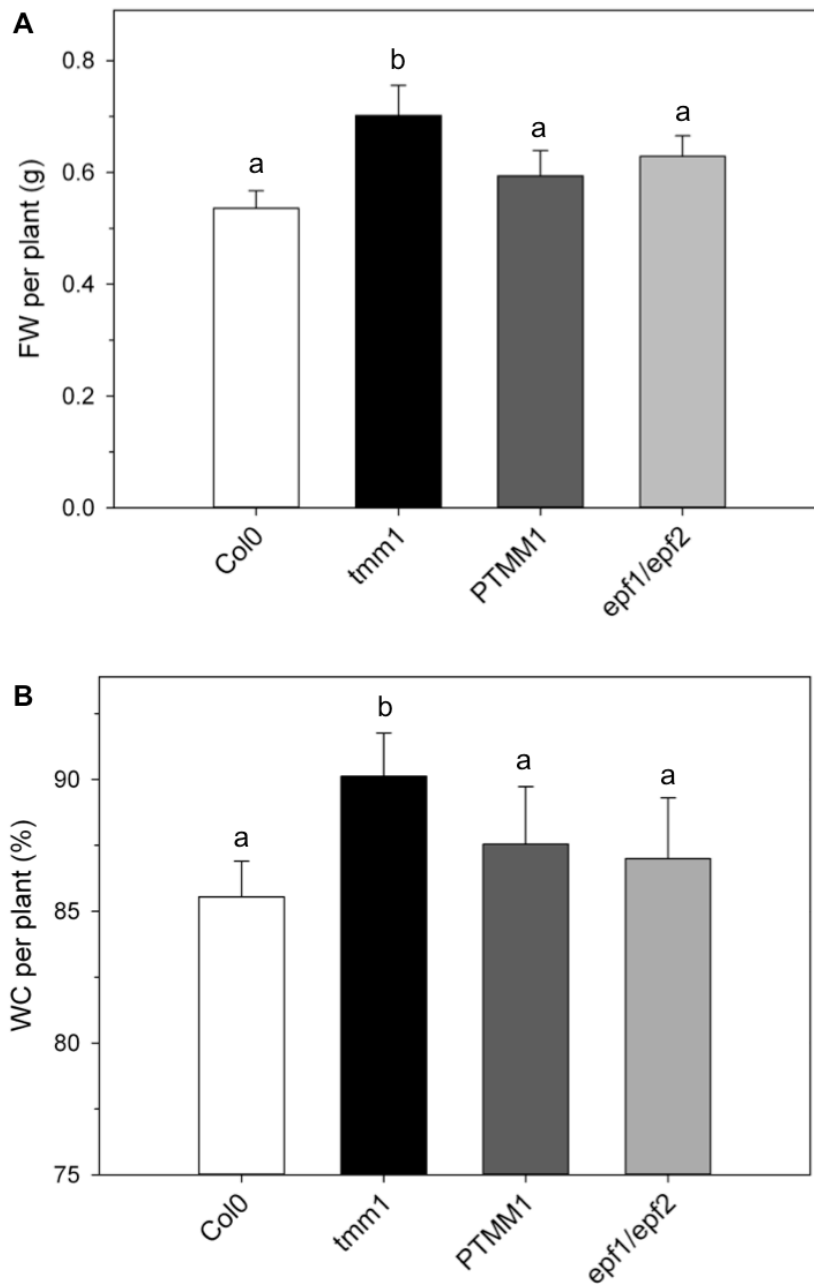


Figure 5. Quantification of sensitivity of *A. thaliana* stomatal patterning mutants to long-term drought stress.

Three week-old *Arabidopsis* wild type (white), *tmm1* (black), PTMM1 (dark grey) and *epf1/epf2* (grey) plants were exposed to drought stress by withholding watering for 30 days. Graphs represent (A) Fresh weight and (B) water content per plant. Data are means \pm SE of n=3 independent experiments. Lettering indicates significance after t-test (P<0.05).

The higher water content of *tmm1* plants under drought stress might arise from a higher accumulation of osmotically active compounds in these mutants. Although I did not carry out an analysis of osmotic contents under drought stress, the osmotic content of *Arabidopsis* plants grown under the control conditions ($70 \mu\text{mol m}^{-2} \text{s}^{-1}$ of PAR and 60% RH) did not display any substantial differences among the four lines (Figure 6). The osmotic contents were 327 ± 9 mOsm for wild type, 334 ± 14 mOsm for PTMM1 and 335 ± 12 mOsm for *epf1/epf2* leaves, when analysed using a vapour pressure depression osmometer. Although the *tmm1* yielded osmotic content of 360 ± 18 mOsm suggesting a minor increase, this difference was not statistically significant. Thus, stomatal patterning defects seem to not influence the accumulation of osmolytes at the leaf level.

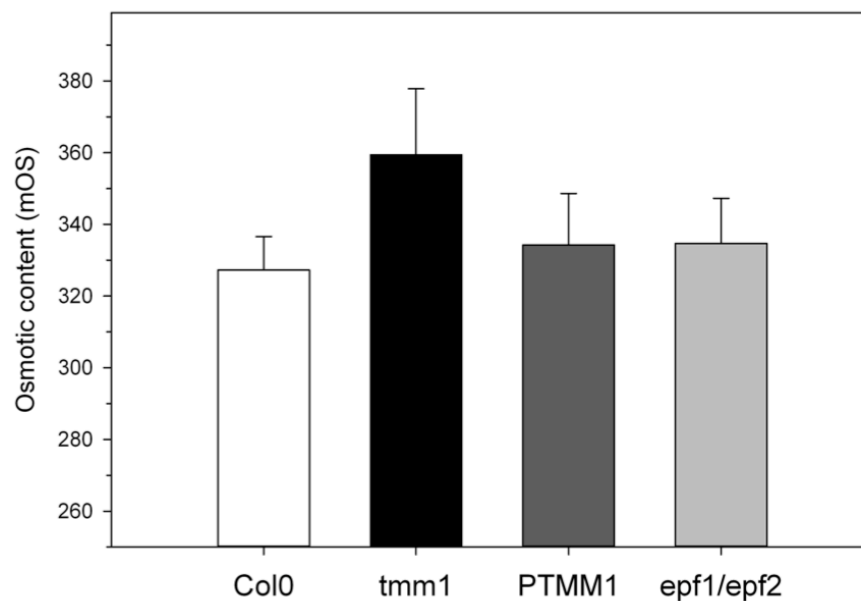


Figure 6. Osmotic content of *A. thaliana* stomatal patterning mutants.

Leaves from three-week old *Arabidopsis* wild type (white), *tmm1* (black), PTMM1 (dark grey) and *epf1/epf2* (grey) plants grown under $200 \mu\text{mol m}^{-2} \text{s}^{-1}$ of PAR and 60% RH were harvested to measure osmotic content. Data are means \pm SE of $n=6$ independent experiments. No statistical differences after ANOVA ($P < 0.05$) were detected.

4.2.3 Stomatal patterning mutants affected in root architecture

Stomatal closure is one of the best-defined responses of plants against drought stress. Yet, plants possess additional strategies to alleviate such stress, including the production of ABA, the induction of drought- and ABA-responsive genes and the modification of their root system. Indeed, plants respond to drought stress by altering their root system in order to reach deeper soil strata and ensure water uptake. This adaptive response includes the expansion of the main root as well as the inhibition of the lateral root formation, a phenomenon also observed during exogenous application of ABA (Smith & De Smet 2012). However, Vartanian et al. (1994) concluded on that progressive drought promotes the formation of short lateral roots, to not only withstand the stress, but also to allow the generation of the root system upon rehydration. This inconsistency in the literature results from the different experimental procedures used to apply and measure drought stress. Interestingly, here, I presented that the stomatal clustering of *tmm1* mutants impeded the proper stomatal function, but it also improved the resilience of plants to severe water stress as the result of minimized transpirational water loss. However, to exclude for the possibility of non-stomatal factors acting for this drought-resistant phenotype, I was interested in investigating the root system of the stomatal patterning mutants and assess both the size and its organization.

For this reason, *Arabidopsis* seedlings were grown on vertical agar plates containing 0.5 MS in the absence and presence of sucrose (0% and 0.5% sucrose, respectively). Light was supplied at moderate intensity ($150 \mu\text{mol m}^{-2} \text{s}^{-1}$) for 9 hours per day. Plates were scanned on day 8 post germination and the root system architecture was quantified using the EZ-Rhizo software (Armengaud et al. 2009). The root system architecture (RSA), which accounts for the organization of the main and lateral roots as well as other secondary roots, is highly influenced by both genetic and environmental factors. For instance, low availability of nitrogen or phosphorus led to longer lateral roots, whereas the reversed was detected when plants grown in low K (Kellermeier et al. 2013). EZ-Rhizo provides a considerably fast but reliable tool for the analysis of root system by enabling the quantification of several parameters contributing to the

RSA. For instance, EZ-Rhizo detects lateral roots of 0.1 mm in length that allows investigation of the RSA from very early stages. In addition, the software automatically adds up the length of individual lateral roots and that of the main root, reporting on overall growth of the root system. Another important property of the software is its non-invasiveness that allows the user to follow a given parameter over time and thus study the kinetics of root growth (Armengaud et al. 2009). The authors reported on the validity of the EZ-Rhizo software by carrying out quantitative trait loci analysis with different *Arabidopsis* accessions and showing that the natural variation of the root system was uncovered by eight root parameters. In addition, another study, using the EZ-Rhizo software and testing fourteen different *Arabidopsis* accessions under K-starved conditions, highlighted the impact on the RSA of more root-related parameters than the usual main root length and number of lateral roots (Kellermeier et al. 2014). This study also showed the presence of two different strategies in coping with K-starvation; the plants maintained main root length by compromising the lateral root elongation or they stopped growing in main root and favour lateral root branching.

Although a range of parameters are available through the EZ-Rhizo software, here, I only measured five parameters: 1) The total root size (TRS), which describes the sum of the main and lateral root length, 2) the main root (MR) path length, 3) the lateral root (LR) path length, 4) the number of lateral roots and 5) the lateral root density per main root, which accounts for the number of lateral roots per cm of the main root length. Figure 7 displays representative images of the four *Arabidopsis* lines taken 8 days post germination. Addition of external sucrose caused the alteration of the RSA of the *tmm1* and *epf1/epf2* mutant lines when compared to the wild type and PTMM1 lines. Additionally, the *epf1/epf2* mutants showed differences in the RSA under sucrose starvation.

Quantification of the root phenotype resulted in observations that did not link the RSA of the *tmm1* plants with the drought-resistant phenotype reported earlier. Under sucrose starvation, no discernible differences were detected in any of the root parameters between the wild type, PTMM1 and *tmm1* lines. The *epf1/epf2* double mutant showed a minor increase in TRS, MR and LR length and number of LRs, but this difference was not statistically significant when

compared to the wild type plants. However, the *epf1/epf2* seedlings showed a denser root system, producing 2.5 ± 0.3 roots per cm of MR comparing to 1 ± 0.4 of wild type. Supplementing the medium with sucrose resulted in the expansion of root system for the wild type and PTMM1 plants, since all parameters appeared larger than the sucrose deficient conditions. In particular, the TRS of wild type and PTMM1 plants was 5.8 ± 0.8 cm and 4.6 ± 0.6 cm, respectively, corresponding to 62% increase compared to that in sucrose-deficient conditions. A similar situation was also apparent for the MR length and the number of LRs, where the parameters were 45-56% greater than those under sucrose starvation. Although the *tmm1* mutant produced a bigger root system under sucrose-abundant conditions, it exhibited a stunting in root expansion in comparison with the wild type and PTMM1 plants. Indeed, the TRS of *tmm1* mutant was 2-fold smaller than the wild type plants, with its MR length being 3.1 ± 0.1 cm compared to 4.4 ± 0.2 cm of wild type and 4 ± 0.2 cm of PTMM1. The *tmm1* mutants produced 56% fewer LRs, with a mean LR length of 0.17 ± 0.01 cm compared to 0.25 ± 0.02 cm for the wild type plants. This set of data ensued that stomatal clustering was associated with significant changes in the root system architecture of the plants only when the carbon status, which was apparent as the sucrose supply, was not limited.

Remarkably, supplementing the medium with 0.5% sucrose did not alter the RSA of the *epf1/epf2* double as it did with the rest of *Arabidopsis* lines. The MR length of the *epf1/epf2* mutants was slightly reduced to 2.2 ± 0.08 , when sucrose was included on the medium, whereas the LR density was marginally increased in the *epf1/epf2* plants, corresponding to 2.8 ± 0.1 roots per cm of MR. In contrast, the LR length remained unchanged between the two sets of conditions, yielding a value of approximately 0.25 cm. The inhibited growth of *epf1/epf2* seedlings under full media was also detected when compared this mutant line with the wild type plants, with the TRS of *epf1/epf2* seedlings being reduced by about 26%. Indeed, the length of MR was half of the wild type under sucrose abundant conditions. Similarly, the number of LR was declined resulting in 3.5 ± 1 LRs compared to 5.9 ± 1.3 LRs of the wild type. However, both in the presence and absence of sucrose, the LR density of the *epf1/epf2* seedlings was consistently higher than the wild type. Overall, the *epf1/epf2* seedlings

exhibited a more compact and denser RSA comparing with the wild type, and they appeared defective in root growth when conditions became favourable. This finding implied a potential role of the *EPF1* and *EPF2* genes in developmental processes, distinct from the stomatal developmental program, as it is discussed below.

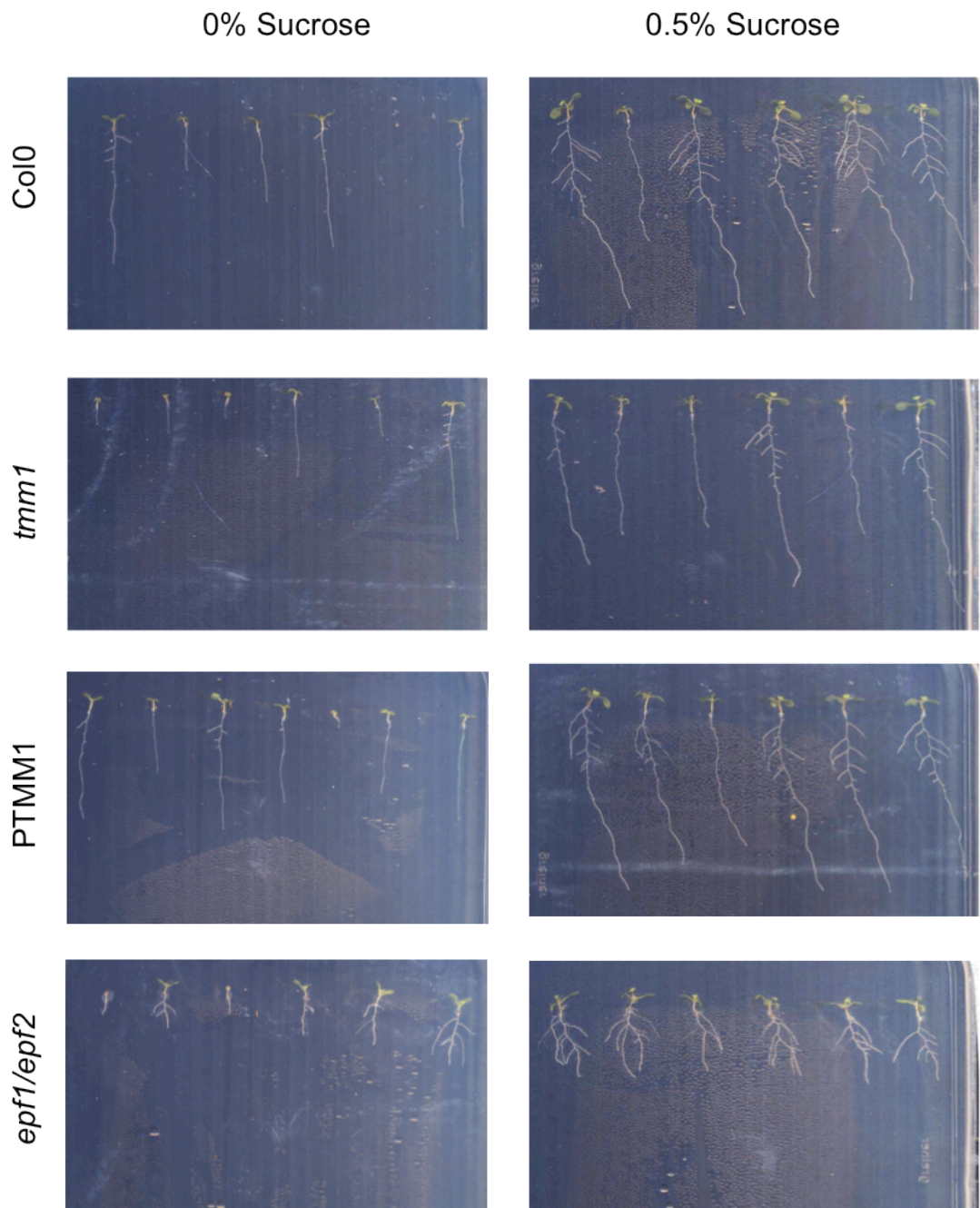


Figure 7. Effects of sucrose starvation on *A. thaliana* stomatal patterning mutants.

Representative pictures of *Arabidopsis* wild type, *tmm1*, PTMM1 and *epf1/epf2* seedlings grown on agar plates containing 0.5 MS and supplemented with 0% (left panel) and 0.5% (right panel) sucrose conditions. Photographs were taken 8 days post germination.

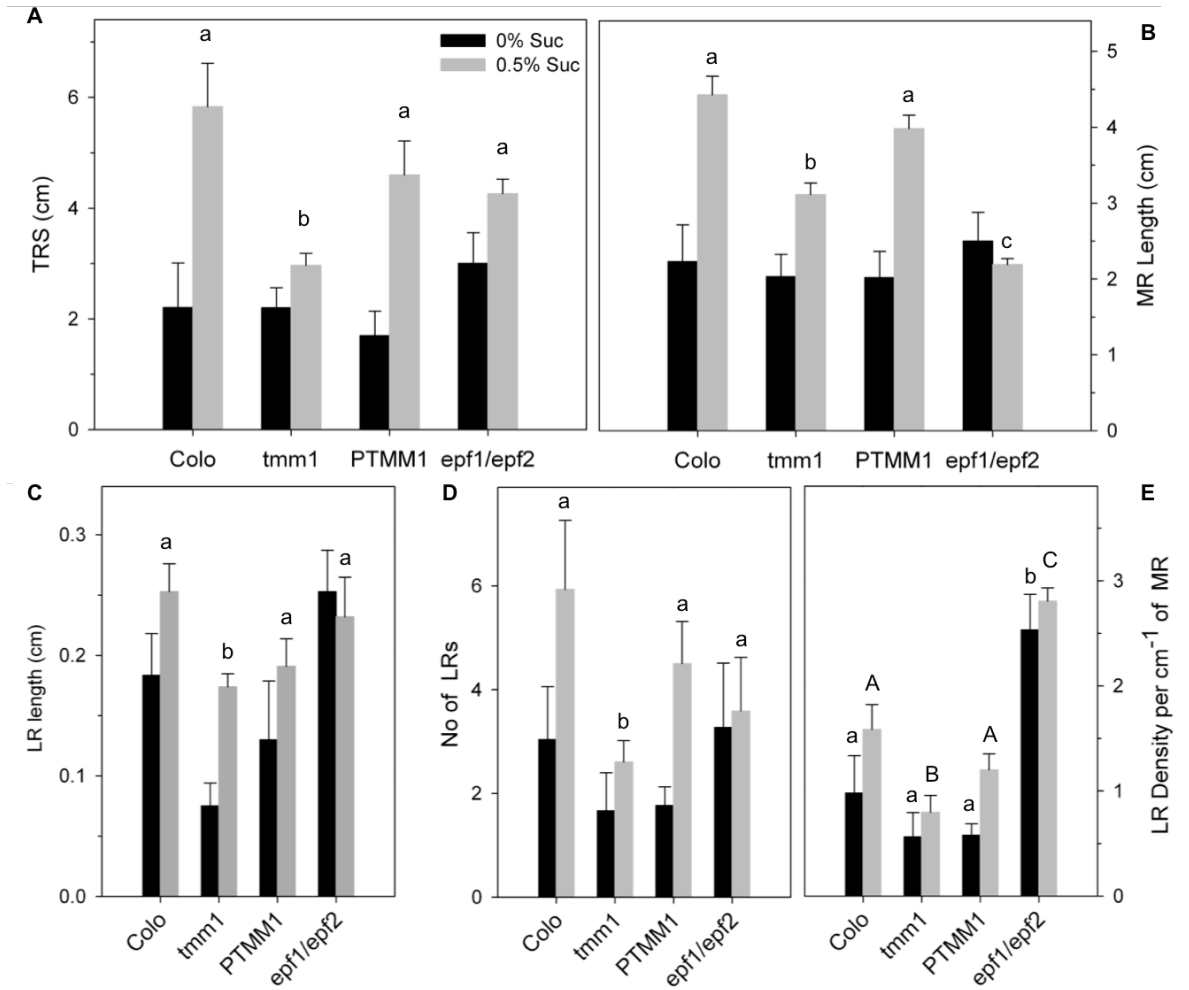


Figure 8. Quantification of sensitivity of *A. thaliana* stomata mutants to sucrose starvation.

Root architecture was quantified from *Arabidopsis* seedlings grown under sucrose deficient (black) and normal (gray) conditions, at 8 days post germination. Graphs represent (A) total root size, (B) main root length, (C) lateral root length, (D) number of lateral roots and (E) density of lateral roots. Data are means \pm SE of n=6 independent experiments. Lettering indicates statistical differences after ANOVA ($P < 0.05$) as determined by Student-Newman-Keuls test performed between lines at each condition.

4.3 Discussion

As mentioned in the previous chapter, manipulation of stomatal numbers can improve WUE through altering gas exchange responses (Yoo et al. 2009; Yoo et al. 2010; Tanaka et al. 2013; Lawson & Blatt 2014). I additionally presented evidence that stomatal clustering has a big impact on gaseous exchange and that stomata in “clustered” plants showed much attenuated behaviours when compared to stomata in plants without clusters. It is suggested that stomatal clustering in *Begonias* is involved in water conservation, albeit no quantitative data exist to support that (Hoover 1986; Tang et al. 2002). The little information available on the impact of stomatal clustering in plant growth and fitness attracted me to investigate whether the unique spatial arrangements of stomata in stomatal clusters confer any advantage when plants were grown under adverse environmental conditions. On the basis of three following key observations, I proposed that the stomatal impairment of the “clustered” mutant plants resulted in better performance of the plant only when the water status of the plant was important for the plant growth: 1) Plant biomass and WUE were altered in *tmm1* plants exposed to conditions of elevated light and of low evaporative demand, 2) drought stress did not lead to any obvious drought phenotype in *tmm1* mutants and 3) root growth of *tmm1* was suppressed under nutrient and water abundant conditions.

4.3.1 Does stomatal clustering hinder plant growth under growth-favourable conditions?

The altered gas exchange and stomatal responses in the “clustered” plants could be translated in the growth suppression of these plants, since these processes are crucial for cell and leaf expansion as well as biomass production (Tardieu et al. 2014). Under favourable conditions, the optimization of the trade-off between photosynthesis and transpiration is translated into improvement of WUE and thus biomass production (McAusland et al. 2013). Indeed, here I reported that improper spacing between stomata affected the biomass production via suppressing CO₂ assimilation (Figure 2). My experimental scenario was based on

the concept that under high light conditions the stomatal aperture becomes the limiting factor for photosynthesis, whereas under low light conditions photosynthesis mainly depends on the photon density rather than stomatal conductance (Hummel et al. 2010; Lawson & Blatt 2014). It is also proposed that CO₂ assimilation will reach saturation even though stomatal conductance continues to elevate due to the non-stomatal limitations imposed by the biochemistry of photosynthetic machinery (Farquhar & Sharkey 1982). Transpiration, on the other hand, rises linearly with the increase of stomatal conductance (Yoo et al. 2009). Therefore, elevating the RH at high light conditions reduces the vapour pressure difference between the leaf and atmosphere allowing plants to overcome the restriction of stomatal aperture.

Three lines of evidence underlined these concepts and pointed to the attenuated stomatal behaviour of the *tmm1* mutants:

1) When RH was saturated and at low light of 70 $\mu\text{mol m}^{-2} \text{s}^{-1}$, the photosynthetic assimilation was not affected in the lines with single stomata, suggesting that stomatal conductance actually was not the limiting factor. Considering the impaired stomatal conductance of “clustered” plants (see Chapter 3, Figure 12), the same argument holds true from the observation of no difference in the gas exchange responses between single stomata and clustered plants at control conditions.

2) At 200 $\mu\text{mol m}^{-2} \text{s}^{-1}$ of PAR, which is close to saturating light, the wild type and PTMM1 plants reached CO₂ assimilation rate of 5.28 ± 0.36 and 5.31 ± 0.03 $\mu\text{mol m}^{-2} \text{s}^{-1}$, in agreement with the A_{max} observed from the light curves (4.5 ± 0.26 and 4.09 ± 0.32 $\mu\text{mol m}^{-2} \text{s}^{-1}$; see Chapter 3, Fig. 6B). Nevertheless, the *tmm1* mutants showed a significant reduction in photosynthesis and biomass, emphasizing on the impaired stomatal movements in these plants and the importance of stomatal conductance as a limiting factor under these conditions.

3) At 200 $\mu\text{mol m}^{-2} \text{s}^{-1}$ of PAR, the wild type and PTMM1 plants exhibited similar levels of A independently of the level of RH. The biomass production of these lines was higher when RH was elevated to >90% and this is in accordance with their higher WUE efficiency under this condition. Although the *tmm1* plants grew bigger at saturating light and RH, they failed to grow at moderate light levels to

the same extent as the “single stomata” lines. Also, the WUE of *tmm1* plants under this condition was significantly suppressed, since they showed similar CO₂ assimilation but significantly higher transpiration rate than the “single stomata” plants. This latter finding suggests that the abnormal spacing of *tmm1* impairs stomatal function, which in turn prevents balancing of gas exchange to ensure maximum growth under optimum conditions.

Eisenach et al. (2012) employed a similar experimental design with the *syp121* mutant, which shows delayed stomatal reopening due to inhibition of K_{IN} channel trafficking, demonstrating its stunted growth and suppressed photosynthesis when the parameters were mainly dependent on stomatal conductance. As presented here and previous chapter, stomatal density also has a huge impact on plant physiology and growth. Studies with the *Arabidopsis* mutants of the EPF family reported the enhancement of plant growth in conditions of high evaporative demand, when the stomatal density was decreased (Doheny-Adams et al. 2012). The authors suggested that the improved biomass of plants with reduced number of stomata was due to the higher temperature, which facilitates photosynthesis, the improved water status of the plant as well as to the lower metabolic cost of developing stomata. Another study showed that *gtl1* improves WUE efficiency and therefore biomass production because of the lower transpirational water loss that is caused of the lower stomatal density in the abaxial side of the leaf (Yoo et al. 2010). However, it is considered that changes in stomatal density associate with parallel changes in stomatal aperture and thus the latter has a greater impact on stomatal conductance (Lawson 2009). In agreement with this, the presented data highlighted the significance of functional stomata in plant growth and particularly the inhibitory effect of impaired stomatal opening of *tmm1* plants on plant growth when conditions were favourable.

4.3.2 Evidence on drought resilience due to stomatal clustering?

The maximum WUE is commonly observed at situations where stomatal conductance is not the limiting factor, such as in drought stress, in mutants with low number of stomata or even in mutants with small apertures (Yoo et al. 2009).

Hence, I was interested in addressing whether the impaired stomatal movements of *tmm1* plants enabled them to sustain drought stress. My hypothesis was based on the observation that “clustered” stomata could maintain their water status due to reduced stomatal conductance. Of course, reduced conductance would prevent the enhancement of CO₂ assimilation when the stress is removed, thereby leading to a relative decline in WUE under favourable conditions. This greater capacity for water conservation would possibly lead to higher resilience to drought stress, comparing to functioning single stomata.

The mild drought stress data did not indicate any differences in the final biomass between the *tmm1* and wild type plants, as depicted from the fresh shoot weight and rosette area measurements (Figure 3). Similarly, the fresh shoot weight of *epf1/epf2* mutants was not suppressed. When the water stress was relieved, the shoot biomass of all four *Arabidopsis* lines was boosted. The *epf1/epf2* mutants reached similar biomass levels as the wild type plants, while the *tmm1* mutants showing slightly suppressed growth comparing to “single stomata” lines. This observation suggests that when conditions are favourable, high stomatal density might improve growth via enhanced CO₂ assimilation.

A positive correlation between stomatal density and CO₂ assimilation was observed in studies using *STOMAGEN* transgenic lines (Tanaka et al. 2013). The authors suggested that the higher photosynthetic rate of *STOMAGEN*-overexpressing lines was due to the higher stomatal conductance while the carboxylation activity was unaffected. Another study with the stomatal patterning mutant *gtl1* showed that high WUE is linked to the decreased stomatal conductance, which was the result of the lower stomatal density of this mutant (Yoo et al. 2010). These conclusions are consistent with the smaller increase in the shoot growth observed in *tmm1* mutants, indicating the significance of stomatal conductance and therefore aperture in WUE efficiency. CO₂ response (A-Ci) curves, stomatal conductance and chlorophyll fluorescence measurements with these lines would directly address whether the observed increase in shoot growth, when stress was alleviated, was due to differences in photosynthetic capacity or stomatal conductance.

The higher number of stomata of the *epf1/epf2* plants resulted in the greater transpirational water loss, which was reflected in the reduced water content of the shoots at the final day of drought stress (Figure 3C). Doheny-Adams et al. (2012) reported that *epf1/epf2* mutants were more able to adjust the transpiration rate in regard with the water availability. They also showed a positive correlation between the transpiration rate and temperature, whereas the opposite was observed between the transpiration rate and biomass. Interestingly, the *tmm1* plants did not show any substantial difference in the water content during drought stress despite the higher stomatal number. Apart from the altered transpiration, changes in the water content of the *epf1/epf2* plants could possibly be due to alterations in the osmotic content of the leaf. The osmotic content analysis of plants grown under control conditions did not show any difference in the accumulation of osmolytes in the shoots of the *epf1/epf2* and *tmm1* plants, inferring that this process was not influenced by the altered stomatal patterning (Figure 6). Hence, I suggested that the impaired stomatal function allowed the *tmm1* plants to maintain their initial water status during water stress, but it also hindered them from reaching a “single stomata”-like growth biomass level, when the water availability was not limiting.

Considering the above conclusions, we can hypothesize that the impaired stomatal conductance of plants with stomata in clusters might be beneficial under long-term water scarcity, since plants do not sense the stress given their consistent water status during the drought period. Indeed, the *tmm1* plants displayed improved fresh weight and water content compared to the single stomata plants after 30 days of water scarcity (Figure 4 and 5). Notably, the potential advantage of “clustered stomata” species under drought stress is in accordance with the habitat where the “clustered” *B. plebeja*. Moreover, studies with *B. heracleifolia* and *B. nelumbiifolia* showed that stomatal clustering can act as a way of water conservation, since this trait was apparent in niches that were limited of water supply (Hoover 1986). The same outcome from studies with *B. peltatifolia* was obtained, highlighting to a positive correlation of stomatal clustering and multiple epidermises, which is described as drought adaptation trait (Tang et al. 2002). Additionally, negative correlation between the degree of stomatal clustering and moisture of soil was

demonstrated in the species *C. camphora* (Zhao et al. 2006). Gan et al. (2010) reported 20% and 16% induction of stomata clustering under severe drought and salinity stress, respectively, in various plant species including *C. camphora*, *Melilotus suaveolens* and *Ginkgo biloba*. The authors proposed that in non-contiguous clusters, the close proximity of stomata produces a boundary layer of low vapour pressure difference, and therefore the water gradient is minimized resulting in lower transpirational water loss (Wilmer & Fricker, 1996; Gan et al. 2010).

All together the results suggested that stomatal clustering might provide an ecological advantage over single stomata when water conditions are limited and plant growth and physiology depends substantially on stomatal conductance. However, in order to further verify these proposition gas exchange measurements in stomatal clustered mutants under severe drought stress must be carried out. As shown in Figure 13 of chapter 3, the *tmm1* mutants close their stomata in response to ABA, though to a much lesser extent than the wild type plants. It would be important to examine whether the *tmm1* mutants contain different contents of ABA than single stomata and whether ABA-signaling is altered in these mutants.

4.3.3 Does stomatal patterning restrain root system architecture?

Plants respond to drought stress through the expansion of root system (Hummel et al. 2010) as well as via changes in stomatal patterning and behaviour to minimize the evaporative area (Fricke et al. 2006; Gan et al. 2010; Claeys & Inzé 2013). Remarkably, both *tmm1* and *epf1/epf2* mutants exhibited an altered root system architecture when compared with the wild type plants (Figure 7). To my knowledge, this is the first report of a root phenotype regarding stomatal patterning mutations. The root phenotype of *tmm1* plants was only apparent when the medium was supplemented with sucrose, whereas in the sucrose-deficient conditions the root system architecture of *tmm1* plants did not differ from that of wild type and PTMM1 plants (Figure 8). It is known that root elongation and LR emergence are controlled at post-embryonic level and highly

depend on the nutrient availability of the surrounding environment (López-Bucio et al. 2003; Malamy 2005; Kellermeier et al. 2014). In the current experimental design, the aerial parts of the seedlings were in contact with the medium enabling sucrose uptake through the shoots. Macgregor et al. (2008) showed that sucrose uptake via shoots in culture media were necessary and sufficient for LR emergence using the *lateral root development 2 (lrd2)* mutant, which is defective in cutin biosynthesis and it reverses the osmotic inhibition of LR emergence. They suggested that reduced permeability of shoots allows sucrose uptake via two routes, the composition of the cuticle and/or the stomatal aperture. When the *speechless* mutant (i.e. no stomata phenotype) was placed in media supplemented with sucrose, there was a substantial decrease in sucrose uptake and this was intensified upon exogenous application of ABA, which induces cuticle formation (Macgregor et al. 2008).

The special experimental design used to quantify the root phenotype also involved the growth of the *Arabidopsis* seedlings under saturating humidity -i.e. sealed agar plates - and this could further explain the reduced root growth of *tmm1* plants. In such situation, stomata can fully open and therefore the unrestricted transpiration enables water flow and nutrient uptake, which eventually promote the root expansion. Given the attenuated function of stomata in clusters, one can assume that the smaller root growth expansion of *tmm1* plants was due to the lack of the transpirational driving force. Yet, this was not apparent in the case of sucrose-deficient media, where *tmm1* plants grew comparably to the “single stomata” plants. Thus, I ruled out that the observed root growth defects were brought by the altered water flow in these mutants.

Regarding the *epf1/epf2* root phenotype, the picture is more complicated. The mutants produced considerably denser root systems compared to wild type plants with or without sucrose supply, confirming that stomata function to promote sucrose uptake and therefore LR emergence. However, addition of exogenous sucrose resulted in significant repression of main root elongation. This phenotype is typical of that observed under low-P conditions, where plants promote extension of LRs to optimize the uptake of phosphate that tends to localize in the topsoil layers (Williamson et al. 2001; Abel 2011; Kellermeier et

al. 2014). Several studies have reported higher number of root hairs as well as clustered root hairs under P-starvation (Williamson et al. 2001; Muller & Schmidt 2004; Sánchez-Calderón et al. 2005). The factors acting to alter root system architecture in response to P-starvation are manifold, including auxin, ABA, NO and ROS (Smith & De Smet 2012; Niu et al. 2013). Moreover, it is known that several genes involved in root hair formation play a role in the formation of stomata in hypocotyl and of trichomes in leaves (Serna 2004). Whether the *epf1/epf2* mutants trigger different epidermal patterning in the roots and how the nutrient availability affects the root system architecture in these mutants required further in-depth investigation that was out of the scope of this project. However, it is known that cysteine-rich peptides, like the EPFs, are involved in diverse plant processes including the root development, plant defence and seed germination (Marshall et al. 2011). For instance, cysteine-rich peptides from the RALF (Rapid Alkanisation Factor) family have been shown to arrest the root growth and produce abnormal root hairs in tobacco (Pearce et al. 2001). Similarly, overexpression of RALF23 in *Arabidopsis* inhibited the root development when seedlings were treated with brassinolide, a hormone that induces root growth (Srivastava et al. 2009). It was also suggested that RALFs act via the activation of MAP kinases, a mechanism that is also shown for the EPFs and especially their involvement in MAPKKK signaling cascade during stomatal development (Bergmann et al. 2004; Sack 2004; Rodriguez et al. 2010).

The results from the above experiments (Figure 8) suggested that the *tmm1* mutant affected the growth of the root system in a stomata-dependent manner, linking sucrose uptake from aerial parts with the expansion of the roots. In contrast, the root growth of *epf1/epf2* seedling was similarly affected with and without sucrose, suggesting that the defects observed were not associated with the carbon supply and stomatal function. Indeed, one cannot exclude the possibility that EPFs are required beyond the stomatal developmental program, and that mutation in these genes result in an ectopic root phenotype. A priority now should be to design experiments in which the aerial parts of the seedlings are prevented from touching the media in order to ascertain the stomatal-dependent root phenotype of the *tmm1* plants. Albeit, the similar growth of plants on soil under control conditions implies that the observed root phenotype

is conditional that explains the lack of previous reports on the growth defects in the *tmm1* plants.

4.3.4 Outlook

In conclusion, the data showed, for the first time, a conditional growth phenotype of *tmm1* mutants under a range of environmental stresses. The suppressed growth of *tmm1* mutants under conditions with elevated light was designated as being the result of the impaired stomatal movements. Surprisingly, the distinctive stomatal behaviour of the *tmm1* mutants enabled the avoidance of transpirational water loss and thus the better survival of the plants under severe drought stress. This observation is in accordance with the proposed role of stomatal clustering to be an adaptive strategy for water-stressed habitats of various species, including *Begonia* species. Finally, a novel phenotype of both *tmm1* and *epf1/epf2* mutants was described, potentially coupling stomatal epidermal defects with changes in root system. Although more experiments are needed, I postulated that the *tmm1* root phenotype was linked to the defective stomatal function that in turn prevented sucrose uptake required for the expansion of the root system.

5 H₂S regulates stomatal movements via a novel pathway

5.1 Introduction

The repertoire of molecules inducing stomatal movements is vast, including several phytohormones as well as bioactive compounds. In the past, research has been highly focused on the role of ABA in stomatal movements and the mechanisms underlying it (Blatt 1990; Blatt & Thiel 1993; Blatt 2000; Roelfsema & Hedrich 2005; Mori & Murata 2011; MacRobbie 1998; Joshi-Saha et al. 2011). ABA signalling pathway involves a number of cytosolic mediators that promote stomatal closure, such as $[Ca^{2+}]_i$ and pH_i and ROS. A simplified diagram of the ABA pathway leading to stomatal closure is shown in Figure 1. Briefly, ABA triggers rise of $[Ca^{2+}]_i$ via the activation of Ca^{2+} -sensitive channels residing at the plasma membrane and via its release from the intracellular compartments. Elevated $[Ca^{2+}]_i$ levels inhibit the inward-rectifying K^+ channels, which prevent K^+ influx to the cell, and they also activate anion channels through the action of the calcium-dependent kinase proteins, which phosphorylate the anion channels. This later event enables the movement of anion out of the cell causing depolarisation of the plasma membrane. The parallel inhibition of the plasma membrane H^+ -ATPase by ABA further shifts the membrane potential towards more positive values. Hence, the combined depolarisation events of plasma membrane together with the elevated cytosolic alkalisation activate the outward-rectifying K^+ channels, in *Arabidopsis* defined by the GORK channel, and enable the efflux of K^+ . The activation of K_{OUT} and anion channels as well as the inhibition of K_{IN} causes loss of the guard cell turgor required for stomatal closure.

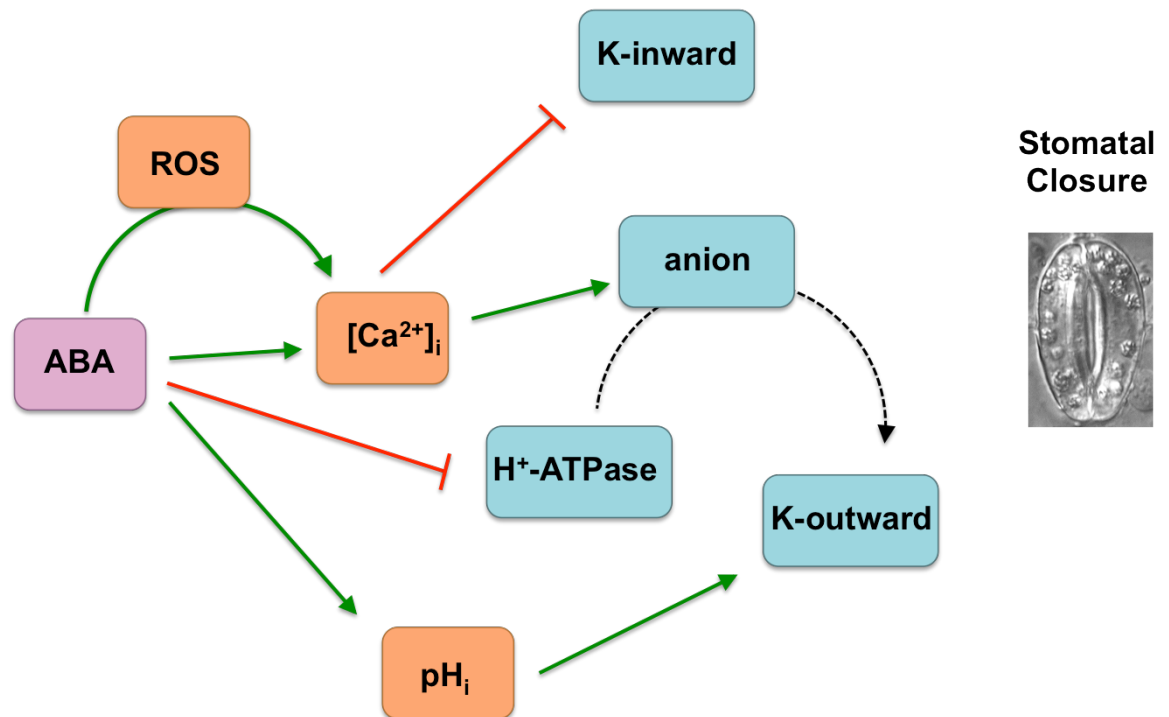


Figure 1. Simplified schematic diagram of the ABA signalling pathway.

Diagram displays the major mediators of the ABA pathway, where activation and inhibition events are shown with green and red arrows, respectively. ABA increases [Ca²⁺]_i via the activation Ca²⁺-sensitive channels residing at the plasma membrane and intracellular compartments, but also through the generation of ROS. The elevated [Ca²⁺]_i, in turn, inhibits the inward-rectifying K⁺ channels and activates the anion channels. Activation of anion channels results in efflux of Cl⁻ and the depolarisation of the plasma membrane (black arrow). The latter also occurs due to the suppression of the plasma membrane H⁺-ATPase, and the combined depolarisation effect activates the outward-rectifying K⁺ channels. Additionally, rise in intracellular pH activates the K⁺_{out} channels that drive the efflux of K⁺. Together the K⁺ and Cl⁻ efflux and inhibition K⁺ influx result in the loss of turgor of the guard cells and thus stomatal closure.

In recent years the bioactive gaseous molecule, hydrogen sulfide (H₂S), has been considered to be a novel stomatal effector as well as to promote tolerance to various biotic and abiotic stresses. H₂S is endogenously generated if plants are supplied with various sulfur sources such as SO₂ (Rennenberg 1983), and its emission occurs in a light-dependent way relying on reductants produced during photosynthetic reactions (Wilson et al. 1978). In the last decade, several H₂S-releasing donors have been discovered, with the most widely used being the NaHS and GYY 4137 that were shown to exert similar effects (García-Mata & Lamattina 2010; Lisjak et al. 2010). However, these H₂S donors differ in the speed of H₂S-release, with GYY 4137 being a more slow-releasing H₂S molecule

than NaHS (Li et al. 2008). The positive effects of H₂S on abiotic tolerance have been shown to rely on the antioxidant properties of the molecule. For instance, treatment of wheat plants with H₂S donors resulted in the reduction of ROS production via the altered regulation of genes involved in oxidative stress, conferring osmotic stress tolerance and enabling seed germination (Zhang et al. 2010a). Similar altered gene expression was observed in soybean seedlings treated with NaHS, which alleviated the drought stress, further supporting an antioxidant property for H₂S (Zhang et al. 2010b). Chen et al. (2011) showed that NaHS treatment improved photosynthetic capacity of *Spinacia oleracea* through enhancing the expression and activity of RuBISCO and other proteins participating in thiol redox modification. They also reported that biomass, chlorophyll content, number of granular lamellae in chloroplasts and protein content of *S. orelacea* were saturated at 100 µM NaHS (Chen et al. 2011).

Yet the effect of H₂S on stomatal aperture remains controversial. Lisjak et al. (2011) showed that treatment of epidermal peels with H₂S triggered stomatal opening under light and it prevented stomatal closing under darkness. However, another study suggested the stomatal closure upon treatment with H₂S, via an ABA-dependent manner (García-Mata & Lamattina 2010). These authors made use of NaHS, hypotaurine, which is a H₂S scavenger, and ABA and tested their actions in stomatal aperture measurements. They showed that the scavenger indeed blocked the effect of H₂S on stomatal closure, but it also led to a recovery in the stomatal apertures (at least partially) when guard cells were treated with ABA (Figure 2). From this latter observation they suggested that H₂S could be a downstream product of the ABA signalling pathway.

Apart from the effect of H₂S in stomatal movements, the mechanism by which it drives stomatal dynamics is not yet known. García-Mata & Lamattina (2010) found that use of glibenclamide, an inhibitor of ABC transporters, blocked the H₂S-induced stomatal closure and therefore they suggested that H₂S might act through regulation of these proteins, which in turn regulate various ion channels at the plasma membrane (Leonhardt et al. 1999a; Suh et al. 2007).

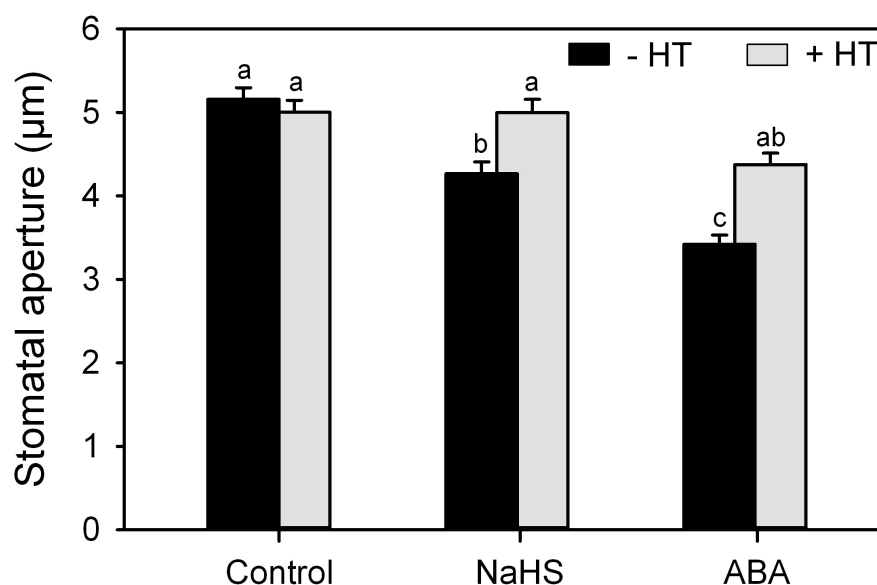


Figure 2. Hydrogen sulfide is involved in ABA-dependent stomatal closure in *Vicia faba*.

Epidermal strips were treated with opening buffer (10 mM KCl-MES, pH 6.1) for 2 hours in the absence (black) or presence (grey) of 200 µM hypotaurine. The peels were subsequently treated with 100 µM NaHS or 25 µM ABA. Hypotaurine fully recovered stomatal closure induced by NaHS and partially blocked the ABA effect.

The guard cell plasma membrane facilitates the diffusion of environmental signals, including molecules, to allow stomata perceiving and responding to the surrounding environment in an independent manner, since they do not possess plasmodesmata (Wilmer & Fricker, 1996). In the previous chapters, I presented the impaired stomatal function of “clustered” stomata due to the altered ion transport through the guard cell plasma membrane. Whether the perception of gaseous signals is similarly altered in the “clustered” stomata remains to be answered. To address this question, I used the novel H₂S gasotransmitter to perform stomatal aperture measurements and investigate the response of both “single” and “clustered” stomata. In addition, the lack of information on the mechanism by which H₂S acts on stomata led me to investigate its effect on guard cells *per se*. For this purpose, I decided to employ *Nicotiana tabacum* plants because of the large stomata and the ease with which they permit electrophysiological studies. I made use of GYY 4137 donor as the H₂S source because of its similar effects to NaHS (Lisjak et al. 2010), but its lower corrosion effect on the electronic equipment. I performed both stomatal aperture measurements and electrophysiological studies focusing on the K⁺ and Cl⁻

channels residing at the plasma membrane. Also, the previously reported sensitivity of H₂S-induced stomatal closure on ABA was revisited. To identify the mechanisms underlying the H₂S effect on stomata, I investigated whether H₂S led to changes in [Ca²⁺]_i. Finally, the experimental data were fed into the OnGuard model, which confers a holistic view of the stoma incorporating all the transporters and salient features of osmolytes, [Ca²⁺]_i and pH_i (Chen et al. 2012; Hills et al. 2012). Doing so, I exploited its potential as a prediction model in order to give insight into the parallel changes occurred in guard cells.

5.2 Results

5.2.1 Stomatal clustering prevents H₂S-induced stomatal closure

Firstly, the effect of H₂S on stomatal movements needed to be determined given the controversial data in the literature. Thus, I performed stomatal aperture measurements of tobacco epidermal peels treated with increasing concentrations of H₂S donor. The epidermal peels were submerged into opening buffer (60 mM KCl-MES, pH 6.1) and placed under light of ~150 μmol m⁻² s⁻¹ for 2 hours to ensure maximum opening of stomata. Subsequently, they were bathed for 90 minutes in control buffer (10 mM KCl-MES; pH 6.1) supplemented with 0, 0.1, 1 or 10 μM GYY 4137. Stomatal aperture measurements were determined before and after H₂S treatment. Figure 3 presents the H₂S-induced stomatal closure relative to that of the control treatment. Exposure to the control buffer yielded stomatal apertures of 6.63 ± 1.77 μm whereas treatment with H₂S donor resulted in stomatal apertures ranging from 5.94 to 4.83 μm. Fitting the data to hyperbolic decay function, the K_{1/2} was determined with 0.16 ± 0.04 μM of GYY 4137 resulting in 50% stomatal closure. The data supported the previously proposed stomatal closing effect of H₂S and they also indicated a dose-dependent response, since elevating the levels of H₂S donor resulted in augmented stomatal closure.

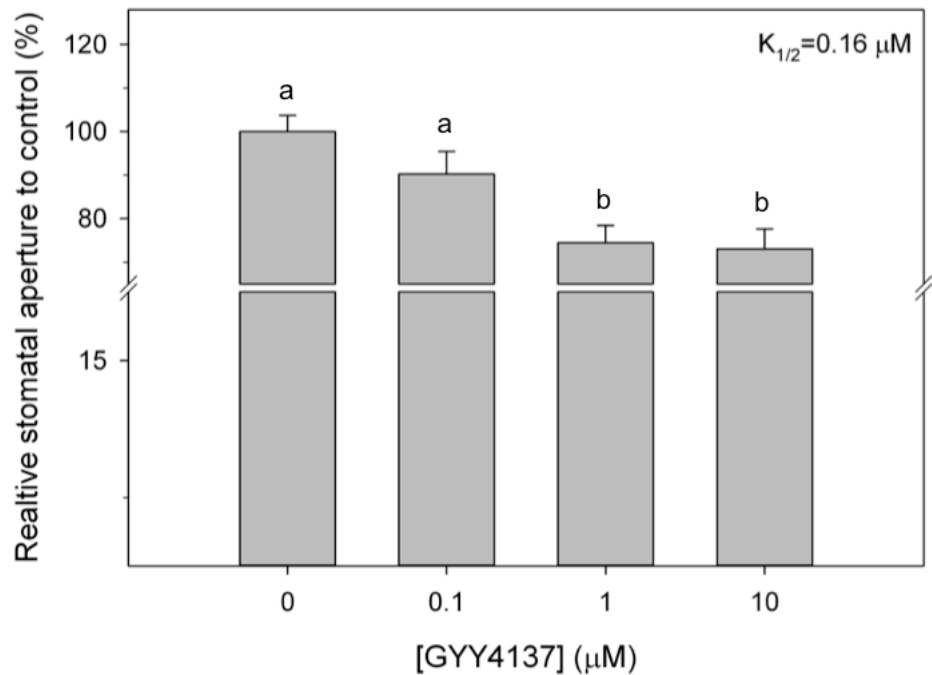


Figure 3. H₂S triggers stomatal closure in a dose-dependent manner.

Epidermal peels from *N. tabacum* were pretreated in opening buffer (60 mM KCl-MES, pH 6.1) and placed under light for 2 hours to ensure maximum stomatal opening. They were subsequently treated with control buffer (10 mM KCl-MES, pH 6.1) containing 0.1, 1 or 10 μM GYY 4137 for 90 minutes. Stomatal apertures were normalized to the control treatment (0 μM GYY 4137). Data are means ± SE of n=50 stomata. Hyperbolic decay function was fitted to data, resulting to a $K_{1/2}$ of $0.16 \pm 0.04 \mu\text{M}$. Lettering indicates statistical differences after ANOVA ($p < 0.05$), as determined by Student-Newman-Keuls test.

In chapter 3, the defective stomatal closure of the “clustered” *tmm1* mutant upon exposure to high external Ca²⁺ and ABA was presented (Figure 14). In order to examine the effect of stomatal clustering on the perception of gaseous signals, I performed stomatal aperture measurements from *A. thaliana* wild type, *tmm1* and PTMM1 epidermal peels that were with H₂S donor. The experimental design was the same as above, but only 10 μM GYY 4137 was used. Figure 4 represents the stomatal closure that was induced by the H₂S donor and was determined on cell-by-cell basis. Treatment of stomata with H₂S donor triggered approximately 58% stomatal closure in both wild type and PTMM1 plants. However, the stomata of *tmm1* mutant responded weakly to H₂S, reaching only 32% stomatal closure. This finding further highlighted the importance of proper spacing between stomata to respond on stimuli independent of these being of soluble or gaseous nature.

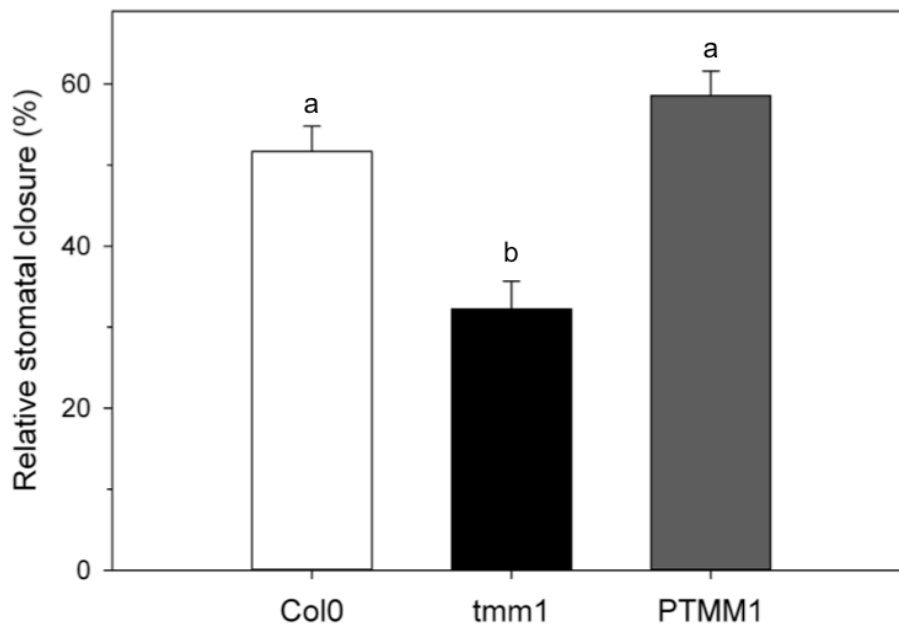


Figure 4. Stomatal clustering inhibits H₂S-induced stomatal closure.

Epidermal peels from *A. thaliana* wild type (white), *tmm1* (black) and PTMM1 (dark grey) were pretreated in opening buffer (60 mM KCl-MES, pH 6.1) and placed under light for 2 hours to ensure maximum stomatal opening. They were subsequently treated with control buffer (10 mM KCl-MES, pH 6.1) supplemented with 10 μM GYY 4137 for 90 minutes. Relative stomatal closure was determined on cell-by-cell basis. Data are means ±SE of n>20 stomata. Lettering indicates statistical differences after ANOVA (p<0.001), as determined by Student-Newman-Keuls test.

5.2.2 H₂S-induced stomatal closure is linked to inhibition of inward-rectifying K⁺ channels

As described in previous chapters, stomatal movements require the fluxes of osmolytes, mainly the K⁺ ions, across the plasma membrane of guard cells. K⁺ fluxes depend on the voltage-dependent K_{IN} and K_{OUT} channels. Making use of the two-electrode voltage clamp technique, I recorded I_{KIN} and I_{KOUT} under the effect of H₂S donor. Epidermal peels were bathed in control buffer (10 mM KCl-MES; pH 6.1) and subsequently were treated with control buffer supplemented with 10 μM GYY 4137 (10 mM KCl-MES; pH 6.1 + 10 μM GYY 4137). Current recordings were carried out by clamping at voltages ranging from -220 to +40 mV, following a holding voltage at -100 mV. Figure 5 presents current traces and average steady-state currents as a function of voltage (I-V curve) from guard cells before (control buffer) and after at least 5 minutes of exposure to 10 μM GYY 4137. I-V curves displayed voltage dependence of both I_{KOUT} and I_{KIN}, as previously described (Gradmann et al. 1993; Blatt 1992). Voltages positive of -40 mV yielded I_{KOUT} that were higher in amplitude as voltage was increased. The mean amplitude of I_{KOUT} at +27 mV was 120 ±28 and 91 ±30 μA cm⁻² before and after exposure to GYY 4137, though this difference was not statistically significant. Voltages negative of -100 mV were marked by I_{KIN}, with decreasing voltage resulting in higher amplitudes of I_{KIN}. The mean I_{KIN} at -220 mV of the H₂S treatment was reduced by 90%, yielding mean current amplitude of -21 ±8 μA cm⁻² compared to -169 ±12 μA cm⁻² of the control. Hence, the data suggested the exclusive inhibition of K_{IN} channels by H₂S donor. For this reason, in the following experiments I focused on the investigation of K_{IN} channels. Exposure to GYY 4137 also affected the activation half times of K_{IN} channels. I_{KIN} recorded under control treatment relaxed to a new steady-state within ~900 ms, whereas the response to H₂S treatment was significantly slower and completed within ~1400 ms (Figure 6). Mean half times of I_{KIN} activation at -220 mV was 710 ±70 ms for control treatment and 1230 ±230 ms after exposure to 10 μM GYY 4137, implying a change in the gating of the K_{IN} channels.

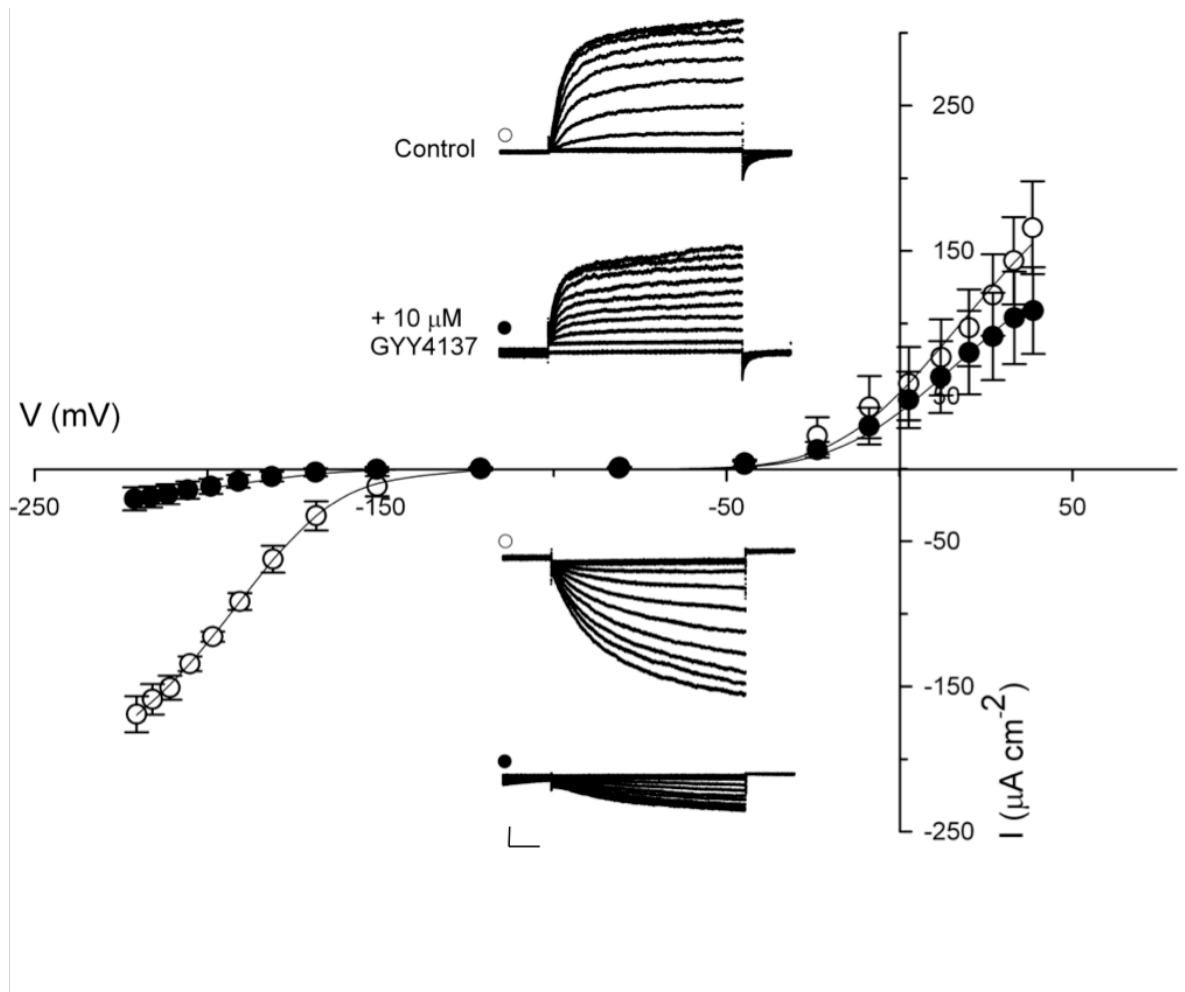


Figure 5. H₂S selectively inactivates currents from inward-rectifying K⁺ channels in *N. tabacum*.

Currents were recorded for outward- (I_{KOUT} ; top) and inward-rectifying (I_{KIN} ; bottom) K⁺ channels under voltage clamp. Voltage clamp protocol consists of steps (20 mV) of 6 seconds between -220 and 0 and 4 seconds between 0 and +40 mV, following a holding voltage at -100 mV. Guard cells were bathed in 10 mM KCl (white circles) and 10 mM KCl supplemented with 10 μ M GYY4137 (black circles). Data are means \pm SE of $n=5$. Curves were jointly fitted to Boltzmann function (solid lines), with $V_{1/2}$ and gating charge δ held in common. Insets present current traces recorded under voltage clamp. Scale bar: horizontal line 2 seconds and vertical line 50 μ A cm⁻².

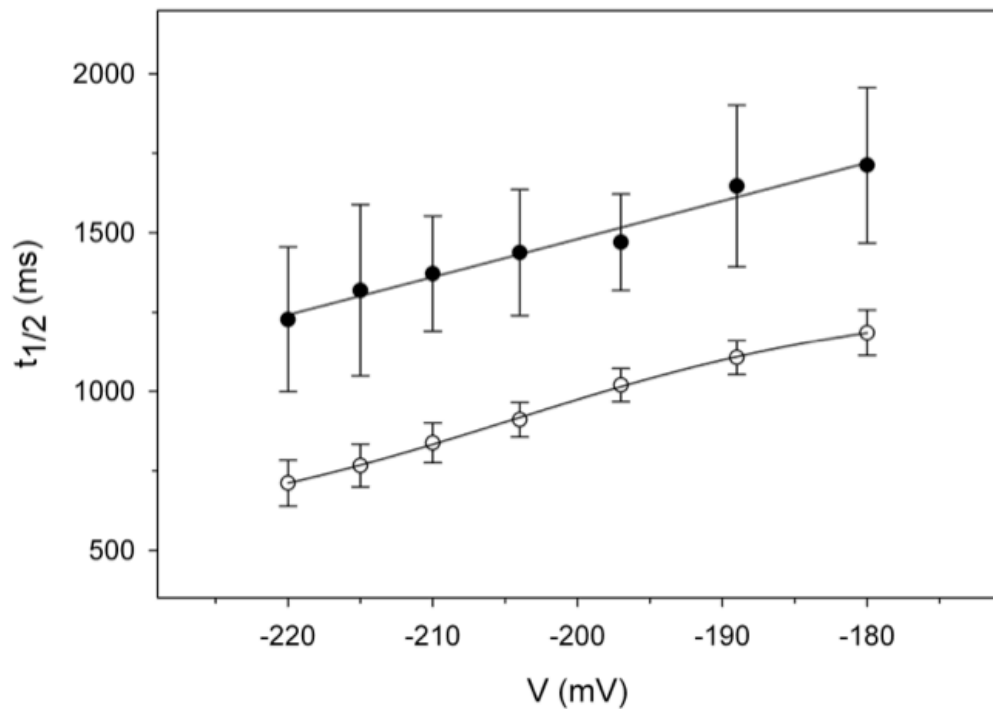


Figure 6. Activation half times of currents from inward-rectifying K⁺ channels.

Mean activation half times as a function of voltage. Data are from the same guard cells as in Figure 3 that were bathed in 10 mM KCl (white) and 10 mM KCl supplemented with 10 μM GYY 4137 (black). Data are means ±SE of n=5.

The steady-state current depends on the ensemble conductance (G), which is a product of the number of functional channels at the plasma membrane (N), the single channel conductance for a given ion species (G_X) and the gating characteristics of the channel that describe the open probability of the channel (P_o), as shown in the following formula.

$$G = N \times G_X \times P_o, \quad \text{Eq 8.}$$

Thus, plotting the conductance of K_{IN} channels (G_{KIN}) before and after exposure to H₂S as a function of voltage allows a clear separation of the differences in the gating characteristics of the response. Figure 7 presents the conductance-voltage (G - V) curves before and after exposure to 10 μM GYY 4137. The G - V curves were jointly fitted to a modified Boltzmann function (omitting the $V-E_K$ component from Eq. 7) to determine the G_{KINmax} , which describes the conductance of K_{IN} at saturating voltages, the half-maximal activation voltage

($V_{1/2}$) and the gating charge (δ) that refers to the charge moved across the membrane electric field during gating (Table 1). For joint fittings the δ was held in common and yielded a value of -1.66 ± 0.04 . The maximum conductance (G_{KINmax}) reflects on the number of channels and the individual capacity of each channel. As expected from the I-V data, the G_{KINmax} increased when voltages got more negative despite the presence or absence of 10 μ M GYY 4137. Albeit, the H₂S donor significantly suppressed the G_{KINmax} across all voltages, showing up to 90% reduction at -220 mV. Moreover, H₂S donor displaced the $V_{1/2}$ by approximately -12 mV (Table 1 and Figure 7; black arrows), indicating that the H₂S did not only result in a decrease of the maximum G_{KIN} but it also affected the open probability of the K_{IN} channels.

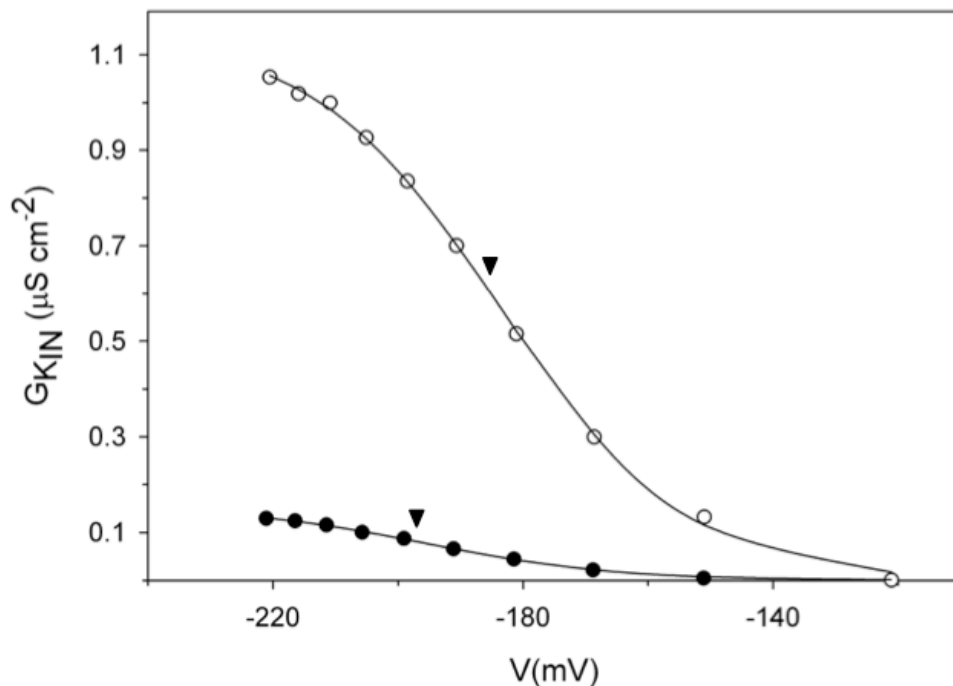


Figure 7. Sensitivity of conductance of inward-rectifying K⁺ channels to H₂S.

Steady-state conductance as a function of voltage was determined from instantaneous currents of Figure 3. Data are from n=5 guard cells bathed in 10 mM KCl (white) and 10 mM KCl supplemented with 10 μ M GYY4137 (black). Curves were jointly fitted to Boltzmann function (solid lines), with gating charge δ held in common. Voltages for half activation ($V_{1/2}$) of the channels for each treatment are indicated with black arrows.

Table 1. Gating characteristics of conductance of inward-rectifying K⁺ channels.¹

	V _{1/2} (mV)	δ	G _{KINmax} (μS cm ⁻²)
	P=0.006		P<0.001
Control	-184 ±0.5		1.15 ±0.01
+10 μM GYY4137	-195 ±3	-1.67 ±0.04	0.15 ± 0.01

1. Statistical differences after ANOVA, as determined by Student-Newman-Keuls test. P values are shown under each parameter tested between control and H₂S treatment.

To investigate whether the dose-dependence of stomatal closure on H₂S was also manifested in the I_{KIN}, I recorded the currents from guard cells that were bathed in buffer supplemented with 0, 0.1, 1 or 10 μM GYY 4137. Figure 8 shows the raw and mean values of I_{KIN} compared to the control treatment under the four distinct GYY 4137 concentrations. Increasing the concentration of H₂S donor indeed resulted in higher reduction of I_{KIN}, indicating the dose-dependence of I_{KIN} on H₂S. Fitting the mean data to hyperbolic decay function, I determined the K_{1/2} to 0.13 ±0.09 μM GYY 4137. The K_{1/2} of stomatal closure (Figure 3) and that of I_{KIN} inhibition did not significantly differ between each other, when compared by t-test (P=0.735).

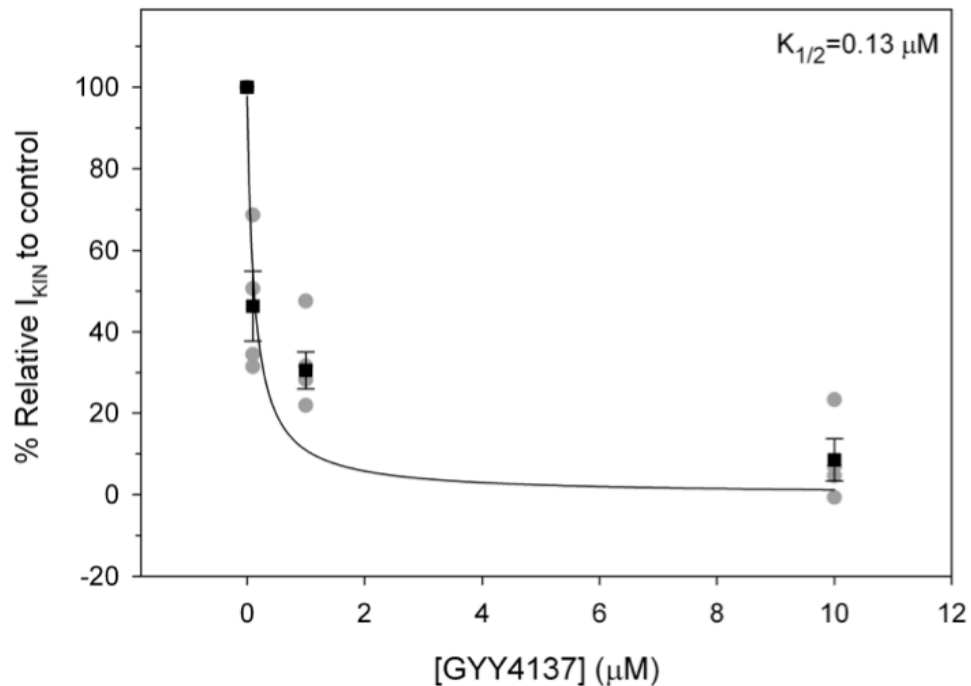


Figure 8. H₂S affects currents from inward-rectifying K⁺ channels in a dose-dependent manner.

Currents for I_{KIN} were recorded under voltage clamp as in Figure 3. Data are the raw values of I_{KIN} at -220 mV for 0, 0.1, 1 and 10 μM GYY4137 (grey circles), normalized to control (10 mM KCl). Mean ±SE of I_{KIN} also shown (black squares). Data were fitted in hyperbolic decay function and K_{1/2} was determined to 0.13 ±0.09 μM of GYY 4137.

5.2.3 H₂S acts via ABA-independent pathway

Given the similar effect of H₂S and ABA on I_{KIN} and stomatal aperture, I was interested in investigating the possibility of H₂S being a downstream event of the ABA signalling pathway, as also suggested by García-Mata & Lamattina (2010). In order to address this, I included treatments of epidermal peels with ABA and hypotaurine (HT) in addition to H₂S. HT interacts with free sulfide to form thiotaurine, and therefore it scavenges the toxic effect of H₂S (Ortega et al. 2008). For stomatal aperture measurements, the same protocol as above was employed, where epidermal peels were pretreated for 2 hours with opening buffer and light to determine the maximum opening of stomata. Afterwards, the peels were submerged for 90 minutes to control buffer supplemented with five distinct combinations of stomatal effectors: 10 μM GYY 4137, 10 μM HT, 10 μM GYY 4137 + 10 μM HT, 20 μM ABA and 20 μM ABA + 10 μM HT. Figure 9A presents

the percentage of stomatal closure induced by each treatment relative to the control. Control treatment yielded stomatal apertures of $4.93 \pm 0.11 \mu\text{m}$. Exposure to $10 \mu\text{M}$ GYY4137 and $20 \mu\text{M}$ ABA resulted in 60% and 80% reduction of stomatal aperture, corresponding to stomatal apertures of 3.25 ± 0.10 and $2.24 \pm 0.07 \mu\text{m}$, respectively. Treatment with HT alone did not affect stomatal aperture, however, when epidermal peels were treated with both $10 \mu\text{M}$ GYY 4137 and HT, the effect of the H₂S donor was alleviated yielding apertures of $4.57 \pm 0.12 \mu\text{m}$. Treatment of epidermal peels with $20 \mu\text{M}$ ABA + $10 \mu\text{M}$ HT partially blocked the ABA-induced stomatal closure, which was approximately 70% reduced in comparison to the control treatment. This set of data suggested that H₂S-induced stomatal closure may occur in a parallel pathway of the ABA.

To further confirm this idea, I investigated the effect of the above compounds and their combinations on I_{KIN} , employing the same protocol as in Figure 3. Figure 9B displays the mean percentage reduction of the I_{KIN} amplitude at -205 mV before and after the exposure to each of the treatments. H₂S resulted in almost complete abolishment of I_{KIN} , as also shown in Figure 5. The ABA treatment reduced the I_{KIN} only by 62%, resulting in currents of $-170 \pm 39 \mu\text{A cm}^{-2}$. Interestingly, exposure of guard cells to $10 \mu\text{M}$ HT yielded currents of $-292 \pm 64 \mu\text{A cm}^{-2}$ that were marginally higher in amplitude compared to $-241 \pm 40 \mu\text{A cm}^{-2}$ the control I_{KIN} . The H₂S-induced I_{KIN} inhibition was blocked when guard cells were treated with the combination of $10 \mu\text{M}$ GYY 4137 + $10 \mu\text{M}$ HT and currents recovered to similar amplitude as the control treatment. In contrast, the reduction of I_{KIN} caused by the ABA treatment was not prevented by adding HT, yielding I_{KIN} of $-174 \pm 35 \mu\text{A cm}^{-2}$. The latter finding clearly shows that H₂S does not act downstream of ABA to evoke stomatal closure.

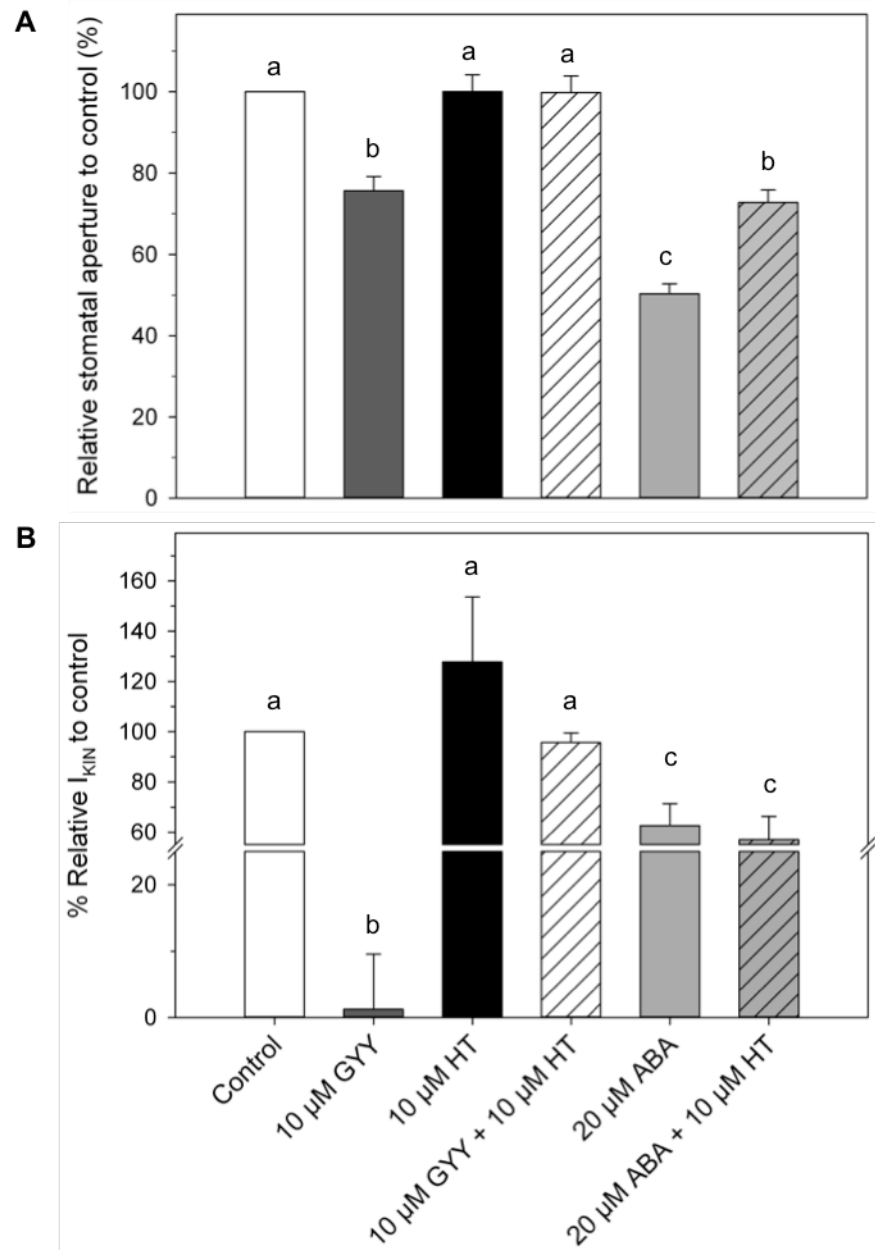


Figure 9. ABA effect on stomata does not require H₂S to trigger stomatal closure.

(A) Epidermal peels from *N. tabacum* were pretreated in opening buffer (60 mM KCl-MES; pH 6.1) and placed under light for 2 hours to ensure maximum stomatal opening. They were subsequently treated with 10 mM KCl supplemented with 10 μ M GYY 4137 (dark grey), 10 μ M HT (black), 10 μ M GYY 4137 + 10 μ M HT (white serrated), 20 μ M ABA (grey) or 20 μ M ABA + 10 μ M HT (grey serrated) for 90 minutes. Data were normalized to the control treatment (10 mM KCl; white) and are means \pm SE of $n > 190$ stomata. (B) Currents for inward-rectifying K⁺ channels were recorded under voltage clamp as in Figure 3. Graph represents I_{KIN} at -205 mV for same conditions as above. Data are means \pm SE of $n > 4$ after normalisation to control treatment (10 mM KCl). Lettering indicates statistical differences after ANOVA ($p < 0.05$), as determined by Student-Newman-Keuls test.

5.2.4 H₂S effect is partially dependent on intracellular Ca²⁺ rises

Taken into account that cytosolic Ca²⁺ affects I_{KIN} (Blatt 1990; Blatt & Armstrong 1993), I was interested to examine whether the H₂S-induced stomatal closure is mediated by augmented intracellular Ca²⁺ (Ca²⁺_i) levels. I utilized ethylene glycol tetraacetic acid (EGTA), which chelates Ca²⁺ ions, to buffer Ca²⁺ in the cytosol of the guard cells and then record the I_{KIN} before and after exposure to 10 μ M GYY4137. For this set of experiments, the filling solution of microelectrode was supplemented with 50 mM EGTA. Once a guard cell was impaled, I waited for approximately 5 minutes to ensure buffering of cytosolic Ca²⁺ and subsequently a voltage clamp protocol similar to that of figure 3 was carried out. Figure 10A presents the mean quasi steady-state currents and current traces of I_{KIN} channels with and without 10 μ M H₂S donor and under the presence of 50 mM EGTA. The mean amplitude of I_{KIN} at -205 mV was -217 ± 29 and -61 ± 11 μ A cm⁻² before and after H₂S treatment (Figure 10B). Fittings of the I-V curves to Boltzmann function carried out by holding in common the δ and $V_{1/2}$ to values of -2.38 ± 0.14 and -193 ± 0.74 mV, respectively. G_{max} of the H₂S treatment was 0.60 ± 0.02 μ S cm⁻² and was significantly reduced compared to 2.06 ± 0.05 μ S cm⁻² of the control, suggesting a scalar decrease in I_{KIN} conductance triggered by H₂S. Compiling the data of I_{KIN} inhibition with and without EGTA, a small recovery of I_{KIN} towards control amplitude upon exposure to H₂S and EGTA was observed (Figure 10C). However, the H₂S effect was still apparent, since the I_{KIN} was reduced by approximately 30% of the control treatment. The data suggested that H₂S caused small changes in intracellular Ca²⁺ that partially mediated the H₂S-induced stomatal closure and inactivation of I_{KIN} .

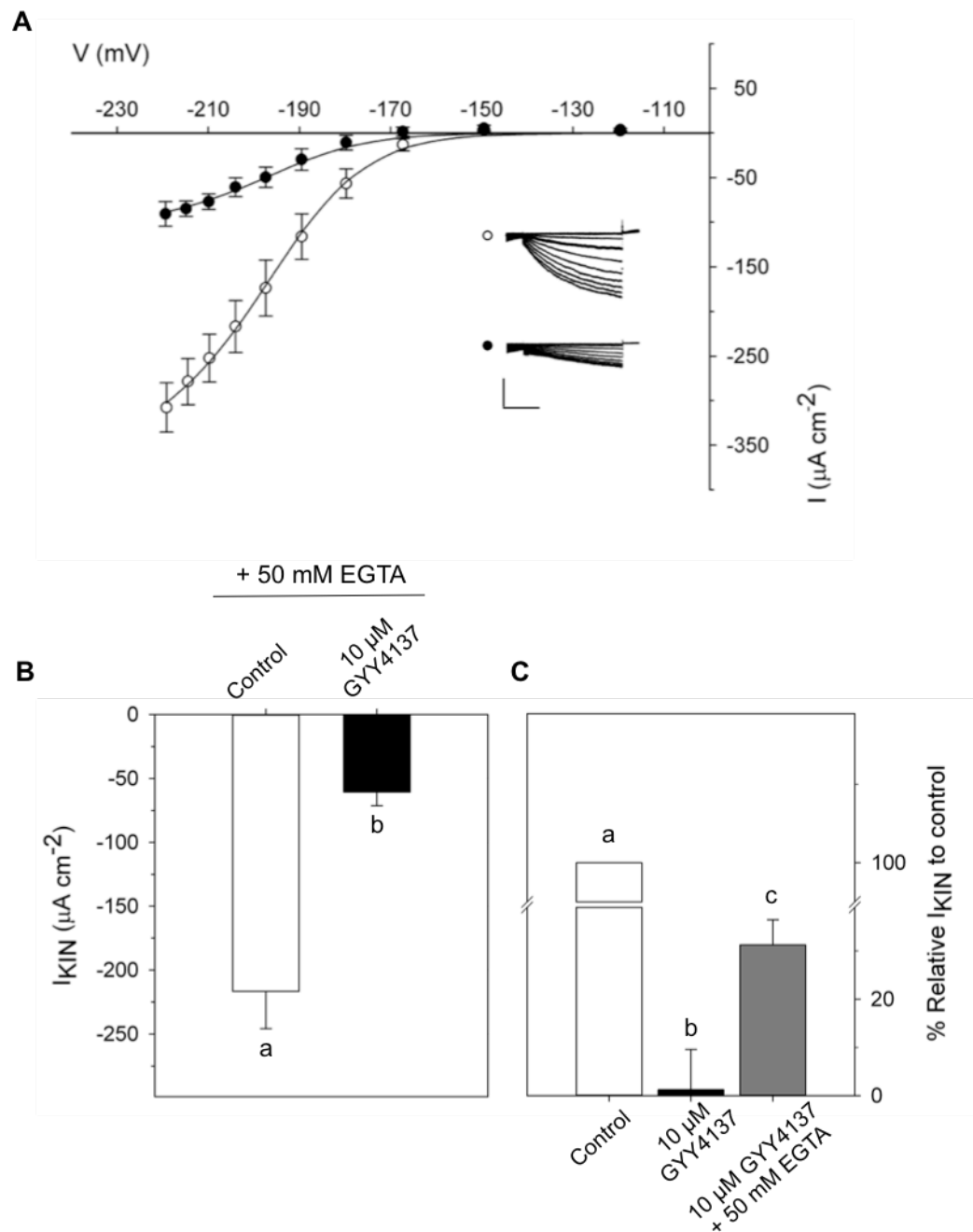


Figure 10. H₂S inactivates currents from inward-rectifying K⁺ channels in Ca²⁺- independent manner.

(A) Quasi steady-state currents were recorded for inward-rectifying K⁺ channels under voltage clamp, as in Figure 3. Guard cells were bathed in 10 mM KCl (white) or 10 mM KCl supplemented with 10 μM GYY4137 (black) and were buffer-loaded with microelectrode containing 50 mM EGTA. Data are means \pm SE of n=5 guard cells. Curves were jointly fitted to Boltzmann function (solid lines), with $V_{1/2}$ and gating charge δ held in common. Insets present current traces recorded under voltage clamp. Scale bar: horizontal line 2 seconds and vertical line 150 $\mu\text{A cm}^{-2}$. (B) Mean I_{KIN} at -205 mV from the current recordings for control (10 mM KCl; white) and 10 μM GYY 4137 (black) treatments. (C) Compiled data of the mean percentage reduction of I_{KIN} at -205 mV under exposure 10 μM GYY 4137 (black) and 10 μM GYY 4137 + 50 mM EGTA (grey) compared to the control (white). Lettering indicates statistical differences after ANOVA ($p < 0.05$), as determined by Student-Newman-Keuls test.

5.2.5 H₂S does not influence the activity of anion channels

Considering that stomatal closure additionally requires the anion efflux, I investigated the effect of H₂S on the activity of anion channels. To test this, I carried out two electrode voltage clamp in intact guard cells of epidermal peels bathed in control buffer (15 mM CsCl and 15mM TEA-Cl) and control buffer supplemented with 10 μ M GYY 4137. The presence of TEA⁺ in the buffer blocks the activation of all K⁺ channels. In addition, the filling solution of the microelectrode consisted of 100 mM CsCl that enables the loading of the cytosol with Cl⁻ to stimulate the anion currents (I_{Cl}). The epidermal peels were submerged in opening buffer and illuminated for 2 hours to obtain open stomata before the impalements. Current recordings were performed at voltages from +0 mV to -220 mV, following a holding voltage +40 mV. Figure 11A presents the averaged steady-state currents and the representative current traces recorded before and after exposure to the H₂S donor. Decreasing voltage produced instantaneous I_{Cl} of increasing amplitude, with mean I_{Cl} at -200 mV being -179 ± 36 and $-151 \pm 38 \mu\text{A cm}^{-2}$ before and after exposure to GYY 4137, respectively. Normalizing the I_{Cl} produced by H₂S treatment to that of the control indicated the suppression of Cl⁻ channel activity by approximately 20%, though this difference was not significant (Figure 10B). This latter finding implies a paradoxical effect of H₂S on stomatal movements, since the H₂S donor did not stimulate the activity of anion channels to promote anion efflux, which is required for stomatal closure.

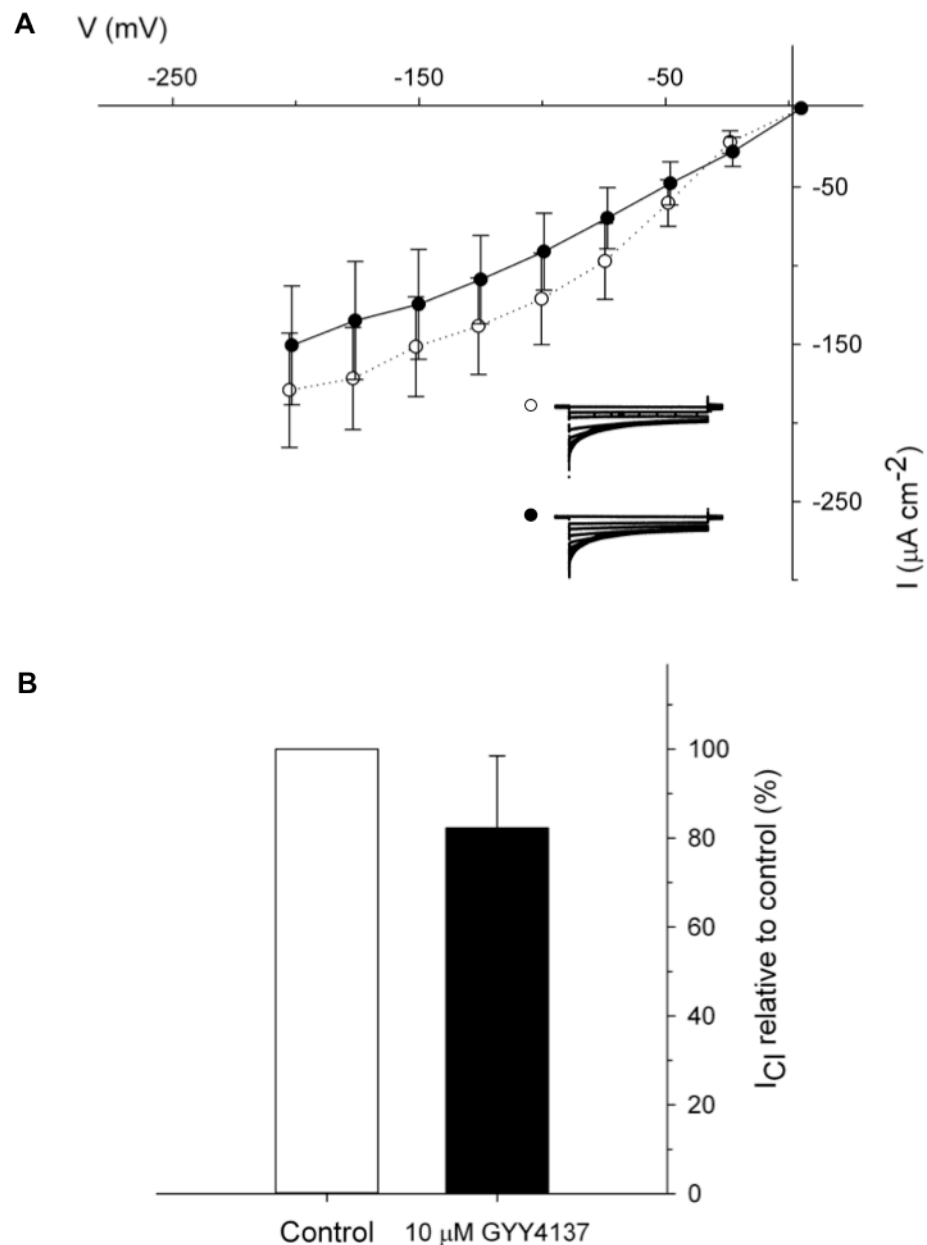


Figure 11. H₂S does not stimulate anion channels.

(A) Currents were recorded for anion channels under voltage clamp. Voltage clamp protocol consists of steps (20 mV) of 10 seconds between -220 and 0 following a holding voltage at +40 mV. Guard cells were bathed in 10 mM KCl (white) or 10 mM KCl supplemented with 10 μM GYY 4137 (black). Data are means \pm SE of n=5. (B) Mean I_{Cl} at -200 mV from above current recordings for control (white) and 10 μM GYY4137 (black) treatments.

5.2.6 Changes in intracellular Ca²⁺ and pH mediate H₂S response

To ascertain the complexity of H₂S effect on the I_{KIN}, I employed a quantitative systems dynamic approach to model the guard cell properties under the influence of H₂S donor. In the previous chapters, I discussed the dependence of stomatal movements on the assembly of the transporters at the plasma membrane and tonoplast, the solutes found in the cytosol as well as the buffering properties of [Ca²⁺]_i and pH. The OnGuard model gives one the opportunity to investigate the ion transport of the guard cells and elucidate the changes in stomatal aperture that it causes (Chen et al. 2012; Hills et al. 2012; Wang et al. 2012; Blatt et al. 2014). OnGuard implements the kinetic characteristics of transporters residing at the plasma membrane and tonoplast, the buffering properties of Ca²⁺ and pH within the cellular compartments as well as the equations coupling the volume, turgor and solute content of the cell to stomatal aperture. The potency of OnGuard relies on the user's ability to define a Reference state of the cell and subsequently modify the parameters in such away to simulate a query for a particular ion, solute or other experimental condition. Despite the fact that the mechanistic information on the regulation of transport by H₂S is still lacking, OnGuard bypasses such limitations by enabling the user to subsume the effects of an experimental challenge within the properties of one or more transporter parameters, effectively 'black boxing' the phenomenology. By doing so it minimizes computational complexity. More important, it enables testing of a range of models to effectively modify and/or discard the experiment after comparison with biological data.

Comparison of the *Vicia* and *Arabidopsis* models suggested that there is little difference between the two, except the stomatal size. Because *Vicia* and tobacco are similar in size, I used OnGuard with the published model for *Vicia* to reproduce the changes observed from my experimental data in order to uncover the role of intracellular Ca²⁺ and pH in the H₂S-induced response. To drive stomatal movements, I simulated the diurnal cycle and I adjusted the guard cell volume and stomatal aperture to the geometry of stomatal complex found in *Vicia faba*, which is the closest approximation to the stomatal complex of *N. tabacum*. I ran the model for 3 days under control conditions - simulating the

situation in the absence of H₂S - and then for 3 more days under H₂S conditions, where the parameters were modified according to the experimental data obtained from the above electrophysiological studies. In particular, the $V_{1/2}$ for K_{IN} channels was changed from -184 mV to -195 mV and the number of K_{IN} channels was reduced by 90% to account for the change in maximum for G_{KIN} upon exposure to H₂S donor (Table 2). Additionally, the populations of both R- and S-type anion channels were reduced by 20% in order to reproduce the anion reduction observed in Figure 11B. All the other parameters involved in the model remained unchanged.

In the subsequent figures, the outputs of the modelling are presented for day 1 and day 5 corresponding to diurnal cycle of the guard cell under control and H₂S conditions, respectively. Figure 12A presents the diurnal changes in turgor and volume of guard cell as well as stomatal aperture under both set of conditions. At the control conditions, the turgor of the cell was 6.6 and 3.8 atm in the open and close state, respectively; while the cell volume changed from 5.8 pl in the open state to 4.6 pl in the close state. The stomatal aperture ranged between 10.6 and 3 μ m during the diurnal cycle (Figure 12B). Modulating the parameters according to H₂S conditions, the model yielded a substantial reduction in all three parameters. In particular, the stomata opened to an aperture of 9.39 μ m during daylight cycle, while transition to night resulted in closing of stomata to an aperture of 3.49 μ m (Figure 12B). H₂S simulation predicted 50% slower opening rate of stomata than at the control conditions. Similarly, stomata upon the H₂S query required more time to reach the close state, though the differences were not as pronounced as those during the opening process (Figure 12C). As in the control conditions, the turgor of the cell followed the stomatal aperture, ranging from 5.7 to 4 atm. The volume of the cell was not substantially different from the control conditions, reaching a maximum of 5.5 pl during daytime and 4 pl during nighttime (Figure 12A).

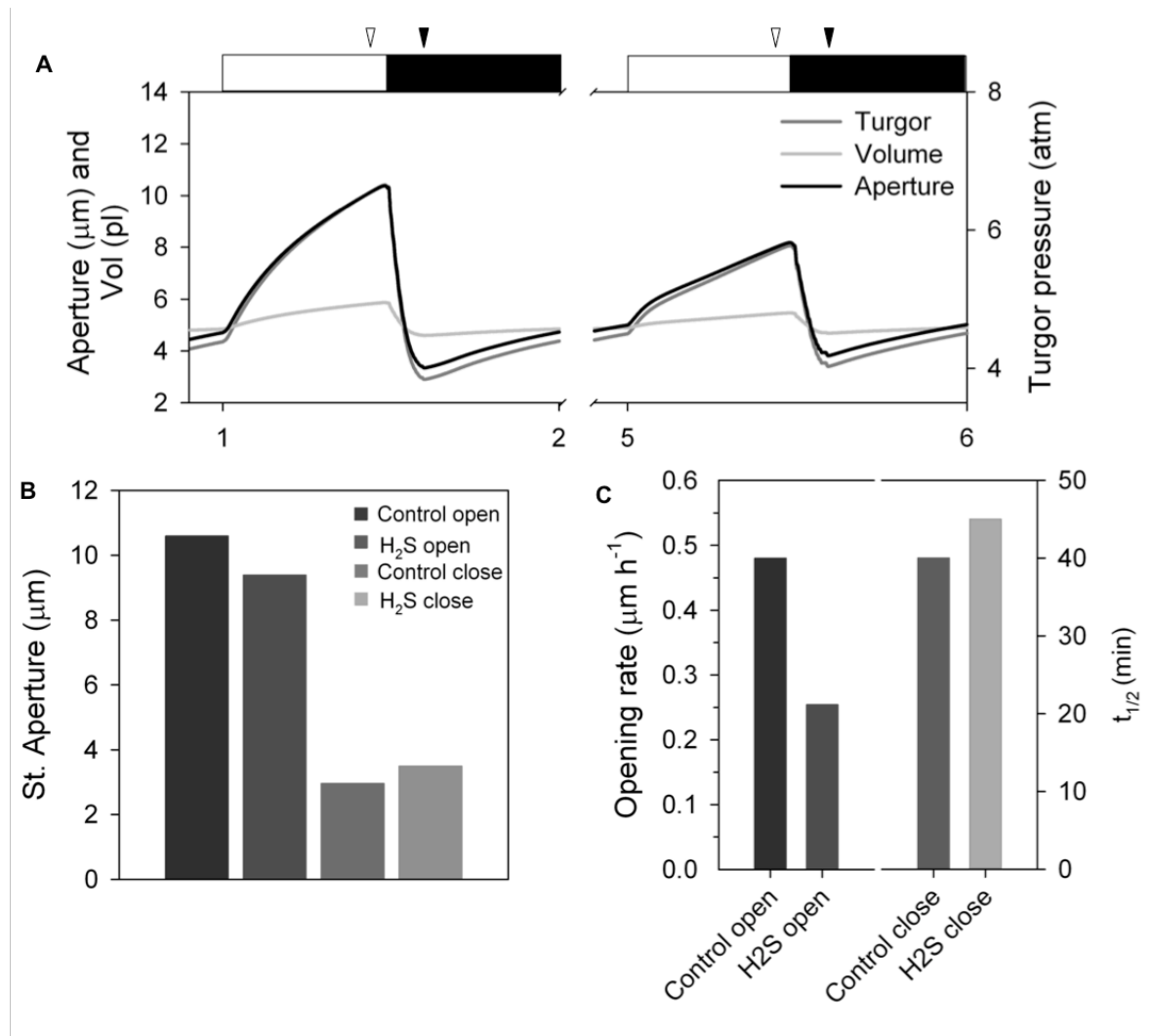


Figure 12. Quantitative modelling reproducing H₂S effect on stomatal opening and closure.

Outputs are derived by modelling the diurnal cycle and altering the activities of K⁺ and anion channels according to the data obtained from the above electrophysiological studies. Data represent 6-days window, with first three days corresponding to control treatment and the last three days corresponding to H₂S treatment. Only one day per treatment is shown, with day 1 (left panel) corresponding to control conditions and day 5 (right panel) to the H₂S conditions. (A) Graph presents the turgor pressure (grey line) and volume (light grey line) of guard cells and the stomatal aperture (black line) during control and H₂S-related conditions. White and black bar above the graph indicates the light and dark period, respectively. Arrows indicate the points at which the maximum responses at light and dark period were estimated. (B) Maximum stomatal aperture during opening and closing processes, with bars indicating from left to right the control open state, the H₂S open state, the control close state and the H₂S close state. (C) Graph represents the opening rate of stomata (left panel) and closing half time (right panel) under control and H₂S conditions.

The concentration of the two major osmolytes, K⁺ and Cl⁻, in the cytosol and vacuole during the open and close states of stomata and under the control and H₂S conditions are presented in Figures 13 and 14. In the cytosol, the K⁺ concentration rose during the daytime to a maximum of 166 mM, before declining to 94 mM at the end of the day. A similar pattern was also detected for vacuolar K⁺ concentration, though it ranged from 90 to 10 mM during the diurnal cycle (Figure 13A). When H₂S-related modifications were applied, the content of K⁺ in the cytosol and in the vacuole were significantly reduced by approximately 13% and 19%, respectively. In particular, upon H₂S simulation, the maximum cytosolic [K⁺] was 144 mM, while the vacuolar [K⁺] was 75 mM (Figure 13B). The reverse was observed during nighttime, when the [K⁺] in the cytosol and vacuole was slightly elevated under H₂S conditions, reaching values of 92 mM and 17 mM, respectively (Figure 13B). The diurnal changes in the K⁺ content were reflected on the fluxes of K⁺ ions through the K_{IN} and K_{OUT} channels (Appendix I, Figure 2). The model reproduced the reduction in K⁺ influx during daytime and a marginal inhibition of the K⁺ efflux during nighttime. In addition, K⁺ flux via the H⁺-K⁺ symport is also shown, though not substantial difference was observed between the control and H₂S query throughout the diurnal cycle.

At the control conditions, the cytosolic Cl⁻ concentration varied between 5 mM in the open state and 14 mM in the close state (Figure 14A and B). A similar pattern was observed upon H₂S simulation, but the maximum cytosolic Cl⁻ levels were 1.87 mM during daytime. Remarkably, H₂S conditions in the close state exhibited a substantially rise of [Cl⁻]_{cyt} by 10 mM compared to the control conditions, reaching a maximum of 17.35 mM (Figure 14B). These H₂S-mediated predictions were also evident from the approximately 2-fold enhanced S-type activity during the daytime that was followed by a great suppression of both S and R-type channels at the start of the night. Cl⁻ influx via the H⁺-Cl⁻ symport was also altered at the open state under the H₂S conditions, whereas it remained unchanged during night (Appendix I, Figure 2). The model also produced a dramatic effect of H₂S on vacuolar Cl⁻ in the open state. The Cl⁻ concentration in the vacuole was 75% decreased compared to control conditions, reaching a concentration of 2 mM. However, during nighttime, the Cl⁻ content in the vacuole was similar between the control and H₂S conditions, resulting in a

maximum of 13.77 and 12.62 mM, respectively. The Cl⁻ flux at the tonoplast was dominated throughout the diurnal cycle by the VCL channel and the H⁺-Cl⁻ antiport. The latter appeared to be stimulated at open state by the H₂S, reflecting on the changes in vacuolar [Cl⁻].

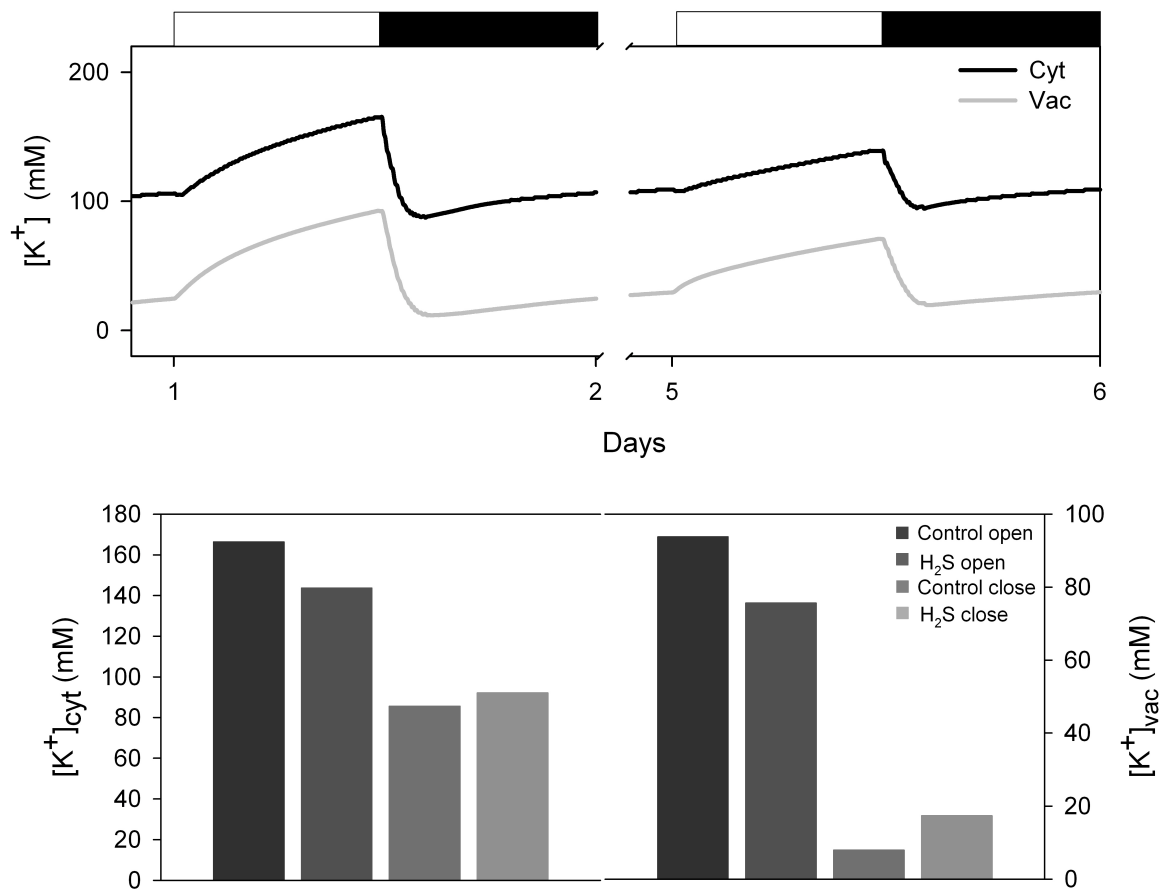


Figure 13. Quantitative modelling reproducing H₂S effect on K⁺ ions in guard cells.

Outputs are derived as in Figure 12. (A) Graph presents the K⁺ content of cytosol (black line) and vacuole (grey line) during the 6-d window simulation, with day 1 and day 5 representing the control and H₂S treatment, respectively. White and black bar above the graph indicates the light and dark period, respectively. (B) Maximum cytosolic and vacuolar K⁺ concentration during opening and closing processes, with bars indicating from left to right the control open state, the H₂S open state, the control close state and the H₂S close state.

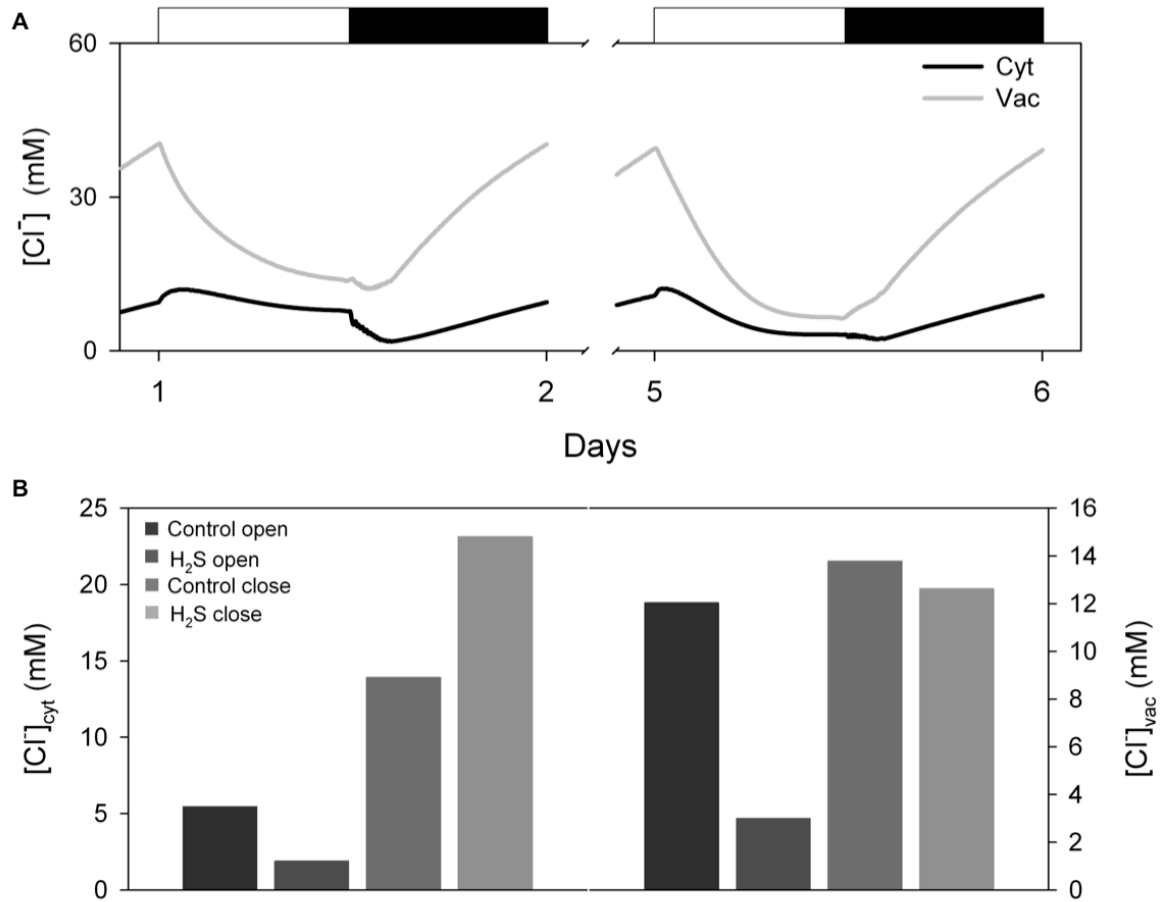


Figure 14. Quantitative modelling reproducing H₂S effect on Cl⁻ ions in guard cells.

Outputs are derived as in Figure 12. (A) Graph presents the Cl⁻ content of cytosol (black line) and vacuole (grey line) during the 6-d window simulation, with day 1 and day 5 representing the control and H₂S treatment, respectively. White and black bar above the graph indicates the light and dark period, respectively. (B) Maximum cytosolic and vacuolar Cl⁻ concentration during opening and closing processes, with bars indicating from left to right the control open state, the H₂S open state, the control close state and the H₂S close state.

The power of the model became apparent when I explored the buffering properties of pH and Ca²⁺, and how these were affected by H₂S. Figure 15A presents the diurnal changes in the cytosolic and vacuolar pH at the control conditions and under the influence of H₂S. The control conditions were characterized by a small acidification of the cytosol at the start of the day before resting to 7.7 during the late hours of the daylight cycle, whereas at nighttime the pH dropped to 7.3 (Figure 15B). It is clear that H₂S conferred dramatic alterations in the pH of the cytosol compared to the control conditions. The pH_{cyt} between the open and close state was not significantly altered, with that ranging by only 0.1 units during the diurnal cycle. Especially, the H₂S query resulted in the acidification of the cytosol during the daytime, as the pH was about 0.2 units reduced compared to the control conditions reaching a maximum of 7.5. In the close state, the opposite phenomenon was observed, with pH_{cyt} being bigger than control by 0.3 units and reaching a value of 7.6. The H₂S simulation did not reproduce any differences in the vacuolar pH compared to the control conditions during the daylight period, resulting in pH of approximately 4.6. Yet, in the close state, H₂S reduced the pH_{vac} by 0.3 units, corresponding to a value of 5.1 compared to the 5.4 of the control conditions (Figure 15B). The acidification of the cytosol during daytime is also suggested from the fluxes of H⁺ via the various channels at the plasma membrane and tonoplast (Appendix I, Figure 4). In particular, the lower cytosolic pH was associated with the reduced activity of H⁺-ATPase but also with the enhanced activity of H⁺-Cl⁻ symport. Also, the vacuolar H⁺-Ca²⁺ antiport (CAX) was significantly altered by H₂S, resulting in 30% lower H⁺ flux via this route and therefore causing the further acidification of the cytosol.

Interestingly, the model also predicted big differences in the Ca²⁺ content of both cytosol and vacuole between the control and H₂S conditions. During the daylight cycle, the vacuolar [Ca²⁺] was rested to approximately 22 mM for control conditions and to 19 mM for the H₂S conditions (Figure 16A). The free Ca²⁺ in the cytosol at the control open state was about 340 nM, while it reached a maximum of 405 nM when H₂S-related modulations were applied (Figure 16B). However, the H₂S simulation predicted a compensatory effect on the activity of

Ca²⁺ channels despite the hyperpolarisation of the plasma membrane, since the fluxes were slightly reduced during daytime (Appendix I, Figure 3).

At the end of the daytime and first hours of the night, Ca²⁺ oscillations were observed consistent with previous reports (Wang et al. 2012; Chen et al. 2012). Surprisingly, a distinct pattern of Ca²⁺ oscillations was detected between the two different sets of conditions (Figure 16C). At the control conditions, the pattern of Ca²⁺ oscillations resembled of a bell shape, with oscillations being of greater amplitude at the beginning and end of the oscillation cycle and with almost a uniform frequency. In contrast, the Ca²⁺ oscillations upon H₂S query were of similar amplitude throughout the oscillation cycle, but with more variable frequency. Therefore, the H₂S resulted in shorter and faster Ca²⁺ oscillations than these of the control conditions. All together, these data suggested that H₂S-induced stomatal closure might be partially depended on the ion channel modulation occurring via changes in the buffering properties of Ca²⁺ and pH of the guard cell.

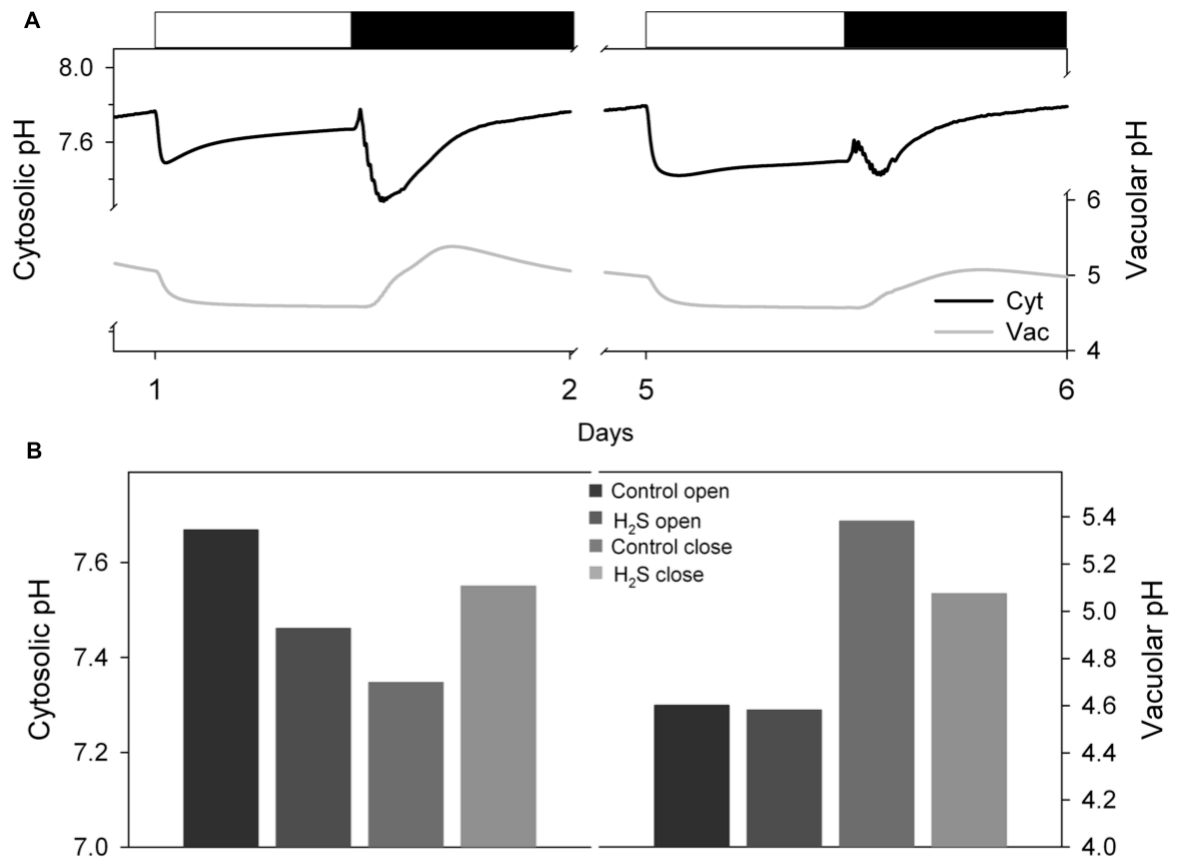


Figure 15. Quantitative modelling predicting changes in pH due to H₂S-induced changes in ion channels.

Outputs are derived by modelling the diurnal cycle and altering the activities of ion channels, as in Figure 12. (A) Changes in cytosolic (black line) and vacuolar (grey line) pH during the 6-d window simulation, with day 1 and day 5 representing the control and H₂S treatment, respectively. White and black bar above the graph indicates the light and dark period, respectively. (B) Cytosolic and vacuolar pH during opening and closing processes, with bars indicating from left to right the control open state, the H₂S open state, the control close state and the H₂S close state.

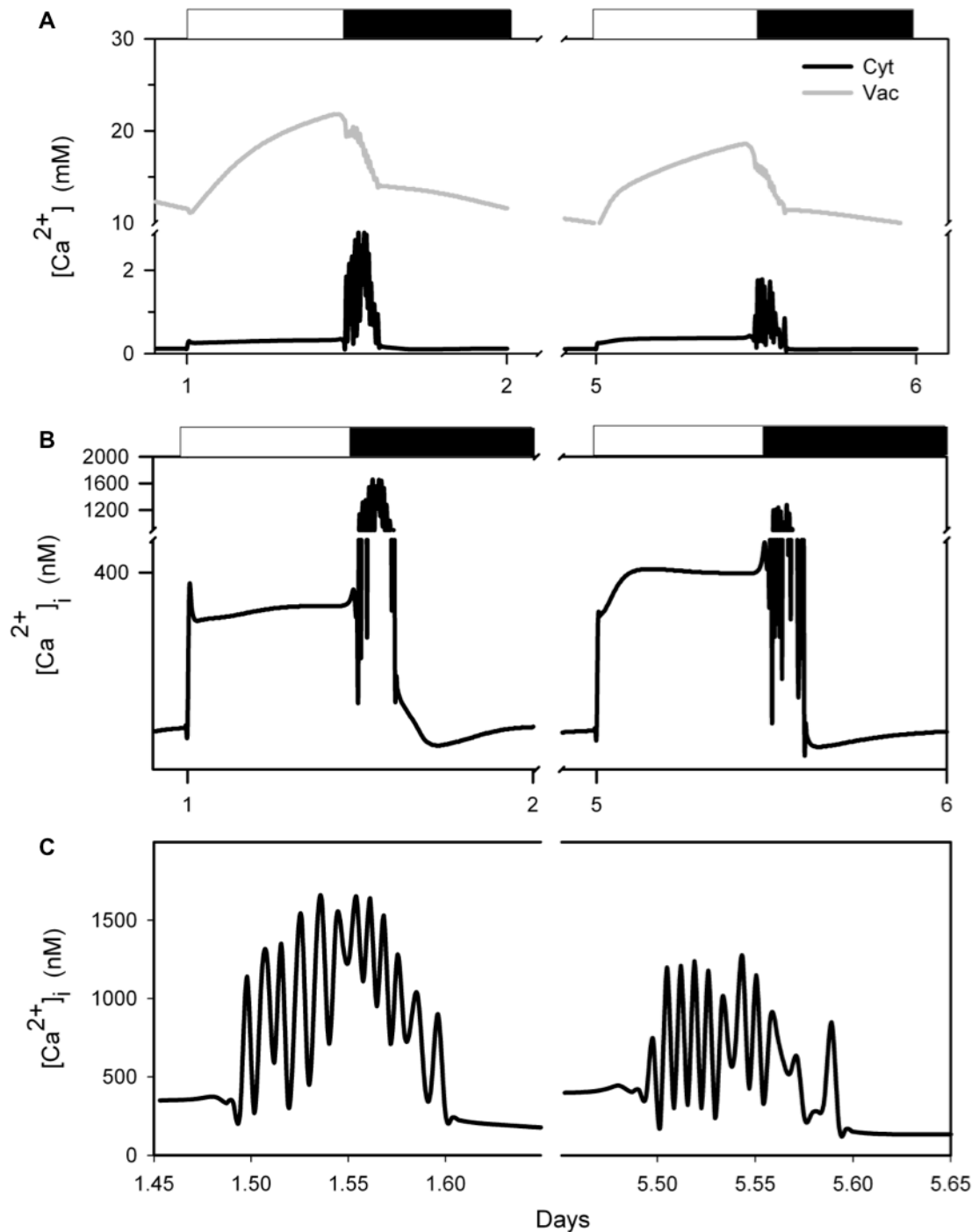


Figure 16. Quantitative modelling predicting changes in intracellular Ca²⁺ due to H₂S-induced changes in ion channels.

Outputs are derived by modelling the diurnal cycle and altering the activities of ion channels, as in Figure 12. (A) Changes in cytosolic and vacuolar Ca²⁺ and (B) in free intracellular Ca²⁺ during the 6-d window simulation, with day 1 and day 5 representing the control and H₂S treatment, respectively. White and black bar above the graph indicates the light and dark period, respectively. (C) Graph presents solely the oscillations of free intracellular Ca²⁺ at the start of nighttime.

5.3 Discussion

While gaseous bioactive molecules like NO and CO have been known as key regulators of plant physiology for the last decades, H₂S has just emerged. The most information on this novel gasotransmitter and its effect on plants comes from studies with crops subjected under various abiotic stresses (Zhang, et al. 2010a; 2010b; 2010c). The controversial effect of H₂S on stomatal apertures (García-Mata & Lamattina 2010; Lisjak et al. 2010) attracted me to examine in depth the effect of H₂S at the stoma level using *N. tabacum* as the model organism. Also, given the gaseous nature of H₂S, I was able to explore whether stomatal clustering influences the perception of gaseous signals. I postulated that H₂S is a novel modulator of stomatal function adding a further hub into the signalling network that governs stomatal behaviour (Hetherington & Woodward 2003). I based this on four key observations. 1) Exogenously applied H₂S induced stomata closure. 2) H₂S exclusively inhibited the inward K⁺ channel activity. 3) The H₂S effect was independent of the ABA pathway, and 4) it involved changes in cytosolic calcium levels and acidification of the cytosol. Finally, stomatal clustering prevented the H₂S-induced stomatal closure, emphasizing on the requirement of spacing to allow proper stomatal function and movement.

5.3.1 Evidence on stomatal closure?

H₂S can be considered to become a potential tool for improving drought stress tolerance via regulation of stomatal aperture and thereby lessening the transpirational water loss. Here, I demonstrated that H₂S induced stomatal closure in abaxial epidermis of tobacco plants, an outcome in accordance with previous reports (García-Mata & Lamattina 2010; Jin et al. 2011). This observation further substantiates the description of H₂S being the third gasotransmitter, as it exerted similar results as CO and NO (Song et al. 2008; Neill et al. 2002; García-Mata & Lamattina 2003). Stomatal closure was sensitive to the concentration of H₂S, as the elevated concentration of H₂S resulted in greater stomatal closure (Figure 3). Particularly, the effective concentrations of H₂S were at low micromolar range, with a K_{1/2} of 0.13 µM being sufficient to

induce stomatal closure. Although not tested here, concentrations of H₂S >100 µM were shown to reverse the stomatal closure and appeared toxic to the cell, since cell viability was highly reduced (García-Mata & Lamattina 2010). In addition, the sensitivity of H₂S effect on its concentration was also presented in the adaptive responses to adverse stresses, including drought and osmotic stress (Zhang et al. 2009a; Zhang et al. 2009b; Zhang et al. 2010). For instance, soybean seedlings showed higher survival rate under prolonged drought stress as the concentration of the H₂S donor NaHS was increased, with the highest survival occurring at 1 mM of NaHS (Zhang et al. 2010). ABA and NO also promote a dose-dependent stomatal closure (Garcia-Mata & Lamattina 2002; Puli & Raghavendra 2012). For instance, Ghassemian et al. (2000) showed that root elongation in *Arabidopsis* upon exposure to ABA was sensitive to its concentration. Although exogenous application of 0.1 µM ABA stimulated the elongation of roots, raising the ABA concentration to 1 µM inhibited the response. A similar response was also shown for the H₂S-triggered root organogenesis in sweet potato and soybean seedlings (Zhang et al. 2009). The authors used NaHS as the H₂S source and measured for lateral root number and root length under varying concentration of NaHS. The H₂S donor promoted the development of roots in a dose-dependent manner, but NaHS concentrations higher than 0.06 mM slowed down root elongation and inhibited root emergence. Collectively, the data argue in favour of H₂S being a novel mediator of stomatal closure showing similarities with the well-known stomatal effectors, ABA and NO. Future studies with *Arabidopsis* transgenic lines defective in H₂S and NO production, and even defective in ABA response will clarify the role of H₂S in stomatal closing process.

I also examined the H₂S-induced stomatal closure in *Arabidopsis* plants (Figure 4). The *tmm1* mutants exhibited a similar defective stomatal closure as it was observed with the soluble closing stimuli (see Chapter 3, Figure 14). This observation suggested that stomatal spacing is likely to be extremely important for the diffusion of both soluble and gaseous signals. Whether this inhibition of the H₂S-mediated stomatal closure in stomatal patterning mutants was dependent on mechanistic or on intermediated targets controlling stomatal movements has yet to be explored, as also postulated in Chapter 3.

5.3.2 H₂S-induced stomatal closure via modulation of ion channels?

The electrophysiological data reinforced the above proposition that H₂S exerts analogous effects on stomatal function as the NO and ABA. Closing of stomata depends on the reduction of the guard cell turgor pressure and volume that ensues the ion - notably K⁺ and Cl⁻ - efflux through ion channels at the plasma membrane. Several groups over the last two decades have shown that ABA suppresses K_{IN} channel activity via changes in [Ca²⁺]_i levels, whereas it activates K_{OUT} channels through the alkalisation of the cytosol (Blatt 1990; Blatt & Armstrong 1993; Schwartz et al. 1994; Garcia-Mata et al. 2003; Siegel et al. 2009). NO affects solely the K_{IN} channels since electrophysiological studies in *V. faba* guard cells treated with the NO donors, sodium nitroprusside (SNP) and S-nitroso-N-acetyl-penicillamine (SNAP), did not suppress the I_{KOUT} (Garcia-Mata et al. 2003). However, a latter study showed the effect of NO on the K_{OUT} channels, possibly via a direct nitrosylation of the K_{OUT} channels or an associated regulatory protein (Sokolovski & Blatt 2004). In the present study, the electrophysiological data with the H₂S donor suggested the exclusive repression of I_{KIN} to basal levels. Indeed, I_{KIN} was reduced by about 90%, while the I_{KOUT} remained largely unaffected by the H₂S treatment (Figure 5). Moreover, I demonstrated that the I_{KIN} inhibition was increased with augmented levels of H₂S, an outcome consistent with the dose-dependent effect on stomatal closure (Figure 8). The imposed suppression in the K_{IN} activity was also reflected from the modelling data as reduction in the cytosolic K⁺ content, which at daytime appeared substantially lower when the H₂S-related modifications were applied (Figure 13). However, the kinetic analysis of I_{KIN} was not adequate to elucidate the mechanism underlying the H₂S-mediated inactivation of K_{IN} channels. The H₂S-triggered changes in K_{IN} gating - i.e. negative shift of V_{1/2} - suggested that H₂S exerts its effect through the regulation of ion channels, whereas the differences in G_{KINmax} implied changes in the population of channels, which in turn rely on the transcription regulation and/or trafficking of the channels (Hille 2001) (Figure 7 and Table 1).

ABA and NO have also been shown to trigger stomatal closure by activating the anion channels, involving the elevation of cytosolic Ca²⁺ (Schroeder & Hagiwara

1989; Schmidt et al. 1995; Grabov et al. 1997; Allen et al. 1999; Garcia-Mata et al. 2003). Remarkably, the exogenously release of H₂S exerted an opposite response to both ABA and NO, as it suppressed the I_{Cl} by 20% but this difference was not statistically significant (Figure 11). Yet, this observation contradicts the data reproduced by the model, which showed a significantly lower [Cl⁻] in the cytosol. This latter finding implies the action of additional transporters mediating Cl⁻ fluxes, such as the H⁺-Cl⁻ symport. Yet, this observation evidently complicates the understanding of the mechanism that promotes H₂S-induce stomatal closure, since activation of Cl⁻ channels have been shown to be a requisite for this process. The data altogether also imply a different mode of action for H₂S from that of ABA and NO, a notion that will be discussed in the following section.

Modulation of K_{IN} and anion channels depends on several events, such as elevation of cytosolic Ca²⁺, alkalinisation of the cytoplasm as well as on posttranslational modification events. The role of cytosolic Ca²⁺ and pH will also be separately addressed in the following sections. Protein phosphorylation has been proposed to have a crucial role in K_{IN} and S-type anion channel regulation (Schmidt et al. 1995; Gosti et al. 1999; Liu et al. 2006; Nishimura et al. 2010). Inhibitors of calcium-dependent protein phosphatase, PP2B, prevented the inactivation of I_{KIN} in *V. faba* and therefore stomatal closure (Luan et al. 1993). In contrast, inhibitors of PP2A down-regulated the K_{IN} channel and up-regulated the S-type anion channel activity to promote stomatal closure (Li et al. 1994; Thiel & Blatt 1994; Schmidt et al. 1995). Moreover, mammalian studies have shown that H₂S triggers additional types of post-translational modifications. For instance, in mice, the sulfhydration of the proteins has been shown to be enhanced with endogenous production H₂S, while in the presence of the reducing agent dithiothreitol (DTT) or in defective H₂S production mutants the modification was reversed (Mustafa et al. 2009).

In addition, regulation of the guard cells plasma membrane proteins involves the actions of scaffolding proteins that enable protein-protein interactions (Leonhardt et al. 1999b; Shimazaki et al. 2007; Christie 2007). In mammals, H₂S has been proposed to promote decrease in arterial blood pressure via the opening of K_{ATP} channels, which are formed by two sulfonylurea receptor (SUR)

ABC proteins and Kir6.2 channel (Babenko et al. 2000). Addition of the SUR inhibitor glibenclamide antagonized the H₂S response and prevented the hypotensive effect of H₂S (Zhao et al. 2001). Glibenclamide has also been shown to abolish stomatal closure triggered by ABA and external Ca²⁺ via the inhibition of anion and K_{OUT} channels (Leonhardt et al. 1999b). However, (García-Mata & Lamattina 2010) presented only partial block of the ABA-induced stomatal closure by glibenclamide, while the H₂S response was completely abolished, suggesting that ABC proteins facilitate the regulation of ion channels upon H₂S exposure. More information on the ion modulation triggered by H₂S is required and will enable the better understanding of its role in both plant and mammalian systems.

5.3.3 H₂S a new branch of the guard cell signalling?

To this point, the data implied that H₂S does not mediate ABA-induced stomatal movements, implying that it may act upstream or even in parallel of ABA. Both stomatal aperture and electrophysiological data using the H₂S scavenger and ABA endorsed this assumption. Although the H₂S scavenger did reverse the H₂S-induced stomatal closure and I_{KIN} inhibition to normal levels, it did not block the ABA effect on either response. Treatment with ABA and HT resulted in 40% bigger stomatal aperture in comparison to that upon exposure to ABA alone, while I_{KIN} were equally inhibited in both treatments (Figure 9). This deviation between the two experimental approaches is expected, since I_{KIN} data represent only a part of the assembly of factors affecting the stomatal aperture.

The ABA signalling pathway involves several signalling intermediates such as ROS and NO that trigger the elevation of cytosolic free Ca²⁺ required for stomatal closure (Pei et al. 2000; Garcia-Mata & Lamattina 2002; García-Mata & Lamattina 2003) . Guard cells produce NO in response to ABA via the activity of nitrate reductases (NR) (Desikan et al. 2002). NO effect on stomata has been shown to be partially dependent on the seconder messenger cGMP and cADPR, a Ca²⁺-mobilizing molecule (Neill et al. 2002). Garcia-Mata et al. (2003) showed that NO promoted the inhibition of I_{KIN} and activation of I_{Cl} through the stimulation of Ca²⁺ release from internal stores. In contrast, stomatal closure

evoked by ROS was dependent on the Ca²⁺ influx rather than Ca²⁺ release. H₂O₂ directly affected the gating of plasma membrane Ca²⁺-permeable channels, stimulating the I_{Ca} to allow the efflux of Ca²⁺ into the cytosol (Pei et al. 2000).

Hence, it was important to ascertain whether the inhibitory effect of H₂S on I_{KIN} was dependent on the [Ca²⁺]_i levels. The OnGuard model indicated a slight increase in [Ca²⁺]_i, which could explain the small but significant recovery of the I_{KIN} in response to H₂S combined with the Ca²⁺ chelator EGTA (Figure 10). It is known that [Ca²⁺]_i close to 330 nM suppress the I_{KIN} (Grabov & Blatt 1999), and indeed the daytime [Ca²⁺]_i was predicted be close to 405 nM (Figure 16). Accordingly, the displacement of the membrane potential of K_{IN} channels to more negative voltages also argue in favour of the predicted elevated cytosolic Ca²⁺ levels (Table 1). The hyperpolarisation event was additionally evident from the H₂S query imposed on the OnGuard model (Appendix I, Figure 1).

When the model was adjusted to H₂S conditions, the Ca²⁺ oscillations were reduced in amplitude but they were more prolonged (Figure 16), underlying the decrease in stomatal aperture under the H₂S treatment. Stomatal closure has been shown to be governed by Ca²⁺ oscillations from experiments using closing stimuli such as CO₂ and ABA (Blatt 2000). However, the intracellular Ca²⁺ content was sufficient to trigger only a mild stimulation of the I_{Cl}, while previous reports have shown the consequent activation of Cl⁻ channels due to the rise in [Ca²⁺]_i (Hedrich et al. 1990; McAinsh et al. 1990; Schroeder & Keller 1992). H₂S has been described as antioxidant agent with a particular potency to eliminate ROS species. Zhang, et al. (2010a; 2010b; 2010c) showed that H₂S-mediated improved tolerance of soybean and wheat seedlings to drought and osmotic stress and aluminium toxicity relies on the reduced levels ROS species. Although this observation excludes the possibility of H₂S-triggered [Ca²⁺]_i rises to take place via the same pathway as H₂O₂, it does not exclude the rise in [Ca²⁺]_i due to H₂S by other means. Which is the origin of this elevation in the guard cell cytosolic Ca²⁺ has to be experimentally addressed in future studies. Hence, the data ascribe Ca²⁺ as a necessary but not sufficient intermediate for H₂S-induced stomatal closure.

The function of several ion channels also depends on the cytosolic pH. ABA is known to stimulate alkalisation of the cytosol that in turn drives the up- and down- regulation K_{OUT} and K_{IN} channels, respectively (Blatt 1991; Blatt 1992; Blatt & Armstrong 1993). The model predicted that H₂S resulted in relatively small changes in cytosolic pH throughout diurnal cycle, but it also anticipated the acidification of the cytosol at the daytime (Figure 15). The predictions for pH do not dictate the mechanism underlying the exclusive suppression of K_{IN} channel activity, suggesting that missing intermediate effectors may contribute to this response. Nevertheless, combining the outputs for Ca²⁺ and pH, one can hypothesize that the changes in the [Ca²⁺]_i are coupled with the changes in the cytosolic H⁺ load. The reduced influx of K⁺ caused the hyperpolarisation of the plasma membrane that in turn gated the voltage-sensitive Ca²⁺ channels to accumulate Ca²⁺ in the cytosol, which eventually stimulated the CAX antiport resulting in the influx of Ca²⁺ into the vacuole at the expense of the acidification of the cytosol. Nevertheless, the experimental characterisation of the subtle changes occurring in the cytosolic Ca²⁺ and pH, using Ca²⁺- and H⁺- sensitive dyes, should be prioritized for future studies in order to dissect the mechanism by which H₂S exerts stomatal closure. Also, further exploitation of the predictive power of OnGuard and by imposing different queries might elucidate the changes occurring at the cellular level required for stomatal closure. For instance, changing the number of Ca²⁺ channels at the plasma membrane could potentially mirror the changes occurring due to H₂S treatment. Recently, a study in HEK293 cells using patch-clamp electrophysiology reported the inhibition of the T-type Ca²⁺ channels by H₂S (Elies et al., 2014). Also, using OnGuard, Wang et al. (2012) showed that malate together with the Cl⁻ hyperaccumulation in the cytosol accounted for the *slac1* stomatal phenotype. Hence, imposing changes in metabolism, reflected as the malate synthesis, could also shed light on the changes in the pH predicted with the H₂S simulation.

5.3.4 Outlook

Two main outcomes summarized the above data. 1) Stomatal clustering prevented the proper stomatal behaviour under the influence of H₂S, despite of that being a gaseous signal. 2) The data identified H₂S as a novel effector of stomata that causes stomatal closure. In tobacco, the exogenous release of H₂S from the GYY 4137 H₂S donor induced stomatal closure in a dose-dependent manner. The stomatal closing effect of H₂S was described as complex and distinct from that of other known stomatal closing stimuli, because of its exclusive blockade to K_{IN} channels. Moreover, the experimental data implied that H₂S is independent of the ABA signalling pathway, possibly placing a new branch in the network governing stomatal behaviour. Considering the effect of H₂S on the kinetic characteristics of plasma membrane K⁺ and anion channels as well as the predicted outputs of the OnGuard model, I finally argue that I_{KIN} inhibition is linked to an elevation of cytosolic Ca²⁺ that in turn is sensitive to changes in pH.

6 General Discussion

6.1 *Summary*

In this study I presented evidence on the effect of stomatal clustering in the plant physiology and growth using two different populations of plants, an experimental one consisting of *A. thaliana* plants and a natural one containing two *Begonia* species. Quantification of the stomatal pattern of these two populations identified two distinct types of stomatal clustering, contiguous clusters for *Arabidopsis* and non-contiguous clusters for *Begonia*. Along with the stomatal clustering in *tmm1* and *B. plebeja*, stomata appeared in greater numbers relative to their respective “single stomata” plants. To separate the effect of stomatal clustering from the stomatal density, I included into my study an additional *Arabidopsis* mutant, the *epf1/epf2*, which exhibits high stomatal density. Using light and dark treatments to drive stomatal movements, I investigated the gas exchange responses and I associated them with the stomatal patterning of each plant. Remarkably, only the *tmm1* mutant showed altered CO₂ assimilation and transpiration rates compared to the “single stomata” *Arabidopsis* lines, while the “clustered” *B. plebeja* did not exhibit such differences when compared to *B. coccinea* with single stomata.

To ascertain the underlying mechanism for altered gas exchanges responses due to stomatal clustering, I investigated the ion transport at the plasma membrane of the guard cells from *Arabidopsis* plants having either single or “clustered” stomata. Astonishingly, stomatal clustering attenuated K⁺ transport at the plasma membrane via alterations in the gating characteristics of the outward-rectifying and inward-rectifying K⁺ channels. Also, the accumulation of K⁺ ions into the guard cells appeared defective in the *tmm1* mutant guard cells. Thus, I postulated that the altered stomatal behaviour of the *tmm1* mutant is partially the result of the compromised ion transport at the plasma membrane but it was also influenced by the limited ion supply from the surrounding epidermal cells.

Whether the altered stomatal behaviour of the *tmm1* plants was manifested as a conditional phenotype under diverse stresses was also investigated. I subjected the *Arabidopsis* plants to different degrees of evaporative demand and drought stress. Stomatal clustering of the *tmm1* mutant resulted in the suppressed shoot biomass when environmental conditions were normally favourable for growth, which was also evident from the WUE measurements. Interestingly, the *tmm1* mutant was more resilient to prolonged drought stress, as the plants appeared more rigid with higher water content at the shoot tissue. Hence, I concluded that stomatal clustering resulted in a conditional phenotype that was underlined by the impaired function of stomata that appeared beneficial when the plants were limited from water availability.

I also presented a novel root phenotype of the stomatal patterning mutants *tmm1* and *epf1/epf2*. The *tmm1* mutant exhibited an attenuated growth of the root system that was sensitive to sucrose uptake via aerial parts, whereas the *epf1/epf2* mutant plants showed an altered root system independent of the sucrose supply. Thus, I postulated that the conditional root phenotype of *tmm1* mutant was associated with the altered stomatal function of these plants. Although no in depth investigation of the *epf1/epf2* root phenotype was undertaken, I speculated that this might be the result of altered patterning in the root epidermis of the plant.

Finally, I also reported on the effects of a novel gasotransmitter on stomatal behaviour. Hydrogen sulfide was here shown to induce stomatal closure in *Arabidopsis* and tobacco plants. Kinetic analysis of three major ion transporters, K_{OUT} , K_{IN} and anion channels, demonstrated the exclusive inhibition of the K_{IN} channels. I also provided evidence on the effect of H_2S to be independent of the well-characterized ABA pathway. Electrophysiological evidence suggested that the H_2S -induced I_{KIN} inhibition was partially mediated by changes in the intracellular Ca^{2+} . This finding was further highlighted from the OnGuard model, which pointed to a role of both intracellular Ca^{2+} and cytosolic pH in the H_2S -mediated stomatal function.

All together this study has indicated six new aspects associating with stomatal behaviour, some of which were also linked to plant growth. 1) The spacing

between stomata is required for proper stomatal movements to allow gaseous exchange and facilitate plant growth under favourable conditions. 2) Stomatal clustering might be beneficial for plants growing in adverse conditions such as dry habitats due to the reduced transpirational water loss. 3) The altered ion transport at the guard cell plasma membrane of the “clustered” stomata underpins the impaired stomatal behaviour of the *tmm1* mutant. 4) Spacing between stomata enables the ionic exchange between guard cells and neighbouring cells. 5) The distinct stomatal movements of the *tmm1* mutant are independent of the soluble or gaseous nature of the stimuli. 6) H₂S is a novel mediator of stomatal movements that possibly creates a new branch of the signaling network governing the stomatal behaviour.

6.2 Stomatal clustering in *Arabidopsis* and *Begonia*

Stomatal clustering is considered to be the result of alterations in the stomatal developmental program, and particularly due to the symmetric division of the meristemoid mother cell (Peterson et al. 2010). Stomatal clustering is naturally found in plants, like in several species of *Begonia* genus (Nebauer, 1967). Although reports on stomatal clustering in *Begonia* do exist (Hoover 1986; Tang et al. 2002), I present the quantification of stomatal phenotype in two *Begonia* species, the *B. coccinea* with single stomata and *B. plebeja* with stomatal clusters. Stomatal clustering in *Begonia* is different from that observed in *Arabidopsis*. Indeed, I noted that *B. plebeja* exhibited non-contiguous stomatal clusters, while the *Arabidopsis tmm1* mutant showed contiguous stomatal clustering. This difference was also accompanied by deviations in additional stomatal parameters. For instance, comparative analysis showed that *B. plebeja* exhibited more stomata of smaller size than the “single stomata” *B. coccinea*, while the *tmm1* mutant had high stomatal density with the stomatal size being not significantly altered. A similar outcome was derived from the stomatal index measurements implying that the non-contiguous stomatal clusters that naturally occur in plants might be an adaptation to minimize the evaporative area on leaves.

The altered stomatal patterning has been previously shown to affect gas exchange responses in *Arabidopsis* (Schluter et al. 2003; Franks et al. 2009; Yoo et al. 2010; Fanourakis et al. 2011; Tanaka et al. 2013; Drake et al. 2013; Dow et al. 2014); high stomatal density resulted in an increase in CO₂ assimilation (Tanaka et al. 2013), while the decrease in stomatal number resulted in the reduction of transpirational water loss (Yoo et al. 2010; Doheny-Adams et al. 2012). It is therefore suggested that stomatal patterning might provide a tool for fine-tuning the trade-off between these two processes and thus improving WUE (Drake et al. 2013; Lawson & Blatt 2014). In this study, I focused on the special pattern of stomatal clusters and on its effects in plant physiology. By employing intra- and inter-species comparison analysis, I provided evidence on the impaired gas exchange responses in the species exhibiting contiguous stomatal clusters. The *tmm1* mutant plants showed a suppressed rate of CO₂ assimilation under light conditions that were not limited for photosynthesis. This is in agreement with Dow et al. (2014) that used plants of different degrees of clustering to measure stomatal conductance and CO₂ assimilation. The authors showed that stomatal clustering had a big impact on stomatal conductance, impeding plants to optimize their photosynthetic capacity to increasing CO₂ concentrations. Another study has shown that increasing stomatal numbers due to higher expression of *STOMAGEN* enhanced the photosynthetic capacity, but did not affect WUE (Tanaka et al. 2013). Nevertheless, I did not observe an enhancement in the CO₂ assimilation in the *epf1/epf2* that have high stomatal density. This discrepancy might be due to the environmental conditions used. Actually, Schluter et al. (2003) demonstrated that photosynthesis was not influenced from stomatal density when light conditions were kept constant, as it is the case here. Here, I also demonstrated that the *tmm1* plants had a consistent greater transpiration rate under darkness in comparison with the *Arabidopsis* lines exhibiting single stomata. In contrast, *B. plebeja* plants with non-contiguous stomatal clusters did not show any difference in gaseous exchange under any condition. This finding clearly emphasized the physiological difference of the two types of stomatal clustering.

Employing mathematical models for the estimation of the maximum stomatal conductance, I presented data that followed the well-established relationship

between stomatal conductance and stomatal density or size. Previous reports have suggested that the more stomata the higher stomatal conductance would be (Hetherington & Woodward 2003; Franks et al. 2009; Franks & Beerling 2009b; Doheny-Adams et al. 2012). However, the experimentally measured stomatal conductance data deviated from the above relationship, with the two “clustered” species showing similar levels of stomatal conductance to the “single stomata” species despite of having higher stomatal density. The data collectively argue on the importance of spacing between stomata to achieve the maximum potential of gas diffusion.

6.3 Stomatal clustering influences plant growth

As mentioned before, stomata play a fundamental role in controlling WUE by facilitating the diffusion of CO₂ and water vapour with their immediate environment (Hetherington & Woodward 2003; Lawson & Blatt 2014). Improving WUE of plants would lead to higher biomass production and is considered to be a key strategy for agricultural practices, especially in habitats that are limited by water availability (Mueller et al. 2012). Wang et al. (2014) demonstrated that by up-regulating the expression of H⁺-ATPase resulted in greater stomatal opening, which in turn enhanced the photosynthetic capacity as well as plant biomass. Stomatal clustering did not result in any change in WUE under normal conditions. Nevertheless, when conditions were adjusted in such a way to promote photosynthesis without the adverse effect of high transpirational water loss, the *tmm1* mutants failed to improve WUE as the “single stomata” plants did. I suggested that this failure was dependent on the inability of stomata in contiguous clusters to effectively adjust their pore according to the environmental conditions. One can assume that the defective “clustered” stomata together with the higher stomatal density of the *tmm1* plants would possibly resulted in hypersensitivity to drought stress. Surprisingly, the *tmm1* plants appeared more resilient to prolonged drought stress, implying that the impaired stomatal movements and thus altered stomatal conductance led to a reduction in the transpirational water loss.

Stomatal clustering has been proposed to be an adaptive trait for dry and saline habitats (Hoover 1986; Gan et al. 2010). In an evolutionary perspective, plants ought to adopt lower stomatal densities because of the reduced developmental cost but also to avoid the contact between adjacent stomata to maintain stomatal function. However, plants that inhabit harsh environments, like those where water is limited, have to balance between metabolic cost and plant growth or even survival. For instance, the development of thicker leaves with multiple epidermis as well as stomatal clusters in *Begonia* has been considered as an adaptation to dry environments. This also holds true for the *B. plebeja* species used in this study, reinforcing the idea of stomatal clustering to be an ecological adaptation to dry niches. Further IRGA measurements of *Arabidopsis* “clustered” plants subjected to water stress will clarify whether stomatal clustering does prevent transpirational water loss.

Another remarkable finding from the current study was related to the novel root phenotype of the stomatal patterning mutants, *tmm1* and *epf1/epf2*. The *tmm1* phenotype was described as conditional, as it was only evident when carbon supply was in abundance. I argued that the defective stomata of the *tmm1* mutant abolished the uptake of sucrose via the aerial parts and therefore preventing the growth of the root system and particularly the emergence and elongation of lateral roots. The requirement of functional stomata to promote lateral root development under the presence of sucrose was also previously presented in the *lrd2* and *speechless Arabidopsis* mutants, which displayed defective or no stomatal phenotypes (Macgregor et al. 2008). In contrast, the *epf1/epf2* root phenotype was insensitive to the external carbon supply implying the potential role of the EPF1 and EPF2 proteins in the regulation of the root developmental program. These observations emphasize on the coupling of stomatal movements and possibly stomatal development with the root system development, a point that is often dismissed. It will be interesting to further test the stomatal patterning mutants in different nutritional compositions, but also investigate if the stomatal patterning is also manifested on the root epidermis by examining the root hair development.

6.4 Stomatal clustering entails changes in stomatal movements via altered ion transport

On a mechanistic basis, the gas exchange responses depend on the opening and closing of stomatal pore and therefore alteration in the capacity of these two processes would dramatically impact the physiology of the plant. Evidently, I argued that the altered gaseous exchange of the *tmm1* mutant was the outcome of the impaired stomatal movements, as depicted from the stomatal aperture measurements. Stomata of the *tmm1* mutant failed to reach a maximum aperture when exposed to light and opening buffer. Similarly, treatment of stomata with soluble closing stimuli as well as with the gaseous stomatal closure inducer, H₂S, resulted in the weakened stomatal closing process in the *tmm1* mutant plants. Yet, the stomata of *B. plebeja* did not exhibit such substantial impaired stomatal movements, highlighting the importance of spacing between stomata.

Stomatal movements depend on changes in the turgor of guard cells, which in turn requires the movement of osmotically active compounds and water across the plasma membrane of guard cells (Blatt 2000; Franks & Farquhar 2007). This procedure is associated with two components: 1) the activity of transport proteins residing at the plasma membrane of the guard cell and 2) the availability of surrounding cells to provide a sink-source of solutes (Raschke & Fellows 1971; Outlaw 1983; Blatt 2000). I here provided evidence on changes in both of these components in the *tmm1* mutants. Firstly, the kinetic analysis of $I_{K_{OUT}}$ and $I_{K_{IN}}$ suggested that stomatal clustering had a big impact on the K⁺ transport. The K_{OUT} channel activity was significantly reduced, while the gating characteristics of the K_{IN} channels were shifted. The change in the activity K_{OUT} channels was not dependent on the homeostatic regulation at the transcriptional level, as it was portrayed from the similar transcript levels of GORK in the three *Arabidopsis* mutants. Similarly, the transcription of K_{IN} channel-encoding genes was not altered due to the *tmm1* mutation. In addition, because changes in the open probability were only apparent for the K_{IN} channel, I postulated that the scarcity of K⁺ ions, which results from the presence of adjacent stomata in contiguous clusters, was not sufficient to impair stomatal function in *tmm1*

plants. The tail current analysis reported that K^+ accumulation in the cytosol of the guard cell from the *tmm1* plants was compromised even when external K^+ supply was in abundance, suggesting that other mechanisms might act to hinder stomatal movements.

Several reports have suggested that the osmotic solutes required for stomatal movements are provided by the surrounding epidermal or subsidiary cells that act as sink-source of ions (Raschke & Fellows 1971; MacRobbie & Lettau 1980; Outlaw 1983; Franks & Farquhar 2007). For instance, MacRobbie & Lettau (1980) using a double barreled K^+ -sensitive microelectrodes showed that K^+ content in the epidermal cells of *C. communis L.* was reduced from 180-300 mM to 80 mM with the opening of stomata. It is suggested that uptake of solutes in *C. communis L.* guard cells occurs at the sites where the cells are adjacent with subsidiary cells (Penny & Bowling 1974). If the above contention is correct then the area where solute shuttling can occur is substantially minimized in contiguous stomatal clusters. Also, Meckel et al. (2007) reported on the specific spatial accumulation of KAT1 channels at the tip of guard cells during stomatal opening. It would be beneficial for future studies to examine the distribution of the plasma membrane ion channels in the *tmm1* guard cells and identify whether the unique arrangements of these cells alters the localization of the ion transport proteins. In terms of the spatial and physical constraints, one can assume that opening of stomata occurs at tandem and that creates a backpressure between them that halts the opening process. However, I here reported that apart from stomatal opening, stomata closure, which should not be limited to the backpressure exerted by guard cells, is also impaired in the *tmm1* mutants. Thus, I ruled out that the stomatal phenotype of *tmm1* was dependent on the lateral physical constraints, though I did not provide direct evidence.

All the above evidence is collectively shown in Figure 1 that demonstrates the stomatal responses under favourable and water-stressed conditions from plants with single stomata and stomata in clusters. Emphasis on the mechanism mediating the impaired behaviour of stomata in clusters is also made. In conclusion, the spacing between stomata is a prerequisite for driving stomatal movements as it is depicted from the physiological, electrophysiological data as

well as the phenotypic analysis of the *tmm1* mutant plants. Stomatal clustering resulted in the suppressed WUE and plant growth when conditions were favourable, yet it allowed the plants to sustain water content and biomass under extreme water scarcity. Hence, stomatal clustering can be beneficial for plants inhabiting extreme environments where water conservation is highly demanded.

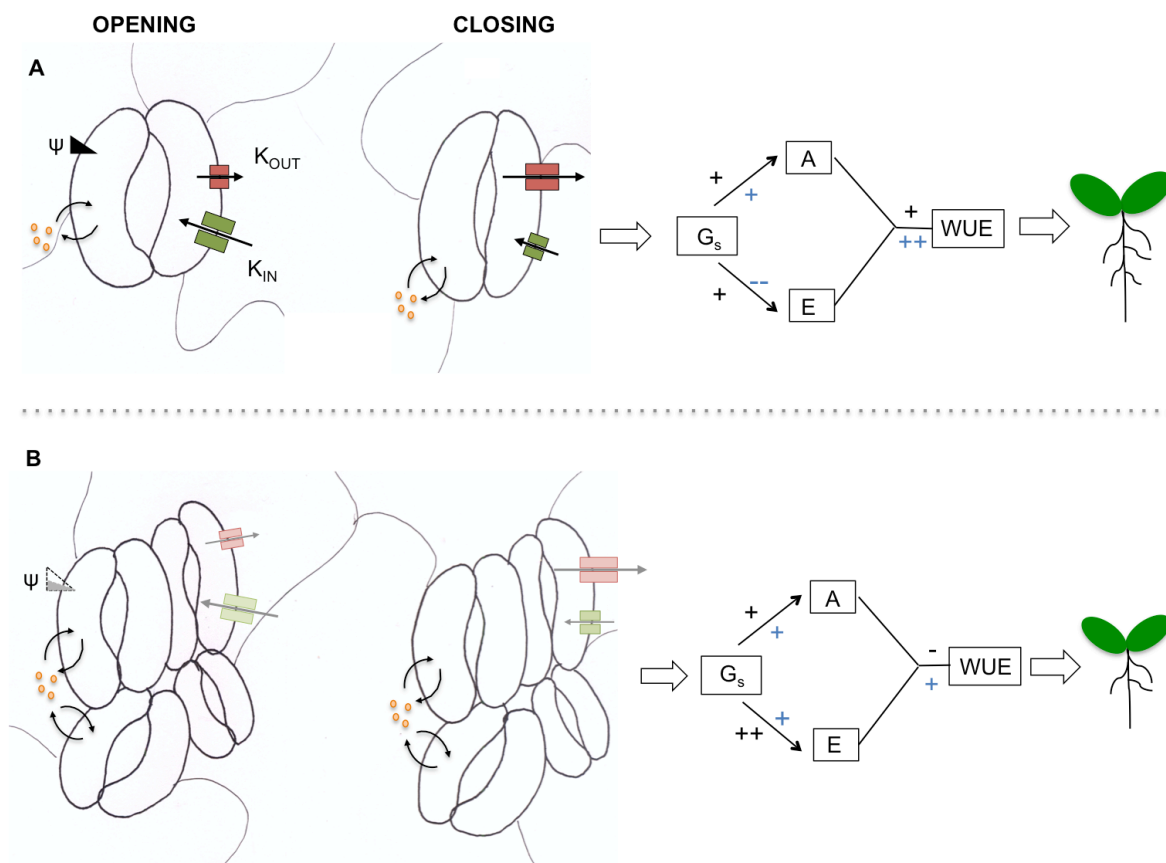


Figure 1. Stomatal clustering impacts plant physiology and growth via changes in ion transport and ionic exchange.

Cartoon collectively illustrates the major findings regarding the consequences of stomatal clustering. Darker coloration of symbols indicates wild-type function, whereas lighter coloration indicates a suppressed function. (+) or (-) symbols indicate the positive or negative effect on the gaseous exchange responses. Black or blue colouration indicates the effect under favourable conditions or under low water availability, respectively. Note, the magnitude of the responses under drought stress are hypothetical, since no IRGA measurements carried out for this condition.

(A) Single stomata responded to opening stimuli by enhancing the activity of K_{IN} channels residing at the plasma membrane via hyperpolarization of membrane voltage (black triangle), while movement of solutes (orange circles) between epidermal guard cells was also enabled. During closing process the efflux of K^+ and Cl^- is a prerequisite and is mediated by the K_{OUT} channels at the plasma membrane. Stomatal movements allow the adjustment of the stomatal pore to enable CO_2 influx at the expense of water vapour release. This is mirrored to stomatal conductance that influences both CO_2 assimilation and transpiration that in turn fine-tune WUE and promote plant growth. When water was limited, the stomatal conductance was reduced to prevent transpirational water loss that eventually affected leaf expansion and plant growth. In long-term, the wild-type stomatal function resulted in plant desiccation.

(B) Stomata in clusters showed impaired stomatal movements that were dependent on the altered activity K_{OUT} and K_{IN} channels. Membrane voltage was shifted to more positive values (depolarization). Also, the movement of solutes between stomata and neighbouring cells was compromised since the pool of solutes was shared between multiple stomata. In turn, under favourable conditions, gaseous exchange via the “clustered” stomata was altered resulting in a lower WUE, eventually causing the attenuated growth of the plants. The impaired function of “clustered” stomata prevented the excessive water loss of via transpiration resulting in a better plant performance under low water availability.

6.5 *H₂S a novel effector of stomatal behaviour*

As in the case with *Arabidopsis*, I also presented that H₂S induces stomatal closure in tobacco plants. Kinetic analysis of the I_{KOUT} , I_{KIN} and I_{Cl} highlighted the mechanism underlying the H₂S-mediated stomatal closure. This novel gasotransmitter exclusively inactivates the I_{KIN} and alters the gating characteristics of the K_{IN} channels. This underpins the separation from other known closing stimuli such as ABA and NO (Blatt 1990; Blatt & Armstrong 1993; Schwartz et al. 1994; Garcia-Mata et al. 2003; Siegel et al. 2009). García-Mata & Lamattina (2010) reported on the H₂S-driven stomatal closure is dependent on ABA. However, I provided strong evidence for the opposite, as pharmacological studies showed that stomata treated with a H₂S scavenger did not bypass ABA-mediated stomatal closure and inhibition of I_{KIN} . The slight stimulation of K_{IN} channels when the intracellular Ca²⁺ was buffered suggested that H₂S-induced stomatal closure might be partially sensitive to the levels of [Ca²⁺]_i. The OnGuard model suggested that changes in intracellular Ca²⁺ are the consequences of changes in the activity of K⁺ and Cl⁻ channels. Additionally, the outputs of the OnGuard model implied that the Ca²⁺ changes brought by H₂S were sensitive to pH since it predicted the acidification of the cytosol. It would be useful to run the OnGuard model backwards and therefore impose changes in both pH and [Ca²⁺]_i and identify whether they are sufficient to give rise to changes in I_{KIN} and I_{Cl} similar to those determined from the electrophysiological studies. Future studies should also include the in vivo ratiometric fluorescence imaging together with the Ca²⁺- and H⁺-sensitive dyes to examine for the specific changes in these secondary messengers by the release of H₂S in the cytosol. Additionally, in the future, the potential use of H₂S as antitranspirant should be addressed by carrying out IRGA measurements on plants that have been exogenously treated with H₂S.

In conclusion, in this study I provided a mechanistic explanation of how H₂S triggers stomatal closure and Figure 2 illustrates all the events that led to this suggestion. Electrophysiological evidence demonstrated that stomatal closure involved the exclusive inhibition of the K_{IN} channels at the guard cell plasma membrane that was partially dependent on intracellular Ca²⁺ levels. Importantly,

the effect of H_2S on stomata and K_{IN} channels *per se* was independent of ABA. Moreover, predictions derived from OnGuard software suggested an additional role of pH in the H_2S -induced stomatal closure. The model coupled the changes in the pH and Ca^{2+} and it predicted the involvement of the tonoplast Ca^{2+} - H^+ tonoplast antiport protein to the H_2S -mediated response.

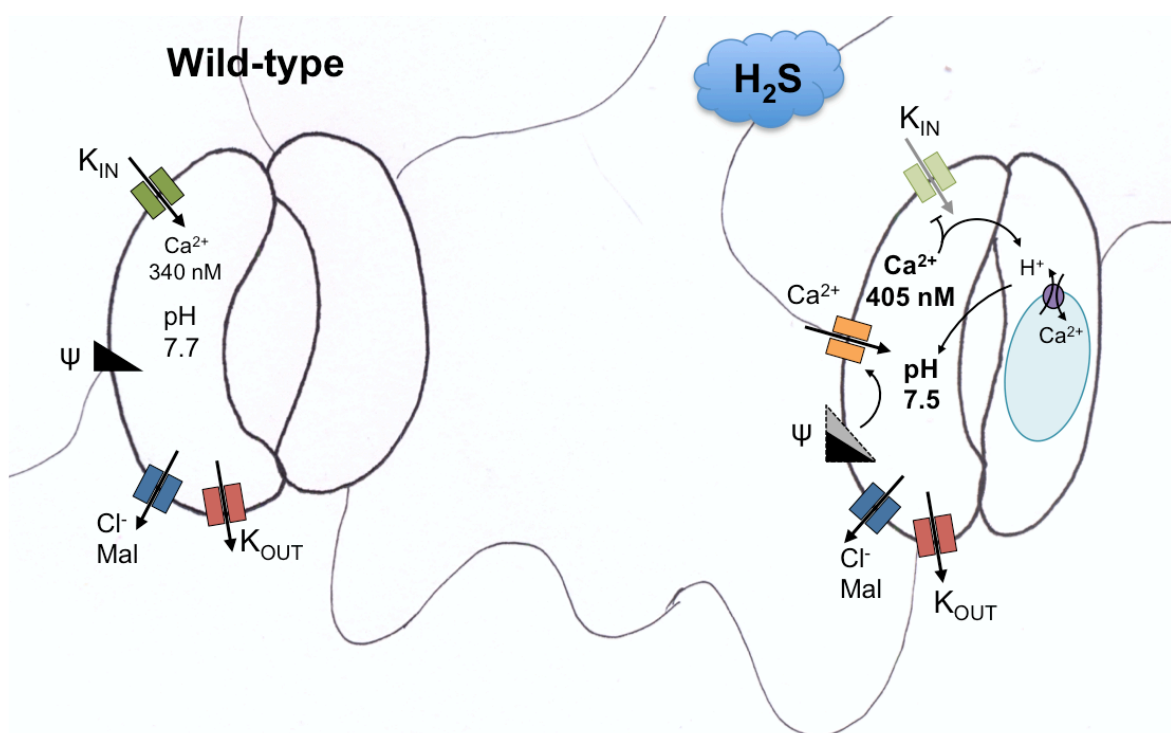


Figure 2. H_2S induces stomatal closure via altering ion transport at the guard cell plasma membrane.

Cartoon collectively illustrates the major findings regarding the H_2S effect on stomata. Stoma at left side indicates the wild type-like function of the major ion transporters residing the plasma membrane and the secondary messengers. Upon exposure to H_2S , stomata close (right). H_2S caused the hyperpolarization of the plasma membrane (grey triangle). Hyperpolarization event was predicted to be associated with a rise in intracellular Ca^{2+} , possibly via the activation of Ca^{2+} plasma membrane channels. Rise in $[\text{Ca}^{2+}]_i$ exclusive inhibited the K_{IN} channels (light green coloration) but did not stimulate either anion or K_{OUT} channels. The H_2S -triggered acidification of the cytosol might be associated with a stimulation of Ca^{2+} - H^+ antiport tonoplast protein as a consequence of the elevated $[\text{Ca}^{2+}]_i$.

6.6 Conclusion

This study provided novel information on the stomatal behaviour and how this is affected by internal and external factors. It highlighted the importance of spacing between stomata in order to promote stomatal movements and enable plant growth. Also, a potentially beneficial property of stomatal clustering against prolonged drought was demonstrated that rationalizes the existence of plant species with stomatal clusters in nature. The mechanistic evidence on the effects of H₂S on stomata was demonstrated, unravelling a new signaling pathway mediating stomatal closure. Collectively, stomatal clustering and H₂S might provide novel insights for manipulating gas exchange responses and thus WUE, especially in crops, to withstand periods of drought.

REFERENCES

- Abel, S. 2011. Phosphate sensing in root development. *Current opinion in plant biology*, 14(3), pp. 303-9.
- Abrash, E. B. & Bergmann, D. C. 2010. Regional specification of stomatal production by the putative ligand CHALLAH. *Development*, 137(3), pp. 447-55.
- Abrash, E. B., Davies, K. & Bergmann, D. C. 2011. Generation of signaling specificity in Arabidopsis by spatially restricted buffering of ligand-receptor interactions. *The Plant cell*, 23(8), pp. 2864-79.
- Ache, P., Becker, D., Ivashikima, N., Dietrich, P., Roelfsema, M. R. G. & Hedrich, R. 2000. GORK , a delayed outward rectifier expressed in guard cells of Arabidopsis thaliana , is a K⁺-selective , K⁺-sensing ion channel. *FEBS letters*, 486, pp. 3-8.
- Allen, G. J., Kuchitsu, K., Chu, S. P., Murata, Y. & Schroeder, J. I. 1999. Arabidopsis abi1-1 and abi2-1 phosphatase mutations reduce abscisic acid-induced cytoplasmic calcium rises in guard cells. *The Plant cell*, 11(9), pp. 1785-98.
- Alvarez, C. Calo, L., Romero, L. C., Garcia, I., & Gotor, C. 2010. An O-acetylserine(thiol)lyase homolog with L-cysteine desulphydrase activity regulates cysteine homeostasis in Arabidopsis. *Plant physiology*, 152(2), pp. 656-69.
- Aphalo, J. & Jarvis, P. G. 1991. Do stomata respond to relative humidity? *Plant, Cell and Environment*, 14, pp. 127-132.
- Armengaud, P. Zambaux, K., Hills, A., Sulpice, R., Pattison, R. J., Blatt, M. R. & Amtmann, A. 2009. EZ-Rhizo: integrated software for the fast and accurate measurement of root system architecture. *The Plant journal : for cell and molecular biology*, 57(5), pp.945-56.
- Assmann, S. M. 1988. Enhancement of the Stomatal Response to Blue Light by Red Light, Reduced Intercellular Concentrations of CO₂, and Low Vapor Pressure Differences. *Plant physiology*, 87(1), pp. 226-31.
- Babenko, A. P., Gonzalez, G. & Bryan, J. 2000. Pharmaco-topology of sulfonylurea receptors. *Journal of biological chemistry*, 275(2), pp. 717-720.
- Bergmann, D. C., Lukowitz, W. & Somerville, C.R. 2004. Stomatal development and pattern controlled by a MAPKK kinase. *Science*, 304(5676), pp. 1494-7.
- Bhave, N. S., Veley, K. M., Nadeau, J. A., Lucas, J. R., Bhave, S. J. & Sack, F. D. 2009. TOO MANY MOUTHS promotes cell fate progression in stomatal development of Arabidopsis stems. *Planta*, 229(2), pp. 357-67.

- Blatt, M. 1990. Potassium channel currents in intact stomatal guard cells: rapid enhancement by abscisic acid. *Planta*, 180, pp. 445-455.
- Blatt, M. R. 1991. Ion Channel Gating in Plants: Physiological Implications and Integration for Stomatal Function. *Journal of Membrane Biology*, 124, pp. 95-112.
- Blatt, M. R. 1992. K⁺ channels of stomatal guard cells. *The Journal of General Physiology*, 99, pp.615-644.
- Blatt, M. R. & Thiel, G. 1993. Hormonal Control of ion channel gating. *Annual review of plant physiology plant molecular biology*, 44, pp. 543-567.
- Blatt, M. & Armstrong, F. 1993. K⁺ channels of stomatal guard cells: Abscisic-acid-evoked control of the outward rectifier mediated by cytoplasmic pH. *Planta*, 191(3), pp. 330-341.
- Blatt, M. R. 2000. Cellular signaling and volume control in stomatal movements in plants. *Annual review of cell. dev. biology*, 16, pp. 221-241.
- Blatt, M. R. 2000. Ca(2+) signalling and control of guard-cell volume in stomatal movements. *Current opinion in plant biology*, 3(3), pp. 196-204.
- Blatt, M.R., Wang, Y., Leonhardt, N. & Hills, A. 2014. Exploring emergent properties in cellular homeostasis using OnGuard to model K⁺ and other ion transport in guard cells. *Journal of plant physiology*, 171(9), pp. 770-8.
- Bloem, E., Haneklaus, S., Salac, I., Wickenhäuser, P. & Schnug, E. 2007. Facts and fiction about sulfur metabolism in relation to plant-pathogen interactions. *Plant biology (Stuttgart, Germany)*, 9(5), pp. 596-607.
- Bloem, E., Haneklaus, S., Salac, I., Wickenhäuser, P. & Schnug, E. 2004. Sulphur supply and infection with *Pyrenopeziza brassicae* influence L-cysteine desulphydrase activity in *Brassica napus* L. *Journal of experimental botany*, 55(406), pp. 2305-12.
- Boghdan & Barkley. 1972. Stomatal patterns in the genus *Begonia*. *Phytologia* 23 (4), pp. 327-333.
- Bouman, F. & de Lange, A. 1983. Structure micropmorphology of *Begonia* seeds. *The Begonian*, 50, pp. 70-78.
- Briggs, W. R. & Christie, J. M. 2002. Phototropins 1 and 2: versatile plant blue-light receptors. *Trends in plant science*, 7(5), pp. 204-10.
- Casson, S. & Gray, J. E. 2008. Influence of environmental factors on stomatal development. *New Phytologist*, 178, pp. 9-23.

Chen, J., Fei-Hua Wu, F. H., Wang, W. H., Zheng, C. J., Lin, G. H., Dong, X. J., He, J. X., Pei, Z. M., & Zheng, H. L. 2011. Hydrogen sulphide enhances photosynthesis through promoting chloroplast biogenesis, photosynthetic enzyme expression, and thiol redox modification in *Spinacia oleracea* seedlings. *Journal of experimental botany*, 62(13), pp. 4481-93.

Chen, Z. H., Hills, a., Bätz, U., Amtmann, A., Lew, V. L. & Blatt, M. R. 2012. Systems dynamic modeling of the stomatal guard cell predicts emergent behaviors in transport, signaling, and volume control. *Plant physiology*, 159(3), pp. 1235-51.

Chen, Z. H. Eisenach, C., Xu, X. Q., Hills, A., Blatt, M. R. 2012. Protocol: optimised electrophysiological analysis of intact guard cells from *Arabidopsis*. *Plant methods*, 8(1), p. 15.

Christie, J. M. 2007. Phototropin blue-light receptors. *Annual review of plant biology*, 58, pp. 21-45.

Claeys, H. & Inzé, D. 2013. The Agony of Choice: How Plants Balance Growth and Survival under Water-Limiting Conditions. *Plant physiology*, 162(4), pp. 1768-79.

Coupe, S., Palmer, B. G., Lake, J. A., Overy, S. A., Oxborough, K., Woodward, F. I., Gray, J. E. & Quick, W. P. 2006. Systemic signalling of environmental cues in *Arabidopsis* leaves. *Journal of experimental botany*, 57(2), pp. 329-41.

Cramer, M. D., Hawkins, H. J. & Verboom, G. A. 2009. The importance of nutritional regulation of plant water flux. *Oecologia*, 161(1), pp. 15-24.

Cutler, S. R., Rodriguez, P. L., Finkelstein, R. R. & Abrams, S. R. 2010. *Abscisic acid: emergence of a core signaling network*. *Annual review of plant biology*, pp. 651-679.

Davies, W. J., 1978. Some Effects of Abscisic Acid and Water Stress on Stomata of *Vicia faba* L. *Journal of experimental botany*, 29(108), pp. 175-182.

De Angeli, A., Zhang, J., Meyer, S., & Martinoia, E. 2013. AtALMT9 is a malate-activated vacuolar chloride channel required for stomatal opening in *Arabidopsis*. *Nature communications*, 4, p.1804.

Desikan, R., Griffiths, R., Hancock, J., & Neill, S. (2002). A new role for an old enzyme: nitrate reductase-mediated nitric oxide generation is required for abscisic acid-induced stomatal closure in *Arabidopsis thaliana*. *Proceedings of the National Academy of Sciences of the United States of America*, 99 (25), pp. 16314-8.

Dewitte, A., Leus, L., Eeckhaut, T., Vanstechelman, I., van Huylenbroeck, J. & van Bockstaele, E. 2009. Genome size variation in *Begonia*. *Genome*, 52, pp. 829-838.

Doheny-Adams, T., Hunt, L., Franks, P. J., Beerling, D. J. & Gray, J. E. 2012. Genetic manipulation of stomatal density influences stomatal size, plant growth and tolerance to restricted water supply across a growth carbon dioxide

- gradient. *Philosophical transactions of the Royal Society of London. Series B, Biological sciences*, 367(1588), pp. 547-55.
- Doorenbos, J., Sosef, M. S. M. & De Wild, J. J. F. E. 1998. The sections of Begonia, including descriptions, keys and species list. *Studies in Begoniaceae VI. Wageningen Agricultural University Papers*, 98 (2), pp. 1-266.
- Dow, G. J., Berry, J. a & Bergmann, D. C. 2014. The physiological importance of developmental mechanisms that enforce proper stomatal spacing in *Arabidopsis thaliana*. *The New phytologist*, 201(4), pp. 1205-17.
- Drake, P. L., Froend, R. H. & Franks, P. J. 2013. Smaller, faster stomata: scaling of stomatal size, rate of response, and stomatal conductance. *Journal of experimental botany*, 64(2), pp. 495-505.
- Dreyer, I. & Blatt, M. R. 2009. What makes a gate? The ins and outs of Kv-like K⁺ channels in plants. *Trends in plant science*, 14(7), pp. 383-90.
- Duby, G., Hosy, E., Fizames, C., Alcon, C., Costa, A., Sentenac, H. & Thibaud, J. B. 2008. AtKC1, a conditionally targeted Shaker-type subunit, regulates the activity of plant K⁺ channels. *The Plant journal : for cell and molecular biology*, 53(1), pp. 115-23.
- Eisenach, C., Chen, Z. H., Grefen, C. & Blatt, M R. 2012. The trafficking protein SYP121 of *Arabidopsis* connects programmed stomatal closure and K⁺ channel activity with vegetative growth. *The Plant journal : for cell and molecular biology*, 69(2), pp. 241-51.
- Eisenach, C., Papapanatsiou, M., Hillert, E. K., Blatt, M. R. 2014. Clustering of the K⁺ channel GORK of *Arabidopsis* parallels its gating by extracellular K⁺. *The Plant journal : for cell and molecular biology*, 78(2), pp. 203-14.
- Elies, J., Scragg, J. L., Huang, S., Dallas, M L., Huang, D., MacDougall, D., Boyle, J. P., Gamper, N. & Peers, C. 2014. Hydrogen sulfide inhibits Cav3.2 T-type Ca²⁺ channels. *The FASEB Journal*, published online 2 September.
- Engineer, C.B., Ghassemian, M., Anderson, J. C., Peck, S. C., Hu, H. & Schroeder, J. I. 2014. Carbonic anhydrases, EPF2 and a novel protease mediate CO₂ control of stomatal development. *Nature*, 410, pp. 327-330.
- Fanourakis, D., Carvalho, S. M. P., Almeida, D. P. F., & Heuvelink, E. 2011. Avoiding high relative air humidity during critical stages of leaf ontogeny is decisive for stomatal functioning. *Physiologia plantarum*, 142(3), pp. 274-86.
- Farquhar, G. D. & Sharkey, T. D. 1982. Stomatal Conductance and Photosynthesis. *Annual Review of Plant Physiology*, 33(1), pp.317-345..
- Flexas, J. 2002. Drought-inhibition of Photosynthesis in C3 Plants: Stomatal and Non-stomatal Limitations Revisited. *Annals of Botany*, 89(2), pp.183-189.
- Franks, P. J. 2013. Commentary Passive and active stomatal control : either or both? *New Phytologist*, 198, pp. 325-327.

- Franks, P. J. & Farquhar, G. D. 1999. A relationship between humidity response, growth form and photosynthetic operating point in C3 plants. *Plant, Cell and Environment*, 22(11), pp. 1337-1349.
- Franks, P. J. & Farquhar, G. D. 2001. The effect of exogenous abscisic acid on stomatal development, stomatal mechanics, and leaf gas exchange in *Tradescantia virginiana*. *Plant physiology*, 125(2), pp. 935-42.
- Franks, P. J. & Farquhar, G. D. 2007. The mechanical diversity of stomata and its significance in gas-exchange control. *Plant physiology*, 143(1), pp. 78-87.
- Franks, P. J. & Beerling, D. J. 2009. Maximum leaf conductance driven by CO₂ effects on stomatal size and density over geologic time. *Proceedings of the National Academy of Sciences of the United States of America*, 106(25), pp. 10343-7.
- Franks, P. J., Drake, P. L. & Beerling, D. J. 2009. Plasticity in maximum stomatal conductance constrained by negative correlation between stomatal size and density: an analysis using *Eucalyptus globulus*. *Plant, Cell and Environment*, 32, pp. 1737-1748.
- Fricke, W., Akhiyarova, G. Wei, W., Alexandersson, E., Miller, A., Kjellbom, P. O. Richardson, A. Wojciechowski, T. Schreiber, L., Veselov, D. Kudoyarova, G. & Volkov, V. 2006. The short-term growth response to salt of the developing barley leaf. *Journal of experimental botany*, 57(5), pp. 1079-95.
- Gaedek, N., Klein, M., Kolukisaoglu, U., Forestier, C., Muller, A., Ansoerge, M., Becker, D., Mammum, Y., Kuchler, K., Schulz, B., Mueller-Roeber, B., Martinoia, E. 2001. The *Arabidopsis thaliana* ABC transporter AtMRP5 controls root development and stomata movement. *The EMBO journal*, 20(8), pp. 1875-87.
- Gambale, F. & Uozumi, N. 2006. Properties of Shaker-type potassium channels in higher plants. *Journal of Membrane Biology*, 210, pp. 1-19.
- Gan, Y., Zhou, L., Shen, Z. J., Shen, Z. X., Zhang, Y. Q., Wang, G. X. 2010. Stomatal clustering, a new marker for environmental perception and adaptation in terrestrial plants. *Botanical studies*, 51, pp. 325-336.
- Garcia-Mata, C. & Lamattina, L. 2002. Nitric Oxide and Abscisic Acid Cross Talk in Guard Cells 1. *Plant phy*, 128, pp. 790-792.
- Garcia-Mata, C., Gay, R., Sokolovski, S., Hills, A., Lamattina, L. & Blatt, M. R. 2003. Nitric oxide regulates K⁺ and Cl⁻ channels in guard cells through a subset of abscisic acid-evoked signaling pathways. *Proceedings of the National Academy of Sciences of the United States of America*, 100(19), pp. 11116-21.
- García-Mata, C. & Lamattina, L. 2003. Abscisic acid, nitric oxide and stomatal closure - is nitrate reductase one of the missing links? *Trends in plant science*, 8(1), pp. 20-6.

- García-Mata, C. & Lamattina, L. 2010. Rapid report Hydrogen sulphide , a novel gasotransmitter involved in guard cell signalling. *New Phytologist*, 188, pp. 977-984.
- Gaymard, F., Pilot, G., Lacombe, B., Bouchez, D., Bruneau, D., Bouchourez, D., Michaux-Ferriere, N., Thibaud, J. B., Sentenac, H. 1998. Identification and disruption of a plant shaker-like outward channel involved in K⁺ release into the xylem sap. *Cell*, 94(5), pp. 647-55.
- Ghassemian, M., Nambara, E., Cutler, S., Kawaide, H., Kamiya, Y., Mc, P. & Court, P. 2000. Regulation of abscisic acid signaling by the ethylene response pathway in Arabidopsis. *The Plant cell*, 12(7), pp. 1117-26.
- Geisler, M., Yang, M. & Sack, F. D. 1998. Divergent regulation of stomatal initiation and patterning in organ and suborgan regions of the Arabidopsis mutants too many mouths and four lips. *Planta*, 205(4), pp. 522-30.
- Geisler, M., Nadeau, J. & Sack, F. D. 2000. Oriented asymmetric divisions that generate the stomatal spacing pattern in arabidopsis are disrupted by the too many mouths mutation. *The Plant cell*, 12(11), pp. 2075-86.
- Gobert, A., Isayenkov, S., Voelker, C., Czempinski, K., & Maathuis, F. J. M. 2007. The two-pore channel TPK1 gene encodes the vacuolar K⁺ conductance and plays a role in K⁺ homeostasis. *Proceedings of the National Academy of Sciences of the United States of America*, 104(25), pp.10726-31.
- Goodall-copestake, W.P., Perez-Espona, S., Harris, D. J., Hollingsworth, M. 2010. The early evolution of the mega-diverse genus Begonia (Begoniaceae) inferred from organelle DNA phylogenies. *Biological journal of the Linnean society*, 101, pp. 243-250.
- Gosti, F., Beaudoin, N., Serizet, C., Webb, A. A. R., Vartanian, N. & Giraudat, J. 1999. ABI1 protein phosphatase 2C is a negative regulator of abscisic acid signaling. *The Plant cell*, 11(10), pp. 1897-910.
- Grabov, A., Leung, J., Giraudat, J. Blatt, M. R. 1997. Alteration of anion channel kinetics in wild-type and abi1-1 transgenic Nicotiana bethamiana guard cells by abscisic acid. *The Plant journal*, 12, pp.203-213.
- Grabov, A & Blatt, M.R. 1998. Membrane voltage initiates Ca²⁺ waves and potentiates Ca²⁺ increases with abscisic acid in stomatal guard cells. *Proceedings of the National Academy of Sciences of the United States of America*, 95(8), pp. 4778-83.
- Grabov, A & Blatt, M. 1999. A steep dependence of inward-rectifying potassium channels on cytosolic free calcium concentration increase evoked by hyperpolarization in guard cells. *Plant physiology*, 119(1), pp. 277-88.
- Gradmann, D., Blatt, M. R. & Thiel, G. 1993. Electrocoupling of ion transporters in plants. *Journal of Membrane Biology*, 136, pp. 327-332.

Gray, J.E., Holroyd, G.H., van der Lee, F. M., Bahrami, A. R., Sijmons, P. C., Woodward, F. I., Schuch, W., Hetherington, A. M. 2000. The HIC signalling pathway links CO₂ perception to stomatal development. *Nature*, 408(6813), pp. 713-6.

Guo, F. Q., Okamoto, M. & Crawford, N. M. 2003. Identification of a plant nitric oxide synthase gene involved in hormonal signaling. *Science (New York, N.Y.)*, 302(5642), pp. 100-3.

Hare, P.D., Cress, W. A. & Van Staden, J. 1998. Dissecting the roles of osmolyte accumulation during stress. *Plant, Cell and Environment*, 21(6), pp. 535-553.

Hara, K., Kajita, R., Torii, K. U., Bergmann, D. C. and Kakimoto, T. 2007. The secretory peptide gene EPF1 enforces the stomatal one-cell-spacing rule. *Genes & development*, 21, pp. 1720-1725.

Hedrich, R., Busch, H. & Raschke, K. 1990. Ca²⁺ and nucleotide dependent regulation of voltage dependent anion channels in the plasma membrane of guard cells. *The EMBO journal*, 9(12), pp. 3889-92.

Hedrich, R. & Schroeder, J. I. 1989. THE PHYSIOLOGY OF ION CHANNELS AND ELECTROGENIC PUMPS IN HIGHER PLANTS. *Annual review of plant physiology*, 40, pp. 539-69.

Hetherington, A. M. & Woodward, F. I. 2003. The role of stomata in sensing and driving environmental change. *Nature*, 424, pp. 901-908.

Hille, B. 2001. Ion channels of excitable membranes. University of Washington, 3rd edition, Washington, USA.

Hills, A., Chen, Z. H., Amtmann, A., Blatt, M. R., Lew, V. L. 2012. OnGuard, a computational platform for quantitative kinetic modeling of guard cell physiology. *Plant physiology*, 159(3), pp. 1026-42.

Hirasawa, T. & Hsiao, T. C., 1999. Some characteristics of reduced leaf photosynthesis at midday in maize growing in the field. *Field Crops Research*, 62, pp. 53-62

Hirsch, R. E., Lewis, B. D., Spalding, E. P. & Sussman, M. R. 1998. A Role for the AKT1 Potassium Channel in Plant Nutrition. *Science*, 280(5365), pp. 918-921.

Honsbein, A., Sokolovski, S., Grefen, C., Campanoni, P., Pratelli, R. Paneque, M., Chen, Z. H. Johansson, I. & Blatt, M. R. 2009. A tripartite SNARE-K⁺ channel complex mediates in channel-dependent K⁺ nutrition in Arabidopsis. *The Plant cell*, 21(9), pp. 2859-77.

Hoover, W. S. 1986. Stomata and Stomatal Clusters in Begonia: Ecological Response in Two Mexican Species. *Biotropica*, 18(1), pp. 16-21.

Hosy, E., Vavasseur, A., Mouline, K., Dreyer, I., Gaymard, F., Poree, F. Boucherez, J., Lebaudy, A., Bouchez, D., Very, A., Simonneau, T. & Thibaud, J. B. 2003. The Arabidopsis outward K⁺ channel GORK is involved in regulation of

stomatal movements and plant transpiration. *Proceedings of the National Academy of Sciences of the United States of America*, 100(9), pp. 5549-54.

Hu, H., Boisson-Dernier, A., Israelsson-Nordström, M., Böhmer, M., Xue, S., Ries, A., Godoski, Kuhn, J. J. M., & Schroeder, J. I. 2010. Carbonic anhydrases are upstream regulators of CO₂-controlled stomatal movements in guard cells. *Nature cell biology*, 12(1), pp. 87-93.

Hughes ., 2003

Hughes, M. & Hollingsworth, P.M., 2008. Population genetic divergence corresponds with species-level biodiversity patterns in the large genus *Begonia*. *Molecular ecology*, 17(11), pp. 2643-51.

Hummel, I., Pantin, F., Sulpice, R., Piques, M., Rolland, G., Dauzat, M., Christophe, A., Pervent, M., Bouteille, M., Stitt, M., Gibon, Y., & Muller, B. 2010. Arabidopsis plants acclimate to water deficit at low cost through changes of carbon usage: an integrated perspective using growth, metabolite, enzyme, and gene expression analysis. *Plant physiology*, 154(1), pp. 357-72.

Hunt, L. & Gray, J. E. 2009. The signaling peptide EPF2 controls asymmetric cell divisions during stomatal development. *Current biology : CB*, 19(10), pp. 864-9.

Imes, D., Mumm, P., Bohm, J., Al-Rasheid, K. A. S., Marten, I., Geiger, D., & Hedrich, R. 2013. Open stomata 1 (OST1) kinase controls R-type anion channel QUAC1 in Arabidopsis guard cells. *The Plant journal : for cell and molecular biology*, 74(3), pp. 372-82.

Jeanguenin, L., Alcon, C., Duby, G., Boeglin, M., Cherel, I., Gaillard, I., Zimmermann, S., Sentenac, H. & Very, A. 2011. AtKC1 is a general modulator of Arabidopsis inward Shaker channel activity. *The Plant journal : for cell and molecular biology*, 67(4), pp. 570-82.

Jin, Z., Shen, J., Qiao, Z., Yang, G., Wang, R. & Pei, Y. 2011. Hydrogen sulfide improves drought resistance in Arabidopsis thaliana. *Biochemical and biophysical research communications*, 414(3), pp. 481-6.

Johansson, I., Wulfetange, K., Poree, F., Michard, E., Gajdanowicz, P., Lacombe, B., Sentenac, H., Thibaud, J. B., Mueller-Roeber, B., Blatt, M. R. & Dreyer, I. 2006. External K⁺ modulates the activity of the Arabidopsis potassium channel SKOR via an unusual mechanism. *The Plant journal : for cell and molecular biology*, 46(2), pp. 269-81.

Joshi-Saha, A., Valon, C. & Leung, J. 2011. A brand new START: abscisic acid perception and transduction in the guard cell. *Science signaling*, 4(201), p. re4

Jr, H. & Outlaw, W. H. 1983. Current concepts on the role of potassium in stomatal movements. , pp. 302-311.

Kanaoka, M. M., Pillitteri, L. J., Fujii, H., Yoshida, Y., Bogenschutz, N. L., Takabayashi, J., Zhu, J. K. & Torii, K. U. 2008. SCREAM/ICE1 and SCREAM2

specify three cell-state transitional steps leading to arabidopsis stomatal differentiation. *The Plant cell*, 20(7), pp. 1775-85.

Kellermeier, F., Armengaud, P., Seditas, T. J., Danku, J., Salt, D. E. & Amtmann, A. 2014. Analysis of the Root System Architecture of Arabidopsis Provides a Quantitative Readout of Crosstalk between Nutritional Signals. *The Plant cell*, 26(4), pp. 1480-1496.

Kellermeier, F., Chardon, F. & Amtmann, A. 2013. Natural variation of Arabidopsis root architecture reveals complementing adaptive strategies to potassium starvation. *Plant physiology*, 161(3), pp. 421-32.

Kim, T.-H., Böhmer, M., Hu, H., Nishimura, N. & Schroeder, J. I. 2010. Guard Cell Signal Transduction Network: Advances in Understanding Abscisic Acid, CO₂, and Ca²⁺ Signaling. *Annual review of plant biology*, 61, pp. 561-591.

Kimura, H. 2011. Hydrogen sulfide: its production, release and functions. *Amino acids*, 41(1), pp. 113-21.

Kondo, T., Kajita, R., Miyazaki, A., Hokoyama, M., Nakamura-Miura, T., Mizuno, S., Masuda, Y., Irie, K., Tanaka, Y., Takada, S. Kakimoto, T. & Sakagami, Y. 2010. Stomatal density is controlled by a mesophyll-derived signaling molecule. *Plant & cell physiology*, 51(1), pp. 1-8.

Kovermann, P., Stefan Meyer, S., Hortensteiner, S., Picco, C., Scholz-Starke, J., Ravera, S., Lee, Y. & Enrico Martinoia, E. 2007. The Arabidopsis vacuolar malate channel is a member of the ALMT family. *The Plant journal: for cell and molecular biology*, 52(6), pp. 1169-80.

Kubo, A., Aono, M., Nakajima, N., Saji, H., Tanaka, K. & Kondo, N. 1999. Differential Responses in Activity of Antioxidant Enzymes to Different Environmental Stresses in Arabidopsis thaliana. *Journal of Plant Research*, 112(3), pp. 279-290.

Kwak, J. M., Murata, Y., Baizabal-Aguirre, V. M., Merrill, J., Wang, M., Kemper, A., Hawke, S. D., Tallman, G., & Schroeder, J. I. 2001. Dominant Negative Guard Cell K⁺ Channel Mutants Reduce Inward-Rectifying K⁺ Currents and Light-Induced Stomatal Opening in Arabidopsis 1. *Plant physiology*, 127, pp. 473-485.

Lake, J. A., Quick, W. P., Beerling, D. J., Woodward, F. I. 2001. Signals from mature to new leaves. *Nature*, 411, pp. 193-203

Lampard, G. R., Lukowitz, W., Ellis, B. E. & Bergmann, D. C. 2009. Novel and expanded roles for MAPK signaling in Arabidopsis stomatal cell fate revealed by cell type-specific manipulations. *The Plant cell*, 21(11), pp. 3506-17.

Lampard, G. R., Macalister, C. A. & Bergmann, D. C. 2008. Arabidopsis stomatal initiation is controlled by MAPK-mediated regulation of the bHLH SPEECHLESS. *Science*, 322(November), pp. 1113-1116.

Lau, O-S, Davies, K. A., Chang, J., Adrian, J., Rowe, M. H., Ballenger, C. H. & Bergmann, D. C. 2014. Direct roles of SPEECHLESS in the specification of stomatal self-renewing cells. *Science*, 345, pp. 1605-09.

Lawson, T. 2009. Guard cell photosynthesis and stomatal function. *The New phytologist*, 181(1), pp. 13-34.

Lawson, T. & Blatt, M.R. 2014. Stomatal size, speed, and responsiveness impact on photosynthesis and water use efficiency. *Plant physiology*, 164(4), pp. 1556-70.

Lee, J. S., Kuroha, T., Hnilova, M., Khatayevich, D., Kanaoka, M. M., McAbee, J. M., Sarikaya, M., Tamerler, C. & Torii, K. U. 2012. Direct interaction of ligand-receptor pairs specifying stomatal patterning. *Genes & development*, 26(2), pp. 126-36.

Lee, S. C. & Luan, S. 2012. ABA signal transduction at the crossroad of biotic and abiotic stress responses. *Plant, cell & environment*, 35(1), pp. 53-60.

Leung, J., Merlot, S. & Giraudat, J. 1997. The Arabidopsis ABSCISIC ACID-INSENSITIVE2 (AB12) and ABI1 Genes Encode Homologous Protein Phosphatases 2C Involved in Abscisic Acid Signal Transduction. *The Plant cell*, 9(May), pp. 759-771.

Leonhardt, N., Vavasseur, a & Forestier, C. 1999a. ATP binding cassette modulators control abscisic acid-regulated slow anion channels in guard cells. *The Plant cell*, 11(6), pp.1141-52.

Leonhardt, N., Vavasseur, a & Forestier, C. 1999b. ATP binding cassette modulators control abscisic acid-regulated slow anion channels in guard cells. *The Plant cell*, 11(6), pp.1141-52.

Li, W., Luan, S., Schreiber, S. L. & Assmann, S. M. 1994. Evidence for protein phosphatase 1 and 2A regulation of K⁺ channels in two types of leaf cells. *Plant physiology*, 106(3), pp. 963-70.

Li, L., Whiteman, M., Guan, Y. Y., Neo, K. L., Cheng, Y., Lee, S. W., Zhao, Y., Baskar, R., Tan, C. H. & Moore, P. K. 2008. Characterization of a novel, water-soluble hydrogen sulfide-releasing molecule (GYY4137): new insights into the biology of hydrogen sulfide. *Circulation*, 117(18), pp. 2351-60.

Li, Q. & Lancaster, J. R. 2013. Chemical foundations of hydrogen sulfide biology. *Nitric oxide: biology and chemistry / official journal of the Nitric Oxide Society*, 35, pp. 21-34.

Lisjak, M., Srivastava, N., Teklic, T., Civale, L., Lewandowski, K., Wilson, I., Woodc, M. E., Whitemand, M. & Hancock, J. T. 2010. A novel hydrogen sulfide donor causes stomatal opening and reduces nitric oxide accumulation. *Plant physiology and biochemistry: PPB / Société française de physiologie végétale*, 48(12), pp. 931-5.

- Lisjak, M., Teklic, T., Wilson, I. D., Wood, M. E., Whiteman, M. & Hancock, J. T. 2011. Hydrogen sulfide effects on stomatal apertures. *Plant signaling & behavior*, 6(10), pp. 1444-1446.
- Liu, F., Yoo, B. C., Lee, J. Y., Pan, W. & Harmon, A. C. 2006. Calcium-regulated phosphorylation of soybean serine acetyltransferase in response to oxidative stress. *The Journal of biological chemistry*, 281(37), pp. 27405-15.
- López-Bucio, J., Cruz-Ramírez, A. & Herrera-Estrella, L., 2003. The role of nutrient availability in regulating root architecture. *Current Opinion in Plant Biology*, 6(3), pp. 280-287.
- Losch, R., Tenhunen, J. D., Pereira, J. S. & Lange, O. L. 1978. Diurnal courses of stomatal resistance and transpiration of wild and cultivated Mediterranean perennials at the end of summer dry season in Portugal. *Flora*, 172, pp. 138-160.
- Luan, S., Li, W., Rusnak, F., Assmann, S. M. & Schreiber, S. L. 1993. Immunosuppressants implicate protein phosphatase regulation of K⁺ channels in guard cells. *Proceedings of the National Academy of Sciences of the United States of America*, 90(6), pp. 2202-6.
- MacAlister, C., Ohashi-Ito, K. & Bergmann, D. C., 2007. Transcription factor control of asymmetric cell divisions that establish the stomatal lineage. *Nature*, 445(7127), pp. 537-40.
- Macgregor, D. R., Deak, K. I., Ingram, P. A. & Malamy, J. E. 2008. Root system architecture in Arabidopsis grown in culture is regulated by sucrose uptake in the aerial tissues. *The Plant cell*, 20(10), pp. 2643-60.
- MacRobbie, E. 1998. Signal transduction and ion channels in guard cells. *Philosophical transactions of the Royal Society of London. Series B, Biological sciences*, 353(1374), pp. 1475-88.
- Malamy, J. E. 2005. Intrinsic and environmental response pathways that regulate root system architecture. *Plant, cell & environment*, 28(1), pp. 67-77.
- Marshall, E., Costa, L. M. & Gutierrez-Marcos, J. 2011. Cysteine-rich peptides (CRPs) mediate diverse aspects of cell-cell communication in plant reproduction and development. *Journal of experimental botany*, 62(5), pp. 1677-86.
- McAdam, S. M. & Brodribb, T. J. 2014. Separating Active and Passive Influences on Stomatal Control of Transpiration. *Plant physiology*, 164(4), pp. 1578-86.
- McAusland, L., Davey, P. A., Kanwal, N., Baker, N. R. & Lawson, T. 2013. A novel system for spatial and temporal imaging of intrinsic plant water use efficiency. *Journal of experimental botany*, 64(16), pp. 4993-5007.
- McAinsh, M. R., Brownlee, C. & Hetherington, A. M. 1990. Abscisic acid-induced elevation of guard cell cytosolic Ca²⁺ precedes stomatal closure. *Nature*, 343, pp. 186-188.

Medrano, H. 2002. Regulation of Photosynthesis of C3 Plants in Response to Progressive Drought: Stomatal Conductance as a Reference Parameter. *Annals of Botany*, 89(7), pp. 895-905.

Meidner, H. 1990. The Absorption Lag , Epidermal Turgor and Stomata. *Journal of Experimental Botany*, 41, pp. 1115-1118.

Melcher, K., Ng, L. M., Zhou, X. E., Soon, F. F., Xu, Y., Suino-Powell, K. M., Park, S. Y., Weiner, J. J., Fuji, H., Chinnusamy, V., Kovach, A., Li, J., Wang, Y., Li, J., Peterson, F. C., Jensen, D. R., Yong, E. L., Volkman, B. F., Cutler, S. R., Zhu, J. K. & Xu, H. E. 2009. A gate-latch-lock mechanism for hormone signalling by abscisic acid receptors. *Nature*, 462(7273), pp. 602-8.

Meyer, S., Mumm, P., Imes, D., Endler, A., Weder, B., Al-Rasheid, K. A. S., Geiger, D., Marten, I., Martinoia, E. & Hedrich, R. 2010. AtALMT12 represents an R-type anion channel required for stomatal movement in Arabidopsis guard cells. *The Plant journal : for cell and molecular biology*, 63(6), pp. 1054-62.

Meyer, S., Scholz-Starke, J., De Angeli, A., Kovermann, P., Burla, B., Gambale, F. & Martinoia, E. 2011. Malate transport by the vacuolar AtALMT6 channel in guard cells is subject to multiple regulation. *The Plant journal : for cell and molecular biology*, 67(2), pp. 247-57.

Mori, I. C. & Murata, Y. 2011. ABA signaling in stomatal guard cells: lessons from Commelina and Vicia. *Journal of plant research*, 124(4), pp. 477-87.

Mott, K. A. & Buckley, T. N. 1998. Stomatal heterogeneity. *Journal of experimental botany*, 49, pp. 407-417.

Mott, K. A., Shope, J. C. & Buckley, T. N. 1999. Effects of humidity on light-induced stomatal opening: evidence for hydraulic coupling among stomata. *Journal of Experimental Botany*, 50(336), pp. 1207-1213.

Mott, K. A. & Buckley, T. N. 2000. Patchy stomatal conductance: emergent collective behaviour of stomata. *Trends in plant science*, 5(6), pp. 258-62.

Mueller, N. D., Gerber, J. S., Johnston, M., Ray, D. K., Ramankutty, N. & Foley, J. A. 2012. Closing yield gaps through nutrient and water management. *Nature*, 490(7419), pp. 254-7.

Muller, M. & Schmidt, W. 2004. Environmentally Induced Plasticity of Root Hair Development in Arabidopsis 1. *Plant physiology*, 134, pp.409-419.

Mustafa, A. K., Gadalla, M. M. Sen, N., Kim, S., Mu, W., Gazi, S. K., Barrow, R. K., Yang, G., Wang, R., & Snyder, S. H. 2009. H2S signals through protein S-sulfhydration. *Science signaling*, 2(96), p.ra72.

Mustilli, A., Merlot, S., Vavasseur, A., Fenzi, F. & Giraudat, J. 2002. Arabidopsis OST1 Protein Kinase Mediates the Regulation of Stomatal Aperture by Abscisic

- Acid and Acts Upstream of Reactive Oxygen Species Production. *The Plant cell*, 14(December), pp. 3089-3099.
- Nadeau, J. A. & Sack, F. D. 2002. Control of stomatal distribution on the Arabidopsis leaf surface. *Science (New York, N.Y.)*, 296(5573), pp. 1697-700.
- Nebauer . 1967. Bemerkungen uber den Bau der Begoniaceen. Ber. Deutch Bot. Ges., 80, pp 80-97.
- Negi, J., Matsuda, O., Nagasawa, T., Oba, Y., Takahashi, H., Kawai-Yamada, M., Uchimiya, H., Hashimoto, M. & Iba, K. 2008. CO₂ regulator SLAC1 and its homologues are essential for anion homeostasis in plant cells. *Nature*, 452(7186), pp. 483-6.
- Neill, S. J., Desikan, R., Clarke, A. & Hancock, J. T. 2002. Nitric Oxide Is a Novel Component of Abscisic Acid Signaling in Stomatal Guard Cells. *Plant Physiology*, 128(January), pp. 13-16.
- Neill, S. J., Desikan, R. & Hancock, J. T. 2003. Nitric oxide signalling in plants. *New Phytologist*, 159(1), pp. 11-35.
- Nishimura, N., Sarkeshik, A., Nito, K., Park, S. Y., Wang, A., Carvalho, P. C., Lee, S. Caddell, D. F., Cutler, S. R., Chory, J., Yates, J. R. & Schroeder, J. I. 2010. PYR/PYL/RCAR family members are major in-vivo ABI1 protein phosphatase 2C-interacting proteins in Arabidopsis. *The Plant journal : for cell and molecular biology*, 61(2), pp. 290-9.
- Niu, Y. F., Chai, R. S., Jin, G. L., Wang, H., Tang, C. X. & Zhang, Y. S. 2013. Responses of root architecture development to low phosphorus availability: a review. *Annals of botany*, 112(2), pp. 391-408.
- Ohashi-Ito, K. & Bergmann, D. C. 2006. Arabidopsis FAMA controls the final proliferation/differentiation switch during stomatal development. *The Plant cell*, 18(10), pp. 2493-505.
- Ortega, J. A, Ortega, J. M. & Julian, D. 2008. Hypotaurine and sulfhydryl-containing antioxidants reduce H₂S toxicity in erythrocytes from a marine invertebrate. *The Journal of experimental biology*, 211(Pt 24), pp. 3816-25.
- Park, S., Fung, P., Nishimura, N., Jensen, D. R., Fujii, H., Zhao, Y., Lumba, S., Santiago, J., Rodrigues, A., Chow, T. F., Alfred, S. E., Bonetta, D., Finkelstein, R., Provart, N. J., Desveaux, D., Rodriguez, P. L., McCourt, P., Zhu, J. K., Schroeder, J. I., Volkman, B. F. & Cutler, S. R. 2009. Abscisic Acid Inhibits Type 2C protein phosphatase via the PYR/PYL family of START proteins. *Science*, 1068, pp. 1068-1071.
- Pearce, G., Moura, D. S., Stratmann, J. & Ryan Jr., C. A. 2001. RALF, a 5-kDa ubiquitous polypeptide in plants, arrests root growth and development. *Proceedings of the National Academy of Sciences*, 98(22), pp. 12843-12847.

- Peers, C., Bauer, C., Boyle, J. P., Scragg, J. L. & Dallas, M. L. 2012. Modulation of ion channels by hydrogen sulfide. *Antioxidants & redox signaling*, 17(1), pp. 95-105.
- Pei, Z. M., Ward, J. M., Harper, J. E. & Schroeder, J. I. 1996. A novel chloride channel in *Vicia faba* guard cell vacuoles activated by the serine/threonine kinase, CDPK. *The EMBO journal*, 15(23), pp. 6564-74.
- Pei, Z. M., Murata, Y., Benning, G., Thomine, S., Klusener, B. 2000. Calcium channels activated by hydrogen peroxide mediate abscisic acid signalling in guard cells. *Nature*, 406(6797), pp. 731-4.
- Peterson, K. M., Rychel, A. L. & Torii, K. U. 2010. Out of the mouths of plants: the molecular basis of the evolution and diversity of stomatal development. *The Plant cell*, 22(2), pp. 296-306.
- Pillitteri, L. J., Daniel B. Sloan, D. B., Bogenschutz, N. L. & Torii, K. U. 2007. Termination of asymmetric cell division and differentiation of stomata. *Nature*, 445(7127), pp. 501-5.
- Pillitteri, L. J. & Dong, J. 2013. Stomatal development in Arabidopsis. *The Arabidopsis book / American Society of Plant Biologists*, 11(12), p.e 0162.
- Pillitteri, L. J. & Torii, K. U. 2012. Mechanisms of stomatal development. *Annual review of plant biology*, 63, pp. 591-614.
- Pilot, G., Pratelli, R., Gaymard, F., Meyer, Y. & Sentenac, H. 2003. Five-group distribution of the Shaker-like K⁺ channel family in higher plants. *Journal of molecular evolution*, 56(4), pp. 418-34.
- Puli, M. R. & Raghavendra, A. S. 2012. Pyrabactin, an ABA agonist, induced stomatal closure and changes in signalling components of guard cells in abaxial epidermis of *Pisum sativum*. *Journal of experimental botany*, 63(3), pp. 1349-56.
- Quarrie, S. A. & Jones, H. G. 1977. Effects of Abscisic Acid and Water Stress on Development and Morphology of Wheat. *Journal of experimental botany*, 28(102), pp. 192-203.
- Raschke, K. & Fellows, M. P. 1971. Stomatal movement in *Zea mays*: Shuttle of potassium and chloride between guard cells and subsidiary cells. *Planta*, 101(4), pp. 296-316.
- Rennenberg, H. 1983. Role of o-acetylserine in hydrogen sulfide emission from pumpkin leaves in response to sulfate. *Plant physiology*, 73(3), pp. 560-5.
- Riemenschneider, A. et al., 2005. Isolation and characterization of a D-cysteine desulphydrase protein from *Arabidopsis thaliana*. *The FEBS journal*, 272(5), pp. 1291-304.
- Rodriguez, M. C. S., Petersen, M. & Mundy, J. 2010. Mitogen-activated protein kinase signaling in plants. *Annual review of plant biology*, 61, pp. 621-49.

- Roelfsema, M. R. G. & Hedrich, R. 2005. In the light of stomatal opening: new insights into “the Watergate”. *The New phytologist*, 167(3), pp. 665-91.
- Roelfsema, M. R. G., Hedrich, R. & Geiger, D. 2012. Anion channels: master switches of stress responses. *Trends in plant science*, 17(4), pp. 221-9.
- Sack, F. D. 2004. Plant sciences. Yoda would be proud: valves for land plants. *Science (New York, N.Y.)*, 304(5676), pp. 1461-2.
- Sánchez-Calderón, L., López-Bucio, J., Chacón-López, A., Cruz-Ramírez, A., Nieto-Jacobo, F., Dubrovsky, J. G. & Herrera-Estrella, L. 2005. Phosphate starvation induces a determinate developmental program in the roots of *Arabidopsis thaliana*. *Plant & cell physiology*, 46(1), pp. 174-84.
- Schluter, U., Muschak, M., Berger, D. & Altmann, T. 2003. Photosynthetic performance of an *Arabidopsis* mutant with elevated stomatal density (sdd1-1) under different light regimes. *Journal of Experimental Botany*, 54(383), pp. 867-874.
- Schroeder, J. I. & Hagiwara, S. 1989. Cytotoxic calcium regulates ion channels in the plasma membrane of *Vicia faba* guard cells. *Nature*, 338, pp. 427-430.
- Schroeder, J. I., Hedrich, R. & Fernandez, J. M. 1984. Potassium-selective single channels in guard cell protoplasts of *Vicia faba*. *Nature*, 312, pp. 361-362.
- Schroeder, J. I. & Hagiwara, S. 1989. Cytotoxic calcium regulates ion channels in the plasma membrane of *Vicia faba* guard cells. *Nature*, 338, pp. 427-430.
- Schroeder, J. I. & Keller, B. U. 1992. Two types of anion channel currents in guard cells with distinct voltage regulation. *Proceedings of the National Academy of Sciences of the United States of America*, 89(11), pp. 5025-9.
- Schmidt, C., Schelle, I., Liao, Y. J. & Schroeder, J. I. 1995. Strong regulation of slow anion channels and abscisic acid signaling in guard cells by phosphorylation and dephosphorylation events. *Proceedings of the National Academy of Sciences of the United States of America*, 92(21), pp. 9535-9.
- Schwartz, A., Wut, W. H., Tucker, E. B. & Assmann, S. M. 1994. Inhibition of inward K⁺ channels and stomatal response by abscisic acid: an intracellular locus of phytohormone action. *Proceedings of the National Academy of Sciences of the United States of America*, 91(9), pp. 4019-23.
- Serna, L. 2004. A network of interacting factors triggering different cell fates. *The Plant cell*, 16(9), pp. 2258-63.
- Shimazaki, K., Doi, M., Assmann, S. M. & Kinoshita, T. 2007. Light regulation of stomatal movement. *Annual review of plant biology*, 58, pp. 219-47.
- Shpak, E. D., McAbee, J. M., Pillitteri, L. J. & Torii, K. U. 2005. Stomatal patterning and differentiation by synergistic interactions of receptor kinases. *Science*, 309(5732), pp. 290-3.

Siegel, R. S., Xue, S., Murata, Y., Yang, Y., Nishimura, N., Wang, A. & Schroeder, J. I. 2009. Calcium elevation-dependent and attenuated resting calcium-dependent abscisic acid induction of stomatal closure and abscisic acid-induced enhancement of calcium sensitivities of S-type anion and inward-rectifying K channels in Arabidopsis guard cells. *The Plant journal : for cell and molecular biology*, 59(2), pp. 207-20.

Smith, S. & De Smet, I. 2012. Root system architecture: insights from Arabidopsis and cereal crops. *Philosophical transactions of the Royal Society of London. Series B, Biological sciences*, 367(1595), pp. 1441-52.

Song, X.-G., She, X.-P. & Zhang, B. 2008. Carbon monoxide-induced stomatal closure in *Vicia faba* is dependent on nitric oxide synthesis. *Physiologia plantarum*, 132(4), pp. 514-25.

Spalding, E. P., Hirsch, R. E., Lewis, D. R., Qi, Z., Sussman, M. R. & Lewis, B. D. 1999. Potassium uptake supporting plant growth in the absence of AKT1 channel activity: Inhibition by ammonium and stimulation by sodium. *The Journal of general physiology*, 113(6), pp. 909-18.

Srivastava, R., Liu, J. X. Guo, H., Yin, Y. & Howell, S. H. 2009. Regulation and processing of a plant peptide hormone, AtRALF23, in Arabidopsis. *The Plant journal : for cell and molecular biology*, 59(6), pp. 930-9.

Sugano, S. S., Shimada, T., Imai, Y., Okawa, K., Tamai, A., Mori, M. & Hara-Nishimura, I. 2010. Stomagen positively regulates stomatal density in Arabidopsis. *Nature*, 463(7278), pp. 241-4.

Suh, S. J., Wang, Y. F., Frelet, A. Leonhardt, N., Klein, M., Forestier, C., Mueller-Roeber, B., Cho, M. H., Martinoia, E. & Schroeder, J. I. 2007. The ATP binding cassette transporter AtMRP5 modulates anion and calcium channel activities in Arabidopsis guard cells. *The Journal of biological chemistry*, 282(3), pp. 1916-24.

Sullivan, S., Thomson, C. E., Kaiserli, E. & Christie, J. M. 2009. Interaction specificity of Arabidopsis 14-3-3 proteins with phototropin receptor kinases. *FEBS letters*, 583(13), pp. 2187-93.

Sutter, J. U., Sieben, C., Hartel, A., Eisenach, C., Gerhard Thiel, G. & Blatt, M. R. 2007. Abscisic acid triggers the endocytosis of the arabidopsis KAT1 K⁺ channel and its recycling to the plasma membrane. *Current biology : CB*, 17(16), pp. 1396-402.

Taiz, L. & Zieger, E. 2010. Plant physiology, University of California, 3rd edition, California, USA.

Tanaka, Y., Sugano, S. S., Shimada, T. & Hara-Nishimura, I. 2013. Enhancement of leaf photosynthetic capacity through increased stomatal density in Arabidopsis. *The New phytologist*, 198(3), pp. 757-64.

- Tang, M., Hu, Y. X., Lin, J. X., Jin, X. B. 2002. Developmental mechanism and distribution pattern of stomatal clusters in *Begonia peltatifolia*. *Acta Botanica Sinica*, 44(4), pp. 384-390.
- Tardieu, F., Reymond, M., Hamard, P., Granier, C., & Muller, B. 2000. Spatial distributions of expansion rate, cell division rate and cell size in maize leaves: a synthesis of the effects of soil water status, evaporative demand and temperature. *Journal of experimental botany*, 51(350), pp. 1505-14.
- Tardieu, F., Parent, B., Caldeira, C. F. & Welcker, C. 2014. Genetic and physiological controls of growth under water deficit. *Plant physiology*, 164(4), pp. 1628-35.
- Tebitt, M. C. 2005. *Begonias: Cultivation, Identification and Natural history*. Oregon Timber Press, Portland, USA
- Tenhunen, J. D., Lange, O. L., Gebel, J., Beyschlag, W. & Weber, J. A. 1984. Changes in photosynthetic capacity, carboxylation efficiency, and CO₂ compensation point associated with midday stomatal closure and midday depression of net CO₂ exchange of leaves of *Quercus suber*. *Planta*, 162, pp. 193-203.
- Thiel, G. & Blattt, M. R. 1994. Phosphatase antagonist okadaic acid inhibits steady-state K⁺ currents in guard cells of *Vicia faba*. , 5(January), pp. 727-733.
- Ting, I. P. & Loomis, W. E. 1963. Diffusion through stomates. *American journal of botany*, 50(9), pp. 866-872.
- Ting, I. P. & Loomis, W. E. 1965. Further Studies Concerning Stomatal Diffusion. *Plant physiology*, 40(2), pp. 220-8.
- Torii, K. U., 2012. Mix-and-match: ligand-receptor pairs in stomatal development and beyond. *Trends in plant science*, 17(12), pp. 711-9.
- Torii, K. U., Mitsukawa, N., Oosumi, T., Matsuura, Y., Yokoyama, R., Whittier, R. F., Komeda, Y. 1996. The Arabidopsis ERECTA gene encodes a putative receptor protein kinase with extracellular leucine-rich repeats. *The Plant cell*, 8(4), pp. 735-46.
- Umbrasaitė, J., Schweighofer, A., Kazanaviciute, V., Magyar, Z., Ayatollah, Z., Unterwurzacher, V., Choopayak, C., Boniecka, J., Murray, J. A. H., Bogre, L. & Meskiene, I. 2010. MAPK phosphatase AP2C3 induces ectopic proliferation of epidermal cells leading to stomata development in Arabidopsis. *PLoS one*, 5(12), p.e 15357.
- Vahisalu, T., Kollist, H., Wang, Y. F., Nishimura, N., Chan, W. Y., Valerio, G., Lamminmaki, A., Brosche, M., Moldau, H., Desikan, R., Schroeder, J. I. & Kangasjarvi, J. 2008. SLAC1 is required for plant guard cell S-type anion channel function in stomatal signalling. *Nature*, 452(7186), pp. 487-91.

Vartanian, N., Marcotte, L. & Giraudat, J. 1994. Drought Rhizogenesis in *Arabidopsis thaliana* (Differential Responses of Hormonal Mutants). *Plant physiology*, 104(2), pp. 761-767.

Vlad, F., Rubio, S., Rodrigues, A., Sirichandra, C., Belin, C., Robert, N., Leung, J., Rodriguez, P. L., Lauriere, C. & Merlot, S. 2009. Protein phosphatases 2C regulate the activation of the Snf1-related kinase OST1 by abscisic acid in *Arabidopsis*. *The Plant cell*, 21(10), pp. 3170-84.

Wang, H., Ngwenyama, N., Liu, Y., Walker, J. C. & Zhang, S. 2007. Stomatal development and patterning are regulated by environmentally responsive mitogen-activated protein kinases in *Arabidopsis*. *The Plant cell*, 19(1), pp. 63-73.

Wang, R., 2002. Two's company, three's a crowd: can H₂S be the third endogenous gaseous transmitter? *FASEB journal: official publication of the Federation of American Societies for Experimental Biology*, 16(13), pp. 1792-8.

Wang, Y. & Blatt, M. R. 2011. Anion channel sensitivity to cytosolic organic acids implicates a central role for oxaloacetate in integrating ion flux with metabolism in stomatal guard cells. *The Biochemical journal*, 439(1), pp. 161-70.

Wang, Y., Papanatsiou, M., Eisenach, C., Karnik, R., Williams, M., Hills, A., Lew, V. L. & Blatt, M. R. 2012. Systems dynamic modeling of a guard cell Cl⁻ channel mutant uncovers an emergent homeostatic network regulating stomatal transpiration. *Plant physiology*, 160(4), pp. 1956-67.

Wang, Y., Noguchi, K., Ono, N., Inoue, S., Terashima, I. & Kinoshita, T. 2014. Overexpression of plasma membrane H⁺-ATPase in guard cells promotes light-induced stomatal opening and enhances plant growth. *Proceedings of the National Academy of Sciences of the United States of America*, 111 (1), pp. 533-38.

West, J. D., Peak, D., Peterson, J. Q., MOTT, K. A. 2005. Dynamics of stomatal patches for a single surface of *Xanthium strumarium* L. leaves observed with fluorescence and thermal images. *Plant, Cell and Environment*, 28(5), pp. 633-641.

Williamson, L. C., Ribrioux, S. P. C. P., Fitter, A. H. & Leyser, O. H. M. 2001. Phosphate availability regulates root system architecture in *Arabidopsis*. *Plant physiology*, 126(2), pp. 875-82.

Wilkinson, S. & Davies, W. J. 2002. ABA-based chemical signalling: the coordination of. *Plant cell environment*, 25, pp. 195-210.

Willmer, C. M. 1988. Stomatal sensing of the environment. *Biological journal of the Linnean society*, 34, pp. 205-217.

Willmer, C. M. & Fricker, M. 1996, *Stomata*, 2nd edition, Chapman & Hall, London, UK

- Wilson, L. G., Bressan, R. a & Filner, P. 1978. Light-dependent Emission of Hydrogen Sulfide from Plants. *Plant physiology*, 61(2), pp. 184-9.
- Woodward, F. I. & Kelly, C. K. 1995. The influence of CO₂ concentration on stomatal density. *New Phytologist*, 131, pp. 311-327.
- Woodward, F. I., Lake, J. A. & Quick, W. P. 2002. Stomatal development and CO₂: ecological consequences. *New Phytologist*, 153(3), pp. 477-484.
- Yang, M. & Sack, F. D. 1995. The too many mouths and four lips mutations affect stomatal production in Arabidopsis. *The Plant cell*, 7(12), pp. 2227-39.
- Yoo, C. Y., Pence, H. E., Hasegawa, P. M. & Mickelbart, M. V. 2009. Regulation of Transpiration to Improve Crop Water Use. *Critical Reviews in Plant Sciences*, 28(6), pp. 410-431.
- Yoo, C. Y., Pence, H. E., Jin, B., Miura, K., Gosney, M. J., Hasegawa, P. M. & Mickelbart, M. V. 2010. The Arabidopsis GTL1 transcription factor regulates water use efficiency and drought tolerance by modulating stomatal density via transrepression of SDD1. *The Plant cell*, 22(12), pp. 4128-41.
- Zeiger, E., Assmann, S. M. & Meioner, H. 1983. RESEARCH NOTE THE PHOTOBIOLOGY OF Paphiopedilum STOMATA: OPENING UNDER BLUE BUT NOT RED LIGHT. *Photochemistry and Photobiology*, 38(5), pp. 627-630.
- Zhang, H., Ye, Y. K., Wang, S. H., Luo, J. P., Tang, J. & Ma, D. F. 2009. Hydrogen sulfide counteracts chlorophyll loss in sweetpotato seedling leaves and alleviates oxidative damage against osmotic stress. *Plant Growth Regulation*, 58(3), pp. 243-250.
- Zhang, H., Wang, M. J., Hua, L. Y., Wang, S. H., Hua, K. D., Bao, L. J. & Luo, J. P. 2010a. Hydrogen sulfide promotes wheat seed germination under osmotic stress. *Russian Journal of Plant Physiology*, 57(4), pp. 532-539.
- Zhang, H., Jiao, H., Jiang, C. X., Wang, S. H., Wei, Z. J., Luo, J. P. & Jones, R. L. 2010b. Hydrogen sulfide protects soybean seedlings against drought-induced oxidative stress. *Acta Physiologiae Plantarum*, 32(5), pp. 849-857.
- Zhang, H., Dou, W., et al., 2010c. Hydrogen sulfide stimulates β -amylase activity during early stages of wheat grain germination. *Plant signaling & behavior*, 5(8), pp. 1031-3.
- Zhao, W., Zhang, J., Lu, Y. & Wang, R. 2001. The vasorelaxant effect of H₂S as a novel endogenous gaseous K(ATP) channel opener. *The EMBO journal*, 20(21), pp. 6008-16.
- Zhao, X., Yang, Y., Shen, Z., Zhang, H., Wang, G., Gan, Y. 2006. Stomatal clustering in Cinnamomum camphora. *South African Journal of Botany*, 72(4), pp. 565-569.
- Zonia, L. & Munnik, T. 2007. Life under pressure: hydrostatic pressure in cell growth and function. *Trends in plant science*, 12(3), pp. 90-7.

Appendix I

The OnGuard model was used to simulate the guard cell properties under control and H₂S conditions. For the latter, I imposed changes in the K_{IN} channels by reducing the population of channels as well as shifting the V_{1/2} of the K_{IN} channels. Here, I present the diurnal changes occurred in the voltage of plasma membrane and tonoplast upon the H₂S query (Figure 1). Also, the model predicted changes in the ion fluxes via the major K⁺ and anion transporters residing at the plasma membrane are shown in Figure 2. Importantly, the model predicted changes in the buffering properties of Ca²⁺ and pH. In particular, the changes included the altered activity of transporters mediating Ca²⁺ fluxes at the plasma membrane and tonoplast (Figure 3) as well as changes involving the major transport proteins that contribute the H⁺ load in the cytosol (Figure 4).

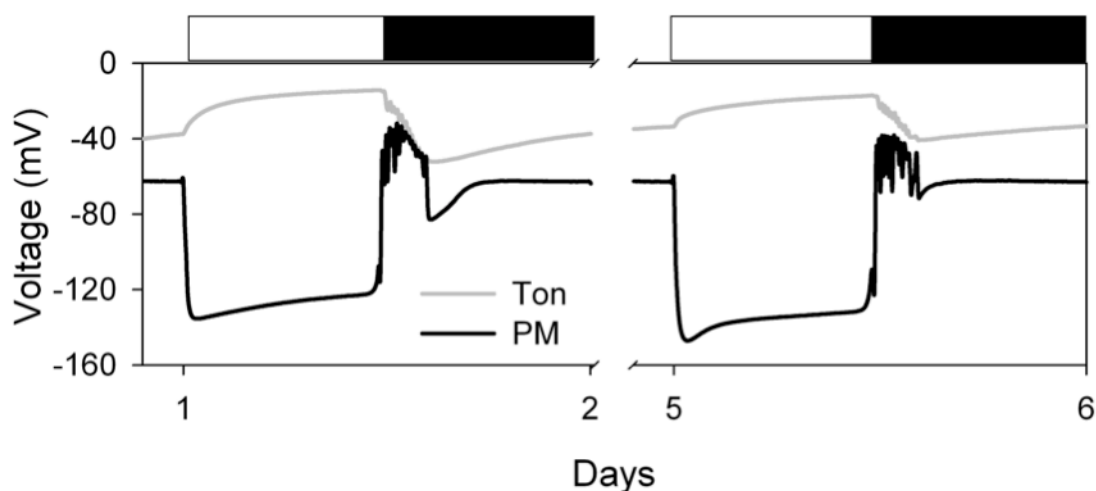


Figure 1. Quantitative modelling predicting changes in the membrane potential at the plasma membrane and tonoplast.

Outputs are derived by modelling the diurnal cycle and altering the activities of K⁺ and anion channels according to the data obtained from the above electrophysiological studies. Data represent 6-days window, with first three days corresponding to control treatment and the last three days corresponding to H₂S treatment. Only one day per treatment is shown, with day 1 (left panel) corresponding to control conditions and day 5 (right panel) to the H₂S conditions. Graph presents the changes in membrane potential of the plasma membrane (black) and tonoplast (grey).

H₂S did not cause any substantial changes in the voltage of the tonoplast throughout the diurnal cycle. The H₂S query predicted the hyperpolarisation of the plasma membrane during the daytime, while the plasma membrane voltage appeared more positive under H₂S conditions than the control. The hyperpolarization during the day can be explained by the loss of the inward current through K_{IN}.

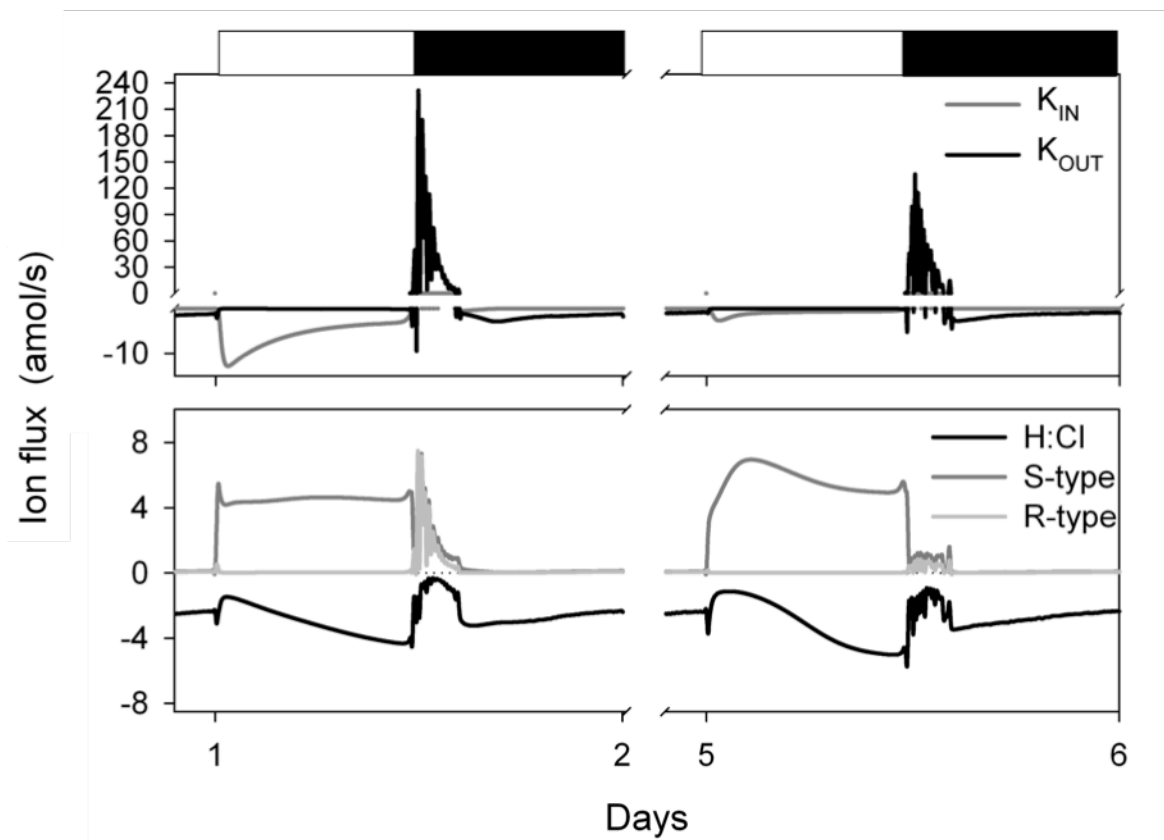


Figure 2. Quantitative modelling predicting changes in the fluxes through the K^+ and Cl^- channels at the plasma membrane.

Outputs are derived by modelling the diurnal cycle and altering the activities of K^+ and anion channels according to the data obtained from the above electrophysiological studies. Data represent 6-days window, with first three days corresponding to control treatment and the last three days corresponding to H_2S treatment. Only one day per treatment is shown, with day 1 (left panel) corresponding to control conditions and day 5 (right panel) to the H_2S conditions. Upper graph presents the diurnal changes in K^+ fluxes through the K_{IN} (black) and K_{OUT} (grey) channels. Bottom graph shows the diurnal changes in Cl^- fluxes via the H^+Cl^- symport (black), S-type (dark grey) and R-type (grey) channels. Positive values indicate the flux out of the cytosol across the plasma membrane.

The predictions are consistent with the experimental observation indicating the substantial reduction in K_{IN} current. Also, the model predicted alterations in H^+Cl^- transport and in the anion channels, despite the changes in membrane voltage.

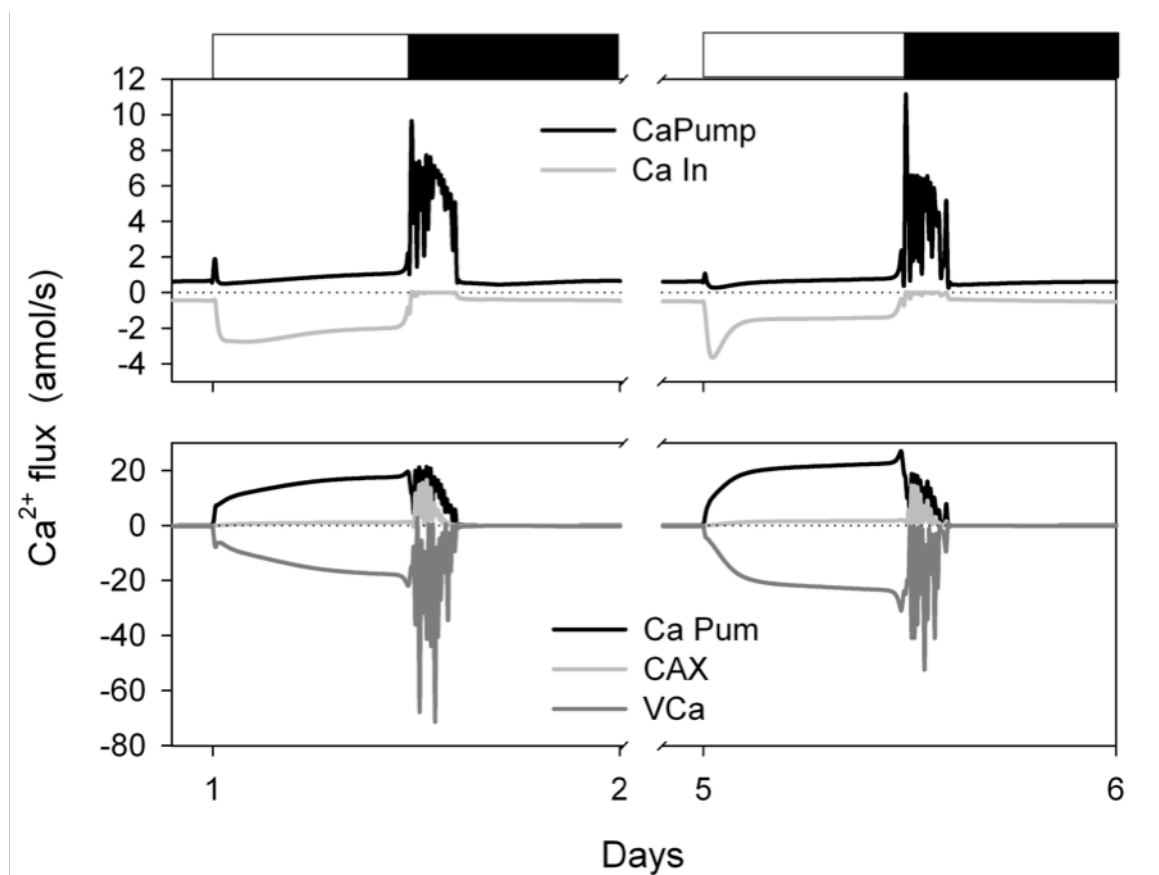


Figure 3. Quantitative modelling predicting changes in Ca^{2+} fluxes at the plasma membrane and tonoplast.

Outputs are derived by modelling the diurnal cycle and altering the activities of K^+ and anion channels according to the data obtained from the above electrophysiological studies. Data represent 6-days window, with first three days corresponding to control treatment and the last three days corresponding to H_2S treatment. Only one day per treatment is shown, with day 1 (left panel) corresponding to control conditions and day 5 (right panel) to the H_2S conditions. Upper graph presents the diurnal changes in Ca^{2+} fluxes through the Ca^{2+} -ATPase (black) and voltage-sensitive Ca^{2+} channel (grey). Bottom graph shows the diurnal changes in Ca^{2+} fluxes via the Ca^{2+} -ATPase (black), Ca^{2+} channel (dark grey) and H^+ - Ca^{2+} antiport (grey) residing at the tonoplast. Positive values indicate the flux out of the cytosol across the plasma membrane or tonoplast.

The model suggested the gating of the voltage-sensitive Ca^{2+} channels mediated by the hyperpolarisation of the plasma membrane brought by the reduction of K_{IN} . The accumulation of Ca^{2+} in the cytosol, in turn, stimulated the CAX antiport resulting in the influx of Ca^{2+} into the vacuole at the expense of the acidification of the cytosol.

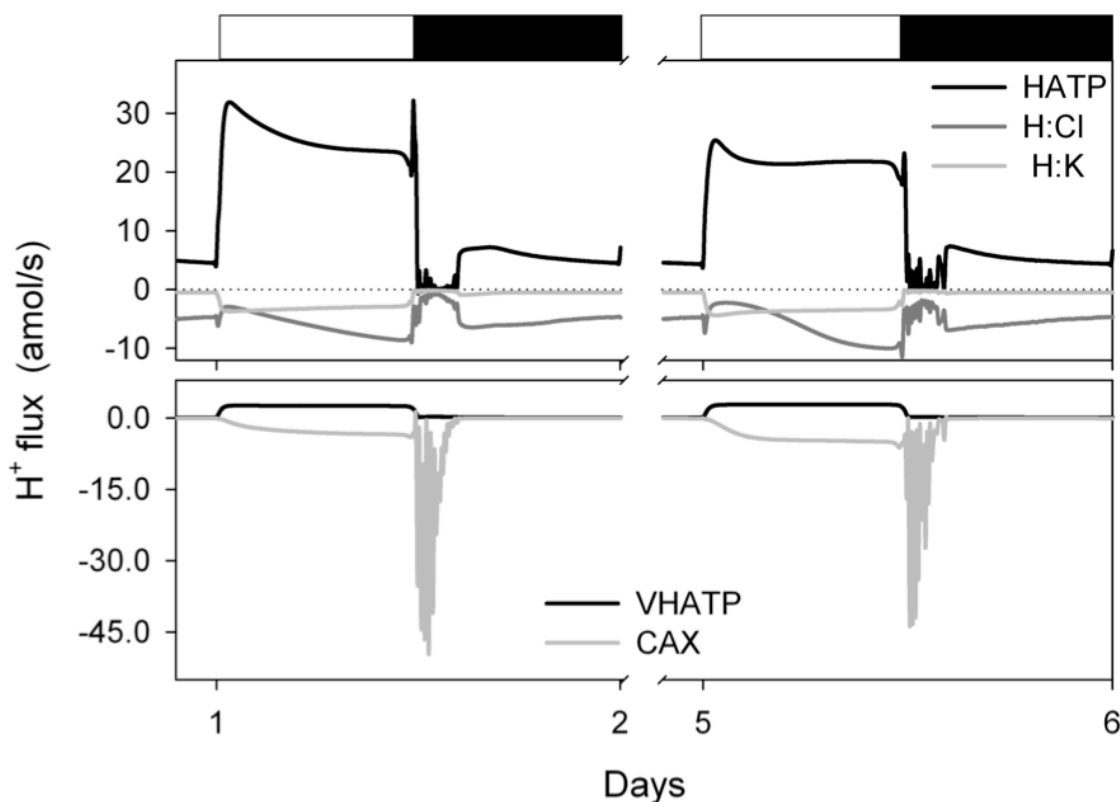


Figure 4. Quantitative modelling predicting changes in Ca^{2+} fluxes at the plasma membrane and tonoplast.

Outputs are derived by modelling the diurnal cycle and altering the activities of K^+ and anion channels according to the data obtained from the above electrophysiological studies. Data represent 6-days window, with first three days corresponding to control treatment and the last three days corresponding to H_2S treatment. Only one day per treatment is shown, with day 1 (left panel) corresponding to control conditions and day 5 (right panel) to the H_2S conditions. Upper graph presents the diurnal changes in H^+ fluxes through the H^+ -ATPase (black), $\text{H}^+\text{-Cl}^-$ symport (dark grey) and $\text{H}^+\text{-K}^+$ symport (grey). Bottom graph shows the diurnal changes in H^+ fluxes via the VH^+ -ATPase (black) and $\text{H}^+\text{-Ca}^{2+}$ antiport (grey) residing at the tonoplast. Positive values indicate the flux out of the cytosol across the plasma membrane or tonoplast.

The H_2S query predicted an increase in the H^+ load in the cytosol, which was associated with the reduced activity of H^+ -ATPase and with the increased activity of the $\text{H}^+\text{-Cl}^-$ symport protein. Additionally the high accumulation of Ca^{2+} (as indicated above) stimulated the CAX tonoplast transporter, further contributing to the acidification of the cytosol.

Appendix II

The following manuscripts were not part of the PhD project. However, I contributed to both manuscripts by carrying out experiments related to gas exchange and confocal microscopy that allow me to get familiar with the techniques used for my project.

Manuscript

Systems Dynamic Modeling of a Guard Cell Cl⁻ Channel Mutant Uncovers an Emergent Homeostatic Network Regulating Stomatal Transpiration

Authors

Yizhou Wang, Maria Papanatsiou, Cornelia Eisenach, Rucha Karnik, Mary Williams, Adrian Hills, Virgilio L. Lew, and Michael R. Blatt

Laboratory of Plant Physiology and Biophysics, Institute of Molecular, Cell, and Systems Biology, University of Glasgow, Glasgow G12 8QQ, United Kingdom (Y.W., M.P., C.E., R.K., M.W., A.H., M.R.B.); American Society of Plant Biologists, Rockville, Maryland 20855 (M.W.); Physiological Laboratory, University of Cambridge, Cambridge CB2 3EG, United Kingdom (V.L.L.)

Published to Plant Physiology, December 2012, Vol. 160, pp. 1956-1967

Manuscript

Clustering of the K⁺ channel GORK of *Arabidopsis* parallels its gating by extracellular K⁺

Authors

Cornelia Eisenach, Maria Papanatsiou, Ellin-Kristina Hillert and Michael R. Blatt

Laboratory of Plant Physiology and Biophysics, Institute of Molecular, Cell, and Systems Biology, University of Glasgow, Glasgow G12 8QQ, United Kingdom

Published to The Plant Journal, February 2014, Vol. 78, pp. 203-214

Systems Dynamic Modeling of a Guard Cell Cl^- Channel Mutant Uncovers an Emergent Homeostatic Network Regulating Stomatal Transpiration¹[W][OA]

Yizhou Wang, Maria Papanatsiou, Cornelia Eisenach, Rucha Karnik, Mary Williams, Adrian Hills, Virgilio L. Lew, and Michael R. Blatt*

Laboratory of Plant Physiology and Biophysics, Institute of Molecular, Cell, and Systems Biology, University of Glasgow, Glasgow G12 8QQ, United Kingdom (Y.W., M.P., C.E., R.K., M.W., A.H., M.R.B.); American Society of Plant Biologists, Rockville, Maryland 20855 (M.W.); and Physiological Laboratory, University of Cambridge, Cambridge CB2 3EG, United Kingdom (V.L.L.)

Stomata account for much of the 70% of global water usage associated with agriculture and have a profound impact on the water and carbon cycles of the world. Stomata have long been modeled mathematically, but until now, no systems analysis of a plant cell has yielded detail sufficient to guide phenotypic and mutational analysis. Here, we demonstrate the predictive power of a systems dynamic model in *Arabidopsis* (*Arabidopsis thaliana*) to explain the paradoxical suppression of channels that facilitate K^+ uptake, slowing stomatal opening, by mutation of the *SLAC1* anion channel, which mediates solute loss for closure. The model showed how anion accumulation in the mutant suppressed the H^+ load on the cytosol and promoted Ca^{2+} influx to elevate cytosolic pH (pH_i) and free cytosolic Ca^{2+} concentration ($[\text{Ca}^{2+}]_i$), in turn regulating the K^+ channels. We have confirmed these predictions, measuring pH_i and $[\text{Ca}^{2+}]_i$ in vivo, and report that experimental manipulation of pH_i and $[\text{Ca}^{2+}]_i$ is sufficient to recover K^+ channel activities and accelerate stomatal opening in the *slac1* mutant. Thus, we uncover a previously unrecognized signaling network that ameliorates the effects of the *slac1* mutant on transpiration by regulating the K^+ channels. Additionally, these findings underscore the importance of H^+ -coupled anion transport for pH_i homeostasis.

Guard cells surround stomatal pores in the epidermis of plant leaves and regulate pore aperture to balance the demands for CO_2 in photosynthesis with the need to conserve water by the plant. Transpiration through stomata accounts for much of the 70% of global water usage associated with agriculture, and it has a profound impact on the water and carbon cycles of the world (Gedney et al., 2006; Betts et al., 2007). Guard cells open the pore by transport and accumulation of osmotically active solutes, mainly K^+ and Cl^- and the organic anion malate²⁻ (Mal), to drive water uptake and cell expansion. They close the pore by coordinating the release of these solutes through K^+ and anion channels at the plasma membrane. The past half-century has generated a wealth of knowledge on guard cell transport, signaling, and homeostasis, resolving the properties of the

major transport processes and metabolic pathways for osmotic solute uptake and accumulation, and many of the signaling pathways that control them (Blatt, 2000; Schroeder et al., 2001; McAinsh and Pittman, 2009; Hills et al., 2012). Even so, much of stomatal dynamics remains unresolved, especially how the entire network of transporters in guard cells works to modulate solute flux and how this network is integrated with organic acid metabolism (Wang and Blatt, 2011) to achieve a dynamic range of stomatal apertures.

This gap in understanding is most evident in a number of often unexpected observations, many of which have led necessarily to ad hoc interpretations. Among these, recent studies highlighted a diurnal variation in the free cytosolic Ca^{2+} concentration ($[\text{Ca}^{2+}]_i$), high in the daytime despite the activation of primary ion-exporting ATPases, and have been interpreted to require complex levels of regulation (Dodd et al., 2007). Other findings wholly defy intuitive explanation. For example, the *tpk1* mutant of *Arabidopsis* (*Arabidopsis thaliana*) removes a major pathway for K^+ flux across the tonoplast and suppresses stomatal closure, yet the mutant has no significant effect on cellular K^+ content (Gobert et al., 2007). Similarly, the *Arabidopsis clcc* mutant eliminates the H^+ - Cl^- antiporter at the tonoplast; it affects Cl^- uptake, reduces vacuolar Cl^- content, and slows stomatal opening; however, counterintuitively, it also suppresses stomatal closure (Jossier et al., 2010). In work leading to this study, we observed that the *slac1* anion channel mutant of *Arabidopsis* paradoxically profoundly alters the activities

¹ This work was supported by the Biotechnology and Biological Sciences Research Council (grant nos. BB/H024867/1, BB/F001630/1, and BB/H009817/1 to M.R.B.), by a Chinese Scholarship Council and Glasgow University PhD scholarship to Y.W., and by a Begonia Trust PhD studentship to M.P.

* Corresponding author; e-mail michael.blatt@glasgow.ac.uk.

The author responsible for distribution of materials integral to the findings presented in this article in accordance with the policy described in the Instructions for Authors (www.plantphysiol.org) is: Michael R. Blatt (michael.blatt@glasgow.ac.uk).

[W] The online version of this article contains Web-only data.

[OA] Open Access articles can be viewed online without a subscription. www.plantphysiol.org/cgi/doi/10.1104/pp.112.207704

of the two predominant K⁺ channels at the guard cell plasma membrane. The *SLAC1* anion channel is a major pathway for anion loss from the guard cells during stomatal closure (Negi et al., 2008; Vahisalu et al., 2008), and its mutation leads to incomplete and slowed closure of stomata in response to physiologically relevant signals of dark, high CO₂, and the water-stress hormone abscisic acid. Guard cells of the *slac1* mutant accumulate substantially higher levels of Cl⁻, Mal, and also K⁺ when compared with guard cells of wild-type Arabidopsis (Negi et al., 2008). The latter observation is consistent with additional impacts on K⁺ transport; however, a straightforward explanation for these findings has not been forthcoming.

Quantitative systems analysis offers one approach to such problems. Efforts to model stomatal function generally have been driven by a “top-down” approach (Farquhar and Wong, 1984; Eamus and Shanahan, 2002) and have not incorporated detail essential to understanding the molecular and cellular mechanics that drive stomatal movement. Only recently we elaborated a quantitative systems dynamic approach to modeling the stomatal guard cell that incorporates all of the fundamental properties of the transporters at the plasma membrane and tonoplast, the salient features of osmolite metabolism, and the essential cytosolic pH (pH_i) and [Ca²⁺]_i buffering characteristics that have been described in the literature (Hills et al., 2012). The model resolved with this approach (Chen et al., 2012b) successfully recapitulated a wide range of known stomatal behaviors, including transport and aperture dependencies on extracellular pH, KCl, and CaCl₂ concentrations, diurnal changes in [Ca²⁺]_i (Dodd et al., 2007), and oscillations in membrane voltage and [Ca²⁺]_i thought to facilitate stomatal closure (Blatt, 2000; McAinsh and Pittman, 2009; Chen et al., 2012b). We have used this approach to resolve the mechanism behind the counterintuitive alterations in K⁺ channel activity uncovered in the *slac1* mutant of Arabidopsis. Here, we show how anion accumulation in the mutant affects the H⁺ and Ca²⁺ loads on the cytosol, elevating pH_i and [Ca²⁺]_i, and in turn regulating the K⁺ channels. We have validated the key predictions of the model and, in so doing, have uncovered a previously unrecognized homeostatic network that ameliorates the effects of the *slac1* mutant on transpiration from the plant.

RESULTS

A Cl⁻ Channel Mutation Alters the Activities of K⁺ Channels and Slows Stomatal Opening

The uptake and release of K⁺ across the guard cell plasma membrane is mediated largely by two subsets of voltage-gated or Kv-like K⁺ channels. Channels mediating K⁺ uptake are dominated by the *KAT1* K⁺ channel gene product in Arabidopsis, and they give rise to an inward-rectifying (inward-directed) K⁺ current (I_{K,in}) that activates at voltages near and negative of -120 mV. K⁺ release in Arabidopsis occurs through the GORK K⁺ channel that gives rise to an outward-rectifying (outward-

directed) K⁺ current (I_{K,out}) at voltage positive of the K⁺ equilibrium voltage (Blatt, 1988, 2000; Schachtman et al., 1992; Nakamura et al., 1995; Blatt and Gradmann, 1997; Ache et al., 2000; Schroeder et al., 2001; Hossy et al., 2003). On recording I_{K,in} and I_{K,out} under voltage clamp (Chen et al., 2012a), we observed the profound suppression of I_{K,in} and moderate enhancement of I_{K,out} in intact guard cells of *slac1-1* mutant Arabidopsis compared with currents from guard cells of wild-type and *pSLAC1::SLAC1*-complemented *slac1-1* mutant (hereafter referred to as *pSLAC1*) plants (Vahisalu et al., 2008). Guard cells of wild-type and *pSLAC1* plants showed similar K⁺ currents, with wild-type plants yielding mean steady-state values for I_{K,in} at -240 mV and I_{K,out} at +40 mV of -821 ± 35 μA cm⁻² (n = 15) and +183 ± 13 μA cm⁻² (n = 12), respectively; guard cells of the *slac1-1* mutant, however, gave currents of -164 ± 37 μA cm⁻² (n = 14) and +295 ± 22 μA cm⁻² (n = 12), corresponding to an 80% reduction and 61% increase at these voltages, respectively (Fig. 1, A and B; Table I). Additionally, the mean membrane voltage of *slac1-1* mutant guard cells was displaced negative relative to values recorded from guard cells of wild-type and *pSLAC1* Arabidopsis, consistent with the loss of inward current through the SLAC1 channel (Fig. 1C).

Thermodynamic considerations preclude the SLAC1 channel from contributing to anion uptake and stomatal opening (Blatt, 2000; Vahisalu et al., 2008; Barbier-Brygoo et al., 2011). Indeed, eliminating the SLAC1 current was expected to accelerate opening by eliminating an efflux shunt that opposed anion accumulation via H⁺-coupled transport and might otherwise slow the accumulation of Cl⁻. By contrast, I_{K,in} is a dominant pathway for K⁺ uptake during opening (Blatt, 2000; Hills et al., 2012); its suppression in the *slac1-1* mutant, therefore, was expected to slow stomatal opening. To monitor opening, we measured apertures from stomata in situ in leaves and after isolation in epidermal peels, and we recorded transpiration from intact Arabidopsis plants in response to step changes in light. Gas-exchange measurements (Fig. 2A) yielded rates of change in transpiration that were slowed significantly in the *slac1-1* mutant when compared with the wild-type and *pSLAC1* plants on transitions to light, and after isolation in epidermal peels, stomata of the *slac1-1* mutant opened in the light at roughly one-half the rate (Fig. 2A) and with half-times more than 2-fold greater than either the wild-type or *pSLAC1* plants (Fig. 2B). Over a 24-h period, stomata in leaves failed to close fully, opened and closed sluggishly, and responded over an elevated range of apertures in the *slac1-1* mutant when compared with the wild-type or *pSLAC1* plants (Fig. 2C), thus confirming the unexpected and ameliorating effect of the *slac1* mutation on water loss through slowed stomatal opening.

Altered K⁺ Channel Activities Are Not Reflected in Channel Gene Transcription

The expression of several ion channel genes in Arabidopsis is subject to environmental cues and,

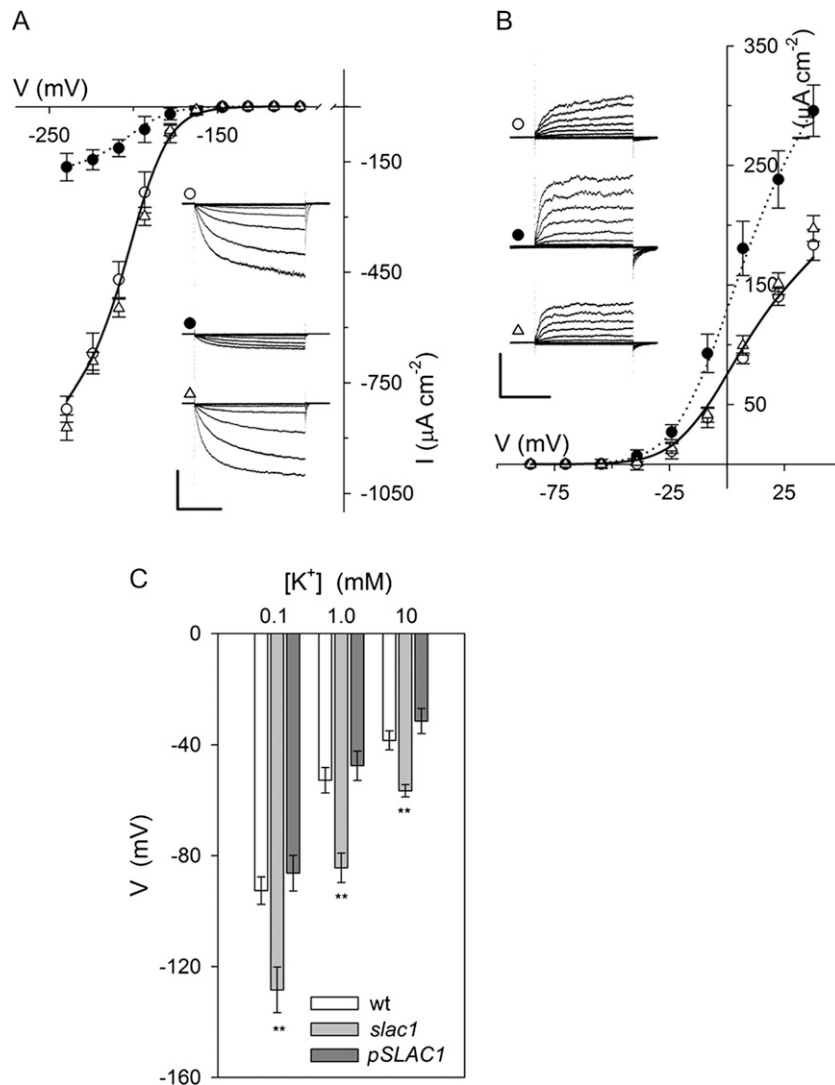


Figure 1. The *slac1* mutant of Arabidopsis alters currents carried by both $I_{K,in}$ and $I_{K,out}$ and hyperpolarizes the membrane voltage. Data are means \pm SE of $n \geq 12$ independent experiments for wild-type (open circles), *slac1-1* (closed circles), and *pSLAC1* (open triangles) plants. A, Steady-state currents recorded under voltage clamp for $I_{K,in}$ show a roughly 80% suppression of channel current. Curves are fittings of wild-type (solid line) and *slac1-1* (dotted line) currents to a Boltzmann function (Table I). The inset shows current traces recorded under voltage clamp and cross referenced by symbol. Scale are as follows: vertical, $500 \mu\text{A cm}^{-2}$; horizontal, 2 s. *slac1-1* currents are significantly different ($P < 0.001$) for all points negative of -180 mV. B, Steady-state currents recorded for $I_{K,out}$ under voltage clamp show a roughly 80% suppression of channel current. Curves are fittings of wild-type (solid line) and *slac1-1* (dotted line) currents to a Boltzmann function (Table I). The inset shows representative current traces recorded under voltage clamp and cross-referenced by symbol. Scale are as follows: vertical, $200 \mu\text{A cm}^{-2}$; horizontal, 2 s. *slac1-1* currents are significantly different ($P < 0.001$) for all points positive of -20 mV. C, Free-running voltages recorded from wild-type (wt), *slac1-1*, and *pSLAC1* Arabidopsis with 0.1, 1, and 10 mM KCl outside. Values for the *slac1-1* mutant differ significantly (** $P < 0.001$) from those of wild-type and *pSLAC1* guard cells at all three KCl concentrations. Note that all values are likely to underestimate the true free-running voltage in this case, given the membrane input resistance (greater than $20 \text{ G}\Omega$; Blatt and Slayman [1983]) and leakage currents (1–2 pA) typical of high-impedance electrometer amplifiers. Such leakage currents are insignificant as a background to clamp currents of ± 300 to 500 pA, so they do not influence measurements under voltage clamp, but they are sufficient to displace the apparent voltage by $+40$ mV or more in the free-running (unclamped) cell.

potentially, to homeostatic regulation (Amtmann and Blatt, 2009). Therefore, we tested whether the *slac1-1* mutation might affect K^+ channel gene transcription. Transcripts for the K^+ channel genes *KAT1*, *KAT2*, *KC1*, *GORK*, *AKT1*, and *AKT2* were assayed by quantitative

PCR using mRNA isolated from plants grown together and harvested 2 h after the start of daylight. We assayed for transcripts of the predominant vacuolar K^+ channel *TPK1* (Gobert et al., 2007) and the K^+ - and Ca^{2+} -permeable channel *TPC1* (Peiter et al., 2005) as

Table 1. Fittings for $I_{K,in}$ and $I_{K,out}$ from *Arabidopsis* guard cells to a Boltzmann function (see Eq. 1)

Fitted curves for wild-type and *slac1-1* currents are as shown (for details, see Figs. 1 and 6). Best fittings were obtained with the voltage sensitivity coefficient (gating charge; δ), held in common in both cases, and with the voltage yielding half-maximal conductance ($V_{1/2}$), held in common for $I_{K,out}$ as indicated. Note the roughly 80% reduction in maximum conductance (g_{max}) for $I_{K,in}$ and its 60% enhancement for $I_{K,out}$ in the *slac1-1* mutant.

Parameter	Wild Type	<i>slac1-1</i>	<i>pSLAC1</i>
$I_{K,in}$ (δ , -1.9 ± 0.1)			
g_{max} ($\mu S\ cm^{-2}$)	4.83 ± 0.08	0.99 ± 0.07	5.20 ± 0.09
$V_{1/2}$ (mV)	-187 ± 3	-202 ± 2	-189 ± 2
$I_{K,out}$ (δ , 2.0 ± 0.1 ; $V_{1/2}$ -7 ± 2 mV)			
g_{max} ($\mu S\ cm^{-2}$)	1.65 ± 0.07	2.83 ± 0.09	1.84 ± 0.08

well as for the vacuolar VH^+ -ATPase C subunit *VHA-C* and the plasma membrane H^+ -ATPases *AHA1*, *AHA2*, and *AHA5* that could affect energization of the membranes (Haruta and Sussman, 2012). No difference between the three plant lines was seen (Fig. 3), thus discounting homeostatic feedback via transcription.

slac1 Is Predicted to Elevate pH and $[Ca^{2+}]_i$, Affecting K⁺ Channels and Stomatal Opening

To explore the physiological context of the *slac1-1* mutation, we next made use of quantitative systems

modeling of the guard cell, incorporating all of the known transporters at the plasma membrane and tonoplast, their biophysical and kinetic characteristics, the salient features of Suc and Mal metabolism, as well as the homeostatic parameters of Ca^{2+} and pH buffering (Hills et al., 2012). We used an equivalent ensemble of model parameters (Chen et al., 2012b) to simulate the diurnal cycle of stomatal movements after scaling guard cell volume and stomatal aperture to the dimensions of the *Arabidopsis* stomatal complex while maintaining transporter surface densities (Supplemental Appendix S1). An essential feature of this modeling approach is that the system is defined by a set of model components (transporters and metabolic and buffering reactions), the parameters of which are fixed constants defined experimentally. Thus, all of the dynamic behavior of the system arises from the emergent interactions between model components and associated dependent variables, notably of ion and solute concentrations, and of the voltages across the two membranes (Chen et al., 2012b). Simulations were carried out first with the full complement of membrane transporters, including the SLAC1 current, and then with the SLAC1 current omitted. The model reproduced the behavior of the wild-type *Arabidopsis* stomata and all of the salient features of the *slac1-1* mutant, notably the elevated range of stomatal

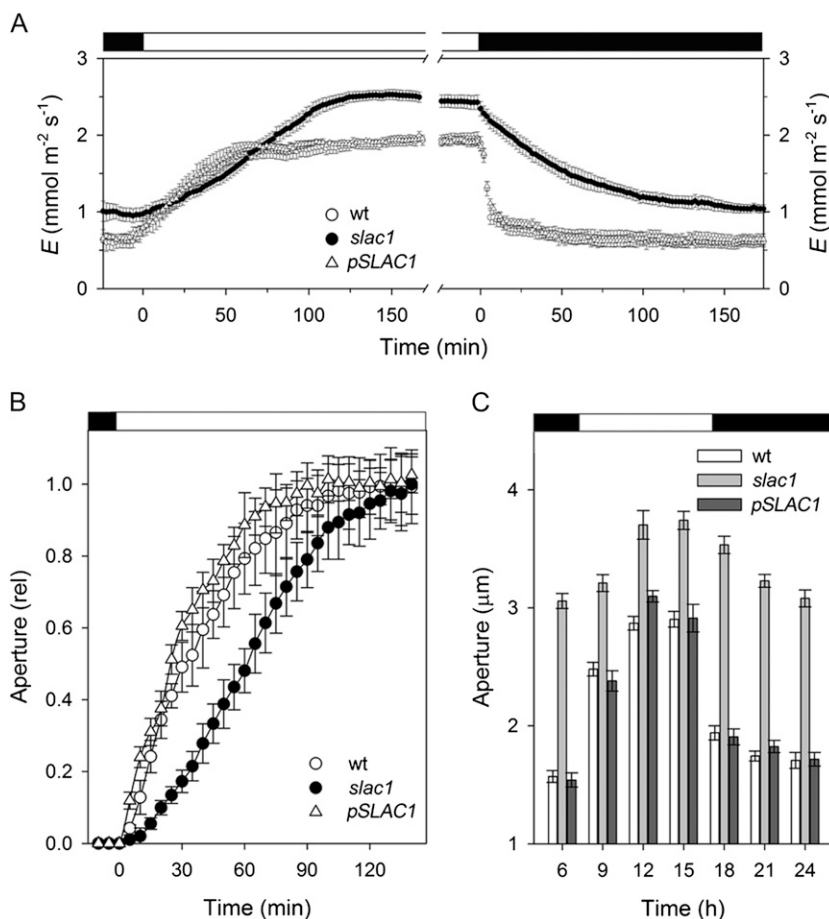


Figure 2. The *slac1* mutant of *Arabidopsis* slows stomatal opening and closing on light-dark transitions. Data are means \pm SE of $n \geq 12$ independent experiments for wild-type (wt; open circles), *slac1-1* (closed circles), and *pSLAC1* (open triangles) plants. A, Transpiration rates recorded from intact *Arabidopsis* on transition from dark to $300\ \mu\text{mol}\ \text{m}^{-2}\ \text{s}^{-1}$ light (left) and back to dark (right). Fitted half-times for opening (sigmoid) and closing (single exponential) are as follows: wild type, 22.4 ± 0.5 and 5.5 ± 0.2 min; *slac1-1*, 65.6 ± 0.4 and 50.7 ± 0.4 min; *pSLAC1*, 27.1 ± 0.4 and 6.3 ± 0.1 min. B, Stomatal apertures from epidermal peels. Data are normalized to initial and final apertures on transition to $300\ \mu\text{mol}\ \text{m}^{-2}\ \text{s}^{-1}$ light. Opening half-times are as follows: wild type, 38 ± 5 min; *slac1-1*, 74 ± 8 min; *pSLAC1*, 34 ± 7 min. Apertures (initial/final, in μm) are as follows: wild type, $2.6 \pm 0.2/4.2 \pm 0.4$; *slac1-1*, $4.0 \pm 0.3/4.8 \pm 0.4$; *pSLAC1*, $2.6 \pm 0.2/4.0 \pm 0.4$. C, Stomatal opening and closing recorded in leaves at 3-h intervals over 24 h. Note the slower response in the first three daylight hours for the mutant. *slac1-1* apertures are significantly different ($P < 0.001$) at all times.

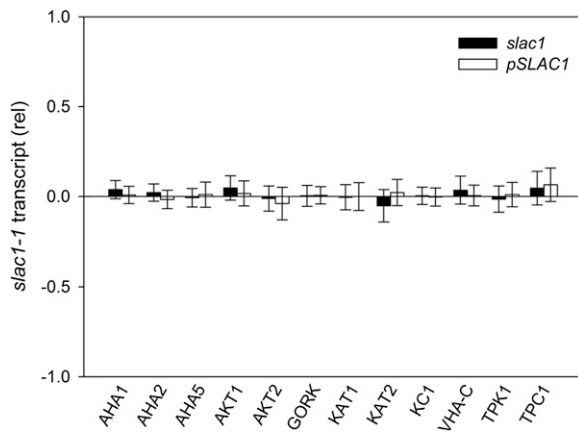


Figure 3. Relative transcript levels for selected plasma membrane and tonoplast transporters from *slac1-1* and *pSLAC1* Arabidopsis assayed by quantitative PCR. Data are means \pm SE of three independent experiments and are reported as the change in expression relative to wild-type levels (=0) after normalizing to the housekeeping *ACT2* actin gene and *TUB9* tubulin gene transcripts.

apertures and accumulation of Cl^- , Mal, and K^+ (Fig. 4A); it returned roughly a 5-fold increase in the half-time for closure and a slowed rate of stomatal opening (Fig. 4B); and it enhanced $I_{\text{K,out}}$ and greatly reduced $I_{\text{K,in}}$ activities in the *slac1-1* simulation (Fig. 4, C and D), much as observed experimentally (Figs. 1 and 2).

The model also yielded two key predictions for the *slac1-1* mutant: (1) it showed roughly a 0.2-unit elevation in pH_i above the means in the wild type, day and night; and (2) it predicted a rise in the daytime $[\text{Ca}^{2+}]_i$ to values near 400 nM (Fig. 4E). Significantly, both elevated pH_i and $[\text{Ca}^{2+}]_i$ are known to suppress $I_{\text{K,in}}$. In *Vicia faba* guard cells, $[\text{Ca}^{2+}]_i$ inactivates $I_{\text{K,in}}$ with an inhibitory constant, k_i of 330 nM and a Hill coefficient of 4 (Grabov and Blatt 1999), and the current activates with cytosolic protein concentration $[\text{H}^+]_i$ (decreasing pH_i), showing an apparent $K_{1/2}$ near 400 nM (pH 6.4) and Hill coefficient of unity (Blatt, 1992; Grabov and Blatt, 1997). Raising pH_i also enhances $I_{\text{K,out}}$ the current exhibiting a K_i for H^+ near 40 nM (pH 7.4) and a Hill coefficient of 2 (Blatt and Armstrong, 1993; Grabov and Blatt, 1997). Such quantitative detail is not available for the guard cells of Arabidopsis, but all evidence (Hoth and Hedrich, 1999; Hosy et al., 2003; Siegel et al., 2009) indicates similar pH_i and $[\text{Ca}^{2+}]_i$ sensitivities. Thus, we suspected that the elevations in pH_i and $[\text{Ca}^{2+}]_i$ predicted for the *slac1-1* guard cells might explain the altered K^+ currents of the mutant.

Direct pH_i and $[\text{Ca}^{2+}]_i$ Measurements and Manipulations Validate Model Predictions

To test these predictions, we recorded pH_i and $[\text{Ca}^{2+}]_i$ in vivo by ratiometric fluorescence imaging using the H^+ -sensitive dye 2',7'-bis-(2-carboxyethyl)-5,(6)-carboxyfluorescein (BCECF) and the Ca^{2+} -sensitive dye 2-

(6-(bis(carboxymethyl)amino)-5-(2-(2-(bis(carboxymethyl)amino)-5-methylphenoxy)ethoxy)-2-benzofuranyl)-5-oxazolecarboxylic acid (Fura2) after iontophoretic injection into guard cells. Recordings of BCECF fluorescence yielded pH_i near 7.6 in wild-type and *pSLAC1* guard cells, similar to guard cells of *V. faba* (Blatt and Armstrong, 1993; Grabov and Blatt, 1997). Recordings from *slac1-1* guard cells showed an elevated pH_i (Fig. 5A), consistent with, and even exceeding, model predictions. We used treatments with butyrate to acid load the cytosol and to calculate the H^+ buffering capacity of the guard cells, much as we have before (Blatt and Armstrong, 1993; Grabov and Blatt, 1997). When protonated, the organic acid is freely permeable across the plasma membrane and sets up coupled dissociation equilibria according to the Henderson-Hasselbalch equation and determined by the dominant pool of protonated acid. For a cell, the near-infinite volume of bathing solution determines the protonated acid concentration. Thus, equilibration of the protonated acid across the plasma membrane and its dissociation generates a substantial cytosolic H^+ load, provided that the bath is 1 to 2 pH units more acidic than the cytosol (McLaughlin and Dilger, 1980). Butyrate treatments carried out while measuring pH_i with BCECF showed a significant acidification of the cytosol (Fig. 5B). From the Henderson-Hasselbalch equation, we calculated a cytosolic buffer capacity of 84 ± 6 mM H^+ per pH unit for guard cells of wild-type Arabidopsis, close to that for *V. faba* guard cells (Grabov and Blatt, 1997), and almost a 2-fold higher buffer capacity of 143 ± 13 mM per pH unit in the *slac1-1* mutant (Fig. 5A). The elevated pH_i buffer capacity of *slac1-1* guard cells is consistent with the substantial retention of organic acids reported previously (Negi et al., 2008). Measurements of $[\text{Ca}^{2+}]_i$ with Fura2 from guard cells of wild-type and *pSLAC1* plants gave resting values near 220 nM, whereas *slac1-1* guard cells showed significantly elevated $[\text{Ca}^{2+}]_i$ with a mean value near 450 nM (Fig. 5C). Thus, in *slac1-1* guard cells, the elevations in pH_i and $[\text{Ca}^{2+}]_i$ alone appeared sufficient to explain both $I_{\text{K,in}}$ suppression and the enhancement of $I_{\text{K,out}}$ assuming kinetic sensitivities similar to those for the K^+ channels in *V. faba*.

To validate this conclusion, we tested the capacity to recover wild-type $I_{\text{K,in}}$ and $I_{\text{K,out}}$ in the *slac1-1* mutant when $[\text{Ca}^{2+}]_i$ and pH_i were chemically "clamped" to suppress their elevation. Guard cells of the *slac1-1* mutant were impaled as before, but with electrolyte including 10 mM of the Ca^{2+} buffer 1,2-bis(2-aminophenoxy) ethane-*N,N,N',N'*-tetraacetic acid (BAPTA; $K_d = 130$ nM) for direct loading from the microelectrode. Loading with Ca^{2+} buffers has been used on many occasions to lower resting $[\text{Ca}^{2+}]_i$ and to suppress $[\text{Ca}^{2+}]_i$ transients (Speknsnijder et al., 1989; Fairley-Grenot and Assmann, 1991; Felle and Hepler, 1997). In our experience, BAPTA loading in guard cells effectively clamps $[\text{Ca}^{2+}]_i$ near 200 nM, even under conditions that normally drive $[\text{Ca}^{2+}]_i$ above 1,200 nM (Chen et al., 2010). Following impalements and BAPTA loading, the guard cells were challenged with 3 mM

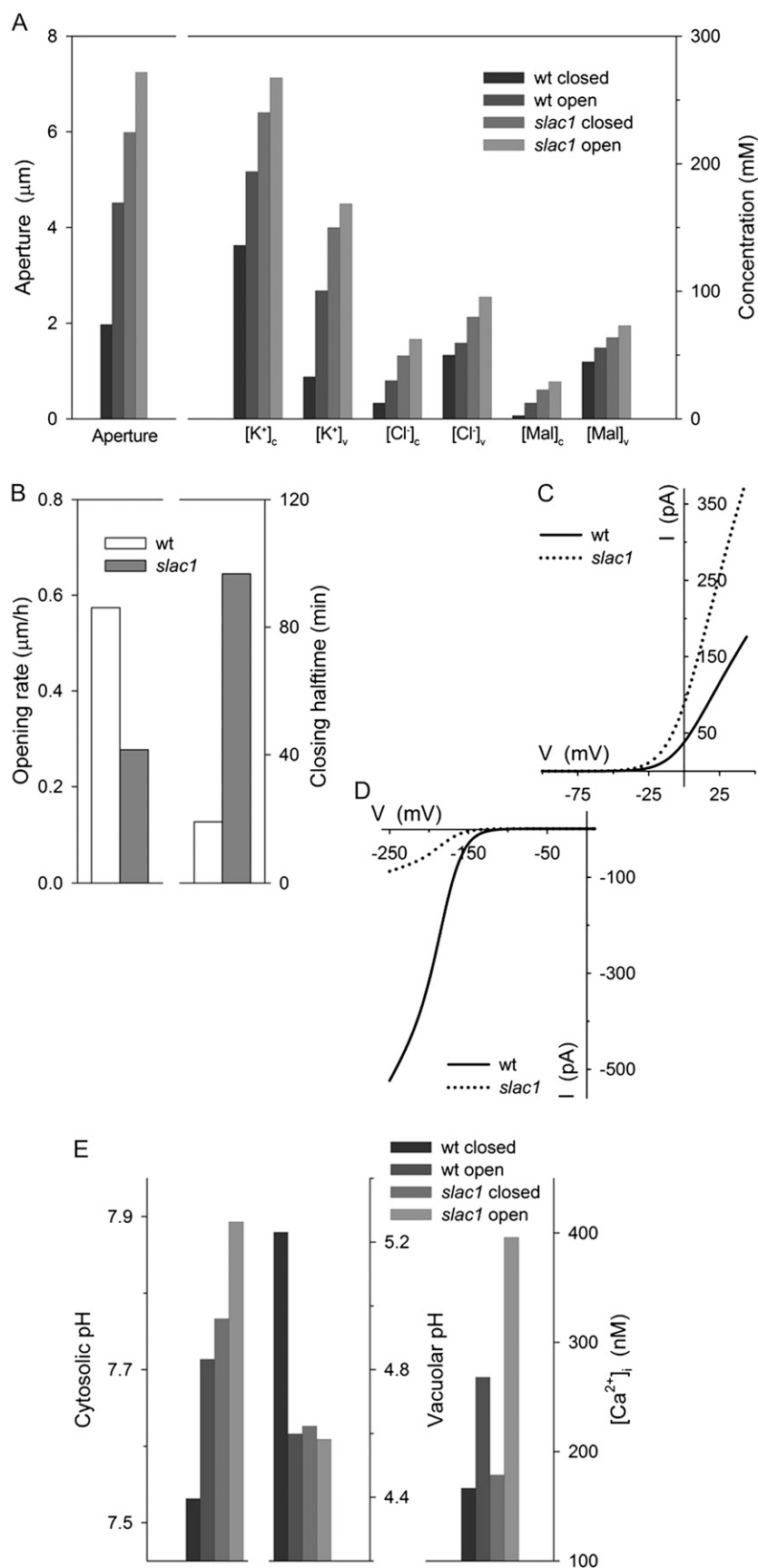
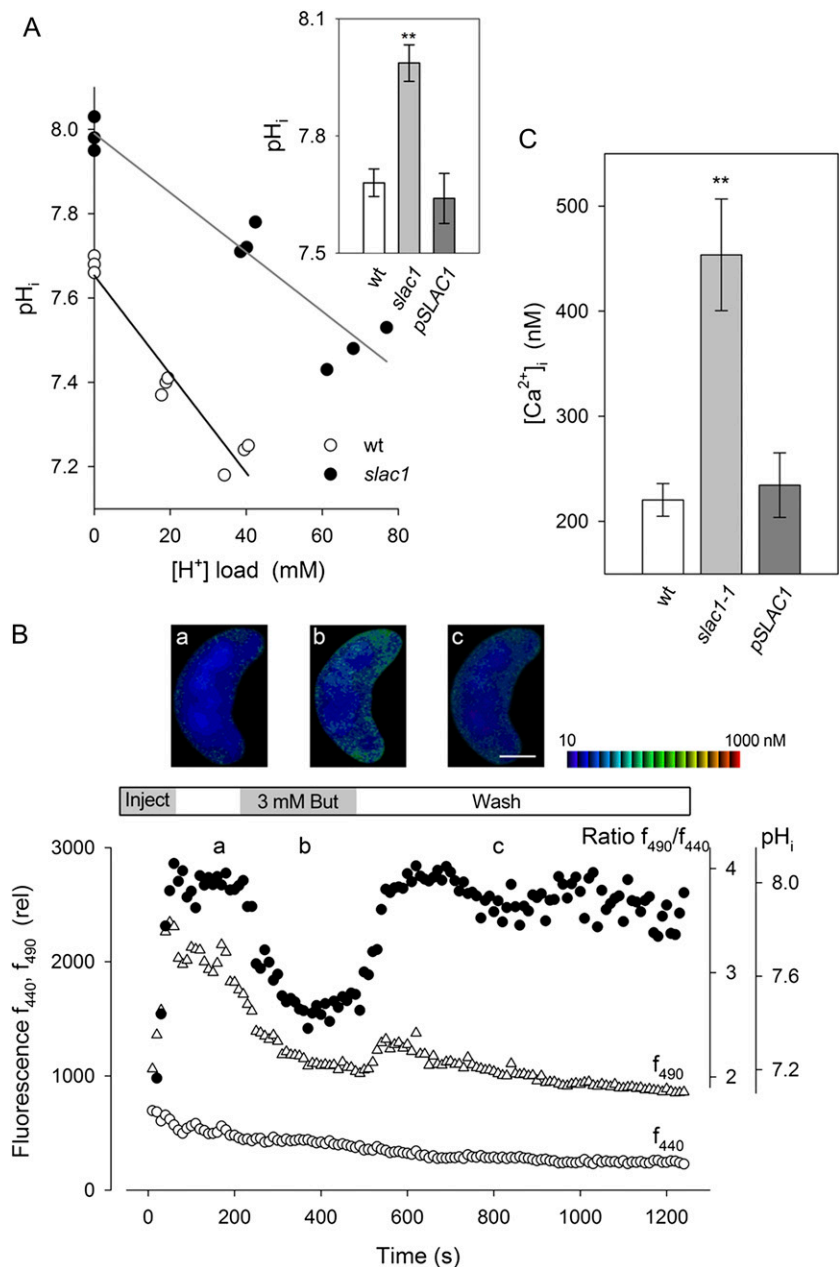


Figure 4. Quantitative systems modeling (Chen et al., 2012b; Hills et al., 2012) reproduces characteristics for *slac1-1* guard cells and accounts for altered K⁺ channel activities through predicted elevations of pHi and [Ca²⁺]_i. Outputs are derived from modeling of the diurnal cycle (Chen et al., 2012b). Additional model outputs and detailed explanations are provided with Supplemental Figures S1 to S7. The full set of model parameters and initializing variables are listed in Supplemental Appendix S1 and are available with the OnGuard software at www.psr.org.uk. A, Mean stomatal apertures and cytosolic and vacuolar solute concentrations for guard cells of stomata in the dark (closed) and light (open). Outputs are for each variable (left to right, wild-type [wt] closed and open, *slac1* closed and open). B, Stomatal opening rates (left) and closure half-times (right) determined from simulated apertures during the first 3 h (opening) and the final 3 h (closing) of the daylight period (compare with Fig. 2; Supplemental Fig. S1). C and D, Current-voltage curves for I_{K,out} (C) and I_{K,in} (D) in wild-type (solid line) and *slac1* (dotted line) simulations taken at 3 h into the daylight period (compare with Fig. 1, A and B). E, Predicted outputs (left to right, outputs for wild-type closed and open, *slac1* closed and open) for pHi (left), vacuolar pH (center), and [Ca²⁺]_i (right).

Figure 5. The *slac1-1* mutant shows elevated pH_i and $[\text{Ca}^{2+}]_i$. A, Mean \pm SE for pH_i (inset; $n \geq 7$) and pH buffering analysis ($n = 3$) from guard cells of wild-type (wt; open circles) and *slac1-1* mutant (closed circles) Arabidopsis using BCECF fluorescence ratio analysis and before and during acid loading with 1 and 3 mM butyrate. Buffering determined by linear fitting (solid lines; Grabov and Blatt 1997) gave 84 ± 6 mM H^+ per pH unit (wild type) and 143 ± 13 mM per pH unit (*slac1-1*). pH_i values from *slac1-1* guard cells differed significantly (** $P < 0.001$) from those of wild-type and *pSLAC1* plants. B, pH_i recording from one *slac1-1* mutant guard cell using BCECF fluorescence ratiometry. Fluorescence at 440 nm (f_{440} ; open circles), 490 nm (f_{490} ; open triangles), and the fluorescence ratio (f_{490}/f_{440}) and calibrated pH_i (closed circles) were recorded at 10-s intervals from 1.5 μm depth around the cell periphery. Representative images (top) were taken at the time points indicated. The intensity-modulated pseudocolor scale (left to right) represents pH 8 to 6. The period of BCECF injection, exposure to 3 mM butyrate (But), and butyrate washout are as indicated. C, Mean \pm SE ($n \geq 5$) for resting $[\text{Ca}^{2+}]_i$. Values for *slac1-1* guard cells differed significantly (** $P < 0.001$) from those of the wild type and *pSLAC1*.



butyrate to lower pH_i near a value of 7.5, close to that of wild-type guard cells (Fig. 5, A and B). Analysis of five independent experiments with *slac1-1* guard cells (Fig. 6, A and B) showed that these manipulations were sufficient to recover both $I_{K,in}$ and $I_{K,out}$ in the *slac1-1* mutant, with characteristics that were quantitatively equivalent to those observed in the wild-type plant. We used a similar strategy in measurements of stomatal opening. Buffering $[\text{Ca}^{2+}]_i$ by BAPTA loading was not possible in this case, so guard cells in epidermal peels were treated with butyrate to suppress pH_i as before. The results yielded rates of stomatal opening statistically equivalent to those of wild-type guard cells (Fig. 6C), consistent with evidence that greater than 70% suppression of $I_{K,in}$ is necessary before a significant

change in opening or its kinetics is measurable (Lebaudy et al., 2008).

DISCUSSION

The detail now available for, and complexity of, guard cell transport defy any simple explanation for how guard cells achieve the range of stomatal apertures observed in vivo, let alone a clear understanding of the properties of the guard cell system as a whole. This gap in understanding is evident especially in the counterintuitive behavior of stomata of the *slac1* mutant of Arabidopsis. *slac1* guard cells lack the major anion channel that mediates anion efflux during stomatal closure; yet paradoxically, the cells show

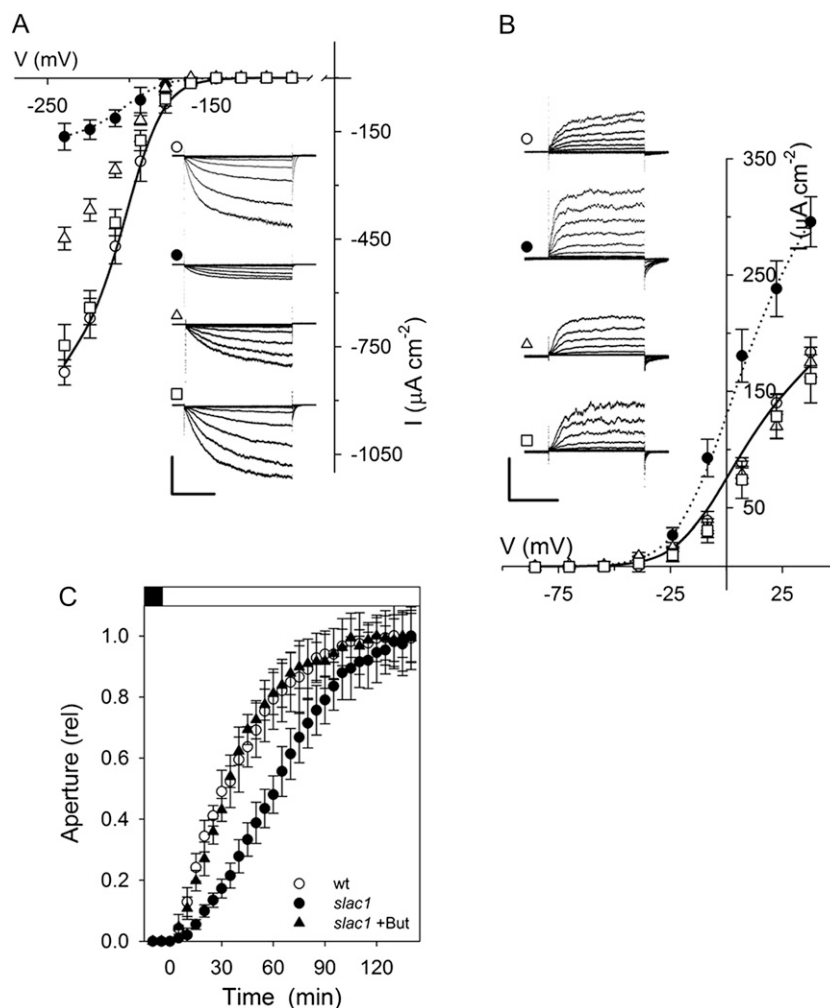


Figure 6. Altered K⁺ channel currents are consequent on elevation of pH_i and [Ca²⁺]_i in the *slac1-1* mutant. A, Mean \pm SE ($n \geq 8$) of steady-state currents for $I_{K,in}$ under voltage clamp show recovery of wild-type characteristics in the *slac1-1* mutant on suppressing [Ca²⁺]_i and pH_i elevations. Wild-type (open circles) and *slac1-1* (closed circles) data are included from Figure 1 for reference. *slac1-1* guard cells were loaded with 10 mM BAPTA to buffer [Ca²⁺]_i (open triangles) and additionally exposed to 3 mM butyrate outside (open squares) to lower pH_i (Fig. 5, A and B). The inset shows current traces recorded under voltage clamp and cross-referenced by symbol. Scales are as follows: vertical, 500 $\mu\text{A cm}^{-2}$; horizontal, 2 s. B, Mean \pm SE ($n \geq 7$) of steady-state currents for $I_{K,out}$ under voltage clamp show recovery of wild-type current characteristics in *slac1-1* mutant guard cells on suppressing pH_i elevation. Wild-type (open circles) and *slac1-1* (closed circles) data are included from Figure 1 for reference. *slac1-1* guard cells were exposed to 3 mM butyrate outside (open squares) to lower pH_i (Fig. 5, A and B) and additionally when loaded with 10 mM BAPTA to buffer [Ca²⁺]_i (open triangles). The inset shows current traces recorded under voltage clamp and cross-referenced by symbol. Scales are as follows: vertical, 200 $\mu\text{A cm}^{-2}$; horizontal, 2 s. C, Stomatal opening in epidermal peels on transition to 300 $\mu\text{mol m}^{-2} \text{s}^{-1}$ light in the presence of 3 mM butyrate (But). Data are normalized to initial and final apertures after correcting for butyrate-induced aperture increase. Results for the wild type (wt) and the *slac1-1* mutant are included from Figure 1 for comparison. Opening half-time was as follows: *slac1-1* + butyrate, 23 \pm 0.8 min. Apertures (initial/final in μm) are as follows: wild type, 2.7 \pm 0.3/4.5 \pm 0.3; *slac1-1*, 4.3 \pm 0.3/5.1 \pm 0.3; *slac1-1* + butyrate, 4.5 \pm 0.2/5.6 \pm 0.2.

profound changes in K⁺ channel activities and a slowed rate of stomatal opening. We have taken a computational approach to quantitative dynamic modeling of the guard cell to understand this behavior. The model incorporates all of the properties for transporters at the plasma membrane and tonoplast, the salient features of osmolyte metabolism, and pH and Ca²⁺ buffering. The results demonstrate the true

predictive power of this systems modeling approach to guide a detailed mechanistic analysis of the signaling pathways responsible. Furthermore, in so doing, they highlight a previously unrecognized homeostatic network that regulates membrane transport for stomatal function. The SLAC1 channel has no direct connection with solute uptake, and especially not with $I_{K,in}$ and K⁺ influx; however, modeling uncovered the feedback

pathway to the K^+ channels, and we confirmed experimentally the link through the effect of *slac1* in elevating pH_i and $[Ca^{2+}]_i$ (Fig. 7). This network ameliorates the effect of the *slac1* mutation by suppressing $I_{K,in}$ and the rise in transpiration during the first hours of daylight, thus explaining the otherwise counterintuitive effects of *slac1* on stomatal movement.

In the model, just as in vivo, changes in $[Ca^{2+}]_i$ and pH_i arise through interactions between the various transporters, metabolism, and associated buffering characteristics (Chen et al., 2012b; Hills et al., 2012).

The model accounts for the emergent effects of the *slac1* mutant on pH_i as a consequence of Cl^- and Mal hyperaccumulation, much as has been observed in vivo (Negi et al., 2008). A detailed analysis of the model outputs is presented in Supplemental Figures S1 to S7. It predicted pH_i in the mutant to rise with Mal transinhibition of Mal synthesis and of Cl^- -mediated transinhibition of H^+ -coupled anion transport. Strongly affected was the H^+ - Cl^- antiport at the tonoplast, which normally transports inorganic anions into the vacuole in exchange for H^+ (De Angeli et al., 2006;

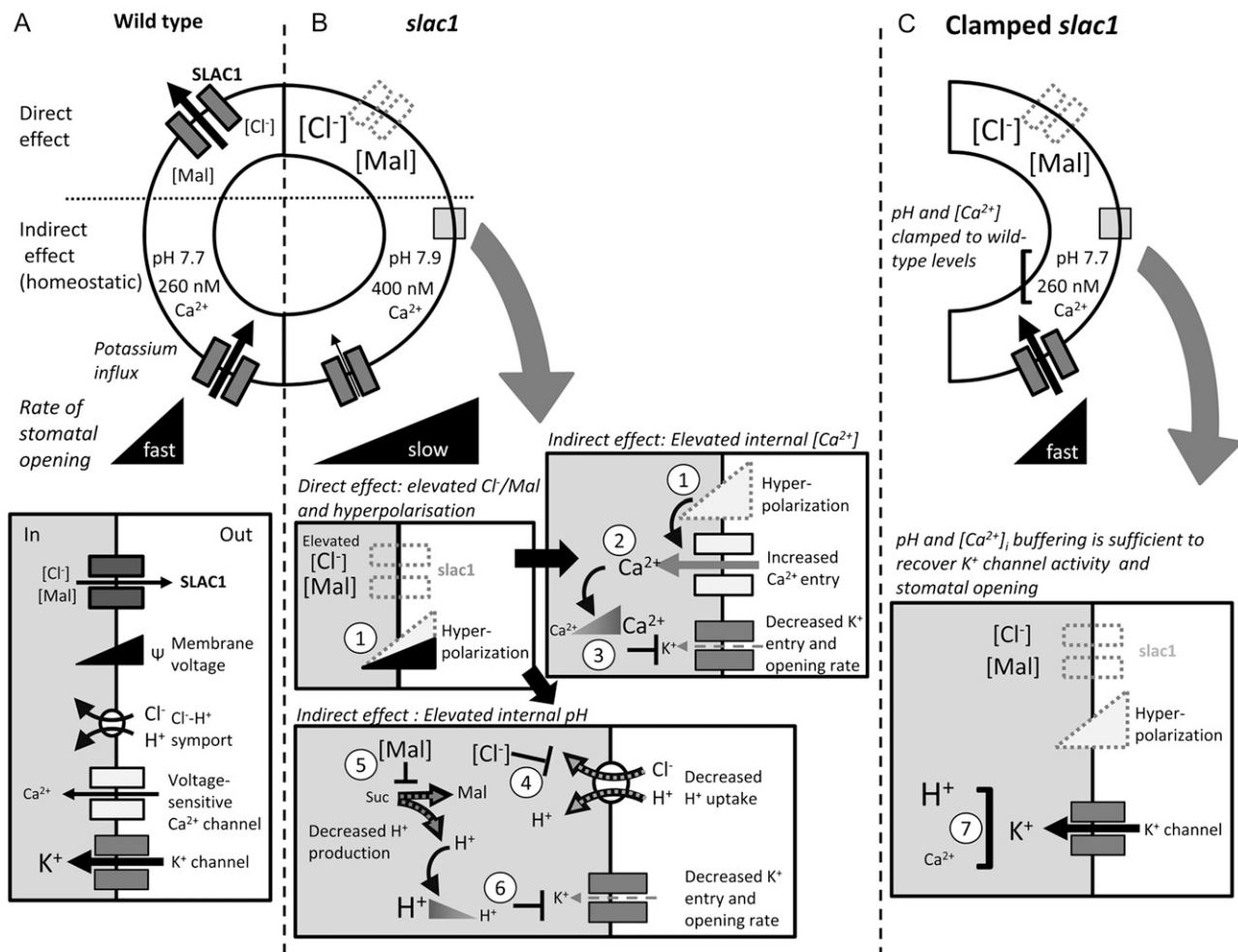


Figure 7. Eliminating the SLAC1 anion channel affects K^+ channel activity, K^+ uptake, and the rate of stomatal opening through its impact on pH_i and $[Ca^{2+}]_i$ as predicted by the OnGuard model (Chen et al., 2012b; Hills et al., 2012). Note that effects on tonoplast transport and on $I_{K,out}$ are not included for clarity, but they are complementary (see text). Black arrows indicate the wild type, and gray arrows indicate *slac1*. A, SLAC1 is a major pathway for Cl^- efflux during stomatal closure and is facilitated when Ca^{2+} channels activate to raise $[Ca^{2+}]_i$. The K^+ channel ($I_{K,in}$) and H^+ -coupled Cl^- transport enable osmotic solute uptake during opening. B, The *slac1* mutation eliminates an inward current (anion efflux), leading directly to Cl^- and Mal accumulation and membrane hyperpolarization (1) in the guard cell (Supplemental Figs. S1–S3). Membrane hyperpolarization promotes Ca^{2+} entry by activating plasma membrane Ca^{2+} channels (2) and elevates $[Ca^{2+}]_i$ (Fig. 5; Supplemental Fig. S6), which in turn suppresses $I_{K,in}$ (3; Fig. 1; Supplemental Fig. S7). Elevated Cl^- and Mal suppress H^+ -coupled Cl^- transport (4; see Supplemental Fig. S2) and Mal synthesis (5; Supplemental Fig. S3), thereby reducing the H^+ load on the cytosol and raising pH_i (Supplemental Fig. S5). The rise in pH_i also suppresses $I_{K,in}$ (6). The predicted increases in $[Ca^{2+}]_i$, pH_i , and their consequences for the K^+ channels were confirmed experimentally (Figs. 5 and 6). C, Suppressing the rise in $[Ca^{2+}]_i$ and pH_i by buffering (7) was sufficient to recover K^+ channel activity and the rate of stomatal opening, thus validating the model (Fig. 6).

Jossier et al., 2010). Overall, the result was to reduce the metabolic and transport H⁺ load on the cytosol, including H⁺ return to balance the H⁺-ATPase at the plasma membrane (Supplemental Fig. S5), hence raising p*H*_i. Thus, one important conclusion to be drawn from this first of the model predictions, and from its experimental validation, is of the central importance played by H⁺-coupled anion transport in controlling p*H*_i. A detailed knowledge of Cl⁻ uptake in plants is restricted to a few cell types (Sanders et al., 1989), but, like that of NO₃⁻ (Meharg and Blatt 1995), it is generally recognized to be mediated in symport with H⁺. In fact, H⁺-coupled anion transport at both membranes has been suggested to contribute to p*H*_i homeostasis (Barbier-Brygoo et al., 2011; Chen et al., 2012b), although direct and quantitative evidence has been lacking until now.

The model ascribes the elevated [Ca²⁺]_i of the mutant to loss of the SLAC1-mediated (inward) current and consequent negative shift in membrane voltage, thus promoting Ca²⁺ entry across the plasma membrane (Fig. 1; Supplemental Figs. S1 and S6). By contrast with the situation for p*H*_i, the effect of membrane hyperpolarization in promoting Ca²⁺ influx and elevating [Ca²⁺]_i in guard cells is well documented (Grabov and Blatt, 1998, 1999; Hamilton et al., 2000; Chen et al., 2010). We note that Vahisalu et al. (2008) reported little difference in [Ca²⁺]_i between wild-type and *slac1* mutant guard cells when recorded using the Cameleon YC3.6 Ca²⁺-sensitive reporter. However, their measurements were determined under experimental conditions known to drive [Ca²⁺]_i, indeed, via control of membrane voltage (Grabov and Blatt, 1998, 1999; Allen et al., 2001), effectively clamping [Ca²⁺]_i either to high or low values. Thus, their measurements cannot speak to the free-running [Ca²⁺]_i, either in the wild-type or *slac1* mutant guard cells.

We stress that our results uncover a homeostatic signaling network that, in itself, is sufficient to explain the physiopathology of the *slac1* mutant and its phenotypic characteristics in altered K⁺ transport and stomatal opening. These findings do not rule out other consequences of the *slac1* mutation, such as might be effected through more subtle changes in p*H*_i or [Ca²⁺]_i sensitivities of one or more of the underlying channels; however, they demonstrate that any such changes are not, in themselves, essential to understanding the effect of the *slac1* mutant either on K⁺ channel activities or on stomatal movement. Our findings also pave the way, through similar dynamic modeling and validation, to addressing many other unresolved observations in stomatal physiology. This strategy is certain to yield a greater understanding of the impacts of transport at the plasma membrane. Furthermore, it should prove a powerful new tool with which to analyze transport at the tonoplast, for which direct access *in vivo* is not possible. Challenges, for example, include resolving the controversial roles for the TPC1 cation channel in stimulus-response coupling (Peiter et al., 2005) and the counterintuitive effects of the TPK1 K⁺

channel and CLC anion antiporter, the deletion of either of which slows stomatal closure but with counterintuitive effects on K⁺ (Gobert et al., 2007) and anion content (Jossier et al., 2010). Analysis of these problems will help refine our current model of the guard cell as well as our understanding of stomatal function.

MATERIALS AND METHODS

Growth and Whole-Plant Physiology

Arabidopsis (*Arabidopsis thaliana*) Columbia wild-type, *slac1-1* mutant, and *pSLAC1*-complemented *slac1-1* plants were grown under 70 μmol m⁻² s⁻¹ light in short-day conditions (8/16 h of light/dark) at 22°C/18°C and 55%/70% relative humidity. All seeds were harvested at the same time from plants grown together. Chemicals were reagent grade from Sigma-Aldrich. Gas exchange was measured using the LI-COR 6400 XT Infrared Gas Analyzer (LI-COR Biosciences) and Arabidopsis Chamber (LI-COR 6400-17). Pots were sealed with Saran Wrap to prevent water vapor and CO₂ diffusion from the soil, and measurements were carried out at 380 μL L⁻¹ CO₂. Gas exchange was recorded in plants adapted to the dark for 2 h with light from an integrated source (LI-COR 6400-18). All plants were analyzed on at least 3 d at the same time of the relative diurnal cycle and were normalized for leaf area using ImageJ, version 1.43 (rsbweb.nih.gov/ij/; Rasband and Bright 1995).

Gene Expression Analysis

Total RNA was extracted from mature leaves, and transcript levels were determined by quantitative PCR as before (Chen et al., 2012b). Unique primers (Supplemental Table S1) were designed for the VH⁺-ATPase C subunit (Dettmer et al., 2006), the plasma membrane H⁺-ATPases *AHA1*, *AHA2*, and *AHA5* (Lopez-Marques et al., 2004), the K⁺ channels *KAT1*, *KAT2*, *KCL1*, *GORK*, *AKT1*, and *AKT2* (Pilot et al., 2001; Hosy et al., 2003; Honsbein et al., 2009), and the vacuolar channels *TPK1* (Gobert et al., 2007) and *TPC1* (Peiter et al., 2005). The *TUB9* tubulin (At4g20890) and *ACT2* actin (At3g18780) genes (Gutierrez et al., 2008) served as internal controls.

Stomatal Assays and Guard Cell Electrophysiology

Stomatal apertures in leaves were determined from impressions made using nail varnish and after peeling at intervals over 24 h (Fig. 2C). Otherwise, guard cells were isolated in epidermal peels and mounted as before (Eisenach et al., 2012). Stomatal apertures were recorded by digital photomicrography under infrared light (greater than 800 nm) and continuous superfusion with 10 mM KCl in 5 mM Ca²⁺-MES buffer, pH 6.1 [5 mM MES buffer titrated to its acid dissociation constant with Ca(OH)₂; Ca²⁺ concentration = 1 mM]. Light treatments were carried out on dark-adapted peels.

Currents from intact guard cells were recorded under voltage clamp using double- and triple-barreled microelectrodes and Henry's EP suite (Y-Science; Blatt and Armstrong, 1993; Eisenach et al., 2012). Microelectrodes were pulled to give tip resistances greater than 500 MΩ for impalement of Arabidopsis guard cells, and microelectrode barrels were filled with 200 mM K⁺ acetate, pH 7.5, to avoid Cl⁻ leakage from the microelectrode (Blatt and Slayman, 1983; Blatt, 1987b; Chen et al., 2012a). Voltage was recorded using a μP electrometer amplifier (WyeScience) with an input impedance of greater than 500 GΩ (Blatt, 1987a) and was typically clamped in cycles with a holding voltage of -100 mV and 6-s steps either to voltages from -120 to -240 mV (I_{K,in}) or to voltages from -80 to +40 mV (I_{K,out}). The Ca²⁺ buffer BAPTA was included as indicated. [Ca²⁺]_i and p*H*_i were determined, as described previously (Grabov and Blatt, 1997; Garcia-Mata et al., 2003), after iontophoretic injection of the fluorescent dyes Fura2 and BCECF, respectively. Fluorescence ratio imaging made use of a GenIV-intensified Pentamax CCD camera and TILL Polychrome II monochromator (Till Photonics), with excitation at 340 and 390 nm for [Ca²⁺]_i and 440 and 490 nm for p*H*_i. Fluorescence was collected after passage through a 535- ± 20-nm bandpass filter and was corrected for background before loading. Dye loading was judged successful by visual checks for cytosolic dye distribution and by stabilization of the fluorescence signals (Grabov and Blatt, 1997; Garcia-Mata et al., 2003). Image analysis was carried out using MetaFluor and MetaMorph (version 6.3; Universal Imaging), and measurements were calibrated *in vitro* and *in vivo* after permeabilization (Grabov and Blatt,

1997). Surface areas of impaled guard cells were calculated assuming a spheroid geometry. Subsequent data analysis and curve fittings were carried out using Henry's EP suite and SigmaPlot 11 (Systat Software). Measurements in the guard cells were validated by acid loading with the weak acid butyrate and by raising $[Ca^{2+}]_i$ on exposures to high external Ca^{2+} concentration (Allen et al., 2001).

Current-voltage analysis and fittings were carried out using Henry's EP suite and SigmaPlot 11 (Systat Software). Currents were fitted by joint, non-linear least squares using a Boltzmann function of the form

$$I = \frac{g_{\max}(V - E_K)}{1 + e^{\delta F(V_{1/2} - V)/RT}} \quad (1)$$

where δ is the voltage sensitivity coefficient (gating charge), E_K is the K^+ equilibrium voltage, g_{\max} is the maximum conductance of the ensemble of channels, $V_{1/2}$ is the voltage yielding half-maximal activation, F is the Faraday constant, R is the universal gas constant, and T is the absolute temperature. Results are reported as means \pm SE of n observations, with significances tested using Student's t test and ANOVA. As appropriate, significance was also verified by multiple pairwise comparisons (Student-Neumann-Keuls method) at $P < 0.05$ unless otherwise indicated.

OnGuard Modeling

The OnGuard software and model was driven through a diurnal 12/12-h light/dark cycle as described previously (Chen et al., 2012b), and all model outputs were derived from this cycle. Model parameters (Hills et al., 2012) were adjusted to reflect the physical dimensions of the Arabidopsis stomatal complex, and transporter numbers were scaled accordingly. Light sensitivity was assigned solely to the plasma membrane H^+ -ATPase and Ca^{2+} -ATPase, the vacuolar VH^+ -ATPase, H^+ -pyrophosphatase, and Ca^{2+} -ATPase, and Suc synthesis in accordance with experimental observation (Chen et al., 2012b). All other model parameters were fixed, the properties of the individual transporters and buffering reactions thus responding only to changes in model variables arising from the kinetic features encoded in the model. The complete parameter set used to initiate modeling is provided in Supplemental Appendix S1, and the OnGuard software is available at www.psrsg.org.uk.

Supplemental Data

The following materials are available in the online version of this article.

Supplemental Figure S1. Macroscopic outputs from the OnGuard model.

Supplemental Figure S2. Chloride contents and analysis of Cl^- fluxes at the plasma membrane and tonoplast.

Supplemental Figure S3. Malic acid synthesis, total malate contents, and analysis of Mal fluxes at the plasma membrane and tonoplast.

Supplemental Figure S4. Cytosolic and vacuolar pH, and analysis of H^+ fluxes across the plasma membrane and tonoplast.

Supplemental Figure S5. Total H^+ distribution summed over a 24-h period.

Supplemental Figure S6. Total cytosolic and vacuolar Ca^{2+} concentration, $[Ca^{2+}]_i$, and analysis of Ca^{2+} fluxes across the plasma membrane and tonoplast.

Supplemental Figure S7. K^+ contents and analysis of K^+ fluxes at the plasma membrane and tonoplast.

Supplemental Table S1. Primers used for quantitative PCR analysis of transcript abundance.

Supplemental Appendix S1.

Supplemental References S1.

ACKNOWLEDGMENTS

We thank Jaakko Kangasjärvi (University of Helsinki) for seeds of the *slac1-1* mutant and *pSLAC1:SLAC1*-complemented lines as well as Christopher Grefen and Anna Amtmann (University of Glasgow) for comments during preparation of the manuscript.

Received September 20, 2012; accepted October 20, 2012; published October 22, 2012.

LITERATURE CITED

- Ache P, Becker D, Ivashikina N, Dietrich P, Roelfsema MRG, Hedrich R (2000) GORK, a delayed outward rectifier expressed in guard cells of *Arabidopsis thaliana*, is a K^+ -selective, K^+ -sensing ion channel. *FEBS Lett* **486**: 93–98
- Allen GJ, Chu SP, Harrington CL, Schumacher K, Hoffmann T, Tang YY, Grill E, Schroeder JI (2001) A defined range of guard cell calcium oscillation parameters encodes stomatal movements. *Nature* **411**: 1053–1057
- Amtmann A, Blatt MR (2009) Regulation of macronutrient transport. *New Phytol* **181**: 35–52
- Barbier-Brygoo H, De Angeli A, Filleul S, Frachisse JM, Gambale F, Thomine S, Wege S (2011) Anion channels/transporters in plants: from molecular bases to regulatory networks. *Annu Rev Plant Biol* **62**: 25–51
- Betts RA, Boucher O, Collins M, Cox PM, Falloon PD, Gedney N, Hemming DL, Huntingford C, Jones CD, Sexton DMH, et al (2007) Projected increase in continental runoff due to plant responses to increasing carbon dioxide. *Nature* **448**: 1037–1041
- Blatt MR (1987a) Electrical characteristics of stomatal guard cells: the contribution of ATP-dependent, "electrogenic" transport revealed by current-voltage and difference-current-voltage analysis. *J Membr Biol* **98**: 257–274
- Blatt MR (1987b) Electrical characteristics of stomatal guard cells: the ionic basis of the membrane potential and the consequence of potassium chloride leakage from microelectrodes. *Planta* **170**: 272–287
- Blatt MR (1988) Potassium-dependent bipolar gating of potassium channels in guard cells. *J Membr Biol* **102**: 235–246
- Blatt MR (1992) K^+ channels of stomatal guard cells: characteristics of the inward rectifier and its control by pH. *J Gen Physiol* **99**: 615–644
- Blatt MR (2000) Cellular signaling and volume control in stomatal movements in plants. *Annu Rev Cell Dev Biol* **16**: 221–241
- Blatt MR, Armstrong F (1993) K^+ channels of stomatal guard cells: abscisic acid-evoked control of the outward rectifier mediated by cytoplasmic pH. *Planta* **191**: 330–341
- Blatt MR, Gradmann D (1997) K^+ -sensitive gating of the K^+ outward rectifier in *Vicia* guard cells. *J Membr Biol* **158**: 241–256
- Blatt MR, Slayman CL (1983) KCl leakage from microelectrodes and its impact on the membrane parameters of a nonexcitable cell. *J Membr Biol* **72**: 223–234
- Chen ZH, Eisenach C, Xu XQ, Hills A, Blatt MR (2012a) Protocol: optimised electrophysiological analysis of intact guard cells from Arabidopsis. *Plant Methods* **8**: 15
- Chen ZH, Hills A, Bätz U, Amtmann A, Lew VL, Blatt MR (2012b) Systems dynamic modeling of the stomatal guard cell predicts emergent behaviors in transport, signaling, and volume control. *Plant Physiol* **159**: 1235–1251
- Chen ZH, Hills A, Lim CK, Blatt MR (2010) Dynamic regulation of guard cell anion channels by cytosolic free Ca^{2+} concentration and protein phosphorylation. *Plant J* **61**: 816–825
- De Angeli A, Monachello D, Ephritikhine G, Frachisse JM, Thomine S, Gambale F, Barbier-Brygoo H (2006) The nitrate/proton antiporter AtCLCa mediates nitrate accumulation in plant vacuoles. *Nature* **442**: 939–942
- Dettmer J, Hong-Hermesdorf A, Stierhof YD, Schumacher K (2006) Vacuolar H^+ -ATPase activity is required for endocytic and secretory trafficking in *Arabidopsis*. *Plant Cell* **18**: 715–730
- Dodd AN, Gardner MJ, Hotta CT, Hubbard KE, Dalchau N, Love J, Assie JM, Robertson FC, Jakobsen MK, Gonçalves J, et al (2007) The *Arabidopsis* circadian clock incorporates a cADPR-based feedback loop. *Science* **318**: 1789–1792
- Eamus D, Shanahan ST (2002) A rate equation model of stomatal responses to vapour pressure deficit and drought. *BMC Ecol* **2**: 8
- Eisenach C, Chen ZH, Grefen C, Blatt MR (2012) The trafficking protein SYP121 of Arabidopsis connects programmed stomatal closure and K^+ channel activity with vegetative growth. *Plant J* **69**: 241–251
- Fairley-Grenot K, Assmann SM (1991) Evidence for G-protein regulation of inward potassium ion channel current in guard cells of fava bean. *Plant Cell* **3**: 1037–1044

- Farquhar GD, Wong SC (1984) An empirical model of stomatal conductance. *Aust J Plant Physiol* **11**: 191–209
- Felle HH, Heppler PK (1997) The cytosolic Ca²⁺ concentration gradient of *Sinapis alba* root hairs as revealed by Ca²⁺-selective microelectrode tests and fura-dextran ratio imaging. *Plant Physiol* **114**: 39–45
- Garcia-Mata C, Gay R, Sokolovski S, Hills A, Lamattina L, Blatt MR (2003) Nitric oxide regulates K⁺ and Cl⁻ channels in guard cells through a subset of abscisic acid-evoked signaling pathways. *Proc Natl Acad Sci USA* **100**: 11116–11121
- Gedney N, Cox PM, Betts RA, Boucher O, Huntingford C, Stott PA (2006) Detection of a direct carbon dioxide effect in continental river runoff records. *Nature* **439**: 835–838
- Gobert A, Isayenkov S, Voelker C, Czempinski K, Maathuis FJM (2007) The two-pore channel TPK1 gene encodes the vacuolar K⁺ conductance and plays a role in K⁺ homeostasis. *Proc Natl Acad Sci USA* **104**: 10726–10731
- Grabov A, Blatt MR (1997) Parallel control of the inward-rectifier K⁺ channel by cytosolic-free Ca²⁺ and pH in *Vicia* guard cells. *Planta* **201**: 84–95
- Grabov A, Blatt MR (1998) Membrane voltage initiates Ca²⁺ waves and potentiates Ca²⁺ increases with abscisic acid in stomatal guard cells. *Proc Natl Acad Sci USA* **95**: 4778–4783
- Grabov A, Blatt MR (1999) A steep dependence of inward-rectifying potassium channels on cytosolic free calcium concentration increase evoked by hyperpolarization in guard cells. *Plant Physiol* **119**: 277–288
- Gutierrez L, Mauriat M, Guéin S, Pelloux J, Lefebvre JF, Louvet R, Rusterucci C, Moritz T, Guerinou F, Bellini C, et al (2008) The lack of a systematic validation of reference genes: a serious pitfall undervalued in reverse transcription-polymerase chain reaction (RT-PCR) analysis in plants. *Plant Biotechnol J* **6**: 609–618
- Hamilton DWA, Hills A, Kohler B, Blatt MR (2000) Ca²⁺ channels at the plasma membrane of stomatal guard cells are activated by hyperpolarization and abscisic acid. *Proc Natl Acad Sci USA* **97**: 4967–4972
- Haruta M, Sussman MR (2012) The effect of a genetically reduced plasma membrane proton motive force on vegetative growth of *Arabidopsis*. *Plant Physiol* **158**: 1158–1171
- Hills A, Chen ZH, Amtmann A, Blatt MR, Lew VL (2012) OnGuard, a computational platform for quantitative kinetic modeling of guard cell physiology. *Plant Physiol* **159**: 1026–1042
- Honsbein A, Sokolovski S, Grefen C, Campanoni P, Pratelli R, Paneque M, Chen ZH, Johansson I, Blatt MR (2009) A tripartite SNARE-K⁺ channel complex mediates in channel-dependent K⁺ nutrition in *Arabidopsis*. *Plant Cell* **21**: 2859–2877
- Hosy E, Vavasseur A, Mouline K, Dreyer I, Gaymard F, Porée F, Boucherez J, Lebaudy A, Bouchez D, Very A-A, et al (2003) The *Arabidopsis* outward K⁺ channel GORK is involved in regulation of stomatal movements and plant transpiration. *Proc Natl Acad Sci USA* **100**: 5549–5554
- Hoth S, Hedrich R (1999) Distinct molecular bases for pH sensitivity of the guard cell K⁺ channels KST1 and KAT1. *J Biol Chem* **274**: 11599–11603
- Jossier M, Kroniewicz L, Dalmás F, Le Thiec D, Ephritikhine G, Thomine S, Barbier-Brygoo H, Vavasseur A, Filleur S, Leonhardt N (2010) The *Arabidopsis* vacuolar anion transporter, AtCLC_c, is involved in the regulation of stomatal movements and contributes to salt tolerance. *Plant J* **64**: 563–576
- Lebaudy A, Vavasseur A, Hosy E, Dreyer I, Leonhardt N, Thibaud JB, Véry AA, Simonneau T, Sentenac H (2008) Plant adaptation to fluctuating environment and biomass production are strongly dependent on guard cell potassium channels. *Proc Natl Acad Sci USA* **105**: 5271–5276
- Lopez-Marques RL, Schiott M, Jakobsen MK, Palmgren MG (2004) Structure, function and regulation of primary H⁺ and Ca²⁺ pumps. In MR Blatt, ed, *Membrane Transport in Plants*, Vol 15. Blackwell, Oxford, pp 72–104
- McAinsh MR, Pittman JK (2009) Shaping the calcium signature. *New Phytol* **181**: 275–294
- McLaughlin SGA, Dilger JP (1980) Transport of protons across membranes by weak acids. *Physiol Rev* **60**: 825–863
- Meharg AA, Blatt MR (1995) NO₃⁻ transport across the plasma membrane of *Arabidopsis thaliana* root hairs: kinetic control by pH and membrane voltage. *J Membr Biol* **145**: 49–66
- Nakamura RL, McKendree WL Jr, Hirsch RE, Sedbrook JC, Gaber RF, Sussman MR (1995) Expression of an *Arabidopsis* potassium channel gene in guard cells. *Plant Physiol* **109**: 371–374
- Negi J, Matsuda O, Nagasawa T, Oba Y, Takahashi H, Kawai-Yamada M, Uchimiya H, Hashimoto M, Iba K (2008) CO₂ regulator *SLAC1* and its homologues are essential for anion homeostasis in plant cells. *Nature* **452**: 483–486
- Peiter E, Maathuis FJM, Mills LN, Knight H, Pelloux J, Hetherington AM, Sanders D (2005) The vacuolar Ca²⁺-activated channel TPC1 regulates germination and stomatal movement. *Nature* **434**: 404–408
- Pilot G, Lacombe B, Gaymard F, Cherel I, Boucherez J, Thibaud JB, Sentenac H (2001) Guard cell inward K⁺ channel activity in *Arabidopsis* involves expression of the twin channel subunits KAT1 and KAT2. *J Biol Chem* **276**: 3215–3221
- Rasband WS, Bright DS (1995) NIH IMAGE: a public domain image-processing program for the Macintosh. *Microbeam Anal* **4**: 137–149
- Sanders D, Hopgood M, Jennings IR (1989) Kinetic response of H⁺-coupled transport to extracellular pH: critical role of cytosolic pH as a regulator. *J Membr Biol* **108**: 253–261
- Schachtman DP, Schroeder JI, Lucas WJ, Anderson JA, Gaber RF (1992) Expression of an inward-rectifying potassium channel by the *Arabidopsis* KAT1 cDNA. *Science* **258**: 1654–1658
- Schroeder JI, Allen GJ, Hugouvieux V, Kwak JM, Waner D (2001) Guard cell signal transduction. *Annu Rev Plant Physiol Plant Mol Biol* **52**: 627–658
- Siegel RS, Xue SW, Murata Y, Yang YZ, Nishimura N, Wang A, Schroeder JI (2009) Calcium elevation-dependent and attenuated resting calcium-dependent abscisic acid induction of stomatal closure and abscisic acid-induced enhancement of calcium sensitivities of S-type anion and inward-rectifying K channels in *Arabidopsis* guard cells. *Plant J* **59**: 207–220
- Speksnijder JE, Miller AL, Weisenseel MH, Chen T-H, Jaffe LF (1989) Calcium buffer injections block fucooid egg development by facilitating calcium diffusion. *Proc Natl Acad Sci USA* **86**: 6607–6611
- Vahisalu T, Kollist H, Wang YF, Nishimura N, Chan WY, Valerio G, Lamminmäki A, Brosché M, Moldau H, Desikan R, et al (2008) *SLAC1* is required for plant guard cell S-type anion channel function in stomatal signalling. *Nature* **452**: 487–491
- Wang Y, Blatt MR (2011) Anion channel sensitivity to cytosolic organic acids implicates a central role for oxaloacetate in integrating ion flux with metabolism in stomatal guard cells. *Biochem J* **439**: 161–170

Clustering of the K⁺ channel GORK of Arabidopsis parallels its gating by extracellular K⁺

Cornelia Eisenach[†], Maria Papanatsiou, Ellin-Kristina Hillert and Michael R. Blatt^{*}

Laboratory of Plant Physiology and Biophysics, Institute of Molecular, Cell and Systems Biology, University of Glasgow, Bower Building, Glasgow G12 8QQ, UK

Received 10 November 2013; revised 18 January 2014; accepted 22 January 2014; published online 12 February 2014.

^{*}For correspondence (e-mail Michael.Blatt@glasgow.ac.uk).

[†]Present address: Institute of Plant Biology, University of Zurich, CH-8008 Zurich, Switzerland.

SUMMARY

GORK is the only outward-rectifying Kv-like K⁺ channel expressed in guard cells. Its activity is tightly regulated to facilitate K⁺ efflux for stomatal closure and is elevated in ABA in parallel with suppression of the activity of the inward-rectifying K⁺ channel KAT1. Whereas the population of KAT1 is subject to regulated traffic to and from the plasma membrane, nothing is known about GORK, its distribution and traffic *in vivo*. We have used transformations with fluorescently-tagged GORK to explore its characteristics in tobacco epidermis and Arabidopsis guard cells. These studies showed that GORK assembles in puncta that reversibly dissociated as a function of the external K⁺ concentration. Puncta dissociation paralleled the gating dependence of GORK, the speed of response consistent with the rapidity of channel gating response to changes in the external ionic conditions. Dissociation was also suppressed by the K⁺ channel blocker Ba²⁺. By contrast, confocal and protein biochemical analysis failed to uncover substantial exo- and endocytotic traffic of the channel. Gating of GORK is displaced to more positive voltages with external K⁺, a characteristic that ensures the channel facilitates only K⁺ efflux regardless of the external cation concentration. GORK conductance is also enhanced by external K⁺ above 1 mM. We suggest that GORK clustering in puncta is related to its gating and conductance, and reflects associated conformational changes and (de)stabilisation of the channel protein, possibly as a platform for transmission and coordination of channel gating in response to external K⁺.

Keywords: GORK K⁺ channel – outward-rectifying, membrane vesicle traffic, plasma membrane, confocal microscopy, K⁺ concentration – extracellular, channel gating – K⁺-dependent, Arabidopsis.

INTRODUCTION

Control of membrane transport is central to solute flux for stomatal regulation. Membrane transport of the predominant, osmotically-active ion, K⁺, is of particular importance and is mediated largely by voltage-dependent K⁺ channels. Inward-rectifying K⁺ channels mediate K⁺ uptake during stomatal opening, while outward-rectifying K⁺ channels mediate its loss during stomatal closing (Blatt and Thiel, 1993; Blatt, 2000; Lebaudy *et al.*, 2007; Dreyer and Blatt, 2009). In Arabidopsis, the former are dominated by the inward-rectifying K⁺ channel KAT1, which is highly-expressed in guard cells, and to a lesser extent the related channel KAT2. K⁺ efflux across the plasma membrane is facilitated by GORK, which is the only outward rectifying K⁺ -channel known to be expressed in the guard cells (Ache *et al.*, 2000; Hosy *et al.*, 2003; Dreyer and Blatt, 2009).

KAT1 and GORK belong to the Kv superfamily of voltage-gated ion channels that are found also in archaea, insects and mammals. These channels open and close, a process referred to as 'gating', in response to membrane voltage. Outward-rectifying K⁺ channels of plants, including GORK, also gate in response to the extracellular K⁺ concentration. Increasing the extracellular K⁺ concentration displaces the voltage-dependence of gating to more positive voltages in parallel with the equilibrium voltage for K⁺ (E_K) and, at concentrations above 1 mM, increases the maximum ensemble conductance (Blatt, 1988; Blatt and Gradmann, 1997; Ache *et al.*, 2000; Johansson *et al.*, 2006). Potassium is the most abundant ionic species in plants; its concentration outside, and its equilibrium, often dominates the membrane voltage in plants. Gating by extracellular K⁺ therefore ensures that these channels activate at a voltage

relative to E_K and adjusts K^+ efflux through the channels in a compensatory manner across a wide range of K^+ concentrations (Blatt, 1988; Blatt and Gradmann, 1997).

The activities of guard cell K^+ channels are subject to a number of regulatory stimuli, including hormones such as abscisic acid (ABA) (Blatt, 2000; Blatt *et al.*, 2007; Kim *et al.*, 2010; Roelfsema and Hedrich, 2010), auxin (Thiel *et al.*, 1993; Blatt and Thiel, 1994; Baulny *et al.*, 2000), metabolites (Hedrich *et al.*, 2001; Wang and Blatt, 2011), and pathogen elicitors (Blatt *et al.*, 1999). Many of these stimuli act through intermediates of cytosolic-free $[Ca^{2+}]_i$, pH and protein (de-)phosphorylation (Blatt *et al.*, 1990; Blatt and Grabov, 1999; Blatt, 2000; Kim *et al.*, 2010). Channel responses to these intermediates are usually very rapid and are underpinned by changes in channel gating, but over longer time periods can extend to membrane vesicle traffic and changes in channel population at the membrane. Much less is known of the scope of channel regulation by vesicle traffic or its regulation. To date, only the KAT1 K^+ channel has been studied in any detail (Hurst *et al.*, 2004; Meckel *et al.*, 2005; Sutter *et al.*, 2006, 2007; Eisenach *et al.*, 2012). KAT1 is localised at the plasma membrane in punctate domains from which ABA and $[Ca^{2+}]_i$ trigger its endocytosis. Its recycling to the plasma membrane depends on the vesicle-trafficking protein SYP121 (=SYR1/PEN1) (Leyman *et al.*, 1999) and underpins the phenomenon of so-called 'programmed closure' of stomata (Eisenach *et al.*, 2012). By contrast, nothing is known of the localisation, distribution and trafficking of the outward-rectifying K^+ channels, including GORK. Here we show that GORK is localised in discrete puncta at the plasma membrane that are similar to, but distinct from, those reported previously for KAT1-GFP. Unexpectedly, GORK-GFP puncta proved to be insensitive to ABA or the presence of SYP121, but channel distribution was affected by increasing external K^+ concentrations in parallel with the dependence of channel gating on the cation. We propose that the gating of GORK with external K^+ concentration is associated with a re-organisation of the channel proteins in clusters within the plane of the plasma membrane.

RESULTS

GORK-GFP is a functional outward rectifying K^+ channel that localises in puncta

We generated GORK-GFP constructs for expression under the control of the Ubiquitin-10 gene promoter to give moderate over-expression *in vivo* (Grefen *et al.*, 2010b) and verified functionality of the recombinant protein after expression in *Xenopus* oocytes. Oocytes injected with GORK-GFP cRNA showed an outward current (Figure S1) when clamped to voltages positive of E_K , with current relaxations typical of the GORK channel and block by TEA⁺ (Figure S2). Relative conductances (G/G_{max}) were

well-fitted to a Boltzmann function (see Figure S1) with a half-maximal activation voltage ($V_{1/2}$) that was displaced in parallel with E_K , much as has previously been shown for GORK (Ache *et al.*, 2000), the outward-rectifier of *Vicia* (Blatt, 1988; Blatt and Gradmann, 1997) and for SKOR, the close homolog of the GORK K^+ channel (Johansson *et al.*, 2006).

We generated stable transformants with GORK-GFP in wild-type Arabidopsis and in the *syp121* mutant that lacks the vesicle-trafficking (SNARE) protein SYP121 (=SYR1/PEN1) (Leyman *et al.*, 1999) and is known to affect K^+ channel traffic and function (Honsbein *et al.*, 2009; Grefen *et al.*, 2010a; Eisenach *et al.*, 2012). Leaves of T_2 and T_3 lines from three independent transformation events were selected; in every case GORK-GFP fluorescence appeared in puncta around the cell periphery (Figure 1), both in wild-type and *syp121* mutant backgrounds. Fluorescence was detected in epidermal cells and guard cells (Figure 1a), distinct from chloroplast fluorescence (Figure 1b), and was localised to the cell periphery (Figure 1c–j). Intracellular GORK-GFP signals were observed in 7% ($n = 72$) of stomata, mostly in very young, developing tissue. Analysis of puncta size yielded diameters of $0.63 \pm 0.01 \mu\text{m}$ ($n = 97$) that were normally distributed and well-removed from the diffraction limit near 300 nm (Figure 1k). These dimensions compare favourably with the mean diameter of $0.5 \mu\text{m}$ observed for microdomains formed by KAT1-GFP in tobacco (Sutter *et al.*, 2006). Although similar in size and distribution, the puncta formed by RFP-tagged GORK did not co-localize (Figures S3 and S4) with puncta formed by the GFP-tagged KAT1 K^+ channel (Sutter *et al.*, 2006, 2007). When expressed in tobacco, fluorescence was occasionally observed within epidermal cells; nonetheless, after plasmolysis GORK-GFP fluorescence was observed in Hechtian strands (Figure S5, arrows), indicating that the punctate structures were localised to the plasma membrane.

GORK-GFP puncta are sensitive to the external KCl concentration

KAT1-GFP is internalised from the plasma membrane following application of ABA (Sutter *et al.*, 2007), and by treatments known to elevate $[Ca^{2+}]_i$ (Grabov and Blatt, 1998), studies showing its recycling by SYP121-mediated traffic underpins programmed stomatal closure (Leyman *et al.*, 1999; Eisenach *et al.*, 2012). We used the treatments to elevate $[Ca^{2+}]_i$, anticipating that GORK traffic would complement that of the KAT1 channel. Intact leaves were incubated for 2 h under light after infiltration with Depolarising Buffer (DB) containing 100 mM KCl and 0 CaCl₂ to open stomata, and stomatal closure was induced by exchange with Hyperpolarising Buffer (HB) containing 0.1 mM KCl and 10 mM CaCl₂ (Eisenach *et al.*, 2012). We found that GORK-GFP did not internalise following HB treatment, unlike KAT1 (Eisenach *et al.*, 2012). Instead, the

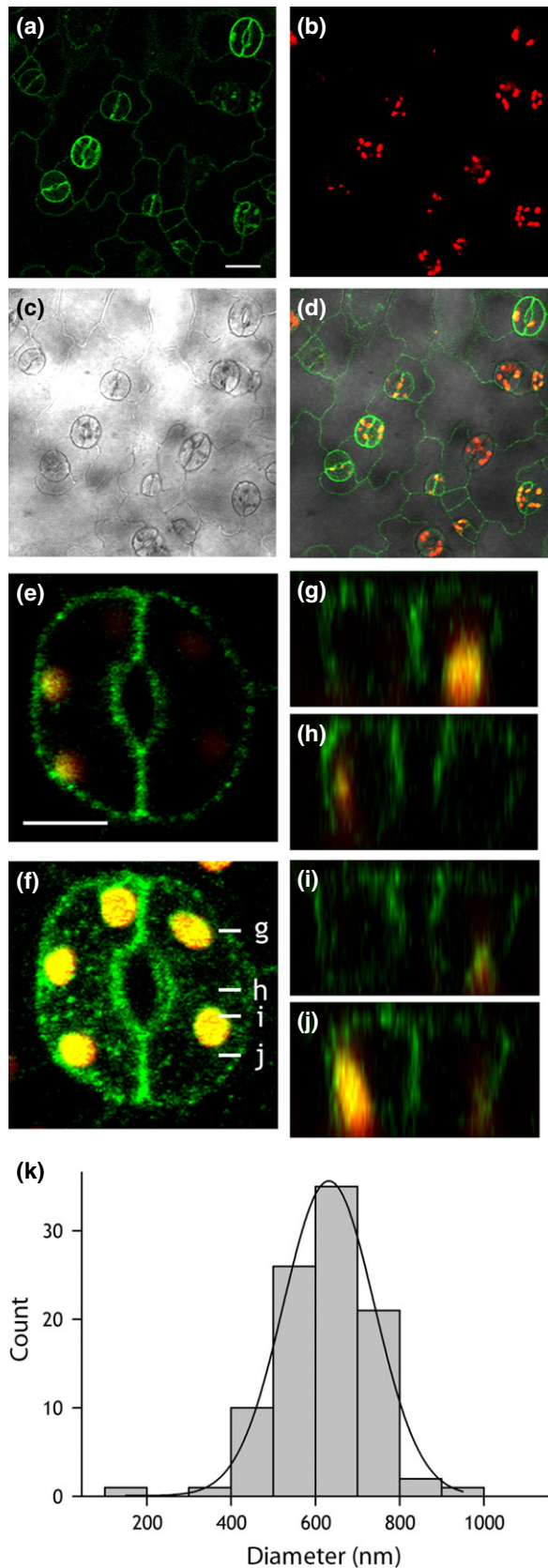


Figure 1. GORK localises in puncta at the periphery of Arabidopsis guard cells and epidermal cells.

(a–d) Confocal fluorescence images of GORK-GFP (green, a), chlorophyll fluorescence (red, b), bright field (c) and the corresponding overlay image (d) from the epidermis of an Arabidopsis leaf expressing *pUBQ10::GORK-GFP*. Scale bar, 20 μm .

(e) Lateral optical section through a single pair of Arabidopsis guard cells showing punctate distribution of GORK-GFP (green) and chloroplasts (yellow). Scale bar, 5 μm .

(f) 3D projection of the same guard cell pair in (e) reconstructed from a z-stack collected at intervals of 0.8 μm .

(g–j) Z-plane sections derived from (f) at the positions indicated by white lines in (f).

(k) Histogram analysis of the diameters of GORK-GFP puncta. Data were fitted to a gaussian function (solid line), indicating a normal distribution of diameters about a mean of 632 ± 1 nm.

punctate distribution of GORK-GFP was lost in DB, the fluorescence redistributing around the cell periphery. This process was fully reversible on transfer back to HB and was evident in both wild-type and *syp121* mutant Arabidopsis. However, treatments with ABA had no effect on GORK-GFP distribution (Figures S6 and S7). We reasoned that the changes in the punctate distribution observed between DB and HB were likely to be related to the ionic content of the buffer rather than to Ca^{2+} or ABA signalling *per se*. We repeated the experiment with solutions of 100 mM KCl and 0.1 mM KCl alone. Again, we found, GORK-GFP puncta were clearly visible in 0.1 mM KCl (Figure 2a,b) but, in the

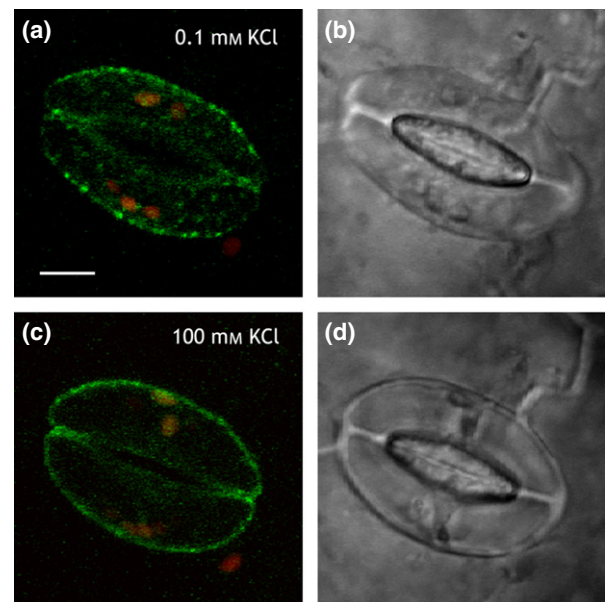


Figure 2. GORK-GFP fluorescence is punctate in 0.1 mM KCl, but is diffuse in 100 mM KCl.

GORK-GFP fluorescence (a, c) and brightfield images (b, d) in a pair of guard cells in 0.1 mM KCl (a, b) and after transfer to 100 mM KCl (c, d). Scale bar, 5 μm . Images in (a) and (c) are overlaid, 3D projections of GORK-GFP (green) and chloroplast (red) fluorescence from z-stacks taken at intervals of 0.7 μm . Equivalent results were obtained with Hyperpolarising and Depolarising Buffers (see text).

same guard cells, the punctate distribution was lost when the external KCl concentration was raised to 100 mM (Figure 2c,d). To exclude an effect of osmotic strength, we repeated these experiments with 0.1 mM KCl including Mannitol to adjust the osmotic strength to that of the 100 mM KCl (200 ± 10 mOsmol). No difference in GORK-GFP distribution was observed between treatments with and without mannitol, thus excluding osmotic effects as the explanation for the changing GORK-GFP distribution.

GORK-GFP redistribution is not associated with endocytic traffic

The dissolution of KAT1 puncta is marked by a substantial increase in mobility and endocytosis of the channels (Sutter *et al.*, 2007; Eisenach *et al.*, 2012). To determine whether GORK-GFP dispersal was similarly associated with endocytosis from the plasma membrane, we first examined the mobility of GORK-GFP by time-lapse and by fluorescence recovery after photobleaching (FRAP) analysis. Figure 3 illustrates one of eight independent time-lapse experiments with GORK-GFP puncta identified at the stomatal surface in tangential scans (Figure 3a,b). Kymographic analysis (Figure 3c) yielded no evidence of lateral movement. We used FRAP analysis in *Arabidopsis* to determine the recovery of fluorescence at the cell periphery, calculating the mobile fraction of GORK-GFP fluorescence from the signal recovery. GORK-GFP was photobleached locally at the periphery of guard cells preincubated in 0.1 and 100 mM KCl, and its recovery within the photobleached regions was monitored. Figure 3(d) summarizes the result of 12 independent experiments. FRAP analysis yielded similar results in 0.1 and 100 mM KCl: fluorescence recovered with a mean half-time of 36 ± 4 sec in 0.1 mM KCl and 28 ± 7 sec in 100 mM KCl, a difference that was not significant at the $P < 0.05$ level. Additionally, in both KCl concentrations the GORK-GFP signal was predominantly non-mobile, with a mobile fraction of $9 \pm 1\%$ in 100 mM KCl and of $14 \pm 6\%$ in 0.1 mM KCl. Again, the difference was not statistically significant at the $P < 0.05$ level.

We used aqueous, two-phase partitioning as an independent test for GORK redistribution between the plasma membrane and endomembranes, including endocytotic vesicles (Sutter *et al.*, 2006, 2007; Honsbein *et al.*, 2009). GORK polyclonal antibodies were raised against a synthetic peptide corresponding to a GORK-specific N-terminal amino-acid sequence (Figure S8). The antibodies were purified and verified for specificity in detecting GORK after immunoblotting. Figure 4(a) shows an immunoblot of soluble (S) and microsomal (M) protein fractions probed with α GORK antibody and the pre-immune serum. The antibody detected a band near the 80 kDa marker in the microsomal protein fraction and close to the 93.8 kDa predicted for GORK. Analysis of microsomal proteins extracts from

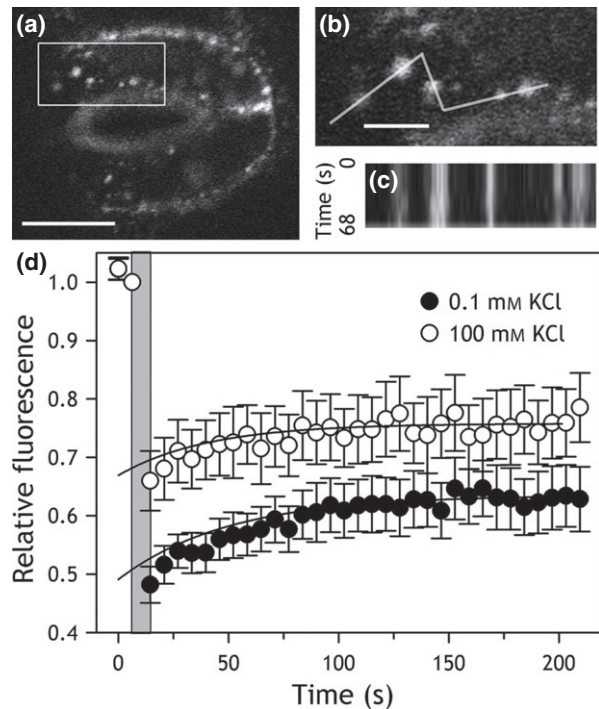


Figure 3. The macroscopic mobility of GORK-GFP at the cell periphery is not affected by extracellular KCl concentration.

(a) Tangential section of a guard cell pair with GORK-GFP puncta in 0.1 mM KCl. Scale bar, 5 μ m.
 (b) Close-up of the boxed region in (a) with the linescan for kymographic analysis as indicated. Scale bar, 2 μ m.
 (c) Kymograph over the linescan in (b) collected over a time interval of 68 sec. The x-axis corresponds to the linescan dimension and the y-axis corresponds to time. The analysis shows that GORK-GFP is positionally stable over this time period.
 (d) Fluorescence recovery after photobleaching (FRAP) of the GORK-GFP recorded from guard cells in 0.1 mM KCl (closed circles, $n = 12$) and in 100 mM KCl (open circles, $n = 11$). Fluorescence was normalized to the signals at the start of the experiments after correcting for fluorescence decay (Sutter *et al.*, 2006, 2007) and fluorescence recoveries after the photobleaching period (grey) were fitted to a single exponential function (solid lines) to derive half-times and amplitudes for recovery.

wild-type plants, a transgenic GORK-GFP overexpressing line probed with α GFP antibody, and the *gork* mutant confirmed this band as the GORK protein (Figure 4b).

We separated plasma membrane and endomembrane fractions after pretreatments of leaf tissues with 0.1 and 100 mM KCl. Figure 4(c) shows an immunoblot of plasma membrane and endomembrane protein fractions from one of two independent experiments, each yielding similar results. Equal loading between samples of plasma and of endomembrane fractions was verified by Ponceau staining and purity was confirmed by probing against the plasma membrane marker AHA3 (Pardo and Serrano, 1989) and the endomembrane marker Sec61 (Yuasa *et al.*, 2005). GORK bands of comparable intensity were observed in plasma membrane fractions irrespective of pretreatments with 0.1 and 100 mM KCl (Figure 4c, left). GORK bands

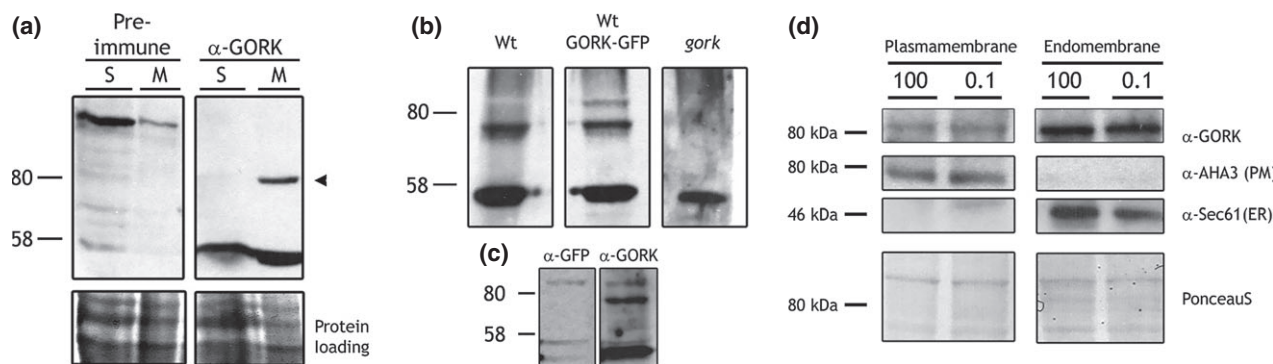


Figure 4. α GORK antibody raised to an N-terminal peptide shows no substantial redistribution of the K⁺ channel between plasma membrane and endomembranes in Arabidopsis.

(a) Immunoblot (top) and Ponceau S stain (bottom) of wild-type Arabidopsis soluble (S) and microsomal (M) protein fractions, probed either with pre-immune serum (*left*) and with the purified α GORK antibody (*right*). The α GORK antibody uniquely detected a single band around 80 kDa in the microsomal fraction (*arrowhead, right*).

(b) Immunoblot of Arabidopsis microsomal fractions from wild type (Wt), a transgenic line expressing GORK-GFP (GORK-GFP), and the *gork* null mutant. Note the double band in the GORK-GFP fraction corresponds to endogenous GORK and recombinant GORK-GFP. The 80 kDa band is missing from the *gork* mutant. The lower intensity of the GORK-GFP band probably is a consequence of co-suppression of the transgene.

(c) Immunoblot of Arabidopsis microsomal fractions from a transgenic line expressing GORK-GFP and probed with α GFP antibody. Note that the antibody detects a specific band above 80 kDa. An additional band is evident on stripping and re-probing with α GORK antibody, consistent with the presence of the native channel.

(d) Endogenous GORK is not affected by the external buffer or KCl concentration.

Immunoblot and PonceauS stain of plasma membrane and endomembrane protein fractions from aqueous two-phase partitioning of Arabidopsis leaves pre-treated with either 0.1 or 100 mM KCl (0.1 and 100, *indicated above*). Molecular weights (*left*) and staining or antibody used for detection (*right*) are indicated. PonceauS stain of the membrane (*bottom*) shows equal protein loading within each gel. The membrane was probed with α GORK antibody (α GORK) before stripping and re-probing, first with an antibody against the plasma membrane H⁺-ATPase AHA3 (α AHA3), and an antibody against the ER-localised translocon Sec61 (α Sec61).

were also detected in the endomembrane fractions (Figure 4c, *right*). An absolute comparison with the plasma membrane fractions is not possible, because of differences in total protein, but a ratiometric comparison between treatments showed little difference in relative distributions. The band density ratios for GORK between plasma membrane fractions in 0.1 and 100 mM KCl yielded values of 1.3 in the first experiment and 1.1 in the second. Thus, KCl treatments did not have a major effect on GORK distribution to the plasma membrane, indicating that vesicle traffic to and from the plasma membrane was unlikely to contribute appreciably to the changes observed in GORK-GFP distribution *in vivo*.

GORK redistribution is fast and mirrors alkali cation-dependent channel gating

We analysed the time-course of puncta dispersal, expressing GORK in tobacco epidermis which showed the same reversible formation of puncta and simplified manipulations. Transformed leaf sections were infiltrated with 0.1 mM KCl and images collected before one half of the sections were re-infiltrated with 100 mM KCl. Samples were randomised and images were collected and analysed in blind assays following the second infiltration. The numbers of cells showing punctate distributions were assessed and then normalised to the measurements prior to the second infiltration. Figure 5 summarises these data with images

collected before (a,c) and after (b,d) infiltration with 100 mM KCl, and shows a rapid decrease in the percentage of cells showing puncta, the count dropping to approximately 40% (Figure 5e) within 10 min of treatments. Exponential fittings yielded a halftime of 2.4 ± 0.5 min for the response. This analysis overestimates the halftime, as the experiments do not take into account the K⁺ diffusion time across the cell wall which can slow diffusion by a factor of 10^{-2} to 10^{-4} (Canny, 1990). Assuming a 10^{-3} -fold decrease, for K⁺ the effect implies a diffusion coefficient of 6.10^{-9} cm² sec⁻¹ and an increase in the root mean square time for bulk diffusion across the 2 μ m of cell wall to 100–200 sec (Hille, 2001), roughly equivalent to the time for GORK-GFP puncta dispersal. These values contrast with the dispersion of KAT1-GFP puncta during endocytosis (Sutter *et al.*, 2007), which displayed a halftime of 10–12 min and was complete only after 40–60 min following ABA treatments. The comparison supports our earlier observations indicating that the redistribution of GORK-GFP is not associated with endocytosis.

The gating of GORK, and its homologs in *Vicia* and tobacco, responds over a similar time course to changes in alkali cation concentrations, including Cs⁺ (Blatt, 1988; Armstrong *et al.*, 1995; Blatt and Gradmann, 1997; Blatt *et al.*, 1999; Baulny *et al.*, 2000). We examined whether the distribution GORK in puncta was sensitive to the K⁺ or to the Cl⁻ concentration, and whether it showed ionic

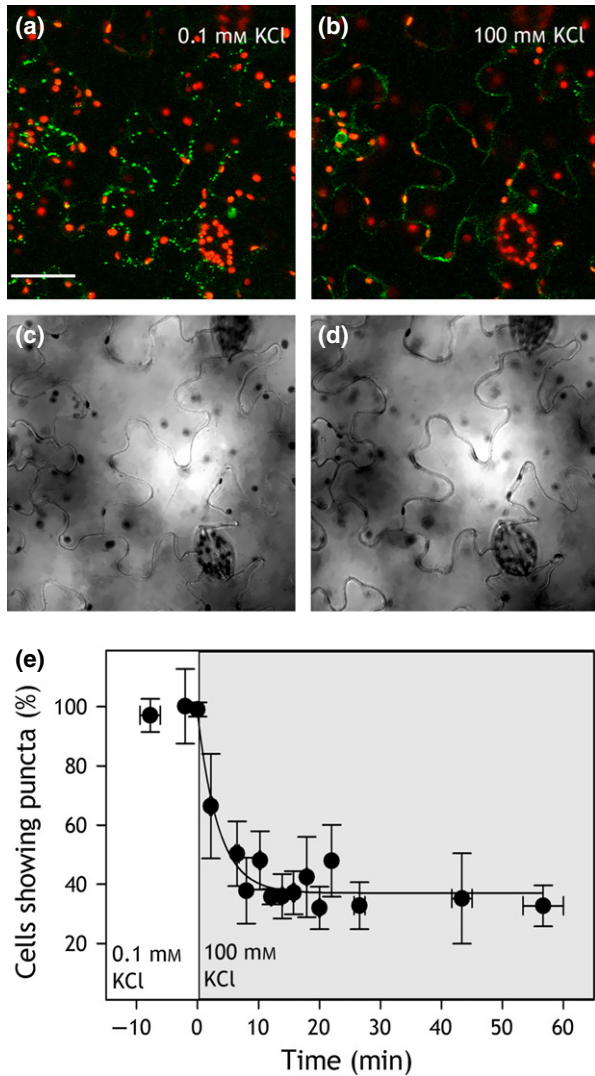


Figure 5. GORK-GFP puncta disperse rapidly on transfer to 100 mM KCl. (a–d) Confocal images (a, b) of GORK-GFP (green) and chloroplast fluorescence (red) expressed in tobacco epidermal cells with corresponding bright field (c, d) images collected in 0.1 mM KCl (a, c) and 30 min after transfer to 100 mM KCl (b, d) showing conversion from punctate to diffuse distribution of the channel. Scale bar, 50 μ m. (e) The percentage of transformed tobacco cells displaying GORK-GFP puncta as a function of time on transfer from 0.1 to 100 mM KCl (grey). Data are means \pm SE of $n \geq 5$ independent experiments and were fitted by non-linear least-squares to an exponential decay function of time (solid line).

sensitivities similar to those of gating. Experiments were carried out as before with pre-infiltrations of 0.1 mM KCl, but with either 100 mM KNO_3 or 50 mM MgCl_2 in the second infiltration. Leaf sections were examined for GORK-GFP distribution after 20 min. The results (Figure 6a) showed a similar decrease in punctate frequency to $45 \pm 10\%$ in leaf sections treated with 100 mM KNO_3 but not with 50 mM MgCl_2 . To avoid the ‘digitizing’ effect of counting cells, we also quantified GORK distribution by

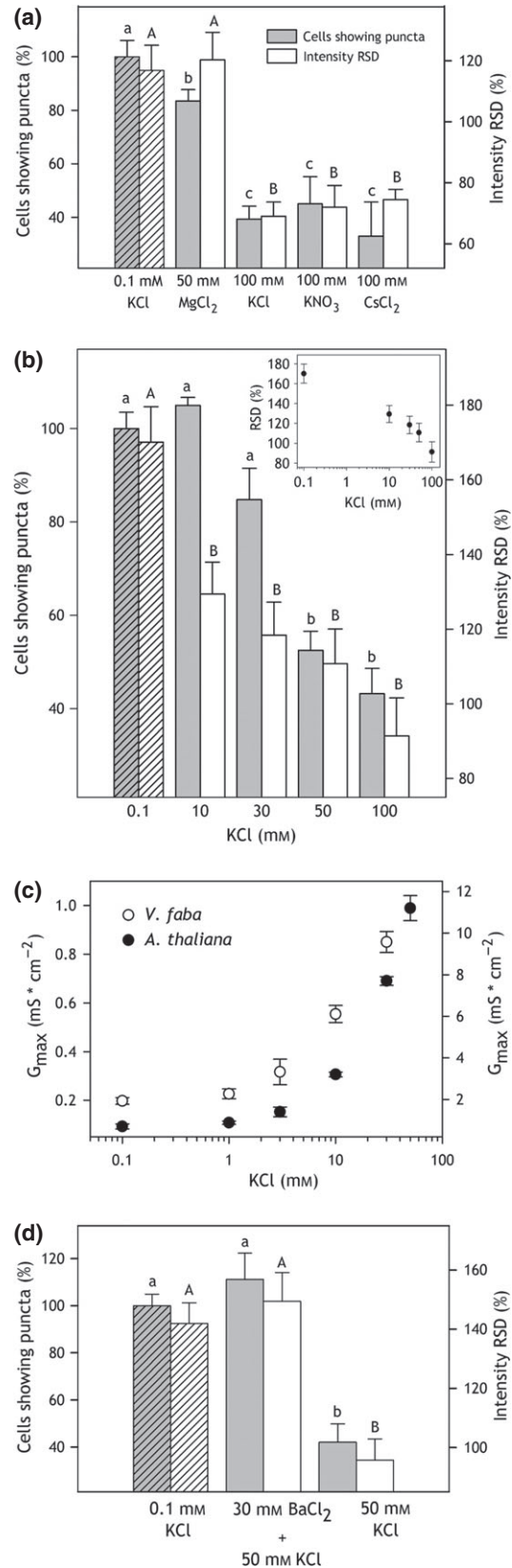


Figure 6. GORK-GFP dispersion is subject to K⁺, not Cl⁻, is equally sensitive to K⁺ substitution with Cs⁺, and is suppressed by pretreatment with the channel blocker Ba²⁺.

(a) Quantification of GORK-GFP puncta in 0.1 mM KCl (diagonal shading) and after treatment with 100 mM KCl, 100 mM KNO₃, 50 mM MgCl₂ and 100 mM CsCl. Punctate distribution was analysed by two methods. The left ordinate and grey bars represent the percentage of cells showing puncta in any one image. The right ordinate and white bars represent the relative standard deviation (RSD) of intensities determined from a 1-pixel-wide line around the periphery of cells and normalized to the intensity means. Data are means ±SE of *n* > 9 independent experiments for each treatment.

(b) Percentage of cells showing GORK-GFP puncta (left ordinate, grey bars) and the intensity SD (right ordinate, white bars) in 0.1 mM KCl (diagonal shading) and after treatment with 10, 30, 50 and 100 mM KCl. Data are means ±SE of *n* > 6 independent for each treatment. *Inset:* Intensity RSD as a function of [KCl] outside plotted on a logarithmic scale.

(c) Maximum ensemble conductance of GORK in Arabidopsis guard cells (filled circles) and the homologous, outward-rectifying K⁺ current in *Vicia* guard cells (open circles) as a function of [K⁺] outside. Data are derived and replotted as means ± SE from prior publications [see (Blatt, 1988; Thiel and Blatt, 1991; Thiel *et al.*, 1992; Blatt and Gradmann, 1997; Brearley *et al.*, 1997; Blatt *et al.*, 1999; Leyman *et al.*, 1999; Sokolovski and Blatt, 2004; Chen *et al.*, 2012; Wang *et al.*, 2012)].

(d) Percentage of cells showing GORK-GFP puncta (left ordinate, grey bars) and the normalized relative standard deviation in intensity (RSD; right ordinate, white bars) in 0.1 mM KCl (diagonal shading), after 30 min pretreatment with 30 mM of the K⁺ channel blocker BaCl₂, and after addition of 50 mM KCl to the 30 mM BaCl₂-treated samples. Data are means ±SE of *n* = 5 independent experiments. Significance at *P* < 0.05 was analysed by ANOVA and pair-wise multiple comparison and are indicated in each case by lettering for the percentage of cells showing puncta (small letters) and RSD (capital letters).

analysis of the relative standard deviations (RSD) in fluorescence intensity around the periphery of the cells. This approach yielded the same pattern in K⁺ dependence. As a further test, we also replaced the KCl solution with 100 mM CsCl. Again, these substitutions gave a punctate distribution of 33 ± 12% and a corresponding decrease in RSD, similar to that 100 mM KCl. We challenged leaf sections with different K⁺ concentrations for comparison with GORK channel gating. Leaf disks were pretreated as before, then split for blind image acquisition and the section fragments re-infiltrated with 0.1, 10, 30, 50 and 100 mM KCl. The results (Figure 6b) showed that the percentage of cells with puncta decreased progressively with increasing KCl concentrations above 10 mM, although a statistical analysis belies the trend. This pattern is similar to that of the ensemble conductance maximum (*G*_{max}) observed for the outward-rectifying K⁺ channels in both *Vicia* and Arabidopsis guard cells (Figure 6c). Quantified by RSD, the effect of KCl concentration is evident across the entire concentration range. Finally, we tested whether the K⁺ channel blocker Ba²⁺ (Armstrong and Taylor, 1980; Roelfsema and Prins, 1997; Romano *et al.*, 1998; Hamilton *et al.*, 2000) might affect the distribution of GORK-GFP. In this case, leaf disks were pretreated with 0.1 mM KCl and split as before, one half of each disk then re-infiltrated either with 50 mM KCl or first with 30 mM BaCl₂ and, after 30 min, with 30 mM BaCl₂ plus 50 mM KCl. Figure 6c shows that infiltrating with

BaCl₂ was sufficient to prevent the dispersal of the GORK puncta. These findings indicate a close association between GORK gating and the distribution of GORK-GFP in puncta and we return to the observations below.

DISCUSSION

Only recently has attention in channel regulation turned to the traffic of ion channel proteins and to changes in the population of ion channels active at the plasma membrane. Notable among the few studies in plants is the ABA-evoked endocytosis of the KAT1 K⁺ channel, its slower recycling to the plasma membrane (Sutter *et al.*, 2007), and a role for the vesicle-trafficking protein SYP121 in recovery from programmed closure of guard cells (Eisenach *et al.*, 2012). Until now, no information has been forthcoming relating to the traffic of GORK, the major outward-rectifying K⁺ channel that facilitates K⁺ efflux during stomatal closure in Arabidopsis, although changes in ensemble channel conductance and the voltage-dependence of gating are known for these and homologous outward-rectifying channels (Blatt, 1990, 1992; Thiel *et al.*, 1992). We anticipated these effects on GORK current might result from channel traffic, but the studies outlined above contradict this expectation. Here we report that the GORK K⁺ channel, like KAT1, appears in discrete puncta at the guard cell periphery. These clusters form independently of the structures assembled by KAT1 (Meckel *et al.*, 2004; Sutter *et al.*, 2006, 2007) and are not affected by ABA, but form and disperse reversibly with external K⁺ concentration. Three additional lines of evidence associate GORK puncta and their dispersal with short-term changes in channel gating and conductance, rather than with channel traffic. (i) The mobility of GORK-GFP was unaffected by ABA, nor was it altered between the punctate and dispersed forms of the channel. (ii) Two-phase partitioning experiments yielded no substantial difference in membrane distribution between punctate and dispersed forms of the channel, unlike KAT1 (Sutter *et al.*, 2007; Eisenach *et al.*, 2012). (iii) Dispersal of the GORK puncta was rapid and demonstrably sensitive to extracellular cations, paralleling gating and block in these channels. We suggest that conformational changes of the channel and its gate with K⁺ are connected structurally to the clustering of GORK within the plane of the plasma membrane. Such clustering may signal changes in the external ionic environment, possibly by exploiting the changing capacity of GORK, when in puncta, to interact with other cytoplasmic or plasma membrane proteins.

GORK puncta are distinct from the trafficking platforms of the KAT1 channel

Clustering of the GORK K⁺ channels within puncta at the surface of tobacco epidermal cells and Arabidopsis guard cells complements studies of the other major K⁺ channel

subgroup, represented by KAT1 (Meckel *et al.*, 2004; Sutter *et al.*, 2006, 2007; Homann *et al.*, 2007), and supports electrophysiological evidence that many functional K⁺ channels in plants are distributed non-homogeneously over the plasma membrane surface (Tester, 1990; Hille, 2001). The puncta formed by GORK are similar in size to those of KAT1, but are physically distinct as evident from co-localisation studies (Figures 1, S3 and S4). GORK puncta also differ from those of KAT1 in their mobility and sensitivity to external stimuli. Whereas the puncta of KAT1 are lost in ABA (Sutter *et al.*, 2007) and reform in a manner sensitive to the vesicle-trafficking protein SYP121 (Eisenach *et al.*, 2012), we found GORK to be insensitive to ABA and SYP121 but dependent on the extracellular K⁺ concentration (Figures 2, 5 and 6). These findings alone distinguish the structural characteristics of the two K⁺ channels.

Physical clustering of channel and other proteins is well known also in animal cells (Lai and Jan, 2006; O'Connell *et al.*, 2010; Zilly *et al.*, 2011; Pristera *et al.*, 2012) and, in neurons, often demarcates platforms for vesicle fusion and channel traffic (Lai and Jan, 2006; Deutsch *et al.*, 2012). Much the same conclusion was reached for the puncta formed of the KAT1 channel when expressed in tobacco (Sutter *et al.*, 2006, 2007): Our analysis of GORK-GFP recovery after photobleaching suggested that roughly 10% may be mobile within the cell (Figure 3), possibly through vesicle traffic. However, two-phase partitioning failed to uncover a substantial change in GORK distribution between plasma- and endomembranes fractions, even following transfer to 100 mM KCl to evoke a dispersal of the puncta. GORK puncta also dissociated reversibly in the *syp121* mutant that is defective in KAT1 trafficking to the plasma membrane (Eisenach *et al.*, 2012). We cannot discount a role for vesicle traffic in the mobility of GORK, but these results indicate that any such contribution to GORK clustering and dispersal is small and of a magnitude that might only be resolved by fluorescence analysis *in vivo* over extended time periods (Luu *et al.*, 2012).

We stress that plant ion channels, including GORK, normally express at levels that are too low for detection by confocal microscopy. We used GORK-GFP constructs driven by the Ubiquitin-10 promoter, *pUBQ10*, that drives expression at lower levels than the 35S CaMV promoter (Grefen *et al.*, 2010b), and we confirmed channel function of GORK-GFP. We cannot rule out that *pUBQ10*-driven expression misrepresents GORK distribution. Nonetheless, GORK-GFP generally was not observed to accumulate in the endoplasmic reticulum, and GORK puncta dissociated reversibly *in vivo*. These findings support the idea that clustering of the K⁺ channels is physiologically relevant. Clustering of membrane proteins in lipid rafts is common and often accompanied by restricted lateral diffusion (Bhat *et al.*, 2005; Lai and Jan, 2006; Mongrand *et al.*, 2010). Such rafts have been implicated in signal transduction,

polarised secretion, membrane traffic and pathogen entry. Membrane rafts are generally acknowledged to form below the resolution limit of the light microscope and, thus, are 5- to 10-fold smaller than the GORK-GFP clusters we observed. However, such small-scale rafts may aggregate in response to external stimuli (Bhat *et al.*, 2005; Mongrand *et al.*, 2010), potentially underpinning the larger clusters observed with the GORK K⁺ channel. Our FRAP analysis (Figure 3) showed that cluster dispersion was not associated with a significant increase in mobility or altered macroscopic diffusion. Thus, it may be that GORK remains anchored with other proteins in raft-like microdomains, even in high external K⁺.

A physiological role for GORK clustering associated with K⁺-dependent gating?

The most striking aspects of the physical organisation of GORK are its parallels to the K⁺-sensitivity of gating and ensemble conductance. The activities of the Kv-like channels GORK and SKOR in Arabidopsis, as well as outward-rectifying K⁺ channels in other plants, show a characteristic dependence on external alkali cation concentration as well as voltage (Blatt, 1988; Armstrong *et al.*, 1995; Blatt and Gradmann, 1997; Blatt *et al.*, 1999; Ache *et al.*, 2000; Bauly *et al.*, 2000; Johansson *et al.*, 2006). These characteristics include a displacement in channel conductance in parallel with the equilibrium voltage for K⁺ (see Figure S1), an increase in the ensemble conductance maximum, and the ability of Cs⁺ to substitute for K⁺ outside. Channel gating responds in a near-instantaneous manner to K⁺ within the timescale of bulk solution changes, and changes in ensemble conductance are only marginally slower (Blatt, 1988; Blatt and Gradmann, 1997). Johansson *et al.* (2006) have shown that external cations affect the K⁺ channel through interactions of the pore loop and pore-lining α -helices that, in turn, are likely to influence the conformational states of the outer ring of polypeptides formed by the voltage-sensor domains of the channels (Dreyer and Blatt, 2009): in effect, occupancy of the inner vestibule of the pore at high K⁺ concentrations appears to favour a temporally-stable, 'locked-closed' state. We speculate that these conformations may affect the local packing of the K⁺ channel proteins within the plasma membrane, which becomes evident at a macroscopic level as cluster dissolution. Barium suppression of the GORK puncta dispersal (Figure 6), and the parallels in timecourse for cluster dissolution and gating in 100 mM K⁺, makes this hypothesis especially compelling. Barium enters the pores of many K⁺ channels (Vergani *et al.*, 1997; Hamilton *et al.*, 2000; Jiang and MacKinnon, 2000; Hille, 2001), including GORK (Roelfsema and Prins, 1997; Ache *et al.*, 2000), and is thought to block by occluding the selectivity filter (Jiang and MacKinnon, 2000; Rowley and Roux, 2013). It follows that, with Ba²⁺ present, the channel is likely to become trapped in the

'locked-closed' state with K⁺ in the inner vestibule of the channel, isolated from the pool of K⁺ in the cytosol and, of course, from changes in K⁺ concentration outside. Thus, the effect on GORK cluster dispersal implies a close connection to channel conformation in gating and to channel conductance.

What role might reversible clustering of the K⁺ channels serve? In addition to the voltage-dependence of the channel gate, at least two physiological phenomena may be connected to this behaviour. First, we suggest that clustering may serve to control the pool of GORK channels active in the plasma membrane by sequestering channels, possibly in a non-activatable state. Such behaviour might be seen to withdraw channels from the active pool at the membrane much as an iceberg constrains a volume of water within a crystalline array, preventing its movement and ability to act as a general solvent. For the channels at low external K⁺ concentrations, the effect of such an 'iceberg' model might be seen to confer a synergy to the voltage-dependence of the channels as the K⁺ concentration decreases while reducing the maximum K⁺ flux capacity of the channel population (Blatt, 1988, 1990, 1992; Thiel *et al.*, 1992; Armstrong *et al.*, 1995; Blatt *et al.*, 1999; Bauly *et al.*, 2000) (see also Figure 6). Similar concepts have been proposed to explain the clustering of mammalian K⁺ channels (Misonou and Trimmer, 2004), although correlating channel clustering and ensemble conductance has proven difficult (O'Connell *et al.*, 2010).

We can propose a second role for GORK clustering that builds on this iceberg analogy. K⁺ flux across the plasma membrane is known to be tightly linked to membrane surface area and volume control (Zonia and Munnik, 2007). Work from this laboratory has uncovered the wide-spread interaction between subsets of vesicle-trafficking (SNARE) proteins and K⁺ channels that have profound effects on channel gating and net K⁺ uptake (Honsbein *et al.*, 2009, 2011; Grefen *et al.*, 2010a). These interactions are implicated in priming the SNAREs to catalyse membrane fusion (Karnik *et al.*, 2013). It is plausible, therefore, that the cell might exploit the K⁺-sensitivity of GORK clustering to regulate vesicle traffic of other membrane components, adjusting the rate of cell surface expansion with K⁺ uptake and cell volume. For example, K⁺ accumulation is enhanced in guard cells at high external K⁺, which also promotes the dissolution of GORK clusters. We can imagine that 'freeing' the channels from within the clusters facilitates SNARE and other interactions to accelerate vesicle traffic for the increase in cell volume.

In conclusion, we have uncovered a new and unusual process that may help to understand how the K⁺ channels of Arabidopsis guard cells, and other plant cells, sense and respond to external K⁺ concentration. To date, the phenomenon of K⁺-dependent channel clustering in plants appears unique to the outward-rectifying K⁺ channel

GORK, but we anticipate that similar characteristics will be forthcoming for other outward-rectifying K⁺ channels in plants. For GORK, the properties of channel clustering shows many hallmarks of K⁺-dependent gating and conductance, implicating a close connection that is now open to testing, for example through a combination of protein domain exchange with a non-clustering channel such as AKT1 (Honsbein *et al.*, 2009). We suspect that the organisation of GORK and other channels in this manner is likely to contribute both as a mechanism regulating the channels and as a platform for sensing and responding to environmental cues.

MATERIAL AND METHODS

Molecular cloning

The GORK coding sequence was amplified from rosette-leaf cDNA using the oligonucleotide primers 5'-attB1 TA ATG GGA CGT CTC CGG-3' and 5'-attB2 G TGT TTG ATC AGT AGT ATC ACT G-3', recombined into Gateway™ entry vector pDONR207 with BP clonase II (Life Technologies, <http://www.lifetechnologies.com>), and transformed into the *E. coli* strain CopyCutter EPI400 (Cambio, <http://www.cam.bio.co.uk>) (Grefen *et al.*, 2009). Clones were verified by sequencing (GATC, <http://www.gatc-biotech.com/>) and recombined into expression vectors via LR-reaction (Life Technologies). The *pUBQ10* vector system was used to generate GORK constructs C-terminally tagged with GFP and RFP (Grefen *et al.*, 2010b). Constructs were transformed into *Agrobacterium tumefaciens* (strain GV3101) and were verified by rescue in *E. coli* and restriction digest analysis. A single *A. tumefaciens* clone was used for transient transformation of tobacco and stable transformation of Arabidopsis.

The coding sequence for GORK-GFP was amplified from the *pUBQ10-DEST* expression construct for re-cloning into the oocyte expression vector *pGT-DEST* (Grefen *et al.*, 2010b) using the oligonucleotide primers 5'-A GTT AAC ATG GGA CGT CTC CGG AGA C-3' and 5'-C AGG CCT TTA TAA CTT GTA CAG CTC GTC CAT GC-3'. These primers incorporated 5' *HpaI* and *StuI* overhangs, respectively. Blunt-end restriction of the oocyte expression vector *pGT-DEST* with *MscI* and of the PCR product with *HpaI* and *StuI* was followed by ligation using T4 DNA Ligase (Promega, <http://www.promega.com/>) before verification by sequencing.

Electrophysiology

GORK-GFP was expressed in *Xenopus* oocytes using *pGT GORK-GFP* plasmid DNA (Vergani *et al.*, 1998; Grefen *et al.*, 2010a), and currents were recorded by two-electrode voltage clamp as described previously (Johansson and Blatt, 2006). Measurements were carried out using

microelectrodes filled with 3 M K⁺-acetate and with oocytes bathed in 10 mM HEPES-NaOH, pH 7.2, with 1.8 mM MgCl₂, 1.8 mM CaCl₂ and additions of 10 mM, 30 mM or 96 mM KCl balanced by NaCl to give a total salt concentration of 100 mM.

Plant growth, transformation and microscopy

Arabidopsis thaliana Col0, *syp121* and *gork* [SALK_082258C (Alonso *et al.*, 2003)] mutant plants were grown and transformed by floral dip (Clough and Bent, 1998) and T₁ transformants were selected for BASTA[®] resistance (1:1000 dilution; Bayer Cropscience, <http://www.cropscience.bayer.com>). Seeds of the T₂, T₃ and T₄ generations were selected in the same manner. Leaves of *Nicotiana tabacum* (tobacco) were transformed by infiltration with *Agrobacterium* carrying the GORK-GFP construct (Geelen *et al.*, 2002), and were analysed 72–120 h after transformation.

GORK-GFP fluorescence was resolved on a LSM510-META confocal microscope (Zeiss, <http://www.zeiss.com>) using the 488-nm line of an Argon laser and fluorescence was collected as reflectance from a 545-nm dichroic mirror after passage through a 505–530 nm interference filter. Chloroplast fluorescence was collected concurrently after passage through the 545-nm dichroic mirror and a long pass 560 nm emission filter. Fluorescence recovery after photobleaching (FRAP) was carried out after fluorophore bleaching with the 488 laser using a pixel time of 1.6 sec (2.4 mJ exposure energy). Bleaching, detection and analysis settings were standardised between experiments for ROI dimensions, laser power, magnification and detection settings and fluorescence was corrected for decay during acquisition.

Imaging was carried out using young rosette leaves of *Arabidopsis* mounted in a custom-build perfusion chamber that enabled continuous perfusion and solution changes during experiments. Buffers included 0.003% Silwet L77 (Lehle Seeds, <http://www.lehleseeds.com>) to ensure cuticle penetration. For tobacco, imaging was carried out on 1-cm diameter leaf discs after vacuum infiltration with treatment buffers before remounting. All buffers were based on 10 mM NaMES, pH6.1. The salts KCl, KNO₃, CsCl₂, MgCl₂ and BaCl₂ were added as indicated and osmotic strength was adjusted using mannitol. Abscisic acid (ABA) was prepared as before (Blatt and Armstrong, 1993) and diluted in buffer to 40 μM for use. For ABA treatments, leaves were infiltrated and incubated in 5 mM Ca²⁺-MES, pH 6.1, 10 mM KCl for 2 h under 100 μmol m⁻² sec⁻¹ white light. Images were collected, the leaves re-infiltrated using the same buffer with the addition of ABA, and the leaves re-imaged after 30 and 60 min. Tobacco disc analysis was carried out in blind assays. GORK puncta were quantified both as the percentage of cells showing puncta and by relative standard deviation (RSD) after normalizing to the intensity means.

Protein biochemistry

GORK distribution between plasma membrane and endomembrane fractions was determined by aqueous two-phase partitioning. Arabidopsis leaf tissues were infiltrated in either 100 mM KCl or 0.1 mM KCl buffers and incubated for 2 h. All subsequent steps were carried out at 4°C as described before (Honsbein *et al.*, 2009). Proteins were separated by electrophoresis and transferred onto PVDF membranes (Honsbein *et al.*, 2009; Karnik *et al.*, 2013) and were probed overnight with primary antibody, either αGORK [1:100]; αAHA [1:5000, (Villalba *et al.*, 1991)], αSec61 [1:3000, (Yuasa *et al.*, 2005)], or αGFP [1:200; Abcam, <http://www.abcam.co.uk>]. Horseradish peroxidase-coupled, α-rabbit IgG secondary antibody (1:100 000) was used for detection with WestFemto SuperSignal (Pierce; Thermo Scientific, <http://www.thermofischer.com>). In some experiments, membranes were re-probed after stripping by incubation in 100 mM β-Mercaptoethanol, 2% SDS, 62.5 mM Tris-HCl, pH 6.7 at 70°C for 45 min.

Data analysis

Statistical analyses were carried out using SIGMAPLOT 11 (Systat Software, Inc., <http://www.sigmaplot.com>). Non-linear least-squares fittings used a Marquardt–Levenberg algorithm (Marquardt, 1963). Significance was tested using Student's *t*-test and analysis of variance (ANOVA). Otherwise, data are reported as means ± SE of *n* observations.

Chemicals and media

All chemicals were from Sigma (<http://www.sigma-aldrich.com>) unless otherwise noted.

ACKNOWLEDGEMENTS

We thank Christopher Grefen and Annegret Honsbein for support in molecular cloning and electrophysiology, respectively, and Amparo Ruiz-Prado for plant maintenance. This work was supported by a postgraduate grant-in-aid from Plant Bioscience Ltd. (CE), by BBSRC grants BB/H009817/1 and BB/I024496/1 (MRB), and by a Begonia Trust scholarship (MP).

SUPPORTING INFORMATION

Additional Supporting Information may be found in the online version of this article.

Figure S1. The GFP-tagged GORK construct encodes a functional K⁺ channel.

Figure S2. GORK current is blocked by the K⁺ channel antagonist tetraethylammonium chloride (TEA⁺).

Figure S3. The K⁺ channels GORK and KAT1 assemble in physically-distinct puncta.

Figure S4. KAT1-GFP and GORK-RFP show intermediate degree of overlap, suggesting that the two channel proteins do not coreside in the same punctate structures at the plasma membrane.

Figure S5. GORK-GFP clusters appear in strands of plasma membrane on cell plasmolysis.

Figure S6. GORK-GFP clusters are unaffected by ABA.

Figure S7. Relative standard distribution (RSD) of GORK-GFP at the guard cell periphery is unaffected by ABA.

Figure S8. GORK peptide antigen design.

REFERENCES

- Ache, P., Becker, D., Ivashikina, N., Dietrich, P., Roelfsema, M.R.G. and Hedrich, R. (2000) GORK, a delayed outward rectifier expressed in guard cells of *Arabidopsis thaliana*, is a K⁺-selective, K⁺-sensing ion channel. *FEBS Lett.* **486**, 93–98.
- Alonso, J.M., Stepanova, A.N., Leisse, T.J. *et al.* (2003) Genome-wide insertional mutagenesis of *Arabidopsis thaliana*. *Science*, **301**, 653–657.
- Armstrong, C.M. and Taylor, S.R. (1980) Interaction of barium ions with potassium channels in squid giant axons. *Biophys. J.* **30**, 473–488.
- Armstrong, F., Leung, J., Grabov, A., Brearley, J., Giraudat, J. and Blatt, M.R. (1995) Sensitivity to abscisic acid of guard cell K⁺ channels is suppressed by *abi1-1*, a mutant *Arabidopsis* gene encoding a putative protein phosphatase. *Proc. Natl Acad. Sci. USA*, **92**, 9520–9524.
- Baully, J.M., Sealy, I.M., MacDonald, H. *et al.* (2000) Overexpression of auxin-binding protein enhances the sensitivity of guard cells to auxin. *Plant Physiol.* **124**, 1229–1238.
- Bhat, R.A., Miklis, M., Schmelzer, E., Schulze-Lefert, P. and Panstruga, R. (2005) Recruitment and interaction dynamics of plant penetration resistance components in a plasma membrane microdomain. *Proc. Natl Acad. Sci. USA*, **102**, 3135–3140.
- Blatt, M.R. (1988) Potassium-dependent bipolar gating of potassium channels in guard cells. *J. Membr. Biol.* **102**, 235–246.
- Blatt, M.R. (1990) Potassium channel currents in intact stomatal guard cells: rapid enhancement by abscisic acid. *Planta*, **180**, 445–455.
- Blatt, M.R. (1992) K⁺ channels of stomatal guard cells: characteristics of the inward rectifier and its control by pH. *J. Gen. Physiol.* **99**, 615–644.
- Blatt, M.R. (2000) Cellular signaling and volume control in stomatal movements in plants. *Annu. Rev. Cell Dev. Biol.* **16**, 221–241.
- Blatt, M.R. and Armstrong, F. (1993) K⁺ channels of stomatal guard cells: abscisic acid-evoked control of the outward rectifier mediated by cytoplasmic pH. *Planta*, **191**, 330–341.
- Blatt, M.R. and Grabov, A. (1999) H⁺-mediated control of ion channels in guard cells of higher plants. In *pH in Biological Systems* (Egginton, S., Taylor, E.W. and Raven, J.A., eds). Cambridge: Cambridge University Press, pp. 155–176.
- Blatt, M.R. and Gradmann, D. (1997) K⁺-sensitive gating of the K⁺ outward rectifier in *Vicia* guard cells. *J. Membr. Biol.* **158**, 241–256.
- Blatt, M.R. and Thiel, G. (1993) Hormonal control of ion channel gating. *Annu. Rev. Plant Physiol. Mol. Biol.* **44**, 543–567.
- Blatt, M.R. and Thiel, G. (1994) K⁺ channels of stomatal guard cells: bimodal control of the K⁺ inward-rectifier evoked by auxin. *Plant J.* **5**, 55–68.
- Blatt, M.R., Thiel, G. and Trentham, D.R. (1990) Reversible inactivation of K⁺ channels of *Vicia* stomatal guard cells following the photolysis of caged inositol 1,4,5-trisphosphate. *Nature*, **346**, 766–769.
- Blatt, M.R., Grabov, A., Brearley, J., HammondKosack, K. and Jones, J.D.G. (1999) K⁺ channels of *Cf-9* transgenic tobacco guard cells as targets for *Cladosporium fulvum* Avr9 elicitor-dependent signal transduction. *Plant J.* **19**, 453–462.
- Blatt, M.R., Garcia-Mata, C. and Sokolovski, S. (2007) Membrane transport and Ca²⁺ oscillations in guard cells. In *Rhythms in Plants* (Mancuso, S. and Shabala, S., eds). Berlin: Springer, pp. 115–134.
- Brearley, J., Venis, M.A. and Blatt, M.R. (1997) The effect of elevated CO₂ concentrations on K⁺ and anion channels of *Vicia faba* L. guard cells. *Planta*, **203**, 145–154.
- Canny, M.J. (1990) Rates of diffusion in wheat leaves. *New Phytol.* **116**, 263–268.
- Chen, Z.H., Eisenach, C., Xu, X.Q., Hills, A. and Blatt, M.R. (2012) Protocol: optimised electrophysiological analysis of intact guard cells from *Arabidopsis*. *Plant Methods*, **8**, 15–25.
- Clough, S.J. and Bent, A.F. (1998) Floral dip: a simplified method for Agrobacterium-mediated transformation of *Arabidopsis thaliana*. *Plant J.* **16**, 735–743.
- Deutsch, E., Weigel, A.V., Akin, E.J., Fox, P., Hansen, G., Haberkorn, C.J., Loftus, R., Krapf, D. and Tamkun, M.M. (2012) Kv2.1 cell surface clusters are insertion platforms for ion channel delivery to the plasma membrane. *Mol. Biol. Cell*, **23**, 2917–2929.
- Dreyer, I. and Blatt, M.R. (2009) What makes a gate? The ins and outs of Kv-like K⁺ channels in plants. *Trends Plant Sci.* **14**, 383–390.
- Eisenach, C., Chen, Z.H., Grefen, C. and Blatt, M.R. (2012) The trafficking protein SYP121 of *Arabidopsis* connects programmed stomatal closure and K⁺ channel activity with vegetative growth. *Plant J.* **69**, 241–251.
- Geelen, D., Leyman, B., Batoko, H., Di Sansabastiano, G.P., Moore, I. and Blatt, M.R. (2002) The abscisic acid-related SNARE homolog NtSyr1 contributes to secretion and growth: evidence from competition with its cytosolic domain. *Plant Cell*, **14**, 387–406.
- Grabov, A. and Blatt, M.R. (1998) Membrane voltage initiates Ca²⁺ waves and potentiates Ca²⁺ increases with abscisic acid in stomatal guard cells. *Proc. Natl Acad. Sci. USA*, **95**, 4778–4783.
- Grefen, C., Obrdlik, P. and Harter, K. (2009) The determination of protein-protein interactions by the mating-based split-ubiquitin system (mbSUS). *Methods Mol. Biol.* **479**, 1–17.
- Grefen, C., Chen, Z.H., Honsbein, A., Donald, N., Hills, A. and Blatt, M.R. (2010a) A novel motif essential for SNARE interaction with the K⁺ channel KC1 and channel gating in *Arabidopsis*. *Plant Cell*, **22**, 3076–3092.
- Grefen, C., Donald, N., Hashimoto, K., Kudla, J., Schumacher, K. and Blatt, M.R. (2010b) A ubiquitin-10 promoter-based vector set for fluorescent protein tagging facilitates temporal stability and native protein distribution in transient and stable expression studies. *Plant J.* **64**, 355–365.
- Hamilton, D.W.A., Hills, A., Kohler, B. and Blatt, M.R. (2000) Ca²⁺ channels at the plasma membrane of stomatal guard cells are activated by hyperpolarization and abscisic acid. *Proc. Natl Acad. Sci. USA*, **97**, 4967–4972.
- Hedrich, R., Neimanis, S., Savchenko, G., Felle, H.H., Kaiser, W.M. and Heber, U. (2001) Changes in apoplastic pH and membrane potential in leaves in relation to stomatal responses to CO₂, malate abscisic acid or interruption of water supply. *Planta*, **213**, 594–601.
- Hille, B. (2001) *Ionic Channels of Excitable Membranes*. Sunderland, MA: Sinauer Press.
- Homann, U., Meckel, T., Hewing, J., Hutt, M.T. and Hurst, A.C. (2007) Distinct fluorescent pattern of KAT1: GFP in the plasma membrane of *Vicia faba* guard cells. *Eur. J. Cell Biol.* **86**, 489–500.
- Honsbein, A., Sokolovski, S., Grefen, C., Campanoni, P., Pratelli, R., Panque, M., Chen, Z.H., Johansson, I. and Blatt, M.R. (2009) A tripartite SNARE-K⁺ channel complex mediates in channel-dependent K⁺ nutrition in *Arabidopsis*. *Plant Cell*, **21**, 2859–2877.
- Honsbein, A., Blatt, M.R. and Grefen, C. (2011) A molecular framework for coupling cellular volume and osmotic solute transport control. *J. Exp. Bot.* **62**, 2363–2370.
- Hosy, E., Vavasseur, A., Mouline, K. *et al.* (2003) The *Arabidopsis* outward K⁺ channel GORK is involved in regulation of stomatal movements and plant transpiration. *Proc. Natl Acad. Sci. USA*, **100**, 5549–5554.
- Hurst, A.C., Meckel, T., Tayefeh, S., Thiel, G. and Homann, U. (2004) Trafficking of the plant potassium inward rectifier KAT1 in guard cell protoplasts of *Vicia faba*. *Plant J.* **37**, 391–397.
- Jiang, Y.X. and MacKinnon, R. (2000) The barium site in a potassium channel by X-ray crystallography. *J. Gen. Physiol.* **115**, 269–272.
- Johansson, I. and Blatt, M.R. (2006) Interactive domains between pore loops of the yeast K⁺ channel TOK1 associate with extracellular K⁺ sensitivity. *Biochem. J.* **393**, 645–655.
- Johansson, I., Wulfetange, K., Poree, F. *et al.* (2006) External K⁺ modulates the activity of the *Arabidopsis* potassium channel SKOR via an unusual mechanism. *Plant J.* **46**, 269–281.
- Karnik, R., Grefen, C., Bayne, R., Honsbein, A., Koehler, T., Kioumourtzoglou, D., Williams, M., Bryant, N.J. and Blatt, M.R. (2013) *Arabidopsis* Sec1/Munc18 protein SEC11 is a competitive and dynamic modulator of SNARE binding and SYP121-dependent vesicle traffic. *Plant Cell*, **25**, 1368–1382.
- Kim, T.H., Bohmer, M., Hu, H.H., Nishimura, N. and Schroeder, J.I. (2010) Guard cell signal transduction network: advances in understanding abscisic acid, CO₂, and Ca²⁺ signaling. *Annu. Rev. Plant Biol.* **61**, 561–591.
- Lai, H.C. and Jan, L.Y. (2006) The distribution and targeting of neuronal voltage-gated ion channels. *Nat. Rev. Neurosci.* **7**, 548–562.
- Lebaudy, A., Very, A.A. and Sentenac, H. (2007) K⁺ channel activity in plants: genes, regulations and functions. *FEBS Lett.* **581**, 2357–2366.

- Leyman, B., Geelen, D., Quintero, F.J. and Blatt, M.R. (1999) A tobacco syntaxin with a role in hormonal control of guard cell ion channels. *Science*, **283**, 537–540.
- Luu, D.T., Martiniere, A., Sorieul, M., Runions, J. and Maurel, C. (2012) Fluorescence recovery after photobleaching reveals high cycling dynamics of plasma membrane aquaporins in *Arabidopsis* roots under salt stress. *Plant J.* **69**, 894–905.
- Marquardt, D. (1963) An algorithm for least-squares estimation of nonlinear parameters. *J. Soc. Ind. Appl. Math.* **11**, 431–441.
- Meckel, T., Hurst, A.C., Thiel, G. and Homann, U. (2004) Endocytosis against high turgor: intact guard cells of *Vicia faba* constitutively endocytose fluorescently labelled plasma membrane and GFP-tagged K⁺-channel KAT1. *Plant J.* **39**, 182–193.
- Meckel, T., Hurst, A.C., Thiel, G. and Homann, U. (2005) Guard cells undergo constitutive and pressure-driven membrane turnover. *Protoplasma*, **226**, 23–29.
- Misonou, H. and Trimmer, J.S. (2004) Determinants of voltage-gated potassium channel surface expression and localization in mammalian neurons. *Crit. Rev. Biochem. Mol. Biol.* **39**, 125–145.
- Mongrand, S., Stanislas, T., Bayer, E.M.F., Lherminier, J. and Simon-Plas, F. (2010) Membrane rafts in plant cells. *Trends Plant Sci.* **15**, 656–663.
- O'Connell, K.M.S., Loftus, R. and Tamkun, M.M. (2010) Localization-dependent activity of the Kv2.1 delayed-rectifier K⁺ channel. *Proc. Natl Acad. Sci. USA*, **107**, 12351–12356.
- Pardo, J.M. and Serrano, R. (1989) Structure of a plasma membrane H⁺-ATPase gene from the plant *Arabidopsis thaliana*. *J. Biol. Chem.* **264**, 8557–8562.
- Priester, A., Baker, M.D. and Okuse, K. (2012) Association between tetrodotoxin resistant channels and lipid rafts regulates sensory neuron excitability. *PLoS One*, **7**, e40078.
- Roelfsema, M.R. and Hedrich, R. (2010) Making sense out of Ca²⁺ signals: their role in regulating stomatal movements. *Plant, Cell Environ.* **33**, 305–321.
- Roelfsema, M.G. and Prins, H.A. (1997) Ion channels in guard cells of *Arabidopsis thaliana* (L.) Heynh. *Planta*, **202**, 18–27.
- Romano, L.A., Miedema, H. and Assmann, S.M. (1998) Ca²⁺-permeable, outwardly-rectifying K⁺ channels in mesophyll cells of *Arabidopsis thaliana*. *Plant Cell Physiol.* **39**, 1133–1144.
- Rowley, C.N. and Roux, B. (2013) A computational study of barium blockades in the KcsA potassium channel based on multi-ion potential of mean-force calculations and free energy perturbation. *J. Gen. Physiol.* **142**, 451–463.
- Sokolowski, S. and Blatt, M.R. (2004) Nitric oxide block of outward-rectifying K⁺ channels indicates direct control by protein nitrosylation in guard cells. *Plant Physiol.* **136**, 4275–4284.
- Sutter, J.U., Campanoni, P., Tyrrell, M. and Blatt, M.R. (2006) Selective mobility and sensitivity to SNAREs is exhibited by the *Arabidopsis* KAT1 K⁺ channel at the plasma membrane. *Plant Cell*, **18**, 935–954.
- Sutter, J.U., Sieben, C., Hartel, A., Eisenach, C., Thiel, G. and Blatt, M.R. (2007) Abscisic acid triggers the endocytosis of the *Arabidopsis* KAT1 K⁺ channel and its recycling to the plasma membrane. *Curr. Biol.* **17**, 1396–1402.
- Tester, M. (1990) Plant ion channels: whole-cell and single-channel studies. *New Phytol.* **114**, 305–340.
- Thiel, G. and Blatt, M.R. (1991) The mechanism of ion permeation through K⁺ channels of stomatal guard cells voltage-dependent block by Na⁺. *J. Plant Physiol.* **138**, 326–334.
- Thiel, G., MacRobbie, E.A.C. and Blatt, M.R. (1992) Membrane transport in stomatal guard cells: the importance of voltage control. *J. Membr. Biol.* **126**, 1–18.
- Thiel, G., Blatt, M.R., Fricker, M.D., White, I.R. and Millner, P.A. (1993) Modulation of K⁺ channels in *Vicia* stomatal guard cells by peptide homologs to the auxin-binding protein C-terminus. *Proc. Natl Acad. Sci. USA*, **90**, 11493–11497.
- Vergani, P., Miosga, T., Jarvis, S.M. and Blatt, M.R. (1997) Extracellular K⁺ and Ba²⁺ mediate voltage-dependent inactivation of the outward-rectifying K⁺ channel encoded by the yeast gene *TOK1*. *FEBS Lett.* **405**, 337–344.
- Vergani, P., Hamilton, D., Jarvis, S. and Blatt, M.R. (1998) Mutations in the pore regions of the yeast K⁺ channel YKC1 affect gating by extracellular K⁺. *EMBO J.* **17**, 7190–7198.
- Villalba, J.M., Lutzelschwab, M. and Serrano, R. (1991) Immunocytolocalization of plasma membrane H⁺-ATPase in maize coleoptiles and enclosed leaves. *Planta*, **185**, 458–461.
- Wang, Y. and Blatt, M.R. (2011) Anion channel sensitivity to cytosolic organic acids implicates a central role for oxaloacetate in integrating ion flux with metabolism in stomatal guard cells. *Biochem. J.* **439**, 161–170.
- Wang, Y., Papanatsiou, M., Eisenach, C., Karnik, R., Williams, M., Hills, A., Lew, V.L. and Blatt, M.R. (2012) Systems dynamic modelling of a guard cell Cl⁻ channel mutant uncovers an emergent homeostatic network regulating stomatal transpiration. *Plant Physiol.* **160**, 1956–1972.
- Yuasa, K., Toyooka, K., Fukuda, H. and Matsuoka, K. (2005) Membrane-anchored prolyl hydroxylase with an export signal from the endoplasmic reticulum. *Plant J.* **41**, 81–94.
- Zilly, F.E., Halemani, N.D., Walrafen, D., Spitta, L., Schreiber, A., Jahn, R. and Lang, T. (2011) Ca²⁺ induces clustering of membrane proteins in the plasma membrane via electrostatic interactions. *EMBO J.* **30**, 1209–1220.
- Zonia, L. and Munnik, T. (2007) Life under pressure: hydrostatic pressure in cell growth and function. *Trends Plant Sci.* **12**, 90–97.